OLENA
HOLOVAN
VIKTOR
KHARCHENKO

TRANSMISSION OF INFORMATION USING METEOR RADIO CHANNELS

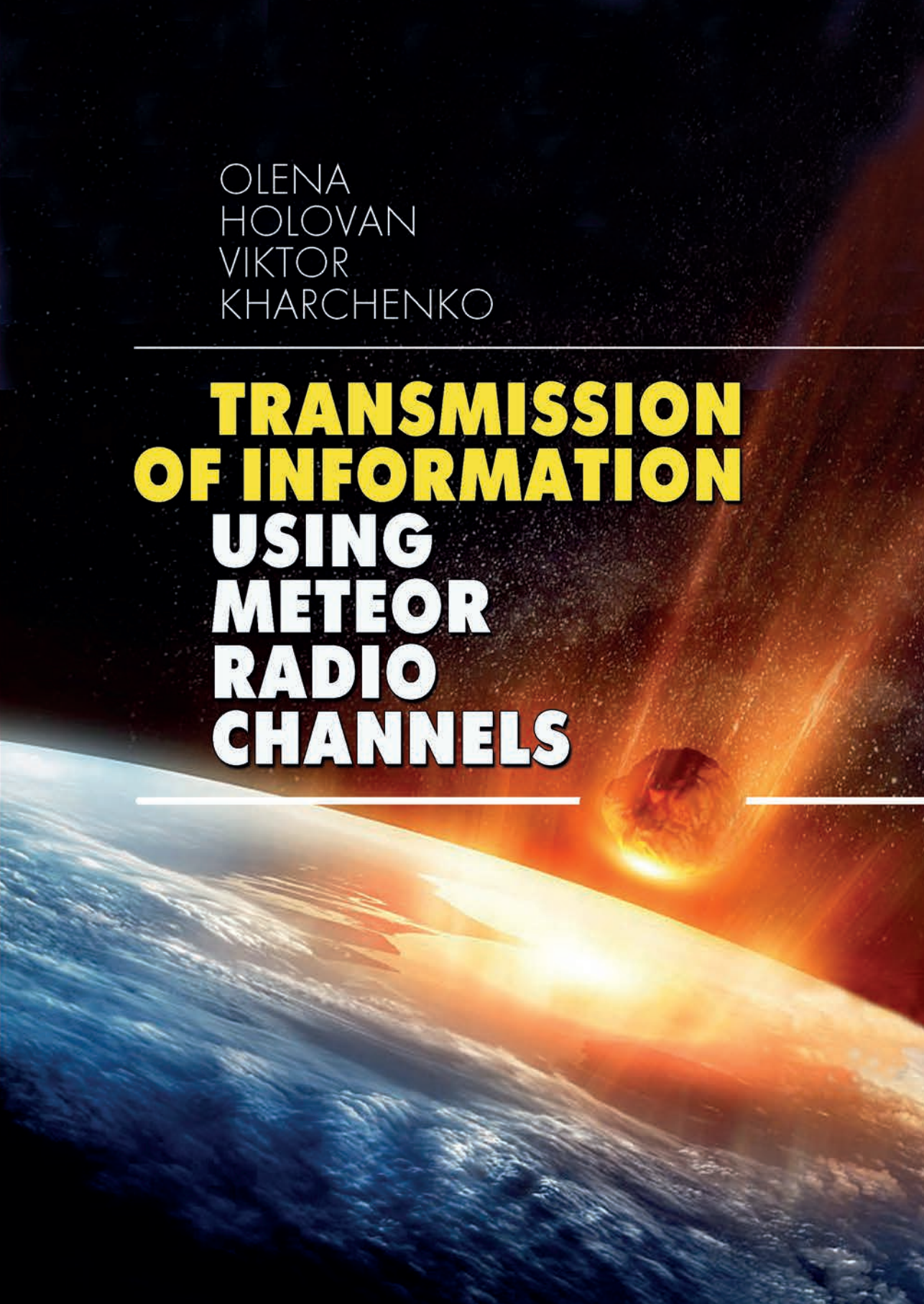

NATIONAL ACADEMY OF SCIENCES OF UKRAINE
O.Ya. USIKOV INSTITUTE FOR RADIOPHISICS
AND ELECTRONICS OF THE NAS OF UKRAINE

НАЦІОНАЛЬНА АКАДЕМІЯ НАУК УКРАЇНИ
ІНСТИТУТ РАДІОФІЗИКИ ТА ЕЛЕКТРОНІКИ
ім. О.Я. УСИКОВА НАН УКРАЇНИ

Олена ГОЛОВАНЬ
Віктор ХАРЧЕНКО

ПЕРЕДАЧА ІНФОРМАЦІЇ ПО МЕТЕОРНИХ РАДІО-КАНАЛАХ

ПРОЄКТ
«УКРАЇНСЬКА НАУКОВА КНИГА
ІНОЗЕМНОЮ МОВОЮ»

КИЇВ
АКАДЕМПЕРІОДИКА
2024

Olena HOLOVAN
Viktor KHARCHENKO

TRANSMISSION OF INFORMATION USING METEOR RADIO CHANNELS

PROJECT
«UKRAINIAN SCIENTIFIC BOOK
IN A FOREIGN LANGUAGE»

KYIV
AKADEMPERIODYKA
2024

https://doi.org/10.15407/akademperiodyka.517.250
UDC 621.371:523.68
H75

Rewiewers:

V.V. DOLZHIKOV, Professor of the Department of Computer Radio Engineering and Technical Information Security Systems, Kharkiv National University of Radio Electronics, IEEE Senior Member, Doctor of Physical and Mathematical Sciences, Professor

A.V. KOBZEV, Honored Science and Technology of Ukraine, Doctor of Technical Sciences, Professor

V.K. IVANOV, Head of the Remote Sensing of the Earth department of O.Ya. Usikov Institute of Radiophysics and Electronics of the National Academy of Sciences of Ukraine, Senior Scientist, Doctor of Physical and Mathematical Sciences

O.Y. IOKHOV, Head of Figure Communication and Informatization department of the National Academy of the National Guard of Ukraine, Doctor of Technical Sciences, Professor

Approved for publication by O.Ya. Usikov Institute for Radiophysics and Electronics of the National Academy of Sciences of Ukraine (September, 14, 2023, Protocol No. 6)

The publication was funded within the framework of the Targeted Complex Program of the NAS of Ukraine "Scientific Bases of Functioning and Providing for Conditions for the Development of the Scientific and Publishing Complex of the NAS of Ukraine"

Holovan O.V.

H75 Transmission of information using meteor radio channels / O.V. Holovan, V.M. Kharchenko; NAS of Ukraine, O.Ya. Usikov Institute for Radiophysics and Electronics. — Kyiv: Akademperiodyka, 2024. 250 p.

ISBN 978-966-360-517-3

The original studies presented in the monograph are based on a systematic analysis of published works in the field of meteor physics. Prognostic models and algorithms for estimating the characteristics of radio signals during bistatic scattering on an ionized meteor trail during its formation and development as well as the concept and technology for constructing a promising meteor radio communication system are proposed. The book may be useful to different categories of readers: scientists and designers involved in meteor radio communications, geophysicists studying the ionosphere in the meteor zone, astronomers searching for new relationships between meteoroids and their parent bodies, graduate students, university professors, and students.

UDC 621.371:523.68

ISBN 978-966-360-517-3

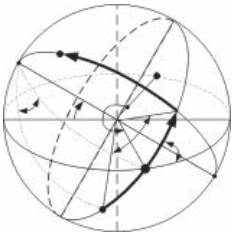

CONTENTS

SECTION 5

SECTION 6

SECTION 7

SECTION 8

SECTION 9

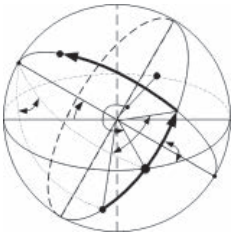

ABBREVIATIONS

ADC — analog-to-digital converter
AMOR — Advanced Meteor Orbit Radar
ANN — artificial neural network
APAA — adaptive phased array antenna
ATCH — amplitude-time characteristics
BS — base station
CDCh — code division of channels
CMOR — Canadian Meteor Orbit Radar
DSSS — direct sequence spread spectrum signals
EIRP — equivalent isotropically radiated power
ESS — effective scattering surface
FDCh — frequency division of channels
FFT — Fast Fourier Transform
FPGA — field-programmable gate array
FR — frequency response
HP — High Power
HPLA — High Power Large Aperture
HRMP — Harvard Radio Meteor Project
IFFT — Inverse Fast Fourier Transform
IMTr — ionized meteoroid trails
IS — incoherent scatter
JFm — Jupiter family
LEDTr — linear electron density of the trail
LFM — linear frequency modulated
LFMS — linear frequency modulated signal
MARS — Meteor Automated Radar System

MBC — meteor burst channel
MRC — meteor radio communication
MRCh — meteor radio channel (meteor burst channel)
MRCS — meteor radio communication systems
MRS — meteor radio system
MST — mesospheric-stratospheric-tropospheric
NBI — narrowband interference
NBIRB — narrow-band interference rejection block
PCP — physical and chemical properties (composition)
PCPAtm — physical and chemical properties (composition) of the atmosphere
PCPMet — physical and chemical properties (composition) of the meteoroid
PDMF — programmable digital matched filter
PLD — programmable logic device,
PPA — phased array antenna
PTR — phase time response
RMS — root mean square
RP — radiation pattern
SAAMER-OS — Southern Argentina Agile Meteor Radar Orbital System
SDR — Software-defined radio
SKiYMET — All-Sky Interferometric Meteor Radar
SMC — sporadic meteor complex
SRP — specular reflection point
SS — subscriber stations
ST — stratospheric-tropospheric
WNLS — wideband noise-like signals

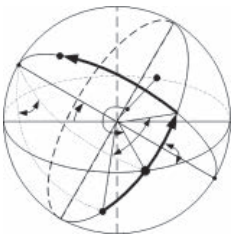

INTRODUCTION

The title of the monograph "Transmission of information using meteor radio channels" reflects the fact that information is transmitted using radio waves, and the information carriers can be meteoroids themselves in the ionosphere at an altitude of 60...130 km, where an ionized meteor trail ("meteor zone") is formed, as well as sources of information directly connected to the transmitting devices that form radio communication systems.

In radar studies of meteoroids, we obtain information about their physical and dynamic parameters by processing signals reflected from the head of meteoroids and meteor trails resulting from the interaction of meteoroids with the Earth's atmosphere. The amplitude-time characteristics (ATCH) of signals scattered by ionized meteoroid trails (IMTr) obtained from radars or radio communications observations implicitly contain information about both the meteoroid itself and the state of the atmosphere at the height of the trail formation. Depending on the path geometry, different ATCHs can be observed for meteoroids identical in all parameters. Knowing the height of the specular reflection point and the velocity of the meteoroid, obtained as a result of measurements or prediction, opens up additional possibilities for extracting information about the meteoroid and the geophysical parameters of the atmosphere. However, this problem cannot be solved using only statistical processing of the results of observations due to the uncontrollability of the initial data. Therefore, prognostic models are necessary to determine the probability of the occurrence of meteor trails with a specular reflection point (SRP) as well as radiophysical scattering models that adequately describe the ATCH of radio reflections from meteor trails.

The radiophysical model of a meteor radio channel (MRCh) is based on the model of a time-varying meteor trail

and the solution of the diffraction problem of signal scattering for a given relative position of the transmitter, receiver, and ionized trail. It is almost impossible to formulate and solve the diffraction problem of radio wave scattering on a meteor trail for all phases of its development in a strict formulation, and it is problematic to obtain reliable empirical calculation formulas directly from the observation results since the initial data are unknown. In this regard, to construct a radiophysical model of signal scattering on a meteor trail, heuristic methods were employed to solve the diffraction problem.

The availability of prognostic and radiophysical models makes it possible to choose the parameters of transceivers and the direction of orientation of antennas toward the zones of the most probable occurrence of meteor trails ("hot areas"), to reasonably use signal-code structures, and, ultimately, to set the topology of the meteor radio communication network and transmission protocols messages. The radiophysical model of the scattering of probing signals on the IMTr can be used to classify meteoroids, as well as to more reliably interpret the results of observations when studying the ionosphere in the meteor zone if the parameters of radio frequency equipment, the type of probing signals, and the geographical coordinates of transmission and reception points are known.

The complexity of constructing a sufficiently complete radiophysical model of MRCh is determined by the fact that astronomy, mathematics, meteoroid physics, geophysics, aerodynamics, radiophysics, plasma physics, spectroscopy, radar, radio engineering, and many other sciences are interconnected during its construction. Specialists in these fields of science often conduct research on meteor phenomena without necessary information from related fields, which sometimes leads to unfortunate misunderstanding.

The absence of a book reflecting the current state of research in the field of physics of meteor phenomena and transmission of information via meteor radio channels has prompted the authors to undertake the task of generalizing and system analysis of the known results and supplementing them with their own research. It should be noted that some problems that are essential for practice have not yet been resolved and require further research, and some solutions are approximate and need to be refined.

The history of the development of the science of meteors is not given in the monograph, since it is described in detail in the works of B. Lovell, T. Kaiser, E. Öpik, D. McKinley, B. Levin, V. Fedynsky, I. Astapovich, L. Katasev, P. Babadzhanov, V. Bronshten, B. Kashcheev, and other authors, where the respective bibliography is also given. The methods of visual, telescopic, and photographic observations, which have been described in detail in many papers and are undoubtedly of great independent importance for studying the physical properties of meteoroids and the lower ionosphere, have not been discussed either. When used together, these methods can significantly complement the data obtained by radio engineering methods.

In the first section of the monograph, the fields of application of meteor radio channels for radio communication, synchronization of time scales, and geophysi-

cal and astrophysical research are considered. The advantages and disadvantages of meteor radio communication systems (MRCS) are assessed. Data on the existing systems and networks of meteor radio communications for general and military purposes, as well as on the principles of constructing these systems, are presented.

In the second section, information from the field of meteor astronomy is presented for readers who may not have relevant knowledge for understanding the material presented in the book.

The coordinate systems used and the design ratios are given, which make it possible to transform the coordinates of meteoroid radiants from one coordinate system to another. The transition from the ecliptic geocentric system to the horizontal system at a given date and time makes it possible to point the antennas at the true or apparent source of radiation, which may be the radiant of a meteor shower or a sporadic meteor complex (SMC). The implementation of the reverse transition provides the possibility of collecting data and mapping the density of the SMC radiant distribution during long-term observations.

The section then discusses the views of modern science on the origin of meteoroids and their genetic relationship with comets and asteroids, which allows making reasonable assumptions about the physicochemical properties of meteoroids that form an ionized trail.

The third section provides the technical characteristics and geographic location of specialized and multifunctional radar systems used in studying atmospheric physics, radiant mapping of sporadic meteor complex**es** and meteor showers, as well as in assessing the parameters of the orbits and velocity of meteoroids. This is necessary because when interpreting the results of observations, one should take into account the features of the systems through which the corresponding data were obtained.

The fourth section is devoted to the development of a physically and astronomically substantiated parametric model of the SMC. The radiant density distribution map serves as the basis for developing a prognostic (probabilistic) model for the frequency of observation of ionized trails that takes into account the orbital motion and axial rotation of the Earth. With the coordinates of the points of transmission and reception and the time of observation, such a model makes it possible to predict the seasonal and diurnal variation in the frequency of occurrence of meteor trails with a specular reflection point belonging to the main SMC sources and meteor showers.

Studying the main sources of SMC and meteor showers allows for reasonable assumptions about the genetic relationship between the meteoroid that generates an ionized trail and its parent body. As a result, assumptions about the physicochemical properties of the meteoroid can be made, which is of interest to both astronomers and astrophysicists, as well as specialists in the field of telecommunications.

Reasonable assumptions about the source of the SMC or the radiant of the meteor shower can provide additional information when choosing the parameters of the radiophysical model of signal scattering on the ionized meteoroid trail.

The fifth section proposes a predictive model for the frequency of observations of IMTr belonging to the main SMC sources or meteor showers. This model opens up additional opportunities for extracting information about the meteoroid and geophysical parameters of the atmosphere in the case of the bistatic scattering of a radio signal.

Given the observation time, zenith angle, and trail azimuth, this model can be used to determine the area where the specular reflection of radio signals is observed with a given probability. This allows one to optimize the parameters of the transmitting and receiving antennas and the protocol for transmitting information while ensuring the maximum throughput of meteor radio communication systems.

The calculation of the coordinates and height of the meteor trail SRP with a given radiant and entry point of the meteoroid into the meteor zone was performed by analytical methods. This required solving a third-degree equation. When solving this equation, Vieta's method was used.

The possibility of using the direction-finding-time radio method for measuring the SRP height under bistatic scattering is shown. A simple and geometrically illustrative method is proposed for finding the SRP coordinates with an unknown radiant of the meteoroid that generated the trail.

The sixth section presents the physical theory of the formation and transformation of an ionized meteoroid trail, which is the basis for creating a generalized model of radio signal scattering on the meteor trail during its formation and development.

An adequate physical model of the formation and transformation of the IMTr takes into account many factors that determine the characteristics of the trail over the interval of its observation. When constructing such a model, the main physical processes occurring during the interaction of a meteoroid with atoms and molecules of the atmosphere were taken into account-preheating, evaporation, and fragmentation of the meteoroid, as well as the formation of the ionized trail head in the thermalization interval and the trail expansion under the ambipolar diffusion.

This model is based on the use of a two-dimensional axisymmetric trail electron density, which is determined by the linear electron density of the trail (LEDTr) created by the meteoroid.

The model uses estimates of the ionization coefficient, the initial radius of the meteor trail, and the ambipolar diffusion coefficient. When calculating these parameters, the physicochemical properties of the meteoroid were taken into account, as well as the physicochemical characteristics of the atmosphere, which, in turn, depend on the height of the specular reflection point, the time of year and day, the latitude of the observation site, and solar activity.

In seventh section, a radiophysical model of signal scattering on a meteor trail is proposed, which takes into account the presence of coherent and incoherent components of the scattered signal and all phases of the trail transformation. Since it is practically impossible to solve such a problem in a strict formulation,

we employed a heuristic method which relies on physical optics approximations used to solve it. An analytical expression based on the use of the MRCh time scatter-function is obtained, which makes it possible to calculate the power of the scattered signal, estimate the lifetime of the meteor trail suitable for information transmission, and describe the features of the observed diffraction oscillations of the received signal amplitude. The scatter-function was obtained by numerical methods for the time-varying equivalent radius of the meteor trail.

The radiophysical scattering model provides the possibility of estimating the signal form at the receiver input at characteristic times and calculating the change in the average signal power over the trail observation interval. This made it possible to suggest such a type and parameters of the used radio signal that could be resistant to fading and provide an increase in the reliability of information transmission over the meteor radio channel. Using the example of linear frequency modulated signals (LFMS or chirp signals), it is shown that the use of broadband signals with a large processing gain ("base" of signal) makes it possible to reduce the diffraction oscillations of the ATCH and provides an increase in the throughput of the MRCh.

Numerical calculations performed using the heuristic model showed good agreement with the results of experimental observations of scattered signals over a time interval from 0 to 3 seconds. Outside this interval, the calculated values of the the scattered signal power somewhat exceed the observed values. The decrease in the signal level may be due to the interference caused by the meteoric body fragmentation and the additional influence of turbulent diffusion, which were not taken into account in the scattering model. The effects of recombination and attachment of free trail electrons, the influence of hyperthermal chemistry and ionic reactions with mesospheric ozone, as well as the possible influence of wind displacement were not taken into account. This indicates the need for further improvement of the radiophysical model of signal scattering on meteor trails of various types.

The eighth section discusses classification methods based on the use of artificial neural networks (ANNs) and proposes a new approach to classifying meteoroids based on the use of model images of signals scattered on IMTr.

When using ANN, the main signs significant for classification are determined. The model image of the signal for the given meteoroid parameters and the atmosphere in the SRP was obtained using the radiophysical model of signal scattering and presented in the form of ATCH. It is indicated that when estimating the mass of a meteoroid, the main feature is the product of the amplitude and duration of the reflection; the necessary additional data are the SRP height and the velocity and expected physicochemical characteristics of the meteoroid.

The possibility of predicting the type and characteristics of the meteor trail from measurements at the initial stage of its existence is estimated, which provides a fundamental possibility of choosing the transmission rate and protocol that maximize the throughput of the meteor radio channel. The possibility of us-

ing early fast Doppler as one of the reflection indicators with large amplitude and duration is considered as well.

In the ninth section, special attention is paid to the development of the concept and technology for building advanced meteor radio communication systems. Several methods are proposed aimed at increasing the throughput of the MRCS, reducing the connection waiting time, increasing the number of subscribers served, and increasing the noise immunity and secrecy of the system. Their implementation is focused on the use of software-controlled antennas, algorithms for adapting to changing operating conditions, and the use of SDR technology, which makes it possible to introduce new signal processing methods and information transfer protocols to unify and subsequently upgrade almost all MRCS elements without a significant change in the circuit design.

The method for optimal reception and synchronization of signals used for large ensembles of signals with direct spread spectrum and based on matched filtering using the fast Fourier transform and narrowband interference rejection in the signal spectrum is described.

Various structures and operating principles of meteor radio communication networks depending on their purpose are considered. It is noted that it is possible to increase the efficiency of using meteor radio communication networks by linking base stations (BS) with satellite or other channels with a sufficiently high bandwidth. It is shown that in solving some problems, it may be expedient to use asymmetric MRCh. In this case, information from BS is transmitted using one type of signals, and when transmitting data from subscriber stations (SS) (or remote stations), signals of a different type are used. Since the protocol for the exchange of information between SS and BS depends on the purpose of the MRCS, its detailed description is beyond the scope of this monograph.

References to the sources of information used are given for each section of the monograph in the order in which they were cited. At the end, there is a bibliography of all sources of information in alphabetical order.

The authors hope that this book will be useful to different categories of readers: scientists and designers involved in meteor radio communications; geophysicists studying the ionosphere in the meteor zone; astronomers looking for new relationships between meteoroids and their parent bodies; graduate students, university professors, and students of relevant specialties.

The authors will be glad to cooperate in the area of research under consideration, as well as to receive constructive comments and suggestions on the content of the monograph. Please send comments and suggestions to the email address: holovan.helen@gmail.com.

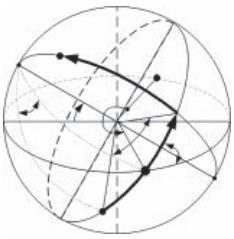

SECTION 1

APPLICATION AREA OF METEOR RADIO CHANNELS

The meteor radio channel is a discontinuous channel with random parameters, such as the time and place of the appearance of the meteor, the number of meteor radio reflections, the duration of existence, and the electron density of the meteor trail.

Despite the discontinuity and relatively small average throughput (up to several kilobits per second), meteor radio communication (MRC) has a number of advantages that distinguish it from other traditional types of communication:

- Significant range of the radio channel (up to 2000 km) and the absence of so-called "dead zones", which allows covering large areas and puts meteor communication on a par with other "above-the-horizon" types of communication.
- The relatively small size of the meteor trail and the radio wave propagation make it possible to receive a signal from a specific meteor in a limited area, which, on the one hand, allows simultaneously serving a large number of correspondents at the same operating frequency, and on the other hand, gives meteor radio communication systems an advantage in electromagnetic compatibility and secrecy of the operation.
- Relatively low energy costs during transmission through the meteor channel are due to the low noise level and low absorption in the ionosphere. This provides a reduction in hardware costs and provides small size and power consumption of communication equipment.
- Resistance to natural and artificial disturbances in the Earth's atmosphere allows one to work in northern latitudes in conditions of ionospheric disturbances. This property is of particular interest in emergent and critical situations, when MRC systems may be the only ones capable of providing communication in a short time.

Meteor radio communication systems can be a low-cost alternative to satellite communication systems and are used:

- in the interests of the Ministry of Defense and diplomatic missions;

- in environmental monitoring systems;
- for automatic monitoring of the state of extended, territorially dispersed technical systems, such as oil and gas pipelines, high-voltage power lines, main cables, etc.;
- to organize service communication between mobile objects;
- for communication in hard-to-reach and remote areas;
- in systems of automatic remote data collection for the benefit of hydrometeorological services;
- in warning systems for emergency events and natural disasters;
- to dispatch control vehicles and collecting information about the location of moving objects (icebergs, buoys, etc.);
- to provide high-precision synchronization of spatially spaced time and frequency standards;
- for geophysical research.

1.1. Overview of foreign meteor radio communication systems for general and military purposes

In the 1950s, MBS received considerable attention. It was considered an alternative to other long–distance communication methods: high-frequency radio, microwave radio, and backbone cable lines. With the development of satellite communications in the early 1960s, interest in MRS diminished. However, growing concern about the vulnerability of satellite communications and its low cost-effectiveness in transmitting information with low traffic made MBS an attractive alternative method for long-distance communication again (Allen, 1989; Weitzen1993; Jernovics, 1990).

1.1.1. JANET meteor radio communication system

One of the first, in 1952, the Canadian Defense Research Council established the MBS JANET system, which provided communication channels of 900 to 1200 km in length at an average data rate of 34 words per minute (Forsyth, 1957).

The US National Bureau of Standards incorporated some of the techniques developed on the JANET system and conducted experiments over 628 and 1277 km paths. These experiments showed an average data rate of up to 30 bits per second with a system error rate of 3.5×10^{-3} per bit (Bartholome, 1968).

1.1.2. COMET operational military meteor radio system

In 1965, NATO's Supreme Headquarters Allied Powers Europe (SHAPE) implemented the meteor communication system COMET (COmmunication by MEteor Trails). This first operational military MBC system oper-

ated between stations in the Netherlands, France, Italy, West Germany, the United Kingdom, and Norway. The COMET system used a 2000 baud signaling rate and **FSK** with a 6 kHz deviation. It could maintain from two to eight 60-word-per-minute teletype circuits and, ensure an average throughput of between 115 and 310 bits per second, depending on the time of year. Hourly average data rates of 150 bps have been achieved. The expediency of using MBC COMET in various conditions of application is shown.

1.1.3. SNOTEL meteor radio communication system

The first civil system SNOTEL was built for the Department of Agriculture by the Western Union. It started operations in 1977 under the management of the Soil Conservation Service (SCS).

SNOTEL collects information on snowpack conditions in the Rocky Mountains. The information is critical to water management planning in the West. The system covers eleven western states with 511 remote MBC stations.

The remote stations are located in harsh, inaccessible terrain. They are unmanned and solar-powered. The remote stations are controlled by two master stations located in Boise, Idaho, and Ogden, Utah. The master stations collect data from the remotes each morning when the meteor activity is the strongest. Each remote sends data collected over the previous 24 hours in a 200-bit message. The collection process averages 20 minutes for the entire system (Hellweg, 1987; Johnson, 1987).

1.1.4. AMBCS and USAF meteor radio systems

Several MBC systems are operating in Alaska; two of them are the Alaska Meteor Burst Communication System (AMBCS) and the USAF Alaska Air Command MBC system.

The AMBCS, operating since 1977, is used by several government agencies. The Bureau of Land Management uses it to communicate with its survey teams operating in the Alaska wilderness. The SCS uses it for the same purposes as the SNOTEL system.

The Federal Aviation Administration (FAA) sends weather information over the AMBCS and employs it during search and rescue operations in remote areas (Hellweg, 1987).

The USAF system is used to provide backup connections among the Regional Operations Control Center (ROCC) located at the Elmendorf Air Base near Anchorage and 13 Long Range Radar (LRR) sites located throughout Alaska. It has demonstrated the ability to deliver enough data to display radar information in real time.

The USAF system includes a limited voice capability, allowing the ROCC to control interceptor aircraft over the MBC system. Routine dialog between a con-

troller at the ROCC and an intercept pilot is limited to a small set of commands. A voice synthesizer added to the aircraft has a coded vocabulary large enough to handle most of these routine commands. When conducting an intercept, the controller types a command code into the MBC terminal, and the pilot hears the command in English. The pilot is limited to acknowledging receipt or non-receipt of the message (Heacock, 1984).

An example of a modern integrated MBC network is the North American Aerospace Defense Command (NORAD) network consisting of three master stations and 18 remote terminals. The network covers two-thirds of the U.S. and is managed by the USAF's 25th Air Division. Headquartered at the United States Air Force Base McCord (Hoff, 1988).

The main purpose of the MBC network is the global control of strategic air transport after a nuclear strike (restoration of control).

Further development of US Air Force meteor communications is aimed at integrating these systems into a unified meteor communication system that will cover all major operational centers.

1.1.5. The concept of constructing a meteor subsystem for the emergency service

The US Federal Emergency Management Agency (FEMA) has developed a concept for the Meteor Burst Warning/Communications Subsystem (MBWCS), which is an addition to the fixed National Warning System (NAWAS). It includes 10 regional master station (MS) meteor terminals, meteor transceivers at Emergency Operations Centers (EOC) of the 48 contiguous countries, and warning receivers at 5,000 designated warning points (including 2,600 NAWAS warning points) throughout the Nation (Cohen, 1989).

Table 1.1. **The main equipment characteristics for the NWC system**

Transmitters	Master stations — 10 State EOCs — 48 (transceivers) Power —1 kW Modulation — Bi-phase shift keyed (BPSK) Directionality — omnidirectional point-to-point connections
Receivers	At master stations sites — 2—4 (about 24 total) State EOCs — 48 (transceivers) At warning points — 5000
Frequency range	40—50 MHz (three frequencies for the system; each MS transmits at one and receives at two frequencies. Each EOC uses one transmit and one receive frequency)
Data Rate	4000 bps

Coded warning messages from the National Warning Center (NWC) or an alternative NWC are acknowledged and broadcast to neighboring MS, state EOCs, and warning receivers. MBWCS also can provide two-way point-to-point communication between adjacent MS, as well as MS and state EOCs within designated areas. The system is non-adaptive. The main characteristics of the equipment for the NWC system in are presented in Table 1.1.

1.2. Meteor radio systems for time scales synchronization

The problem of high-precision synchronization of time scales is one of the actual problems of modern science and technology (Kascheev, 1989; Antipov, 2006; Korneev, 2007; Koval, 2012). At present, systems for transmitting time over long distances have already been created and are constantly being improved, providing measurements with an error not exceeding nanoseconds. There are three main methods for nanosecond synchronization of time scales (Antipov, 2006):

- Passive satellite methods (GPS, GLONASS — accuracy 10—40 ns, GPS Common View — accuracy 1—10 ns).
- Active methods using geostationary satellites (accuracy 1—5 ns).
- Phase meteor synchronization systems (accuracy 0.3—0.9 ns), which are at the stage of further technological development.

The meteor method of transmitting time stamps uses the counter transmission of interrogation and response radio signals in a channel with a high degree of reciprocity of propagation conditions. The measurements are organized in such a way that the request signal is tied to the time scale, and the response signal carries information about the scale shift. The currently available theoretical estimates and experimental results show that the meteor radio channel is very promising for synchronization. This is because the potential accuracy of single measurements of the time discrepancy in the meteor radio channel is fractions of a nanosecond, and these measurements do not require time to accumulate results, as, for example, in the case of GPS/GLONASS. This modern method, which uses measurements of the phase of the carrier oscillations in the GPS, is similar to the meteor time transfer system but so far it is at the stage of technological development and has not been presented in commercial operation.

The main difficulties in using the meteor channel are related to the unequal accuracy and non–uniformity of measurements. Whereas the technology of the measurements themselves is sufficiently developed, the problem of controlling the time scale in the absence of measurements, which is relevant for the meteor radio channel, has not been considered so far. Therefore, work in the field of optimizing the use of uneven and unequal meteor radio measurements for real–time scale control needs further developed.

1.3. Ionospheric research based on radiolocation of meteor trails

The most important problems in the physics of the ionosphere include theoretical and experimental studies of motions in the high layers of the atmosphere, which occupy a large place in international programs of geophysical and space research. Knowledge of the parameters of the velocity field of macroscopic motions of both the neutral and ionized components of the ionospheric plasma is necessary for constructing models of the upper atmosphere, understanding the physical nature of the interaction of various atmospheric layers, and solving several applied problems.

A significant part of the experimental data on motions in the ionosphere was obtained by a meteor trail radar using the method of diversity radio reception in vertical and oblique sounding. The method is based on the study of scattering processes on meteor trails. The speed of movement and lifetime of irregularities at these heights are mainly related to the processes of dissipation and transfer, which makes it possible to estimate the wind speed and temperature gradients, as well as turbulence and ozone concentration in the meteor zone at different latitudes and different times of the year and day (Arnold, 2003; Hocking, 2011; Hocking, 2001; Hocking, 1997; Hocking, 1987; Hajduk, 1999; Jones, 1990; Fukao, 2003; Kawamura, 2007; Kascheev, 2000; Portnyagin, 1978; Fedynsky, 1972; Beldon, 2008; Ye, 2017; Sukara, 2013; Younger, 2014).

1.4. Astrophysical research based on radiolocation of meteor trails

Astrophysics studies the origin (cosmogony), structure, chemical composition, physical properties, and evolution of individual celestial bodies and systems up to the Universe as a whole (cosmology). Unlike physics, which is based on experiments associated with given conditions for the occurrence of a phenomenon, astrophysics is based mainly on observations. At the same time, the researcher cannot influence the course of the physical process but has the opportunity to observe it on many celestial objects under various conditions. Ultimately, this turns out to be no less informative than a physical experiment and often leads to the discovery of new physical laws.

Observation data on small celestial bodies (meteoroids) based on the radiolocation of meteor trails make it possible to obtain information on the genetic relation of meteor showers and sporadic meteoroids to the parent body (comet or asteroid), their chemical composition, mineralogical and bulk density, which is necessary for the development of the theory of origin and evolution of meteoric matter (Babadzhanov, 1991; Obrubov, 1991).

In this case, continuous measurements of the parameters of the orbits of meteoroids entering the Earth's atmosphere are performed. Mapping of a spo-

radic meteor complex (measurement of radiant distribution density) and meteor showers, as well as the measurement of meteoroid orbital parameters and velocity, makes it possible to predict the level and duration of the signal reflected from the meteor trail and optimize the construction of meteor radio communication systems (McKinley, 1961; Voloshchuk, 2011; Kharchenko, 2011; Holovan, 2020a; Holovan, 2020b).

This information can also be used to assess the risks of collisions between small celestial bodies and space vehicles in near and deep space.

1.5. Conclusions

Meteor radio communication systems can be an alternative to satellite and shortwave radio communication systems. They can be used in the interests of the Ministry of Defense of Ukraine, diplomatic missions, and for organizing radio communications in areas of natural disasters, as well as in hard—to—reach and remote areas.

Since MBSs have a relatively low cost, small dimensions, and power consumption, it is advisable to use them in transmission systems where the information delivery time is not critical:

- in environmental monitoring systems;
- in systems for monitoring the state of extended, territorially dispersed technical systems, such as oil and gas pipelines, high-voltage power lines, main cables, etc.;
- in systems of automatic remote data collection for the benefit of hydrometeorological services;
- in service communication between mobile objects in areas with low information infrastructure;
- in dispatching control vehicles and collecting information about the location of moving objects (icebergs, buoys, etc.).

The possibility of using MRCS to provide high-precision synchronization of spatially spaced time and frequency standards is shown.

The use of MRS opens up new opportunities for ionospheric, geophysical, and astrophysical research.

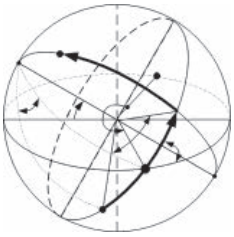

SECTION 2

COORDINATE SYSTEMS USED AND BASIC ASTRONOMIC TERMS

For readers who do not have the appropriate professional training, the section presents some information concerning the field of meteor astronomy, necessary for understanding the essence of the materials presented in the book. Coordinate systems and astronomical quantities characterizing the orbits of celestial bodies are given in (Zharov, 2006; Abalakin, 1979; Blazhko 1954; Kulikov, 1976; Green, 1985).

Celestial coordinate systems are spherical and used in astronomy to describe the position of luminaries in the sky or points on an imaginary sphere. They differ from each other in the choice of the main plane and the origin. Depending on the problem being solved, the corresponding coordinate system or a set of coordinate systems can be used. The most commonly used are horizontal, equatorial, and ecliptic coordinate systems. The expediency of using the apex system of spherical coordinates for studying the distribution density of radiants of celestial bodies is shown. The Galactic coordinate system, which is used in the study of the problem of hyperbolic orbits of small celestial bodies, is briefly described.

2.1. Horizontal coordinate system

The horizontal ("alt-azimuth") coordinate system is used by an observer located in a certain place on the Earth's surface to directly determine the positions of luminaries on the celestial sphere using goniometric instruments mounted on an azimuthal installation or oriented relative to terrestrial objects, the azimuth of which is considered known. During measurements, the observation time should be fixed and corrected to take into account refraction in the atmosphere.

In the horizontal coordinate system, the main plane is the plane of the mathematical horizon. The direction on the object is determined relative to two mutually perpendicular

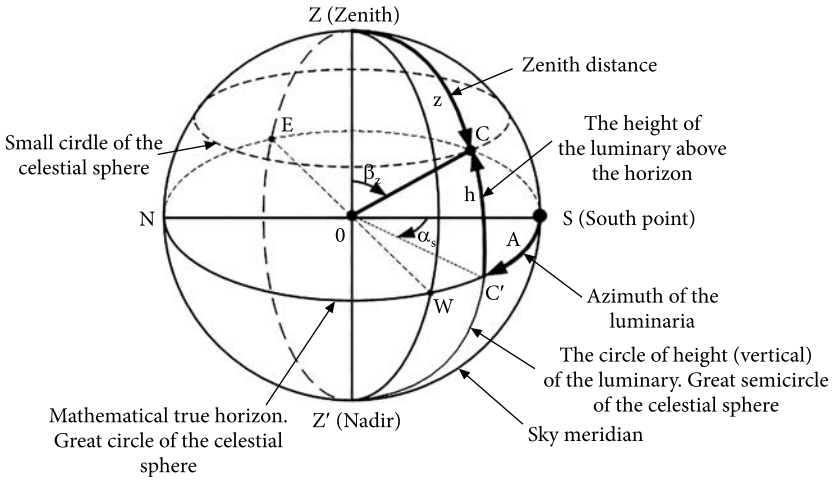

Fig. 2.1. Horizontal coordinate system

planes: the plane of the mathematical horizon and the plane of the celestial meridian, which, when intersecting with the celestial sphere, form large circles.

The object position is given by two coordinates — the zenith distance z (or the height $h = 90° - z$) and azimuth A. The zenith distance is the vertical arc from the zenith to the luminary, which corresponds to angle β_z. The height of the luminary *0* is the arc of the vertical from the horizon to the luminary. The zenith distances vary within $0° < z < 180°$, and the heights for northern hemisphere stars vary within $0° < h < +90°$ and $-90° < h < 0°$ for southern hemisphere stars. Azimuth A (the arc of the mathematical horizon SC') determines the position of the star's vertical relative to the plane of the celestial meridian at the moment of observation (Fig. 2.1). It corresponds to the azimuth angle α_s. The astronomical azimuth is measured from the south point S to the intersection of the star's vertical with the mathematical horizon and increases to the west from 0 to 360°, whereas in geodesy and navigation from the north point to the east. Therefore, before using the azimuth, one need to clarify in which system it is indicated. In the horizontal coordinate system, due to the daily rotation of the celestial sphere, both coordinates of the luminary participating in the daily movement change continuously, that is, they depend on time. Therefore, any measurement of the horizontal coordinates of a luminary must be accompanied by the fixation of the moment at which these coordinates are obtained.

2.2. First equatorial coordinate system

The first equatorial system (declination and hour angle) is used primarily in determining the exact time — one of the main tasks of practical astronomy. In this system (Figure 2.2), the main plane is the plane of the celestial equator QC'Q', which is perpendicular to the axis of the World.

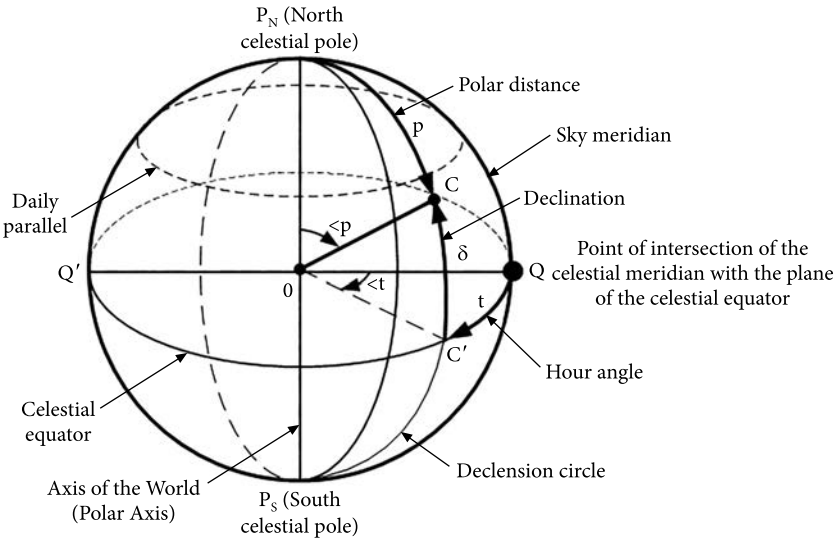

Fig. 2.2. The first equatorial coordinate system

The great circle arc passing through the luminary determines the circle of declination. Declination δ of an astronomical object is the circle arc of declination from the equator to the luminary, which characterizes the angular distance of the luminary from the celestial equator. The declination from the plane of the celestial equator is counted and varies in the direction of the north pole within $0° < \delta < 90°$, and in the direction of the south pole within $-90° < \delta < 0°$. For astronomical objects located near the pole, instead of declination, the polar distance is used – the arc of the circle of declination from the north pole to the luminary. The polar distances vary within $0° < p < 180°$.

The hourly angle *t* is the dihedral angle between the plane of the circle of declination and the plane of the celestial meridian, which passes through the zenith, the north celestial pole, the nadir, and the south celestial pole. It corresponds to the angle QOC' in the plane of the equator, which determines the angle of rotation of the circle of declination relative to the plane of the celestial meridian. The hour angle is measured from the equator point Q to the west (clockwise) from 0 to 360° in degrees or from 0 to 24 h in hours (360° corresponds to 24 h, 1 h — 15°, 1 min —15', 1 s — 15"). In the first equatorial coordinate system, the declinations of the luminaries remain constant if their proper motions are not taken into account, while their hour angles continuously change.

2.3. Second equatorial coordinate system

The second equatorial system is the main one in solving problems of fundamental astrometry. In this system, lists of star positions (star catalogs), star charts, etc. are compiled.

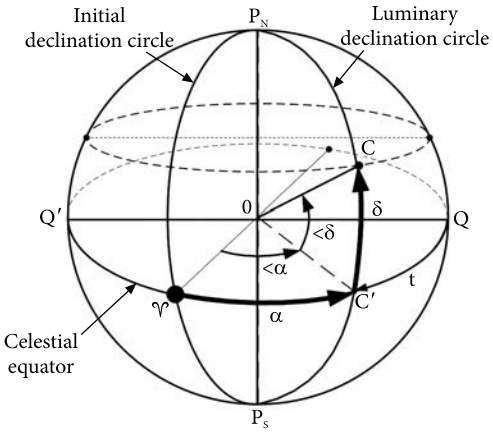

Fig. 2.3. The second equatorial coordinate system: angle QOC' — hour angle of star C; angle QOϒ — hour angle of the vernal equinox point; angle ϒOC' — right ascension of the luminary; α — the arc of the equator from the point of the vernal equinox to the point of intersection of the equator with the circle of the star declination

This system (Fig. 2.3) was introduced to determine the coordinates of the Sun in such a way that, over long time intervals, they do not depend on the daily rotation of the Earth. The declination of a luminary δ satisfies this condition, but the hour angle *t* does not correspond to it. To introduce a second constant coordinate, it is necessary to associate the position of the circle of declination with such a plane that, together with all the luminaries, participates in the visible daily movement. Then, the angle between the circle of the star declination 0 and this plane will be constant.

On the celestial sphere, the circle passing through the vernal equinox ϒ, which lies in the plane of the celestial equator on the line of its intersection with the orbit plane, was taken as the initial circle of declinations. The center of the solar disk passes this point on the day of the vernal equinox.

Right ascension α is counted in the direction opposite to the daily rotation of the celestial sphere (counterclockwise) from 0 to 360° or from 0 to 24 hours . It retains its value, since star hour angles and vernal equinox points change at the same rate due to the daily rotation of the Earth. From the definition of right ascension, the equality of sidereal time and the hour angle of the vernal equinox follows.

Sidereal time S cannot be determined directly from observations, but at any particular moment, it can be represented as the sum of the hour angle and the star's right ascension.

At the moment when the vernal equinox passes the celestial meridian over the south point, its hour angle is equal to zero, hence S = 0h0m. This moment is taken as the moment of the beginning of the sidereal day on the given meridian. In addition, when an arbitrary luminary passes the celestial meridian over the south point, its hour angle is also equal to zero, therefore $S = \alpha_c$ is the sidereal time at the moment of the upper climax of the celestial C on this meridian. Recall that the climax in astronomy is the moment of passage of the star through the celestial meridian in the process of its daily movement. During the day, all the luminaries cross the celestial meridian twice. There are upper and lower climaxes of the

luminary. In the upper climax, the height of the luminary is the greatest, and in the lower — the smallest.

When determining the point of the vernal equinox, one can take into account the precession of the earth's axis and nutation (small oscillations of the earth's axis superimposed on the precessional movement) in different ways, or not take it into account at all. Depending on this, true, quasi-true, and mean sidereal times are distinguished. In the first case, the true point of the vernal equinox Υ_{true}, which has precessional and nutational motion, is considered. It shifts in the plane of the ecliptic at a velocity of 50. 25" per year due to the general precession in longitude and simultaneously fluctuates periodically due to nutation. In the second case, quasi-true sidereal time, its short-period part, is excluded from nutation, and, finally, the exclusion of all nutation gives the point spring equinox Υ_{mean}, which determines the mean sidereal time.

Thus, there are distinguished :

• Local true sidereal time (Local Apparent Sidereal Time, LAST) — the hour angle of the true point of the vernal equinox Ytrue at the given site (for the local meridian).

• Greenwich true sidereal time (Greenwich Apparent Sidereal Time, GAST) — the hour angle of the true point of the vernal equinox Ytrue on the Greenwich meridian.

• Local mean sidereal time (LMST) — the hour angle of the midpoint of the vernal equinox Ymean.

• Greenwich Mean Sidereal Time (GMST) — the hour angle of the average position of the vernal equinox Ymean on the Greenwich meridian.

2.4. Ecliptic coordinate system

When studying the motion of the bodies of the solar system, it is more convenient to use not the equatorial but rather the ecliptic coordinate system. The basis for constructing the latter is the equations of celestial mechanics that describe the movement of the Earth and other objects of the solar system in orbits around the Sun. The middle plane of the Earth's orbit is called the ecliptic plane. According to the International Earth Rotation and Reference Systems Service standards, this is the plane that is perpendicular to the orbital angular momentum vector.

For an observer, the actual movement of the Earth in orbit leads to the apparent movement of the Sun. Thus, the apparent annual movement of the Sun is a reflection of the movement of the Earth around the Sun during the year. The great circle formed by the intersection of the celestial sphere with a plane passing through its center parallel to the plane of the Earth's orbit is commonly called the ecliptic.

In astrometry, several ecliptic coordinate systems are used:

• The ecliptic heliocentric coordinate system, which is used primarily in theoretical astronomy when determining the orbits of celestial bodies — planets, comets, asteroids, meteoroids, etc.

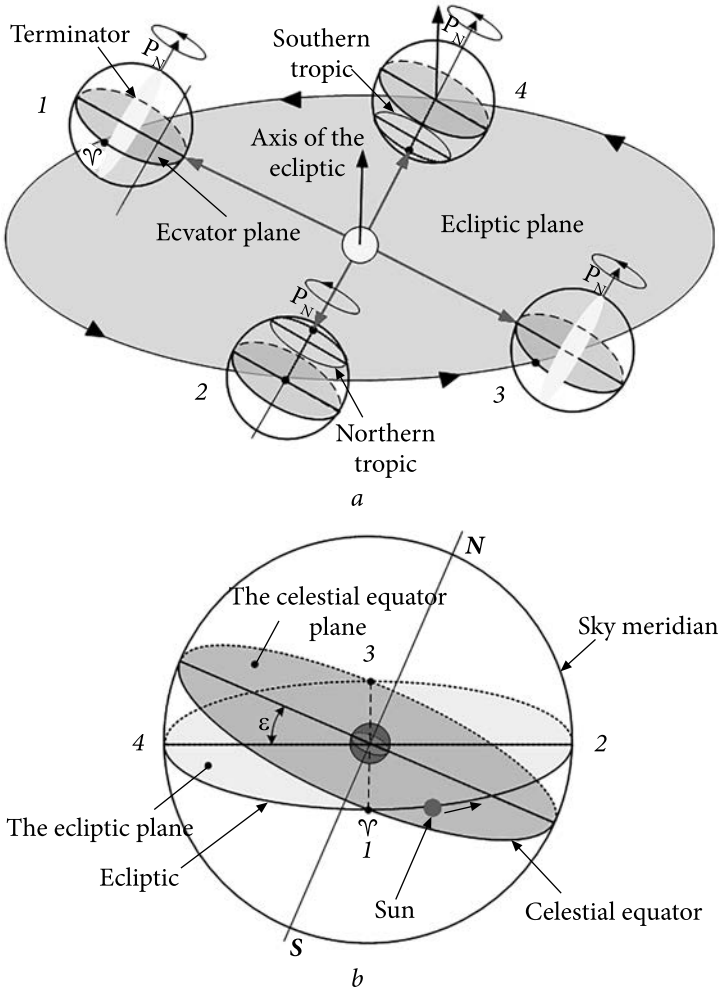

Fig. 2.4. Ecliptic heliocentric (*a*) and ecliptic geocentric (*b*) coordinate systems: *1* — point of the vernal equinox; *3* — point of the autumn equinox; *2* — point of the summer solstice (maximum day length for the northern latitude); *4* — point of the winter solstice (minimum day length for the northern latitude)

• The ecliptic geocentric coordinate system, which is used to display the position of celestial bodies and radiants of sporadic meteoroids and meteor showers in catalogs and on star maps. It is also used to determine the starting point of time reference in the second equatorial and geocentric coordinate systems.

Fig. 2.4 shows the ecliptic heliocentric and ecliptic geocentric coordinate systems. The axis of the Earth's rotation is oriented at an angle of 90°-ε, where ε is the angle of inclination of the ecliptic plane to the plane of the celestial equator. Considering the Earth's orbital movement (Fig. 2.4*a*), one can see that at certain times

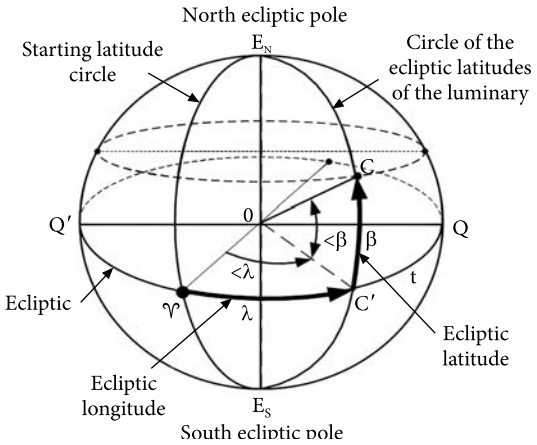

Fig. 2.5. Ecliptic geocentric coordinate system

(positions *1* and *3* in Fig. 2.4*a*), the axis of rotation of the Earth is perpendicular to the Sun rays, the terminator (light-dividing line) passes at such moments through the geographic poles, and there is observed an equinox — the day is equal to the night at all latitudes.

For an observer located on the Earth's surface, the movement of the Sun occurs along the ecliptic (Fig. 2.4*b*). As a starting point of time reference in the second equatorial and geocentric coordinate systems, the moment is chosen when during the equinox period, the Sun passes from the southern hemisphere of the celestial sphere to the northern one. This point of intersection ♈ is called the vernal equinox. The opposite point of the celestial sphere is called the autumnal equinox.

At the beginning of our era, the vernal equinox was in the constellation Aries, from which it received its designation (♈), and the autumn equinox was in the constellation Libra (♎). Since then, point ♈ has moved to the constellation Pisces, and point ♎has moved to the constellation Virgo, but their designations have remained the same.

Without taking into account disturbing factors affecting the position of the plane of the Earth's orbit and short-period oscillations (nutation) of the Earth's rotation axis, we can assume that the ecliptic plane is inclined to the plane of the celestial equator at an angle

$$\varepsilon = 23°26'21.448'' - 46.8150''\,t - 0.00059''\,t^2 + 0.001813''\,t^3, \qquad (2.1)$$

where t is the number of Julian centuries since January 1, 2000. This formula is valid for the coming centuries. In meteor measurements, one can quite often restrict oneself to the value $\varepsilon = 23°26'21.448''$ (for trigonometric calculations, $\varepsilon = 23.439281°$).

The ecliptic geocentric system of celestial coordinates is based on the vernal equinox and the ecliptic — the line of intersection of the plane of the Earth's orbit with the celestial sphere. The main axis in this coordinate system is normal to the plane of the Earth's orbit (straight line $E_N\,E_S$ in Fig. 2.5).

The perpendicular to the ecliptic plane intersects the celestial sphere at two points – the poles of the ecliptic. The north ecliptic pole E_N in the present era has equatorial coordinates α = 18h 0m 0.0s (exact value), δ = +66°33'38.55" and is located in the constellation Draco. The south ecliptic pole E_S is in the constellation Dorado and has equatorial coordinates α = 6h 0m 0.0s (exact value), δ = = –66°33'38.55".

The ecliptic coordinates are similar to the corresponding equatorial coordinates of the second type. The determining factors are the ecliptic (astronomical) latitude β and ecliptic longitude λ. A large circle drawn through the luminary C and the ecliptic poles E_N and E_S is called the circle of ecliptic latitudes. Ecliptic latitudes are measured from 0 to +90° to the north pole (EN) and from 0 to –90° to the south ecliptic pole (E_S).

Ecliptic latitude determines the position of the luminary on the circle of latitude. The position of the circle of latitude itself is determined by another coordinate – the ecliptic longitude λ, which is measured from the vernal equinox Υ in the direction of the apparent annual movement of the Sun along the ecliptic, i.e. from west to east, and can take values from 0 to 360°. With the daily rotation of the celestial sphere, ecliptic latitudes and longitudes do not change.

2.5. Galactic coordinate system

The problem of studying the complex of highly eccentric orbits of meteoroids of the Solar System, observed instrumentally, is connected with the Solar System. Nevertheless, the solar system is not closed, and there is a fundamental possibility of astronomical objects from other parts of our galaxy falling into their limits. The hyperbolic heliocentric velocity of meteoroids is related to their geocentric velocity; therefore, the possibility of registering the hyperbolic orbits of meteoroids is limited by large errors in measuring their observed velocity. There is not a single sufficiently accurately measured orbit not only of meteoroids but also of larger small bodies (asteroids and comets), reliably classified as uniquely hyperbolic, but search in this direction continues. In this regard, we present some data on the Galactic coordinate system used in stellar dynamics.

In the Galactic coordinate system, the main plane is the plane of symmetry of our Galaxy (the Milky Way), which is classified as a spiral galaxy, and the main axis is normal to it, crossing the celestial sphere at points called galactic poles.

The Sun is located on the periphery of the Galaxy (at a distance of about 28,000 light-years from its center) and is one of the stars that make up its disk. It moves at a speed of approximately 230 km/s in the direction of the constellation Cygnus. This movement is explained by the rotation of the galactic disk. The Sun makes a complete revolution around the center of the Galaxy in a period of $\sim 2.5 \cdot 10^8$ years . In this case, the movement relative to the nearest stars (the main movement of the Sun) occurs at a speed of ~15.5 km/s.

A simplified scheme for constructing the Galactic coordinate system is shown in Fig. 2.6 [https://en.wikipedia.org/wiki/Galactic_coordinate_system]

The position of the main plane of the Galactic coordinate system — the Galactic equator, is set relative to the second equatorial system. As a result of processing data from the HIPPARCOS project, the following coordinates of the north galactic pole (located on the same side of the galactic plane as the celestial North

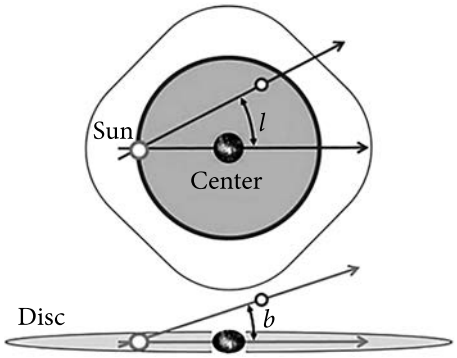

Fig. 2.6. Simplified scheme for constructing the Galactic coordinate system

Pole) in the second equatorial system for the J2000.0 epoch were accepted: α = 192°.85948; δ = 27°.12825.

Galactic coordinates are similar to equatorial and ecliptic ones. In this case, one coordinate is the galactic latitude b, and the other is the galactic longitude l (see Fig. 2.7).

The galactic latitude *b* of a luminary is the circle arc of galactic latitude from the ecliptic to the luminary, or the angle between the plane of the galactic equator and the direction to the luminary. Galactic latitudes are measured from 0 to +90° to the north galactic pole and from 0 to −90° to the south galactic pole. The galactic longitude *l* of the luminary is the galactic equator arc from the reference point *C* to the circle of the luminary's galactic latitude, or the angle between the direction to the reference point *C* and the plane of the circle of the galactic latitude of the luminary. Galactic longitude counted clockwise when viewed from the north galactic pole, that is, east of the reference point C, ranging from 0 to 360°.

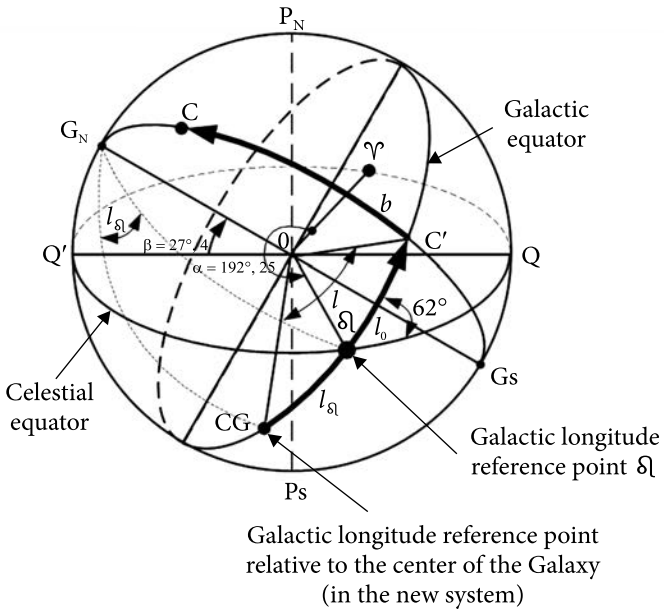

Fig. 2.7. Galactic coordinate system combined with the equatorial coordinate system of the second type

Previously, galactic longitudes l_0 were counted from the ascending node ☊, that is, the intersection point of the galactic and celestial equators, the right ascension of which was ~18h40m.

Since 1971, a new system of galactic coordinates has been adopted. In it, longitude is measured not from the ascending node but from the CG point (Fig. 2.7). This point is $l_{☊} = 32°.93192$ (at epoch J2000.0) to the west of the ascending node and is close to the direction to the galactic center but does not coincide with it, since the latter, due to the slight displacement of the solar system above the plane of the galactic disk, lies approximately 1° south of the galactic equator. Therefore, the galactic longitude l in the new system and the longitude $l_{☊}$ in the old frame of reference are related by a simple relationship

$$l = l_0 + l_{☊} = l_0 + 32°,93192 . \qquad (2.2)$$

If, in this case, it turns out that $l > 360$, 360° should be subtracted from the obtained value of l.

Formulas for the transition from the second equatorial coordinate system to the galactic one and vice versa are derived using known methods (Zharov, 2006).

2.6. Ecliptic geocentric coordinate system centered on the Sun

When the Earth moves along the ecliptic, according to the results of radar and optical measurements, the geocentric ecliptic latitude and longitude (λ and β) of radiants and other parameters of meteoroids are calculated. After obtaining raw results, it is possible to correct them by taking into account the zenithal attraction, diurnal aberration, and the acceleration of gravity at the latitude of the observation site.

Obviously, the measurement results depend not only on the local time of observation but also on the date (date, month, and year) of observation, i.e., on the position of the Earth in the ecliptic heliocentric coordinate system.

The ecliptic geocentric coordinate system makes it possible to fix the distribution density of radiants and other parameters of meteoroids over a given time interval (during a year, several years, or within a month). These results may vary. More informative are the results obtained for a given month. They make it possible to estimate not only the distribution of the radiant density in the geocentric coordinate system but also to make reasonable assumptions about the origin of the observed meteoroids and their relationship with meteor showers. The most informative would be data on the distribution of radiant density for a given day of the year, but this statistics collecting is problematic.

The Earth rotation around the Sun leads to the fact that the maximum value of the zenith angle of radiants of sporadic sources changes during the year. The Earth rotation around its own axis also leads to the fact that the zenith

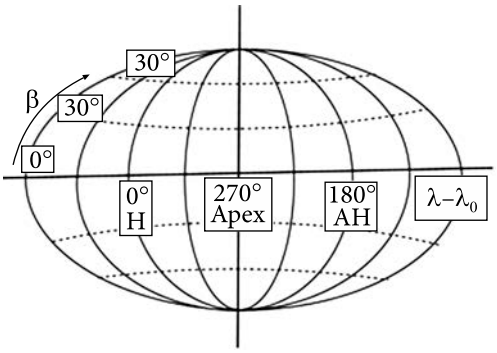

Fig. 2.8. Apex plane of the ecliptic geocentric coordinate system centered relative to the Sun

angle and azimuth of these sporadic sources change during the year and day. In this regard, the quantity of meteoroids that form a specular reflection point varies depending on sources within radio visibility and their location relative to the radio link (geometric factor). Therefore, the motion of the Earth around the Sun and around its own axis will cause both a seasonal change in the total daily meteor count rates and **a** diurnal variation in the meteor count rates.

To unify the representation of the distribution of radiants, an ecliptic geocentric coordinate system centered relative to the Sun is used (Fig. 2.8). In this case, the solar longitude (λ_0) for a given epoch measured relative to the vernal equinox is subtracted from the longitude of the ecliptic, and the apex coordinates become equal to 270° (Campbell-Brown, 2008). The latter is not mandatory, and some researchers associate zero longitude with the apex (Younger, 2009; Kascheev, 1982).

To change from a Sun-centered to an ecliptic geocentric coordinate system, one should add the calculated value of λ_0 and, if the result is more than 360°, subtract 360°.

2.7. Converting data from one coordinate system to another

The coordinate's transformation from one coordinate system to another for celestial bodies or apparent sources (radiants) of sporadic meteoroids is performed to solve the following problems:

1. Star maps based on the results of astronomical observations and measurements. In this case, data transformations are performed sequentially: from the horizontal coordinate system to the equatorial one and then from the equatorial to the ecliptic geocentric coordinate system.

2. To determine the coordinates of a luminary or radiant, the position of which is given in the ecliptic geocentric coordinate system. The coordinates must be determined for a specific date and time and for an observation point with given geographic coordinates. This is necessary for pointing telescopes at the luminaries or optimizing the pointing of antenna patterns to areas of the celestial sphere, where the appearance of meteor trails with a specular reflection point is most likely. In this case, data transformations are performed sequentially: from the ecliptic geocentric coordinate system to the equatorial one, and then from the equatorial to the horizontal coordinate system.

2.7.1. Converting data from horizontal to equatorial coordinates and vice versa

The horizontal coordinate system is used in the collection of data on the radiants of sporadic sources and meteor showers in radar and optical measurements to determine and display the body position on the celestial sphere. Here, it is necessary to fix the geographical coordinates of the observation point (the difference between geographical, geocentric, and topocentric coordinates is insignificant when measuring radiants), as well as the date and time of observations.

The measurement result looks like this:

- geographic coordinates of the observation site (latitude φ and longitude λ);
- date of observation (year, month, day);
- local mean solar observation time T_m (hours, minutes, seconds), which is related to the coordinated universal time T_0 (UTS) by the simple relation $T_m = T_0 + \lambda_h$, where λ_h is the longitude of the observation site, in hours;
- zenith distance z (or height h = 90° – z) of the luminary (radiant) above the horizon;
- azimuth A of the radiant.

To present the results of measurements (mapping) of radiants and other parameters of meteoroids obtained over long observation intervals at observation sites with different geographical coordinates, the second equatorial coordinate system is used. In this system, the influence of the Earth's daily rotation is excluded by introducing a reference point that participates in the visible daily movement along with all the luminaries. As such a point, the vernal equinox Υ_{mean} is used, which determines the local mean sidereal time (LMST), which provides sufficient accuracy for radiant measurements (without taking into account the influence of precession and nutation) (see subsection 2.1.3). In this case, the difference between true and mean sidereal time will not exceed 0.9 s. If necessary, for the transition to the Greenwich true sidereal time (S_{true}), it is necessary to take into account the correction for nutation (N_a) in right ascension at epoch t and perform calculation by the formula $S_{true} = S_p + N_a$. Sidereal time at midnight on the Greenwich meridian is denoted by S_0. The Astronomical Yearbook contains S_0 values for each day of the year.

The transition from the horizontal coordinate system to the second equatorial one and the inverse transformation are illustrated in Figure 2.9. This was performed using the known relations (Zharov, 2006; Abalakin, 1979; Blazhko 1954; Kulikov, 1976; Green, 1985):

$$\sin\delta = \sin h \sin\varphi - \cos h \cos A \cos\varphi, \tag{2.3a}$$

$$\cos h \cos A = \cos\delta \cos t \sin\varphi - \sin\delta \cos\varphi, \tag{2.3b}$$

$$\cos\delta \sin t = \cos h \sin A, \tag{2.3c}$$

$$\sin h = \sin\delta \sin\varphi + \cos\delta \cos t \cos\varphi, \tag{2.3d}$$

$$\cos h \cos A = \cos\delta \cos t \sin\varphi - \sin\delta \cos\varphi, \tag{2.3f}$$

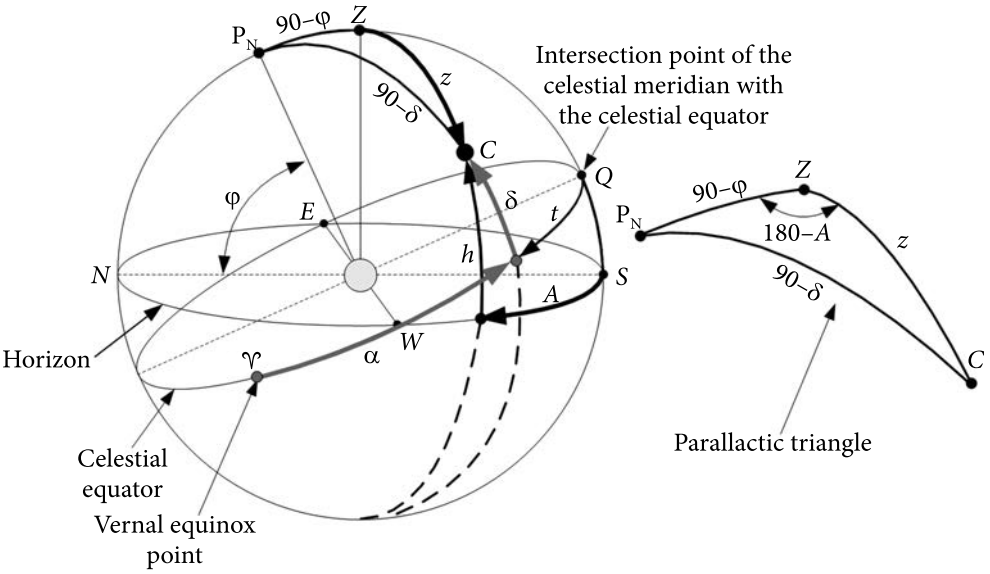

Fig. 2.9. Transition from the horizontal coordinate system to the second equatorial and inverse transformation

where φ is the latitude of the point of observation, and the hourly angle of the star t is related to the local sidereal time s (time on the meridian of the point of observation) by the relation

$$t = s - \alpha.$$

If instead of the luminary (radiant) height h above the horizon, the zenith distance z is used, then based on the relationship $h = 90^\circ - z$, instead of (2.3a – 2.3f), we obtain

$$\sin\delta = \cos z \sin\varphi - \sin z \cos\varphi \cos A, \quad (2.4a)$$

$$\cos\delta \cos t = \cos z \cos\varphi + \sin z \cos A \sin\varphi, \quad (2.4b)$$

$$\cos\delta \sin t = \sin z \sin A, \quad (2.4c)$$

$$\cos z = \sin\delta \sin\varphi + \cos\delta \cos t \cos\varphi, \quad (2.4d)$$

$$\sin z \cos A = \cos\delta \cos t \sin\varphi - \sin\delta \cos\varphi. \quad (2.4f)$$

Formula (2.4a) allows us to calculate δ, (2.4b) and (2.4f) allow us to determine t and $\alpha = s - t$.

To determine the right ascension α at the found t, it is necessary to calculate sidereal time s on the meridian of the observation site from the date and time of observation. It is convenient to represent it using Greenwich true (S_{true}) or mean ($S_{mean} = S_0$) sidereal time measured relative to the Greenwich meridian and given in the Astronomical Yearbooks for each day of the year.

Greenwich mean sidereal time S_0 (midnight time on the Greenwich meridian) for any date can be found using the formulas:

in hours (minutes, seconds)

$$S_0 = 6^h41^m50^s,54841 + 236^s,555367908 \times d + 86400^s \times M + \\ + 0^s,093104 \times \tau^2 - 6^s,2 \times 10^{-6} \times \tau^3; \quad (2.5а)$$

in degrees

$$S_0 = 100°,460618374 + 0°,9856473662 \times d + 360^o \times M + \\ + 3°,879333 \times 10^{-4} \times \tau^2 - 2°,583 \times 10^{-8} \times \tau^3; \quad (2.5б)$$

in radians

$$S_0 = 1,7533685592 + 0,0172027918051 \times d + 6,2831853072 \times M + \\ + 6,7707139 \times 10^{-6} \times \tau^2 - 4,50876 \times 10^{-10} \times \tau^3, \quad (2.5в)$$

where h is the hour, m is the minute, s is the second, and d is the time interval from epoch T_0 to epoch t (number of days elapsed from epoch 2000, Jan. 1, to GMT midnight of the date in question) in mean solar days calculated from the formula

$$d = JD - 2451543.5 = MJD - 51543.0; \quad (2.6)$$

JD (Julian Date) — the number of days that have passed since noon GMT on January 1, 4713 BCE; *MJD* (Modified Julian Date); M — universal time UT1 of the date under consideration, expressed in fractions of a day; τ — time interval from epoch T_0 to epoch t in Julian centuries of 36525 mean solar days calculated by the formula $\tau = d/36525$.

You can calculate the JDN Julian date integer value directly from the calendar date as follows (Schlyter, 2013):

$$JDN = 367 \cdot Y - \left\lfloor \frac{7\left(Y + \left\lfloor \frac{M+9}{12} \right\rfloor\right)}{4} \right\rfloor + \left\lfloor \frac{275M}{9} \right\rfloor + (D-1) - 730530, \quad (2.7)$$

where Y is the year (4 digits), M is the month (1, 2, ... 12), D is the day (1, 2, ... 31), and the parentheses indicate an integer operation (i.e., division remainders are discarded).

$$JD = JDN + \frac{UT}{24,0} = JDN + \frac{h}{24} + \frac{m}{1440} + \frac{s}{86400}, \quad (2.8)$$

where UT — universal time expressed in hours, h — hours, m — minutes, s — seconds.

The above formulas (2.7) and (2.8) provide acceptable accuracy from March 1900 to February 2100.

Sidereal time s used in astronomical observations is related to universal time UT by the relationship:

$$s = S_0 + \mathrm{UT} + \lambda + c, \tag{2.9}$$

where S_0 is the sidereal time at Greenwich midnight; λ is the longitude of the observation point expressed in units of time (λ > 0 for east longitude and λ < 0 for west longitude); c = 9.86UT (UT expressed in fractions of an hour) is the correction in seconds (usually not exceeding 240 seconds).

When calculating sidereal time and hour angle, it should be taken into account that time in any system must take values from 0 to 24^h. Otherwise, it is necessary to subtract $n \cdot 24^h$ from the result obtained, where n is chosen such that it provides the specified condition.

To calculate horizontal coordinates based on given equatorial coordinates, the following working formulas can be used

$$\begin{gathered} t = s - a, \\ \cos z = \sin\delta * \sin\varphi + \cos\delta * \cos t * \cos\varphi, \\ \cos A = \frac{\cos\delta * \cos t * \sin\varphi - \sin\delta * \cos\varphi}{\sqrt{1 - \cos^2 z}}. \end{gathered} \tag{2.10}$$

In this case, the initial data for the calculation are:

1. date — XXXX year, XX month, XX day;
2. standard time M_d — XX hours, XX minutes, XX seconds of a point with longitude λ;
3. time zone P;
4. λ — longitude of the observation place;
5. φ — latitude of the observation place;
6. α — right ascension;
7. δ — declination.

It should be noted that when calculating time and hour angle, their values in any system are in the range from 0 to 24^h. To calculate trigonometric functions, the hour angle must be converted to degrees, according to the formula $t^0 = 15t^h$. All calculations are performed with an accuracy of 10^{-8}.

The procedure for calculating the zenith angle z and azimuth A is as follows:

1. Based on the date, calculate JD and mean sidereal time (S_0) in hourly measure at midnight on the Greenwich meridian. The S_0 value can be taken from the Astronomical Almanac for a given date.
2. Calculate the universal time on the mean Greenwich meridian UT1 ≈ Md – P.
3. Based on S_0, UT1, and λ, calculate the mean sidereal time at the observation site $s = S_0 + \mathrm{UT1} + \lambda$.
4. Determine the hour angle t = s – α.

5. Perform the calculation by the formulas:

$$\cos z = \sin\delta * \sin\varphi + \cos\delta * \cos t * \cos\varphi,$$

$$\cos A = \frac{\cos\delta * \cos t * \sin\varphi - \sin\delta * \cos\varphi}{\sqrt{1-\cos^2 z}}.$$

6. Find the taget values of z and A

$$z = \text{Arccos}(\cos z);\ A = \text{Arccos}(\cos A).$$

7. Since the azimuth A of the radiant (luminary) can be in the range from 00 to 3600, determine the quadrant in which its true value is located. Calculation control can be performed based on the sine theorem, using the expression cos δ sin t = sin z sin A. In this case, the equality sin z / sin t = cos δ / sin A must match up to 7 significant digits.

To quickly convert equatorial coordinates into horizontal ones, instead of calculating by the above formulas, one can use WEB-calculators in the online mode (for example,"Universal coordinates transformer" [http://astro. prao. ru/utilities/utilcoor. html])

2.7.2. Converting data from equatorial to ecliptic geocentric coordinate system and vice versa

Observation data obtained at a given point over time in the horizontal coordinate system are used in the second equatorial system to compile star catalogs, star maps, and the distribution of radiant densities of meteor showers and a sporadic meteor complex (SMC). The ecliptic geocentric coordinate system is used to represent the results of measurements of the coordinates of true or apparent sources of radiation obtained over long observation intervals. These sources can be celestial bodies and radiants of meteor showers or a sporadic meteor complex.

Recalculation of the ecliptic geocentric coordinates λ and β into equatorial coordinates α and δ, followed by transformation into horizontal coordinates (see Section 2.7.1), makes it possible to point antennas at a given radiation source.

Fig. 2.10 presents the ecliptic geocentric coordinate system combined with the second equatorial coordinate system. The formulas for transition

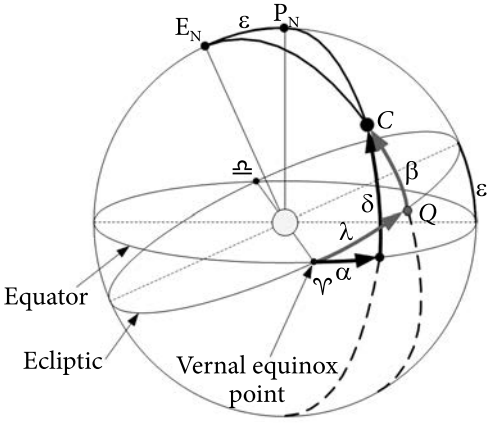

Fig. 2.10. Ecliptic geocentric coordinate system, combined with the second equatorial coordinate system (Zharov, 2006)

from the latter to the former are derived from the spherical triangle formed by the World Pole (P_N), Ecliptic Pole (E_N), and Luminary (C) (Zharov, 2006).

To calculate the ecliptic latitude β and longitude λ from angle ε, right ascension α, and declination δ, the following formulas are used:

$$\sin(\beta) = \sin(\delta) * \cos(\varepsilon) - \cos(\delta) * \sin(\varepsilon) * \sin(\alpha), \quad (2.11a)$$

$$\cos(\lambda) = \cos(\alpha) * \cos(\delta) / \cos(\beta), \quad (2.11b)$$

$$\cos(\beta) * \sin(\lambda) = \sin(\varepsilon) * \sin(\delta) + \cos(\varepsilon) * \cos(\delta) * \sin(\alpha). \quad (2.11c)$$

The calculation order is as follows:

1. Determine sin(β) by formula (2.11a).
2. Calculate angle β using the inverse trigonometric function Arcsin (β),
3. Calculate $\cos(\beta) = \sqrt{1 - \sin^2 \beta}$.
4. Find cos (λ) by formula (2.11b).
5. Calculate angle λ using the inverse trigonometric function Arccos (λ).
6. Based on (2.11b) and (2.11c), determine the quadrant in which angle λ is located and, if necessary, correct its value.

To move from the ecliptic coordinate system to the second equatorial coordinate system, formulas similar to (2.11) and the corresponding calculation order are used:

$$\begin{gathered} \sin(\delta) = \sin(\varepsilon)\sin(\lambda)\cos(\beta) + \cos(\varepsilon)\sin(\beta), \\ \cos(\delta)\cos(\alpha) = \cos(\lambda)\cos(\beta), \\ \cos(\delta)\sin(\alpha) = \cos(\varepsilon)\sin(\lambda)\cos(\beta) - \sin(\varepsilon)\sin(\beta). \end{gathered} \quad (2.12)$$

To quickly convert ecliptic coordinates to equatorial (or vice versa), instead of calculating by the above formulas, WEB-calculators can be used in the "on-line" mode (for example, "Universal coordinates transformer" [http://astro.prao.ru/utilities/utilcoor .html])

If the Sun-centered ecliptic geocentric coordinate system is used, then before performing the conversion to the equatorial coordinate system, it is necessary to add the Sun longitude to the centered longitude. The Sun longitude is calculated using the known formula

$$\lambda_S = \mathrm{L} + 1{,}915^\circ * \sin q + 0{,}020^\circ * \sin 2q, \quad (2.13)$$

where the mean longitude of the Sun at epoch J2000, corrected for light aberration, is

$$\mathrm{L} = 280{,}460^\circ + 0{,}9856474^\circ * d, \quad (2.14)$$

solar mean anomaly

$$q = 357{,}528^{\circ} + 0{,}9856003^{\circ} * d, \tag{2.15}$$

d is the number of days that have passed from the J2000 epoch to the Greenwich midnight of the date under consideration, calculated by formulas (2.6)—(2.8).

If the calculated value of λ_S exceeds 360°, it is necessary to subtract m · 360° from the result obtained, where m is the integer part of λ_S / 360°.

2.8. Conclusions

The systems of astronomical coordinates and the given calculation ratios make it possible to carry out the necessary transformations of the coordinates of meteoroid radiants.

The transition from the horizontal coordinate system to the second equatorial coordinate system with the subsequent transition to the ecliptic geocentric coordinate system provides the possibility of collecting data and mapping the density of the SMC radiant distribution together with the results of studying the frequency of occurrence of meteor trails at certain heights and at certain velocities.

The reverse transformation allows for calculation of the radiant coordinates needed to go from the ecliptic geocentric system to the horizontal system at a given date and time. This makes it possible to point antennas at the true or apparent source of radiation, which may be the radiant of a meteor shower or the region of a sporadic meteor complex.

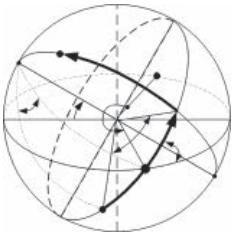

SECTION 3

RADAR SYSTEMS FOR RESEARCH OF SPORADIC METEOROID COMPLEX AND STREAM METEOROIDS

Radar measurements of radiants and orbital parameters of observed sporadic and shower meteoroids, as well as their velocities and masses, make it possible to predict the frequency of occurrence of meteor trails with a specular reflection point and electron density sufficient to transmit information during the year and day for a given geographical area. In this case, various methods of measuring and processing the results of direct observations ("raw" data) are used.

The interpretation of the observation results makes it possible to predict the origin and, on this basis, the physicochemical properties of meteoroids. This provides additional data required for constructing a meteor trail radiophysical model that could be used both for classifying meteor trails and for optimizing the main parameters of the meteor radio communication network and its adaptation algorithms.

Since various radar systems are used to measure the main parameters of meteoroids, in order to interpret the results of observations, it is necessary to take into account the features of the systems through which these results were obtained. In this regard, below are some of the technical characteristics and geographical position of the radars, the observational data of which were used in the study of atmospheric physics, radiant mapping of a sporadic meteor complex and meteor showers, as well as in estimating the parameters of the orbits and velocity of meteoroids.

The review of radar systems provides an opportunity to gain knowledge related to the research of the sporadic meteor complex, providing a basis for analyzing the observation results, as well as creating one's methods and tools for obtaining radar data and algorithms for their processing.

The objects of radar observations are reflections from ionized meteoroids trails (IMTs) and head echoes of meteoroids. To obtain the necessary information, methods of specu-

lar reflection and incoherent scattering on plasma inhomogeneities (inhomogeneities of the permittivity) are used along with interference, correlation, Doppler, and combined methods for data processing.

Typically, radar complexes are multifunctional and focused mainly on the study of the mesosphere, stratosphere, and troposphere of the Earth but they also provide the opportunity for astronomical research. In some cases, the main tasks set in developing and producing radars are their portability and relatively low cost. An example is the Australian interferometric all-sky meteor radar SKiYMET (SKiYMET-All-Sky Interferometric Meteor Radar) jointly developed by Mardoc Inc. and Genesis Software Pty. Ltd., which is designed to measure the parameters of meteoroids entering the Earth's atmosphere and study the atmosphere.

In connection with the above, the following types of radar structures can be distinguished:

- multifunctional multi-position incoherent scatter High Power Large Aperture (HPLA) radars designed to study both local and global characteristics of the Earth's ionosphere, as well as to observe astronomical objects (including mapping of sporadic meteor complexes, study of meteor showers, and measurement of orbit parameters and meteoroid velocities);
- mesospheric-stratospheric-tropospheric (MST) and stratospheric-tropospheric (ST) radars designed mainly to study the processes that determine the global dynamics of the Earth's atmosphere (atmospheric and ionospheric studies of wind and temperature fields, turbulence, ambipolar diffusion, generation and propagation of acoustic gravity waves, etc.), but, like High Power (HP) radars, it makes it possible to determine the meteoroid parameters;
- All-Sky small-sized meteor radars developed by SKiYMET technology that do not require constant maintenance and provide continuous measurement of the parameters of meteoroids entering the Earth's atmosphere, as well as studies of the Earth's atmosphere.

The incoherent scattering method is the most informative radiophysical method for studying the ionosphere. It allows one to simultaneously determine a large number of parameters of the ionospheric plasma in a wide range of heights such as electron density, electron and ion temperatures, ion composition, plasma drift velocity, etc. HP radars are actively used in studies of coherent echoes (radio aurora) - signals scattered by inhomogeneities of the E layer stretched along the the magnetic field lines. The technical characteristics of HP radars make it possible to measure the parameters of astronomical objects with high accuracy and estimate the influx of meteor matter to the Earth.

Despite the large amount and value of data obtained by HP radars, the widespread use of the HP method is limited due to the high cost of installing and operating radars. There are only 9—10 observatories in the world equipped with HP radars, and each of them is individual in terms of its technical parameters and design features related to the direction of research. The geographic location of HP radars is also of great importance. To study the global latitudinal depen-

dences of the ionospheric parameters, the American HP latitudinal radar chain was built including Jicamarca (Peru), Arecibo (Puerto Rico), Millston Hill (USA), and Sanderström (Greenland). To study the polar ionosphere, HP radars were also placed in Scandinavia (Sweden, Norway, Finland) and on about. Spitsbergen (Svalbard). Of great importance are simultaneous, coordinated measurements using all HP radars under the international program Incoherent Scatter Coordinated Observation Day and other joint programs.

Note that the technical characteristics of the IS radar make it possible to implement almost all methods for processing reflected signals used in MST radars such as interference, correlation, Doppler, and combined techniques (Medvedev, 2014).

A feature of the technical implementation of the IS radar is that due to the rotation of the wave polarization plane in the ionospheric plasma associated with the Faraday effect, to prevent the radar signal fading, orthogonal receiving antennas are used, or they emit and receive radio waves with circular polarization. Significant attenuation of signals during incoherent scattering determines the use of high-power transmitters (P ~ 1 MW) and a large–aperture antenna complex (S ~ 3,1000 m^2...100,000 m^2) in IS radars.

When mapping a sporadic meteor complex (measuring the radiant distribution density), as well as measuring the parameters of orbits and the velocity of meteoroids, the HP radars use appropriate operating modes and measurement methods.

MST radars, in terms of construction principles and methods for processing reflected signals, are similar to HP radars and differ from them (and among themselves) in technical capabilities, methods for measuring the studied parameters, and features of antenna systems (Hocking, 1997).

Modern developments of complex multifunctional radar complexes for geophysical and astronomical research are based on the use of technologies and software that were used for HP and MST radars. Examples are the HP-MST radar PANSY in Antarctica (Sato, 2014), the multifunctional radar EISCAT-3D (Kero, 2019; McCrea, 2015), and the advanced HP-MST radar, which is being developed by the Radiotechnical Institute named after Academician A.L. Mintz (RTI) in Russia (Potekhin, 2016).

3.1. SKIYMET Interferometric Radars

The class of interferometric radars operating on the "all-sky" technology includes SKiYMET radars, which are a joint development product of Mardoc Inc. and Genesis Software Pty. Ltd. Australia.

The goals of building the SKiYMET radar were multiple. The idea was to develop a compact multi-purpose system that could receive radar data at the highest possible speed in real time and simultaneously perform many different analyses to interpret the results of observations. An important requirement was also the

ability to work continuously and without constant monitoring, which could make it possible to register and process more than 20,000 meteor trails per day. Many of the scientific aspects, including radar design and antenna placement, the development of universal interferometric and Doppler methods of radar measurements, and methods for analyzing the results obtained, were developed by Mardoc Inc., while Genesis Ltd was involved in the development of electronic control systems for data collection, storage, and transmission. An essential feature of the development is the use of new algorithms for the selection and analysis of meteor trails, which allow for real-time selection of lightning discharges, impulse radio interference, auroral echoes, etc., which previously took hours or days in the case of large data sets.

The system was designed in such a way that new methods for analyzing the signals reflected from the meteor trail could be used with minimal effort. The use of a multitasking UNIX operating system installed on a personal computer made it possible to implement rather complex algorithms for processing multichannel radar information in real time and to repeatedly transfer data to memory. The storage of the results of "online" analysis and raw data associated with any events is provided along with the possibility of transfer them to the user via the Internet for further detailed analysis.

The radar system is easily configured to communicate through any available TCP/IP network point or modem, thus allowing remote control of the radar, and a facility to automatically transfer acquired data to remote hosts.

The SKiYMET hardware consists of two main components: an antenna system with feeders and a radar system including a transmit path and 5 receive paths (according to the number of antennas) (Webster, 1998).

The antenna system typically consists of a three-element transmit Yagi antenna and five two-element Yagis for the receive paths, which are lightweight, compact, and can be assembled quickly and easily at the radar site. The antenna field usually requires an area of less than 2000 m^2.

The diagram of the antenna system is shown in Fig. 3.1*a*, where five receiving antennas are arranged in the form of an asymmetric cross with arms of 2 or 2.5 wavelengths long.

The location of the transmitter antenna is not critical, although it should not be too close to any of the receivers. Fig. 1*b* shows the appearance of the transmitting antenna of the SKiYMET radar as an example.

For phase alignment, each receiving antenna is connected to a separate receiver with cables of the same length (typically ~70 m). The location of the transmitter antenna is not critical and may be in any convenient place. Receiving antennas must be installed strictly in a horizontal plane.

Two compact cabinets contain the remaining elements of the SKiYMET radar system — the RF components and the control and data processing system. They include:

1. A transmitter having (typically) six 1 kW solid-state modules.

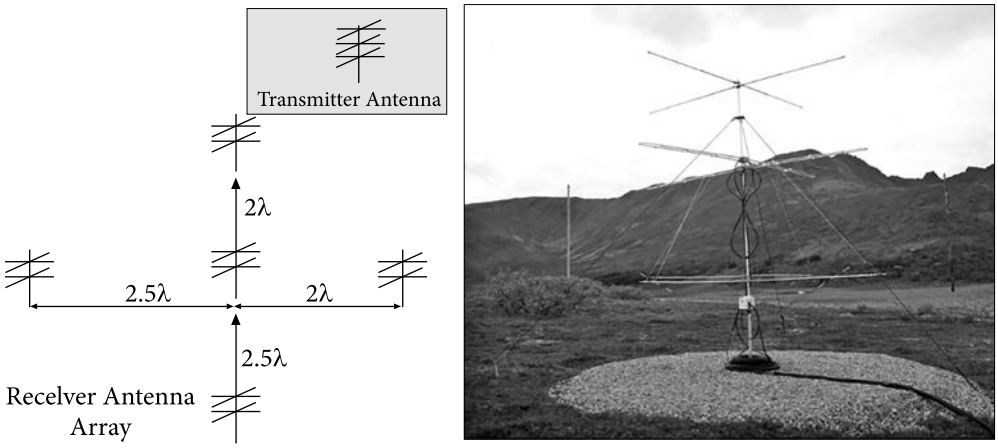

Fig. 3.1. SKiYMET radar antenna array (*a*); transmitting three-element cross-polarized Yagi antenna (*b*) (Foto Ding Tao, Andenes, Norway, June 21, 2009)

2. Radar Data Acquisition System (RDAS) containing five identical receivers, each connected to a separate antenna, which in turn is connected to the received signal digitization system.

3. "Frequency Synthesizer Unit" (FSU), which provides different reference frequencies for the transmitter and receivers and the ability to tune the radar operating frequency the range of 20—50 MHz.

4. A control and self-diagnostics system based on a personal computer, interacted with the FreeBSD UNIX operating system, which provides storage of "raw" data and processed observation results on a hard disk (for 1 second before the appearance of a meteoroid and 3 seconds after that).

5. Real-time clock with GPS-synchronization, providing the system time required for the time reference of meteor events with millisecond accuracy to the selected time scale.

A simplified block diagram of the SKiYMET radar and its software is shown in Fig. 3.2.The main technical characteristics of SKiYMET radars are given in Table 3.1 (Webster, 1998; Hocking, 1998; Hocking, 2000; Hocking, 2001; Brown, 1995; Brown, 1998).

The main parameters displayed when using SKiYMET radars are:

1. Echo detection date relative to Coordinated Universal Time (UTC).
2. Detection time in UTC (millisecond precision).
3. Distance range of the detected echo (in km).
4. Height of the detected echo above the Earth's surface, including correction for the curvature of the Earth's surface.
5. Observed radial drift velocity of the meteor trail.
6. Error related to the radial velocity of the meteoroid (observations with an error exceeding the set value are rejected).

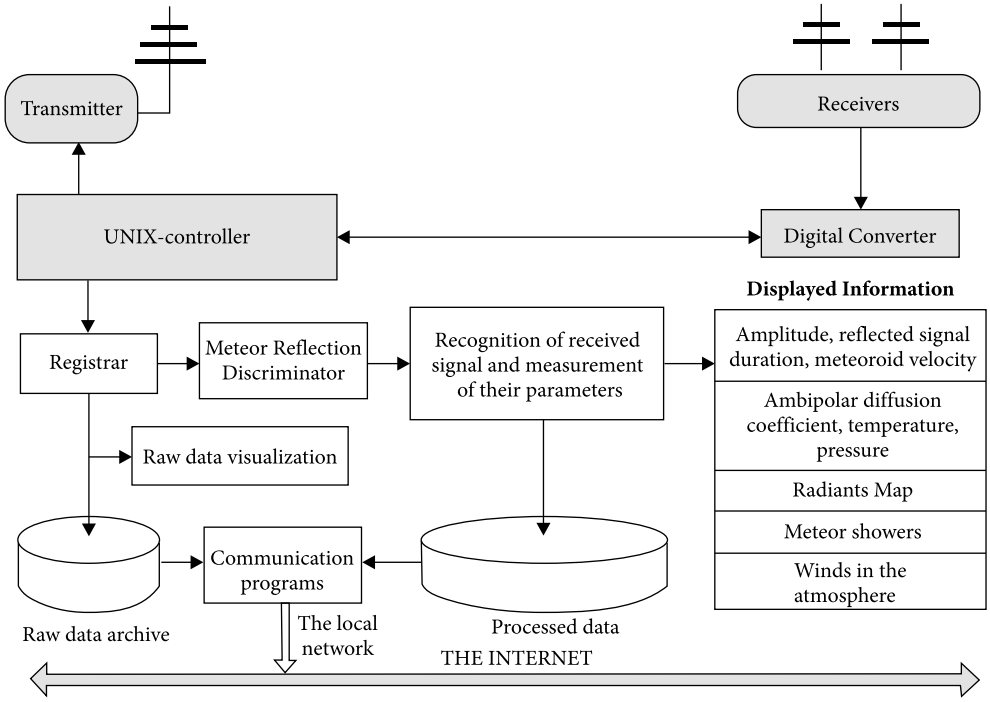

Fig. 3.2. Simplified block diagram of the SKiYMET radar and its software

7. Zenith angle of the meteoroid (specular reflection points) (in degrees).

8. Azimuth angle of the meteoroid (in degrees).

9. The number of possible locations (ranges) that an observed echo can have (in the presence of measurement ambiguity).

10. Decay time (half-life) of the meteor trail (in seconds).

11. Velocity of meteoroid entry into the Earth's atmosphere (available in less than 5% of the observed number of trails).

The method used was discussed in detail in the article (Hocking, 2000).

Attention should be paid to some features of the SKiYMET radar:

1. Data analysis occurs simultaneously with data collection and system management, and the graphical data is automatically updated in real time as results are obtained. The display mode can be changed using the graphical interface so that various statistics could be displayed along with current trends in the data.

2. The radar system can be configured to communicate via any available network point or a TCP/IP modem, allowing remote control of the radar and automatic transmission of received and stored data to remote hosts.

3. It is impossible to determine the radiant of any single meteoroid using a SKiYMET radar, however, it is possible to determine the distribution of radiants when many meteoroids have a common origin.

4. The SKiYMET radar is unique as such that fully uses the backscatter Fresnel diffraction pattern to determine the meteoroid entry velocity, but only ~5% of the observed underdense meteor trails can be used for that. Velocity detection is fully automated but it is problematic to estimate the velocity of meteoroids that create overdense trails. At the same time, to determine meteor shower orbits, it is necessary to compare information on entry velocities and radiants, which complicates the establishment of a relationship between meteoroids and parent bodies. The method used is discussed in detail in (Hocking, 2000).

Table 3.1. **Main technical characteristics of SKiYMET radars**

Parameter	Value
Radar location coordinates	Esrange (67.88°N, 21.10°E) Ascension Island (7.9°S, 14.4°E) Rothera (66.6°S, 68.1°E) Buckland Park (34.6°S, 138.5°E) ALOMAR (69.3°N, 16.0°E)
Operating frequency, MHz	20—60 (31—32,55 MHz for meteor measurements)
Transmitter peak power (depends on the number of modules used), kW	6 and more (Buckland Park — 7,5 kW)
Transmitting antenna type	Three-element Yagi antenna
Selectable receiver gain, dB	Up to 122
Waveform of the emitted uncoded pulse	Rectangular; trapezoidal; Gaussian
Encoded pulse type	Barker code or 4-bit complementary code
Pulse repetition frequency (PRF), selected depending on the measured parameter, Hz	60 — 20000 (for measuring velocity — 2144 Hz)
Pulse length* (selectable), km	0.1—9 (typical ~2 km)
Type of receiving antenna system	5-C hannel interferometer with 2-element cross–polarized Yagi antennas
Bandwidth of the receiving path (selectable), kHz	18—400 (typical 25, 50, 125, and 250)
Duty Cycle of emitted signal, %	Determined by the product of pulse width and repetition rate (typical 15%)
Maximum Duty Cycle for Uncoded Pulse, %	5
Maximum Duty Cycle for Encoded Pulse, %	8.3
Number of coherent accumulations (selectable)	2—16 (typical 2—4)
Range of measured reflection heights from the ionized meteor trail, km	78—120
Angular resolution, degrees	2

* The length of the pulse is determined by the product of the pulse duration and the speed of light.

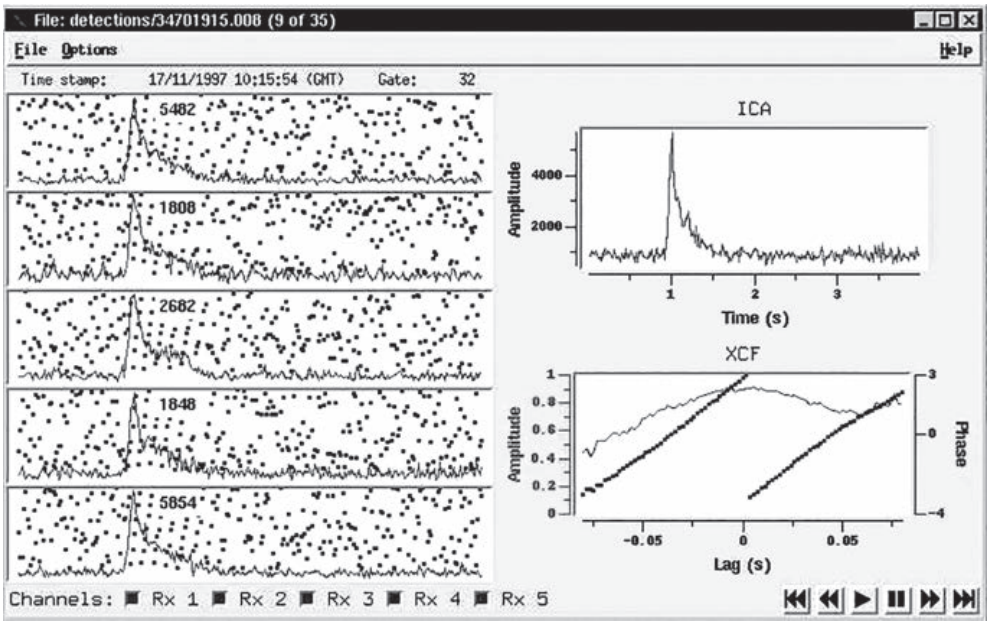

Fig. 3.3. Graphical user interface of the SKiYMET radar

5. To convert the intensity of meteor echoes into parameters such as particle mass, it is necessary to use the received signal amplitude and known transmitted power, antenna gains, received path gain, range estimation, and attenuation in the atmosphere (taking into account the zenith angle and azimuth). Examples of such transformations can be found in a number of publications (Brown, 1995; Brown, 1998; Hocking, 1998) and references given there. The SKiYMET software does not directly perform such transformations but provides all the information necessary for that.

As an example, Figure 3.3 shows the graphical user interface of the SKiYMET radar (SKiYMET, Pty Ltd).

This user interface shows a "screenshot" of the REV (Raw Event) display program, which automatically detects new meteor event data and updates the contents accordingly. The five diagrams on the left show the magnitude and phase recorded by the five receiving channels 1 second before the meteoroid echo and 3 seconds after that (red magnitude and blue phase). The chart on the top right shows the average value for the left channels. The phase information contained in the 5 cross-correlation functions provides the data needed to determine the azimuth and zenith angle of the meteor echo.

The all-sky technology is widely used as an addition to standard MST radars. Examples are Davis Radar, Jicamarca Radar (Peru), National MCT Radar (India), MU Radar (Japan), Resolute Bay Modular Mobile Radar, and others.

3.2. Mesospheric-stratospheric-tropospheric radars

Mesospheric-stratospheric-tropospheric (MST) radars are designed for atmospheric studies of wind and temperature fields, turbulence, the processes of generation and propagation of acoustic gravity waves, and, as a result, the global dynamics of the Earth's atmosphere as a whole. The altitude range of the radar operation covers altitudes from 0.3 to 25…28 km and from 50 to 140 km. Some measurements are carried out with the combined use of MST and SKiYMET radars (Barabash 2004). A number of incoherent scatter (HP) radars occasionally operate in the MST mode.

Lot of works (Hocking, 2011) is directed to the development of methods and means of measurement, as well as to the analysis of data obtained with the help of MST radars.

MST radars are complex and expensive systems with high energy potential (power ~1 MW, antenna gain >30 dB), high sensitivity, modern control and data processing systems (Chilson, 1999).

The main elements of the radar are transmitting and receiving phased antenna arrays, which are complex systems of dipoles covering an area of several thousand square meters.

Table 3.2. **Main technical characteristics of MST radars**

Parameter	Value
Operating frequency, MHz	40—60
Operating frequency tuning step, kHz	50
Maximum pulse power, kW	250—1000
Output power adjustment depth, dB	20
Average power, kW	6—10
Probing pulse duration, μs	1—50
Duration adjustment step, μs	0.5
Random pulse repetition interval, μs	20—700
Types of transmitted signals	Periodic sequence of single radio pulses, a periodic sequence of bursts of radio pulses modulated by the Barker or Golay code
Envelope form of radio pulses	Rectangular, gaussian
Antenna system aperture, m^2	3600
Antenna pattern width at half power, degrees	1—6
Number of beam positions for antenna pattern	1—5
Range of measured reflection heights, km	0.5—140
Height resolution, m	150—450
Range of measured wind speeds, m/s	–50…+50
Range of measured wind directions, degrees	0…360
Time to obtain a wind speed profile, min	5

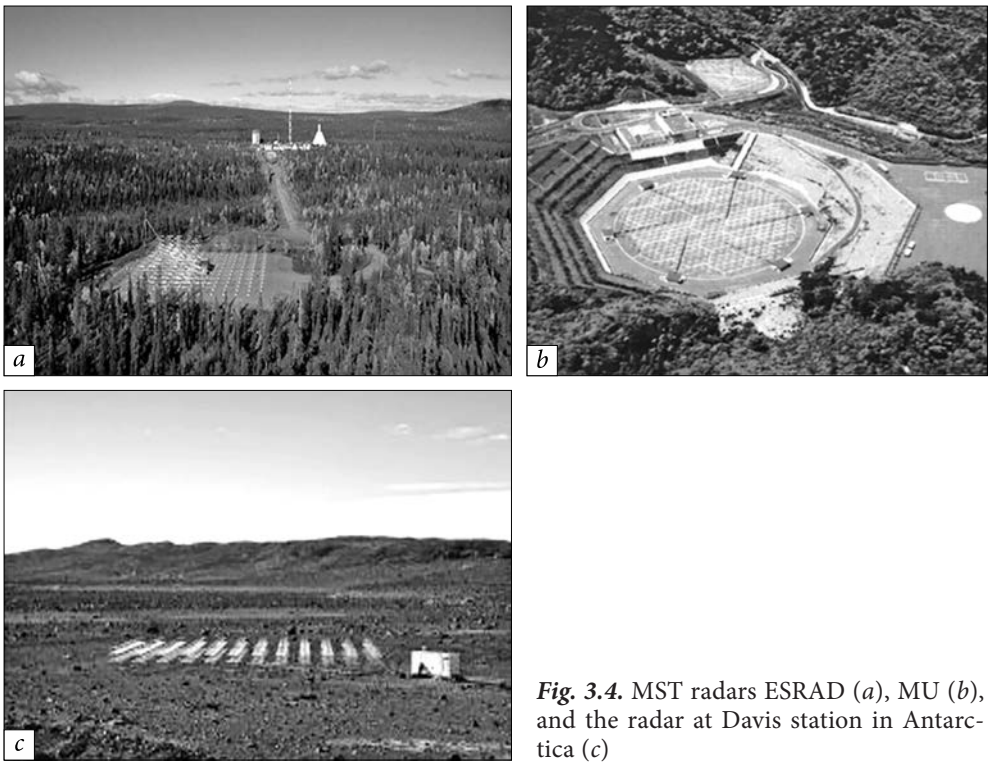

Fig. 3.4. MST radars ESRAD (*a*), MU (*b*), and the radar at Davis station in Antarctica (*c*)

The radar transmitter is a distributed power amplification complex, consisting of a large number of low-power amplifiers that emit signals through their antenna system elements. In each of the power amplifiers, power and phase adjustments are made to phase the total radiated signal. The transmitter includes a frequency synthesizer that provides the choice of the optimal signal frequency in a wide range. The modulator provides the possibility of generating single radio pulses and coded signal sequences (in this case, the choice of the pulse form is possible). The main technical characteristics of MST radars are given in Table 3.2.

At first, simple (non-coded) probing pulses were used to provide the required range resolution. However, their duration did not allow for obtaining sufficiently accurate estimates of the spectral characteristics of incoherently scattered signals. Long pulses give a good spectral representation, but they do not allow for obtaining high spatial resolution and are currently used only for measurements in the F region of the ionosphere. Correlation measurements, in which coded signals were used, turned out to be more effective. This type of measurement became the main one, and to improve it, various schemes of modulation and signal processing were developed to provide high resolution over the entire height range and measurement efficiency. Modern techniques

based on complex radiation and signal processing schemes make it possible to obtain a sufficiently high resolution and accuracy, as well as to optimize measurement modes when solving various problems.

As an example, here are some characteristics of the MST radars ESRAD (Sweden), MU (Japan), and the MST radar at Davis Station in Antarctica (Australia). Their photographs are shown in Fig. 3.4. For meteor measurements, these radars are complemented with interferometric all-sky radars similar to SKiYMET radars.

3.2.1. MST Radar ESRAD

The ESRAD MST radar is a radar complex located in the north of Sweden at Esrang (67.88°N, 21.10°E), near Kiruna (Chilson, 1999). Its operation began in July 1996 and went through several stages of modernization. The purpose of the radar was to provide information about the dynamic state of the atmosphere - winds, waves, turbulence, and stratification of the ionosphere, from the troposphere to the mesopause.

The transmitter and receiver hardware was designed and manufactured under contract with Atmospheric Radar Systems Pty Ltd (ATRAD) in Adelaide, Australia. In 2004 and again in December 2015, the ESRAD radar was upgraded under contract with Genesis Software Pty, Australia.

In the initial version, the antenna array contained 12 × 12 elements. Each element consisted of 5 Yagi antennas, each about 6 meters high and 3 meters across. The antennas are spaced about 4 m apart (corresponding to 0.7 of the radar wavelength). At 4 central unfilled positions in the array, there is an observation post containing transmitters, receivers, and a control computer. Each group of 4 nearest adjacent antennas is separately connected to the control system. This made it possible to use a large number of different antenna configurations, and perform phasing to control the beam in the zenith direction. In 2004, the array was expanded to 16 × 18 five-element Yagi antennas and the phase control option was removed. The width of the main lobe of the radiation pattern at half the antenna power was about 5°. In 2015, at a distance of about 30 m from the southeast corner of the main array, a small array was built with the ability to receive reflected signals. This made it possible to carry out measurements at the lowest altitudes, starting from about 0.5 km and using only a part of the main array. The main technical characteristics of the ESRAD MCT radar are given in Table 3.3.

The transmitter consists of 72 solid-state modules with a power of 1 kW each, connected to 12 power supplies with a power of 6 kW. The radar emits sounding pulses vertically using the entire main antenna array. For reception, the array is divided into 12 segments (6 segments until December 2015), each connected to a separate receiver. In addition, three remote receivers have been installed (since December 2015). The receivers provide separate processing of in-phase and

Table 3.3. **Main technical characteristics of the ESRAD MCT radar**

Parameter	Value
Radar location coordinates	67.9°N, 21°E
operating frequency, MHz	40—60
Operating frequency tuning step, kHz	50
Antenna	
quantity of antennas	140
distance between antennas, λ	0.7 λ
antenna area, m^2	~2000 (45 × 45 m)
beam rotation angle, degrees	7, 14, 20°, ? (in directions N, S, E, W)
product of average power and aperture, $W \cdot m^2$	7×10^6
Transmitter	
peak power, kW	72
duty Cycle, %	5
pulse repetition frequency (PRF), Hz	100—16000
pulse length (selectable), μs	1—50
envelope form of radio pulses	Rectangular, gaussian
types of transmitted signals	Uncoded and coded
coding	Complementary Galley code (2, 4, 8, 10, 16, 32, and 64 bits); Barker code (7, 11, and 13 bits)
product of average power and antenna aperture, $W \cdot m^2$	7×10^6
Receiving path	
configuration	6 separate receivers
sample interval, ms	1—20
main selection filter band, kHz	250, 500, 1000, 2000
Digital processing	
range of measured heights, km	0. 5—140
height resolution, m	150—450

quadrature signal components. This allows for control of the beam after object detection and complete spectral analysis of the reflected signal.

The main software for radar control and data collection in various modes, as the original software for analyzing the received data, works in real-time. The radar operates continuously, switching modes optimized for measurements in the troposphere, stratosphere, or mesosphere. A typical measurement cycle is 1—2 minutes in each mode, repeating every 2—3 minutes.

3.2.2. Middle and upper atmosphere radar

The middle and upper atmosphere radar (Middle and Upper atmosphere) of Kyoto University (Fig. 3.4*b*), located in Shigaraki (Japan), is used in both MST and incoherent scatter modes to study the dynamics of the mesosphere and lower thermosphere, as well as the dynamics of the lower atmosphere and ionosphere. For this, a circular antenna array is used to emit a probing signal that ensures the formation of a radiation pattern of 3.6 degrees at half power.

In meteor mode, to increase the number of observed reflections from meteor trails, the transmit antenna pattern is converted in such a way as to provide maximum radiation at zenith angles of 30—40° with a circular pattern in the azimuth

Table 3.4. **Main technical characteristics of MU radar**

Parameter	Value
MU radar coordinates	34, 85°N and 136.10°E
Central operating frequency, MHz	46.5
Bandwidth of operating frequencies, MHz	1.65
Possible number of frequencies	5
Transmitter peak power, kW	1000
Average transmitter power, kW	50
Duty cycle, %	5
Power distribution	5 separate transmit/receive modules located along the perimeter of the antenna
Antenna array configuration	Circular antenna array with a diameter of 103 m (Aperture 8332.3 m^2)
Elements of the antenna array	475 cross-polarized Yagi antennas
Antenna array gain, dB	34
Beam width of antenna array, degrees	3.6
Beam width of single antenna group, degrees	16
Duration of emitted pulse, μs	0.4—65
Interpulse period, ms	3.12
Pulse coding	Uncoded; 13-bit Barker code; 32-bit code sequence
Receiver bandwidth, MHz	Up to 3.5 (167 kHz in Barker code mode)
Range resolution, m	150
Maximum number of ranges by distance	128
Altitude resolution, km	1
Range of measured heights, km	73—127
Meteoroid radiant localization accuracy, degrees	1
Meteoroid radial velocity measurement accuracy, m/s	10—20

plane. With this, at altitudes from 75 to 100 km, horizontal wind speed and the altitude dependence of the meteor trail ambipolar diffusion coefficient are measured with a height resolution of 1 km.

Due to its high versatility of the MU radar, the use of multi-channel analog and digital signal processing, and channel synchronization by GPS, it is successfully used to determine the trajectories and velocities of meteoroids. In surveillance mode, the MU radar can process about 10,000 meteor trail returns per day.

The main technical characteristics of the MU radar for meteor measurements are presented in Table 3.4.

The antenna configuration used for meteor observations is presented in (Nakamura, 1991). Three antennas form an equilateral triangle with a base of 0.697λ, and the fourth antenna is approximately 2λ apart. Then, to improve the accuracy of measurements, the base distances of the antennas were increased (Nakamura, 1997).

Meteor observations have been regularly made since 2009. They are performed using an upgraded 25-channel digital receiver system and a new head echo observation mode that allows optimizing the determination of the interferometric position of the target and the control of the receiver beam (Kero, 2012).

The location of the meteor target is determined for each received radar pulse and is used to convert the accurately measured radial velocity component into meteoroid velocity. This transformation gives accurate localization of the radiant and meteoroid velocity, but depends on a correct estimate of the trajectory from the lateral motion of the target. The latter is never as accurate as the radial (direct) velocity component. Usually, meteoroid radiants can be measured with an accuracy of 1°, but errors in radiant measurements lead to greater uncertainty in estimating meteoroid velocities. This is due to an error in calculating the angle between the meteoroid trajectory and the radar beam.

3.2.3. Davis MST radar

The Davis MST radar was installed in 2003 at Davis Station (68.6°S, 78.0°E), Antarctica. Although its main purpose was to observe the summer echoes of the polar mesosphere, additional transmitting and receiving antennas were installed to perform large-scale interferometric meteor observations using the all-sky technology. To avoid communication with the main array antennas, they were located outside the main array. The transmitting antenna is located at a distance of about 40 m from the main array, and the nearest receiving antenna is located at a distance of about 20 m from the main array. Meteor receiving antennas are located along two perpendicular branches at intervals of 2 and 2.5λ, which provides an unambiguous estimate of the meteoroid arrival angle while minimizing the mutual coupling between the antennas (Webster, 1998).

To weaken the influence of the Faraday effect, circular polarization is used in the transmission of a probing signal. The principle of radar measurements

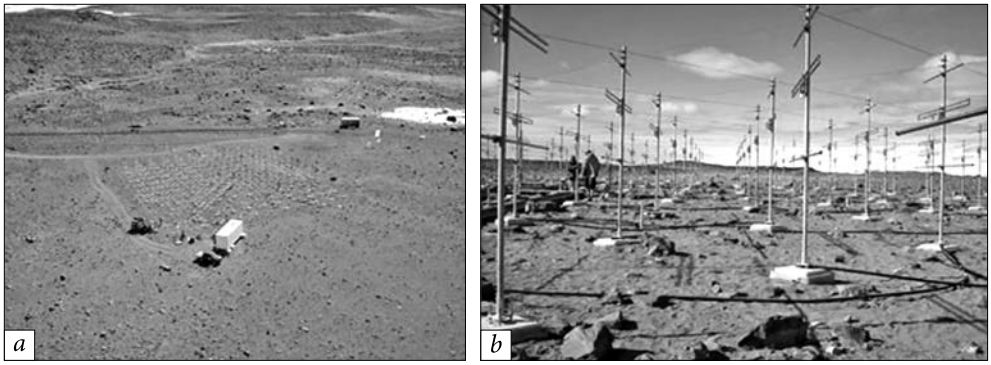

Fig. 3.5. The main antenna array of the MST Davis radar

Table 3.5. **Main technical characteristics of the MST Davis radar for meteor observations**

Parameter	Value
Davis radar MST coordinates	68. 6°S, 78. 0°I
Central operating frequency, MHz	55 and 33. 2 (after modernization)
Transmitter peak power, kW	To 20
Average transmitter power at 5% duty cycle, kW	6
Main transmitting antenna array	Array of 12×12 three-element Yagi antennas combined in groups of four.
Area of the main array, m^2	About 1800 (width 42.427 m, distance between antennas 0.7λ)
Effective area of the main array, m^2	2180
The maximum value of the product of the average power and the effective area of the antenna, $W \cdot m^2$	Approximately 2.5×10^6
Antenna beamwidth (main array), degrees	7 (vertically up)
Antenna array for meteor research	One circularly polarized transmitting Yagi antenna and five dual-element receiving Yagi antennas for interference measurements
Probing pulse type	Gaussian
Pulse repetition frequency, Hz	1960
Radar width of the probing pulse, m	2275
Receiver bandwidth, kHz	20. 1
Number of coherently accumulated pulses	16
Effective time of pulses accumulation,s	0. 1
Number of samplings on observation interval	6700
Observation time interval, s	55
Range of measured distances, km	70—104
Range resolution, m	1000

and data analysis is similar to those used for the interferometric meteor radar of Buckland Park (Holdsworth, 2004). This applies a number of criteria to reject received echoes that exhibit unreliable characteristics.

The main technical characteristics of the Davis MST radar for meteor observations are presented in Table 3.5 (Reid, 2006; Morris, 2004), and the image of the main antenna array is shown in Fig. 3.5*a* and *b* (Davis radar, 2023).

3.2.4. Modular mobile radar at Resolute Bay

The radar system at Resolute Bay is multifunctional and can be used to study meteors and meteor showers, wind and temperature dynamics in the troposphere and mesosphere, and ionospheric physics. This list is not exhaustive, since the system operates under the control of a computer with the UNIX operating system, which allows the development and implementation of other experimental studies, as well as remote control of the system.

The receiver and digital data acquisition system (RDAS) were manufactured by Genesis Software Australia, which specializes in the design and manufacture of radars for studying the Earth's atmosphere and ionosphere and observing meteoroids as they enter the atmosphere. The 12 kW solid-state transmitter (at 8%duty cycle) and transmit/receive switches were manufactured by Tomco Technologies (Australia) and ATRAD. The equipment was supplied through Atmospheric Radar Systems Pty Ltd (ATRAD) in Adelaide (Australia).

The generalized technical characteristics of the Resolute Bay MST radar are presented in Table 3.6 (Hocking, 2001).

Meteor mode is one of the most commonly used. In this mode, probing is carried out with 5-bit Barker codes, and a repetition frequency of 750 Hz is used. At the same time, the decay times of meteor trails and radiant velocities are determined, which makes it possible, when these data are used together, to determine the direction of wind flows and temperatures at mesosphere heights.

Methods of interferometric measurements are similar to those developed for SKiYMET radars and are described in detail in articles (Hocking, 2001).

The software used on the sites of the Resolute Bay radar has a number of significant features that allow one to obtain information about meteoroids that form transitional dense and overdense ionized trails.

First, the observations of a probable meteoroid are initially stored as a 4-second data sequence. It begins to be recorded 1 second before a decision is mode about the expected event (meteoroid detection). Further data processing is applied, in which a correlation analysis of the signals observed at five receiver antenna diversity is performed, and the cross–correlation of the amplitude and phase of the reflected signal is checked. There is no requirement for the signal selection algorithm that the amplitude of the reflected signal decay exponentially. Instead, the software looks for a fast turn followed by a decrease in signal ampli-

tude, typically in the next 2 sec. Small spikes and dips are allowed, provided they are not too large. This means that underdense meteor trails with typical exponential amplitude decay can also be identified by the detection system. At the same time, the system has good discrimination against lightning and other events that create natural impulse noise for receivers.

Typically, meteor trail times recorded are less than 1.5 sec, that is, less than the 2 sec limit. However, to provide additional possibilities for detecting trails with significantly longer lifetimes, the software on the site has been modified in

Table 3.6. **Generalized technical characteristics of the Resolute Bay MST radar**

Parameter	Value
Resolute Bay MST radar coordinates	74.7°N, 94.9°W (height above the sea level 66 m)
Operating modes that can be selected remotely (under computer control)	Research of the mesosphere–troposphere Research of meteoroids and meteor showers Ionospheric research Specialized interferometric studies
Central operating frequency, MHz	51.5
Transmitter peak power, kW	12
Maximum power factor (duty cycle), %	8
Typical power factor (duty cycle), %	5
Transverse structure of the main antenna array	Area about 1500 m^2, width 100 m
Antenna field elements	Four main antenna systems: main antenna array range array? of 4-element Yagi antennas transmitting antenna for meteor measurements meteor receiving antenna built into the main array
The maximum value of the product of the average power and the effective area of the antenna, $W \cdot m^2$	2.3×10^7
Typical value of the product of the average power and the effective area of the antenna, $W \cdot m^2$	1.2×10^6
Antenna beamwidth (main array) at half power, degrees	2
Probing pulse type	Pulse code sequences
Pulse repetition frequency (PRF), Hz	16—16000
Radar width of the probing pulse (software changeable)	From 150 m to several kilometers
Controlled deflection of the main antenna array beam from the vertical (zenith), degrees	10.9
Assignment of additional antennas	1. Research of meteoroids and meteor showers 2. Research based on backscattering

such a way that it is possible to detect meteor trails with significantly longer lifetimes (at least up to 10 s). The requirements for a good cross-correlation of amplitude and phase between the received signals, as well as a decrease in amplitude over time were retained.

3.2.5. Promising IS-MST radar of the National Heliogeophysical Complex of the Russian Academy of Sciences

As part of the creation of the National Heliogeophysical Complex of the Russian Academy of Sciences (NHGC RAS), the work continues on the creation of promising radar that combines the capabilities of IS and MST radars (Zherebtsov, 2011; Potekhin, 2016).

The development is carried out by the Radio Engineering Institute, named after Academician A.L. Mintz (Concern "Radio Engineering and Information Systems"), which has experience in designing radar systems.

The main task of the IS-MST radar is to study the structure and dynamics of the neutral atmosphere of the mesosphere and ionosphere, as well as to study meteor phenomena at heights of the mesosphere and lower thermosphere (Hocking, 2011).

The promising IS-MST radar is a phased array consisting of two spaced antenna arrays, with a digital multi-channel transceiver system that allows for detailed spatiotemporal processing of backscatter signals.

The antenna system of the IS-MST radar consists of two spaced planar arrays of an antenna located along the magnetic meridian at a distance of 100 m from each other and tilted to the north and south by 20° (Fig. 3.12). The incline of the array is compensated by swinging the beam by 20° to ensure vertical measurements (Potekhin, 2016). Each antenna array has dimensions of 40 × 40 m and includes 1536 crossed vibrators located at the nodes of a triangular grid. The field of view of each antenna is ±45°, and the total radar field of view is ±65° in the north-south direction and ±45° in the east–west direction relative to the magnetic meridian.

The configuration of the antenna system provides maximum spatial coverage of the sounding area and creates conditions for interferometric measurements. An evaluation of the interferometric capabilities of the radar showed that it has a high sensitivity to the angular dimensions of an object about 7.5 arc minutes, and the potential accuracy of determining target angles can reach 40 arc seconds.

An image of the promising IS-MST radar of the Russian Academy of Sciences is shown in Fig. 3.6, and the main technical characteristics are given in Table 3.7 (Potekhin, 2016).The main components of the IS-MST radar RAS include:

- Two antenna arrays with dimensions of 40 × 40 m.
- 24 complexes of transceiver equipment built according to the modular principle (12 for each antenna array). Each module is placed in a container with dimensions of 13.5 × 3.2 × 3 m and weighing up to 35 tons.

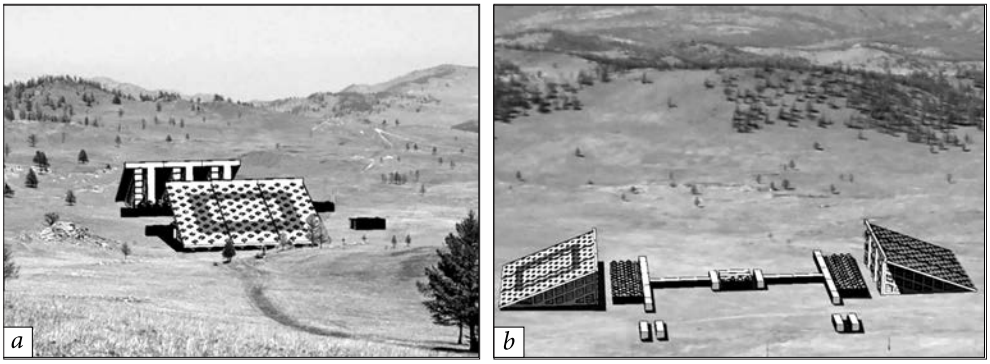

Fig. 3.6. Promising-MST radar of RAS

Table 3.7. **Main technical characteristics of the IS–MST RAS radar**

Parameter	Value
Coordinates of the IS-MST RAS radar	51.9°N, 103.7°E (708 m above the sea level)
Operating frequency range, MHz	154—162.7
Transmitter peak power, kW	2000
Maximum power factor (duty cycle), %	6.8/17.5/37.5 (depending on operating mode)
Antenna type and antenna array elements	2 square phased array antenna containing 1536 crossed vibrators
Polarization	Right and left circular
Effective antenna area (2 grids), m^2	2500
Beam width (1 array), degrees	2.5 × 2.5
Average level of sidelobes, dB	–35
Probing pulse type and coding	Determined by operating mode
Coherent pulses accumulation	Provided
Pulse duration, μs	10—5000
Pulse repetition frequency (PRF), Hz	75—2000 (depending on operating mode)
Minimum height resolution, m	480
Receiver bandwidth, kHz	625

- Complex of control and digital signal processing.
- Four transformer substations.
- Laboratory building equipped with a system for processing, accumulating, and storing data. It is located 2.5 km from the HP-MST radar and connected to it by an optical link.

The available literary sources do not contain information about the use of the National Heliogeophysical Complex of RAS for meteor research. However, with the additional equipment of the IS-MST radar, wide opportunities open up for radar and the study of the physical characteristics of sporadic and shower meteoroids.

3.3. Specialized radars for meteor research

Over the past 50 years, several meteor radar systems have been used for detailed orbital surveys of the sporadic meteor complex. Some of them are discussed below:

- Harvard HRMP Meteor Radio System Project (HRMP).
- Advanced Meteor Orbit Radar (AMOR) located in New Zealand.
- Canadian meteor orbital radar CMOR (CMOR — Canadian Meteor Orbit Radar)
- Orbital system SAAMER (SAAMER-OS — Southern Argentina Agile Meteor Radar Orbital System).
- Ukrainian radar system MARS (MARS — Automated Meteor Radar System).
- Tajik meteor pulse radar MIR-2.

The HRMP observations have processed about 2×10^4 meteoroid orbits from 1968 to 1969 and have been used as a basis for studying many terrestrial meteor showers near the Earth (Sekanina, 1970a; Sekanina, 1970b; Sekanina, 1973; Sekanina1976) and for creating environmental models.

A more significant study was carried out by AMOR, which observed approximately 5×10^5 orbits during 5 years from 1995 to 1999. Since AMOR was located in the Southern Hemisphere (43°34'S, 172°39'E), it provided the most detailed study of meteoroids in this region of the sky for today.

From 2002 to 2008, the CMOR system, which is still functioning, recorded more than 3 million individual meteoroid orbits for particles with an average mass of 10^{-7} kg, and every day ~4000—5000 orbits are added to the statistics.

The SAAMER Orbital System (SAAMER-OS — Southern Argentina Agile Meteor Radar Orbital System) is one of the latest meteor radars entered into service to conduct continuous meteor observations. The resulting dataset contains over 750,000 meteoroid orbits.

Meteor Automated Radar System (MARS), deployed in Ukraine, is multifunctional and designed to collect information about meteor phenomena in solving astronomical and geophysical problems. In the period from 1967 to 1972, about 2 million photographs were taken, which are stored in the archives of the Kharkiv National University of Radio Electronics (KNURE). In 1972—1978, a long-term unique experiment was carried out on the Kharkiv meteor radar, resulting in the registration of about 250 thousand orbits of meteoroids up to +12 magnitude (in the mass range 10^{-3}—10^{-6} g) and construction of an empirical model for the distribution of orbital elements of small meteoroids,

In 1964—1968, a special complex of radar equipment MIR-2 (second-generation meteor pulse radar) was created in Tajikistan. It is located on the territory of the Gissar Astronomical Observatory and designed to measure radiant and meteor velocities using the direction-finding-time radio method. The device, principle of operation, and detailed characteristics of MIR-2 are described below.

3.3.1. AMOR meteor orbit radar

Advanced Meteor Orbit Radar (AMOR) is located near Christchurch in New Zealand (43.57°N, 172.65°E). This is a multi-station high-frequency system of continuous operation, which measures both the geophysical parameters associated with the ablation of meteoroids and the heliocentric orbits of particles (up to a limiting size of ~ 40 μm) entering the near-Earth space.

The radar has been operating since 1990 (Galligan, 2005; Baggaley, 1994; Baggaley, 2001; Baggaley, 2002), capturing meteorite echoes and raw observational records, regularly cataloging the population of meteoroids crossing the Earth's orbit, and providing high quality measurement of ~106 orbits.

Until 2001, the AMOR system consisted of one transmit array and three receive arrays (forming a double interferometer) at a central site. Then it was supplemented with two remote sites, each of which had one receiving array. This ensured the expansion of the system's capabilities for measuring geophysical and astronomical parameters. Fig. 3.7 shows the geographic location of these sites (Taylor, 1991).

A detailed description of the principles of constructing the AMOR radar and the methods used to measure various parameters of meteoroids can be found in (Taylor, 1991).

The main technical characteristics of the AMOR radar are presented in Table 3.8.

The array of receiving antennas, tuned to 26.2 MHz, consists of six collinear sections with a central feed. Collinear compartments are placed with a shift of 2 λ. Fig. 3.8 shows a schematic of the receiving antenna array (Taylor, 1991). Adding two additional sections lengthens the array of receiving antennas up to 16 λ.

Fig. 3.7. Geographic location of AMOR meteor orbit radar sites (Taylor, 1991)

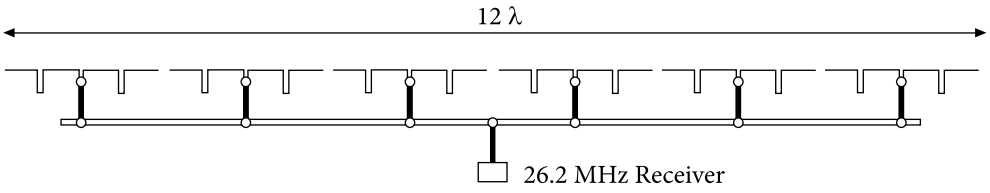

Fig. 3.8. Schematic representation of the array of receiving antennas

Table 3.8. **Main technical characteristics of the AMOR radar**

Parameter	Value
AMOR radar coordinates	43.57°N, 172.65°E
Operating frequency, MHz	26.2
Transmitter peak power, kW	20
Maximum average output power, W	About 700
Probing pulse type	Rectangular
The antenna system elements	Array of 6 collinear receiving antennas; Transmitting matrix of 8 rhombic antennas; Four 3-element Yagi antennas, two of which transmit data to the central site
Transmitting antenna beamwidth at half power, degrees	3—4
Antenna gain of transmit array	635
Gain of the receiving array of antennas	133
Probing pulse duration, μs	66
Pulse repetition frequency, Hz	379
Number of samplings on observation interval	250
Observation time interval, s	9.5
Range of measured distances, km	Up to 400
Range resolution, km	1 (assuming that the meteor trail is observed at altitudes of 70—120 km)
Receiver bandwidth at half power, kHz	20

The transmitting matrix consists of 8 rhombic antennas, which are placed with an interval of 2λ. Fig. 3.9 shows a schematic representation (top view) of a transmitting matrix whose main beam is directedto the south.

Ongoing developments, including the installation of additional antenna systems and independent measurements from separate antennas, as well as new signal processing algorithms, provide enhanced system capabilities for the high–quality measurement of the astronomical parameters of meteoroids entering the near-Earth space and the geophysical parameters of the atmosphere. An important feature of the system AMOR is a continuous operation without maintenance.

3.3.2. Canadian Meteor Orbit Radar CMOR

The Canadian station multifunctional radar complex for measuring meteor orbits CMOR (CMOR — Canadian Meteor Orbit Radar) is a multi-station, pulsed multi-frequency meteor radar of HF-VHF bands. It is located on the territory of the University of Western Ontario (UWO) near Tavistock (43.264°N, 80.772°W) and is operated by the UWO Department of Physics and Astronomy Meteor Array.

CMOR has been operating since the end of 2001 and is currently one of the most productive and active (by 2009, the number of registered orbits had reached 4 million). In 2009, the original CMOR I was replaced by an equivalent but more modern CMOR II. The scientific research that CMOR provides includes:

• Study of the sporadic meteor complex and development of its model, which makes it possible to determine the main sources of sporadic meteors in the solar system.

• Measurement of reflections from meteor trails at several frequencies to estimate the initial radius of the meteor trail.

• Determination of bulk electron density and linear electron density profile for meteor trails using the reflections fixed at several points.

• Determination of the density and probable chemical composition of meteoroids based on the study of their ablation.

• Analysis of the origin and development of a model for the evolution of the population of interplanetary meteoroids, comets, and asteroids.

• The study of the genetic relation of sporadic meteoroids and meteor showers to the parent bodies allowing to make reasonable assumptions about the physicochemical properties of small celestial bodies.

• Detection and study of interstellar meteorites and identification of their astrophysical sources (Weryk, 2005).

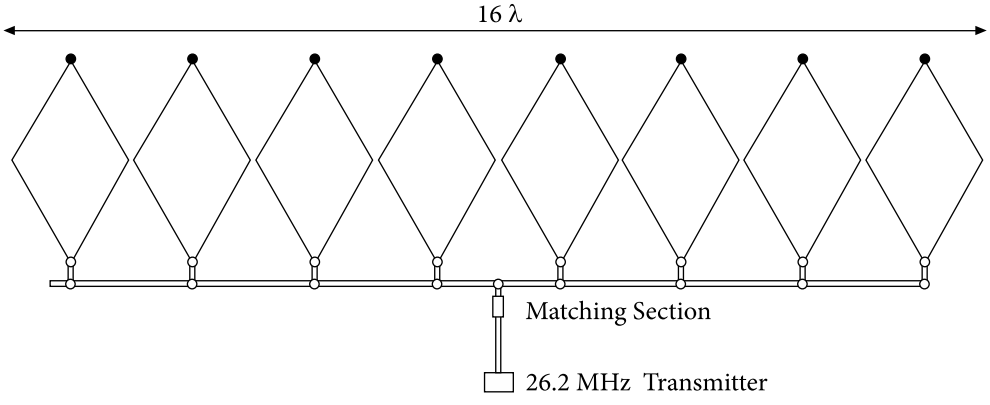

Fig. 3.9. Schematic representation of the transmitting array of 8 rhombic antennas placed at intervals of 2λ and, for matching, having a load of 680 ohms (filled circles)

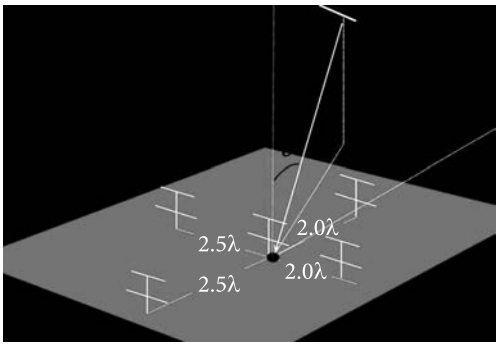

Fig. 3.10. Schematic representation of the five-element interferometer of the CMOR radar complex [available at http://meteor.uwo.ca/research/radar/cmor_science.html]

The radiant directions of meteoroids are determined using interference methods similar to those used in the SKiYMET technology (Hocking, 2001), and the speeds are determined at the same time for all stations. This provides a radiant estimate with a resolution of 6 degrees in direction (due to the uncertainty in measuring time delays) and a speed estimate with ~10% accuracy. Deceleration corrections are computed using empirical expressions determined by comparing raw radar velocities with ones found in photographic studies of large meteor showers (Brown, 2004).

The radiant distribution of sporadic meteors is studied with allowance for observational corrections for a given meteoroid mass and energy.

The limiting magnitude value is +7.5, which at an average meteoroid speed of 30 km s^{-1} corresponds to its limiting mass of ~10^{-7} kg and limiting size ~0.2 mm Brown, 2010). More details are available in (Jones, 2005).

For a system operating at a frequency of 29.85 MHz in the "Orbit" mode, the absolute minimum detectable intensity of the signal reflected from the trail corresponds to trails of meteoroids with magnitudes of about +9. However, due to reduced sensitivity, the count statistics are complete only for magnitudes up to +8.

Vertically directed antenna arrays provide an overview of the sky up to ~20° in elevation. In this case, a five-element interferometer, a schematic representation of which is shown in Fig. 3.10, allows one to determine the direction of the echo with an accuracy of ~1° (Webster, 2004).

In 2009, the main CMOR orbital radar system (29.85 MHz) was replaced with an equivalent but more modern one. The upgraded system has twice the transmission power (12kW instead of 6kW) and a highly stable reference oscillator. As part of the CMOR II upgrade, three more remote sites were deployed with the same high stability crystal oscillators. Each new remote site contains a receiving antenna (for operation at 29.85 MHz) connected to a remote GPS equipped digital receiver. The received UHF signals are transmitted to the main site via a remote UHF connection, which is necessary for measuring the meteoroid radiant and improving the accuracy of measuring its speed, as well as for the possibility of measuring the ionization profile of the meteor trail.

Depending on the tasks to be solved, the components of the CMOR system operate at frequencies of 17.45, 29.85, and 38.15 MHz. The "Orbit" component applies only to a system operating at 29.85 MHz.

The CMOR system consists of three identical radar systems connected to each other for simultaneous transmission and reception. Each of the three components has seven antennas and seven individual receivers. For components operating at 17 and 38 MHz, all seven receivers are used to increase the signal to the noise level, but only five of them are used for interferometry.

The system operating at 17 MHz daytime is subject to strong interference from terrestrial radio stations. This allows for using it only at nighttime.

The main technical characteristics of the CMOR radar system are presented in Table 3.9. Detailed information about the system can be found in (Webster, 2004).

Table 3.9. Main technical characteristics of the CMOR radar system

Parameter	Value
CMOR radar coordinates	43.264°N, 80.772°W
Operating frequency, MHz	17.45, 29.85, and 38.15
Noise level at the receiver input depending on the frequency, dBm	–98, –109, and –113
Transmitter peak power, kW	15
Transmitting antennas	Three-element vertically-directed horizontally-polarized Yagi
Transmitting antenna gain, dB	7.6
Transmitting antenna beamwidth at half power, degrees	30
Probing pulse type	Rectangular
Probing pulse duration, μs	75
Pulse repetition frequency, Hz	532
Receiving antennas	Two-element vertically-directed horizontally-polarized Yagi
Receiving antenna beamwidth at half power, degrees	45
Receiving antenna gain, dB	6.5
Sample rate (per channel), samples per second	42 000
Receiver bandwidth at half power, kHz	28
Limit magnitude	+8
Minimum detectable meteoroid mass (depends on speed), g	10^{-5}
Minimum size of a detected meteoroid, mm	0.1
Range of measured distances, km	15—255
Range of measured reflection heights from the ionized meteor trail, km	70—120
Effective viewing area, km^2	100—300
Accuracy of estimation (resolution) of radiants in direction, degrees	6
Estimation accuracy (resolution) of reflection point in range, km	3

UHF communications at 450 MHz are used to transmit information from remote sites to the Main Site. In this case, nine-element horizontally-polarized Yagi antennas are used as transmitting and receiving antennas.

3.3.3. Multifunctional radar SAAMER

The Southern Argentina Agile Meteor Radar Orbital System (SAAMER-OS) was deployed at the astronomical station in Rio Grande, Tierra del Fuego, Argentina (53.8°S, 67.8°W) in May 2008. It uses a flexible construction technology that provides multifunctionality and the ability to quickly change the parameters of the radar system. In August 2010, the SAAMER radar complex was upgraded to a system capable of determining the parameters of meteoroid orbits. This was achieved by adding two remote receiving stations, located about 10 km from the main site in almost perpendicular directions, which made it possible to create a new generation SKiYMET system. The SAAMER radar emits 10 times more power than conventional meteor radars and uses an 8-antenna transmit array, which focuses the emitted energy upwards instead of the traditional single-antenna of the all-sky configuration. The system is configured so that the transmitting array could also be used as a receiving antenna. The new design significantly increases the sensitivity of the radar and allows for additional studies of meteoroids beyond those that are characteristic for systems focused on the detection of specular reflections. When using high radiation power and a large aperture of the transmitting and receiving antennas, it is possible to detect the head echo and incoherent scattering from ionized meteor trails.

A new high-power transmitting antenna (TX) and a fourth remote receiving station have been deployed and have been operational since October 2019. A new software has been implemented that uses «overdense» and «underdense» echoes and determines orbits using all remote sites simultaneously.

The update has a significantly expanded the scope of scientific research provided by the radar system and makes it possible to detect high-velocity meteoroids at low zenith angles.

At present, SAAMER is the only radar system capable of continuously observing and determining the parameters of meteoroid orbits in the southern hemisphere (Janches, 2014; Janches, 2015; Janches, 2019; Pokorný, 2017).

SAAMER's unique geographic location allows for an additional ("interhemispheric") comparison with the measurements from the Canadian CMOR meteorite orbital radar, which is geographically conjugate. It can effectively observe radiants from the south ecliptic pole down to about 30°N and is ideally suited to provide critical data for the continuous study of the apparent sources of sporadic Southern Toroidal and Southern Apex meteorites.

SAAMER-OS consists of five radar stations:

• Central station (SAAMER-C; 53.786°S, 67.751°W), which houses a transmitting array and receiving arrays with interferometry;

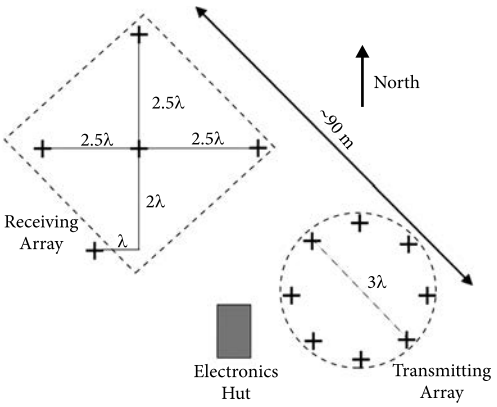

Fig. 3.11. Geographic location of SAAMER-OS (Janches, 2019)

Fig. 3.12. Location of the transmitting array and interference receiver antennas at the SAAMER–C central station (Pokorný, 2017)

• Northern remote station (SAAMER-N; 53.682°S, 67.871°W), located approximately 13 km northwest of the central station;

• Southern remote station (SAAMER-S; 53.682°S, 67.871°W), located approximately 7 km southwest of the central station;

• Western remote station (SAAMER-W; 53.828°S, 67.842°W), located approximately 7 km southwest of the central station.

• Eastern remote station (SAAMER-E; 53.682°S, 67.871°W), located approximately 3.8 km northeast of the central station.

• The geographic location of SAAMER-OS is shown in Fig. 3.11. The location of the transmitting array and interference receiver antennas at the SAAMER-C central station is shown in Fig. 3.12 (individual antennas are marked with plus signs).

SAAMER employs a transmitter phase array configuration of eight three-element crossed Yagi antennas arranged in a 27.6 m diameter octagon (three wavelengths), and the phase difference between the transmit antennas is set by software, which increases the flexibility of the system to perform a number of transmission modes and reception (Pokorný, 2017; Janches, 2015).

The receiving antenna configuration is typical for meteor radar systems, consisting of five antennas, each of which is a three-element cross-polarized Yagi antenna. The receiving array is separated from the transmitting array by about 90 m, which is several orders of magnitude less than the distances at which reflection from meteoroids and meteor trails occurs (~100—400 km). Thus, for the purposes of meteor observations, the SAAMER-C transmitting and receiving arrays can be considered combined.

The two remote stations SAAMER-N and SAAMER-W are equipped with single three-element cross-polarized Yagi antenna. They are located in almost orthogonal directions from SAAMER-C at a distance of about 10 km.

SAAMER uses real-time meteorite echo detection and analysis algorithms developed for SKiYMET systems. These algorithms simultaneously transfer raw data to memory, detect the appearance of meteors, and identify events created by reflections from meteoroids and meteor trails. When analyzing raw data, false detections of the same event are possible. To reduce this probability, the system is typically configured to consider only meteor events that occur in the same altitude range.

The absolute meteoroid velocity is measured by a geometric method similar to that used in AMOR and CMOR. This method is applied to all meteor events detected at all three SAAMER stations, assuming that the received radar signal is specular. When the echo is detected by all three SAAMER-OS stations, the trajectory and velocity of the meteoroid can be determined using the measured time delays (Baggaley, 1994; Brown, 2008; Webster, 2004).

The main technical characteristics of the SAAMER-OS radar system are presented in Table 3.10.

UHF communication is used to transmit and receive information from remote sites to the main site. Horizontally polarized Yagi antennas are used.

3.3.4. Meteor automated radar system MARS

A Meteor automated radar system (MARS) was deployed in Ukraine near the village of Olkhovatka, Balakleysky district (49.42° N, 36.94° E). The MARS system is multifunctional and designed to collect information about meteor phenomena to solve astronomical and geophysical problems.

At the General Assembly of the International Astronomical Union (IAU) in 1958 (in Moscow), the Kharkiv meteor radar observations were recognized the best in the world.

The MARS system has been recommended as a successful prototype for wide distribution (Kolomiyets, 2012; Fedynsky, 1976). Until now, this radar system has been one of the most sensitive meteor radars for astronomical observations.

From 1967 to 1972, on the Meteor automated radar system of the Kharkiv National University of Radio Electronics (KNURE), observations of radio signal reflections from meteor trails were made, moreover, added with fixing oscillograms on film. In total, about 2 million photographs were taken, which are stored in the KNURE archive. Currently, work is underway to convert this information into digital form.

In 1972—1978 on the Kharkiv meteor radar, a unique long experiment was carried out resulting in about 250 thousand orbits of meteors up to a magnitude of +12 (in the mass range 10^{-3}—10^{-6}g) registered (Kascheev, 1982). An empirical model for the distribution of orbital elements of small meteoroids was developed and a description of this model was given (Kascheev, 1979; Tkachuk, 1979).

During radar observations, special attention was paid to the regularity and continuity of measurements, as well as the high and stable sensitivity of the receiving equipment. The observation schedule was organized in such a way that the measurement cycles were distributed as evenly as possible throughout the year. For example, 29 measurement cycles (5 to 8 days long) were taken during 1975, resulting in more than 54,000 meteoroid orbits. The monitoring carried out in the absence of the main meteor showers made it possible to observe mainly the characteristics of the sporadic meteor complex.

Table 3.10. **Main technical characteristics of the SAAMER-OS radar system**

Parameter	Value
SAAMER-C radar coordinates (main site)	53.786°S, 67.751°E
SAAMER-W (removed site)	53.828°S, 67.842°E
SAAMER-N (removed site)	53.682°S, 67.871°E
SAAMER-E (removed site)	53.772°S, 67.727°W
SAAMER-S (removed site)	53.852°S, 67.759°W
Operating frequency, MHz	32.55
Transmitter peak power, kW	64
Transmitting array located on the main site	8 antennas arranged in a circle with a diameter of 27.6 m
Receiving system located at the main site	Five antennas, each is a three-element cross-polarized Yagi antenna
Receiving antenna located at remote site	Three-element cross-polarized Yagi antenna
Probing pulse type	7-bit Barker code (22.5 μs) — the main mode; Monopulse — head echo measurement mode
Pulse repetition frequency, Hz	1765 — the main mode; 500 — head echo measurement mode; 625 — radiant measurement mode
Receiver bandwidth at half power, kHz	300 — the main mode; 50 — head echo and radiant measurement mode
Limit magnitude	+8
Minimum detectable meteoroid mass (depends on speed), g	From 10^{-11} to 10^{-4}
Minimum size of detectable meteoroid, mm	0.1
Range of measured distances, km	15—255
Range of measured reflection, km	70—120
Range of measured velocities, km/s	From 11 to 72
Effective viewing area, km^2	100—300
Accuracy of estimation (resolution) of radiants in direction, degrees	8
Accuracy of estimation (resolution) of reflection point in range, m	2000 — the main mode; 250 — head echo measurement mode

The real-time measurements provided by the MARS II system include:

- fixation of the event (the moment of observation start of the meteor);
- measurement of the slant range to the reflecting area of meteor trails;
- measurement of angular coordinates (azimuth and elevation) of the reflecting area of meteor trails;
- measurement of reflection point height;
- measurement of amplitude, duration, and range of reflected signals;
- registration of temporal variations and the number of observed reflections from meteor trails;
- measurement of the velocity, coordinates of radiants, and elements of orbits of individual meteoroids;
- assessment of the distribution of meteoroids by mass;
- measurement of the radial component of the wind speed in the meteor zone of the atmosphere.

In addition, in the semi-automatic mode, using an electronic radiant indicator with a photo recorder, it is possible to study the diffusion coefficient, the initial radius of meteor trails, resonance effects, meteoroid fragmentation, etc.

The speed and coordinates of the radiants of individual meteoroids are determined by the Davis pulsed diffraction method with one transmitting and three spaced receiving points. The direction of radiation is eastward (astronomical azimuth 270°). The main receiving point is combined with the transmitting one, and remote receiving and relaying points are located at distances of 4.32 km (azimuth 214°) and 8.42 km (azimuth 290°).

Information is received within 0.2 s by interrupt signals from the output of the pre–processing device when reflected signals are detected. This did not allow us to completely process the signals reflected from overdense meteor trails.

The main antenna system (separate transmitting and receiving) generates a radiation pattern 5° wide in the horizontal plane and 30° in the vertical plane. The maximum of the antenna pattern is directed at an angle of 45° to the horizon. As emitters, 20 in-phase biconical vibrators are used, located inside a corner reflector with an opening angle of 60°. The reflector is formed by two grids, which are stretched at angles of 15 and 75° to the horizon. Their length is 193 m in the horizontal plane, and the width in the vertical plane is 27 m. With the help of the corner reflector, the antenna pattern is formed in the vertical plane. The side lobes' level of the radiation pattern is –20 dB, the level of the back lobe is –40 dB, and the antenna gain is 250 (Kascheev, 2002).

Double horizontal rhombuses are used as receiving antennas at remote points. For relaying signals from remote points to the main one, five-element Yagi antennas are used.

The antenna field of the phase goniometer consists of 5 five-element Yagi antennas arranged in the form of an asymmetric cross.

The pulse repetition frequency of the locator is 500 and 100 Hz, which is necessary to eliminate ambiguity in determining the distance to the meteor reflection

(Antipov, 2010). The duration of the probing pulse of the radar is 30 μs. The main technical characteristics of the MARS II radar system are presented in Table 3.11 (Kascheev, 1977; Kascheev, 1980).

3.3.5. Meteor pulse radar MIR-2

A special complex of radar equipment MIR-2 (a second-generation meteor pulse radar) was created in Tajikistan from 1964 to 1968 to measure the radiants and velocities of meteors using the direction-finding-time radio method. The complex is located on the territory of the Gissar Astronomical Observatory (GisAO coordinates: 38°29'23"S, 68°40'58"E). Its device, principle of operation, and detailed characteristics are given in (Chebotarev, 1970a; Chebotarev, 1970b; Narziev, 2017).

The complex includes a transmitter, five receivers, a synchronization block, an anti-jamming unit, a high-accuracy range meter, remote point receivers, remote point relay signal transmitters, relay signal receivers, a meteor simulator,

Table 3.11. **Main technical characteristics of the MARS II radar system**

Parameter	Value
MARS II radar coordinates (main site)	49.42°N, 36.94°I?
Operating frequency, MHz	31.1
Transmitter peak power, kW	Up to 1000
Main antenna (transmitting, receiving) located on the main site	Corner antenna (20 in-phase biconical vibrators located inside the corner reflector)
Main antenna gain	250
Width of the main lobe of the main antenna at half power, degrees	5° horizontal, 30° vertical
Receiving antennas at remote sites	Double horizontal rhombic antennas
Receiving antenna gain at remote sites	16
Antenna field of the phase goniometer	Five antennas, each is a five–element cross–polarized Yagi antenna
Probing pulse type	Monopulse
Probing pulse duration, μs	30
Pulse repetition frequency, Hz	500 and 100
Minimum discernible receiver signal (actual sensitivity at signal-to-noise ratio = 2), uV	5
Limit magnitude	+10 in height measurement mode; +11…+12 in the mode of measuring velocities, radiants, and orbits; +13…+14 in meteor count mode
Minimum mass of a detected meteoroid (depends on speed), g	~10^{-6}
Type of detectable meteor trails	Underdense, ~10^{11} e m^{-1}

a multi-beam frame-by-frame indicator, an indicator with waiting-continuous photo registration, and antennas.

The transmitter together with the receivers of the central point and the receiving–recording equipment are located in the GisAO. Remote points are remote from the central one at a distance of 4.05 km (astronomical azimuth 314°), 3.90 km (azimuth 94°), and 3.85 km (azimuth 202°).

The main parameters of the MIR-2 complex:

- wavelength — 8 m;
- transmitter power in pulse — 65 kW;
- pulse repetition frequency — 500 p/s;
- pulse duration — 6.5 μs;
- main receiver bandwidth — 600 kHz;
- bandwidth of paths of relay signals from remote points — 2 MHz;
- threshold sensitivity of receivers (at $U_s / U_{sh} = 1$) – 8×10^{-14} W (or 2.5 μV);
- sensitivity for measuring radiants and velocities — 17...34 μV;
- antennas in the mode of measuring radiants and velocities-half-wave vibrators located at a height of λ/3 above the ground, having a maximum power gain of ~5.3 at an elevation angle of about 45° in the east and west directions;
- limiting magnitude of meteors when measuring radiants and velocities +5.7...+5. 0 (at a velocity of 40 km s^{-1}, corresponds to the minimum mass of registered meteoroids (0.5—1.0) 10^{-3} g).

The complex of radar equipment allows for each meteor to be determined by its range, speed, coordinates of the reflecting point and radiant, the height of the reflecting point, and the duration of radio reflections with an accuracy of 0.02 sec (by two methods: pulse-diffraction and direction finding time). The latter is superior to the former in terms of both measurement accuracy and sensitivity. In this case, the error in measuring the zenith distance of the radiant does not depend on its position.

3.4. Conclusions

Various radar systems, both specialized and multifunctional, can be used to measure the main parameters of meteoroids. The results of observations allow for determining the main characteristics of meteoroids, mapping their radiants, predicting the origin, and, on this basis, the physicochemical properties of meteoroids. These data are necessary for both astrophysical research and telecommunications.

When interpreting the results of observations, it is necessary to take into account the features of the systems through which the corresponding data were obtained. In this regard, some technical characteristics and geographic location of radars were presented, the observational data of which were used in the study of atmospheric physics, radiant mapping of the sporadic meteor complex and meteor showers, as well as in estimating the parameters of the orbits and velocity of meteoroids.

An essential feature of modern radar systems is the use of new algorithms for selecting and analyzing meteor trails, which allow for the real-time selection of lightning discharges, pulsed radio interference, auroral echoes, etc., which previously took hours or days when working with large data arrays.

The use of the multitasking UNIX operating system installed on a personal computer made it possible to implement rather complex algorithms for processing multichannel radar information in real time and repeatedly transferring it to the database. The storage of the results of "online" analysis and raw data associated with any event is provided along with the possibility of their transfer to the user via the Internet for further detailed analysis.

Radar systems are easily configured to communicate via any available network point or TCP/IP modem, allowing for remote control of radars and automatic transmission of observations to remote hosts.

The review of radar systems offers an opportunity to gain knowledge related to the study of the sporadic meteor complex and provides a basis for analyzing the results of observations, as well as creating new methods and tools for extracting information from existing radar data.

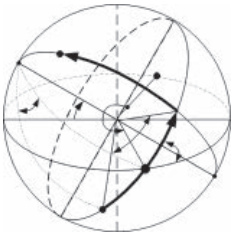

SECTION 4

SPORADIC METEOROIDS AND METEOROID STREAMS

The study of sporadic meteoroids and meteor showers makes it possible to obtain information of interest both to astronomers and astrophysicists, as well as to telecommunications specialists. This information can also be used to assess the risks of collisions between small celestial bodies and a spacecraft in near and deep space.

Obtaining the necessary information is based on data obtained as a result of using modern methods of astronomical observations at scientific institutes, universities, and observatories.

The most complete idea of the nature of the distribution of meteoric matter in near-Earth and interplanetary space is based on radar observations of meteors. In radar studies of meteoroids, information about the physical and dynamic parameters of meteoroids is obtained by processing signals reflected from meteoroid heads and meteor trails resulting from their interaction with the Earth's atmosphere.

A feature of the observation of meteor phenomena is that having observed an event once, we do not have complete and reliable data either about the meteoroid or about the state of the environment in which it occurred. In this regard, the construction of predictive models of meteor phenomena in the Earth's atmosphere is very important for interpreting the results of meteor observations.

In radar observations, the necessary initial data for constructing a fairly complete model of meteor phenomena are the mass of the meteoroid, its velocity, density, and chemical composition, as well as the height of the IMTr formation, the chemical composition of the ionosphere, and pressure and turbulence at a given altitude. The amplitude-time characteristic (ATCH) of the probing radio signal reflected from the meteor trail and its head part depends on all the above initial data and implicitly contains information about them. At the

same time, only the height of the formation of the meteor trail, the radiant and velocity of the meteoroid, as well as, in some cases, its chemical composition (according to the results of spectral analysis of the trail luminosity are available for direct measurements. At meteor velocities, which are hypersonic, aerodynamic braking and aerodynamic heating of a meteoroid in the real (nonisothermal) atmosphere significantly interact, which may lead to meteoroid fragmentation (Bronshten, 1983; Grigoryan, 1979; Stulov, 1998; Fadeenko, 1967; Ceplecha, 1998). The crushing effect leads to a change in the IMTr and, accordingly, to a change in the ATC of the reflected signal.

Due to the incompleteness of the initial data, a model of the meteor phenomenon is prognostic (probabilistic) and can be built based on some assumptions. One of the grounds for such assumptions may be the discovery of the genetic relationship between the meteoroid and its parent body — a comet or an asteroid. The signs that make it possible to judge this relationship are the known radiant (the observation site, zenith angle, azimuth, and time of the event) and the meteoroid velocity . Depending on the height of the formation of the specular reflection point on the meteor trail, one can make assumptions about the density and chemical composition of the meteoroid.

To develop a model, the results of mapping the sporadic meteor complex and meteor showers together with the results of studying the frequency of observation of meteor trails at certain heights and certain velocities can be used.

The amplitude-time characteristic of the signal reflected from the meteor trail provides a fundamental opportunity to solve the inverse problem-based on the ATCH, to predict the genetic relationship of the meteoroid with the parent body, which is necessary for the development of the theory of the origin and evolution of meteoric matter.

To construct advanced meteor communication systems, which are the focus of this monograph, we need an ATCH predictive model and maps of the radiant distribution for a sporadic meteor complex in the geocentric ecliptic coordinate system centered relative to the Sun. Taking into account the characteristics of meteoroids that appear in the radio visibility zone makes it possible to reasonably choose the location of base stations and optimize the orientation of antennas as well as the speed and protocols of information transmission. In this case, it should be taken into account that the distribution density of meteoroid radiants on the celestial sphere in a given geographical region changes during the year (due to the Earth's revolution around the Sun) and day (due to the Earth's axial rotation). The main characteristics of meteoroids, which are necessary for building a model, can also change if, at different time intervals, meteor trails with a specular reflection point are created by meteoroids having parent bodies of different types. Thus, a promising meteor communication system should be adaptive.

When selecting and processing radar observation data necessary for building and updating the ATCH predict model and the sporadic meteor complex model, attention should be paid to where the observation site was located, what equip-

ment was used to obtain the corresponding characteristics, what methods were used to process the observational data, and how the radars were calibrated before measurements.

This section discusses the views of modern science on the origin of meteoroids, their genetic relationship with comets and asteroids, the space location of the orbits of sporadic meteoroids, and meteor showers.

4.1. Relation of meteoroids with parent bodies

According to modern concepts, the main sources of comets and asteroids that give rise to sporadic and shower meteoroids are the Main asteroid belt, Kuiper belt, a family of Trojans orbiting Jupiter, and the hypothetical Oort Cloud, which contains the most distant objects in the solar system. This list also includes asteroids of the Hirayama family, which includes several subfamilies, the main distinguishing feature of which is that each of them was formed owing to the destruction of a large parent body. As a result, the asteroids of these families have similar spectral and chemical characteristics.

4.1.1. Main Belt of asteroids

Main Belt asteroids move in orbits between the orbits of Mars and Jupiter, that is, at distances from 2.1 to 3.3 astronomical units (AU) from the Sun. The planes of their orbits are near the ecliptic, their inclination to the ecliptic lies mainly up to 20 degrees (reaching up to 35 degrees for some), and eccentricities — from zero to 0.35. Most of the orbits of the Main Belt asteroids have eccentricities of 0.1—0.2. However, some asteroids move in highly elongated orbits and have eccentricities up to 0.8, so that their orbits intersect the orbits of Mars and Earth. The main distinguishing feature that characterizes an individual asteroid is its spectrum, which can be used to judge the chemical composition of a given body. In the Main Belt, depending on the chemical composition, 3 main spectral classes of asteroids are distinguished: carbon (class C), silicate (class S), and metallic or iron (class M).

Comets of the Main Belt are a special class of objects that are part of the Main Asteroid Belt and move in almost circular orbits. Unlike asteroids, in certain parts of their orbits (closest to the Sun), they are able to show cometary activity due to ice and frozen gases that were preserved shallowly under the surface of these bodies. It is possible that many asteroids of the Main Belt were generated by long-period comets from the Oort cloud, which, under the influence of planetary disturbances, were captured and transferred to short-period orbits (Asher 1994; Biryukov, 2007; Whitman, 2006). Such comets, having exhausted all the reserves of volatile substances, could turn into specific asteroids that contain “dried” nuclei of long-term comets. Their physical and chemical properties may differ significantly from those of non-comet-produced Main Belt asteroids.

4.1.2. Kuiper Belt

The Kuiper Belt (sometimes also called the Edgeworth-Kuiper Belt) lies beyond the orbit of Neptune and is much larger than the main asteroid belt. It was named in honor of its discover Gerard Kuiper.

The location of the Kuiper Belt in the solar system is conventionally shown in Fig. 4.1.

The first of the objects in this belt was discovered in 1992 and was named "1992 QB 1". The Kuiper Belt itself has not been studied at a close range yet. The first step taken by mankind in this direction was the mission of the spacecraft New Horizons, which was sent by NASA to this region of the solar system on January 19, 2006, to study Pluto and its natural satellite Charon. The information collected by the probe (in the summer of 2015) radically changed the scientific community's ideas about such celestial bodies, demonstrating that at least Pluto is still a geologically active world, under the surface of which an entire ocean can hide. After Pluto, New Horizons continued its journey deep into the Kuiper Belt. In 2019, it performed the flyby of Arrokoth (486958 Arrokoth) — the most "primitive" celestial body ever studied by a spacecraft from a close distance. As of April 2022, New Horizons has moved 53 au away from the Sun. The probe has almost passed the Kuiper belt, and the chances that an object accessible for the close-range study will meet on its trajectory are minimal.

The Kuiper Belt belongs to the solar system and is an ellipse in space (see Fig. 4.1). While the Main Asteroid Belt consists of asteroids, mainly containing rocky components and metals, the Kuiper Belt asteroids mainly contain ice fragments of water, ammonia, and various hydrocarbons.

4.1.3. Short-period comets of the Jupiter family

Of the 1139 known comets in elliptical orbits, a significant proportion (737) of them revolve around the Sun over less than 100 years (How Comets Move, Center for Scientific Creation). They are called short-period and usually move near the ecliptic plane (the average inclination of the orbit to the ecliptic plane is around 18°). Almost all orbits (711) are progressive (that is, they revolve around the Sun in the same direction as the Earth) and have a Tisserand parameter within $2 < T_J < 3$ (Lowry, 2008).

All short-period comets are members of different cometary-planetary families. It is believed that all of them were originally long-period, but due to the long-term gravitational influence of large planets on them, they gradually moved into orbits associated with the corresponding planets and became members of their cometary families.

The largest such family belongs to the Jupiter family (we will designate it as the JFm group). The periods of revolution around the Sun of the JFm comets are within 3.3 — 20 years.

Of all the known short-period comets, Comet Encke, a member of the JFm, has the shortest period of revolution around the Sun — 3.3 Earth years. The predominance of JFm comets is a consequence of Jupiter's much greater gravitational influence on comet bodies compared to other planets: it is 10 times greater than the influence of Saturn and 100 or more times greater than the gravitational influence of any other planet.

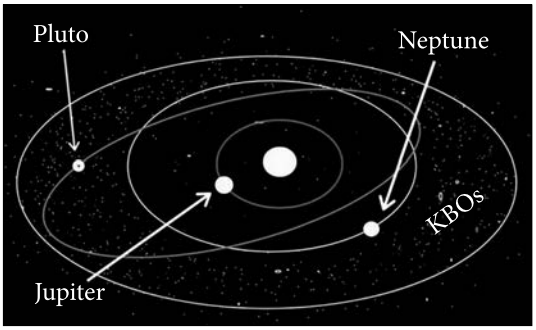

Fig. 4.1. Location of the Kuiper Belt in the solar system (Kuiper Belt, by Planets Education)

The way in which Jupiter has assembled its large family of comets poses a major problem for most comet origin theories. This is because comets originating from the outer solar system, when falling toward the Sun, tend to move fast as they pass inside Jupiter's orbiting.

Although the orbits of JFm comets are inside the orbit of Jupiter or not far from it, there is an assumption that they originate in the Kuiper Belt (the same source may be for the Oort cloud). The physicochemical properties of trans-Neptunian objects and their orbits, which include JFm, are under study (Fraser 2022).

4.1.4. Trojan family orbiting Jupiter

Trojans are asteroids moving along the orbits of planets, the first of which is Achilles, discovered in 1906 by the German astronomer Max Wolf. This was a confirmation of the theoretical result of Lagrange that three mutually attracted bodies (under certain conditions) can remain near the vertices of an equilateral triangle during movement (Fig. 4.2).

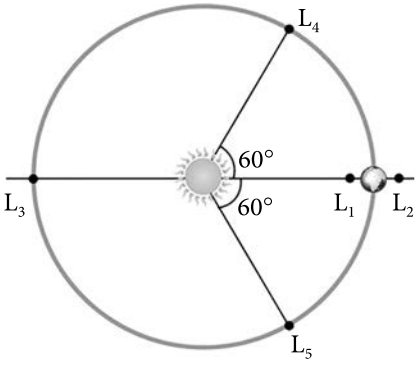

Fig. 4.2. Location of Lagrange Points

The Trojans move near the Lagrange points L4 and L5 — points of stable motion in the three-body problem. Celestial bodies that have fallen into their vicinity make an oscillatory motion without going too far. In Jupiter's orbit, there are two populations of small bodies that orbit Jupiter around the Sun, in a 1:1 orbital resonance with Jupiter. The Greek group is 60° ahead of Jupiter. The Trojans group is 60° behind Jupiter. By the beginning of 2004, this family had included 1640 objects. The Trojans include the Hilda family, a group of dark carbon asteroids located in the main belt between the orbits of Mars and Jupiter. The Hilda family does not

form a true family of asteroids, since its members are not fragments of a common parent body, which is typical for most other asteroid families. This family itself is distributed along the orbit rather unevenly and represents a triangle with three separate local concentrations of asteroids at the vertices of the figure corresponding to three Lagrange points.

Other large planets — Saturn, Uranus, and Neptune — should also have Trojan-like bodies at their respective triangular Lagrange Points. Six Trojans have been discovered orbiting Mars. In 2002, the first Trojan was discovered orbiting Neptune.

4.1.5. Oort Cloud

One of the directions of planetary cosmogony is the hypothesis of the relic origin of long-term comets, which is based on the fact that at a certain stage in the evolution of the solar system, a disk-formed gas and dust protoplanetary nebula were formed near the protosun. When the dust particles that make up the nebula collided, an accumulation process took place with the formation of larger bodies, called planetesimals, from which the planets were formed. The assumption about the ejection of relict planetesimals outside the solar system was taken by Oort and his followers as the basis for the hypothesis of the relict origin of long-period comets (Oort, 1950; Oort, 1951; Safronov, 1972; Fernandez, 1983).

The mechanism of ejection of such bodies by gravitational perturbations is associated with the angular momentum redistribution. Bodies moving with random velocities along a circular orbit in the direction of the gas-and-dust disk rotation had the highest velocities relative to the Sun. When a body approaches a planet, its relative velocity vector rotates without changing its magnitude. If this rotation occurs in the direction of the planet's orbital motion, the absolute velocity increases. The angular momentum of the body relative to the Sun increases due to the orbital momentum of the planet. Thus, bodies are ejected mainly in the direction of the planet's motion.

These assumptions were the basis for substantiating the presence of a hypothetical swarm of comets at heliocentric distances of about 150,000 AU, which is called the "Oort Cloud". The physical mechanism of the formation of this cloud was not considered by either Oort or his followers. The Oort Cloud model is a spherical region that extends over distances from 50 to 100 thousand AU from the Sun. It is considered as a model of the source of long-term comets reaching the inner region of the solar system.

The cloud itself was not instrumentally observed until 2003, but many indirect facts point to its existence. In March 2004, a team of astronomers announced the discovery of a planet-like object (2003VB12), named Sedna, which moves in a highly elliptical orbit with a period of 10,500 years. The orbit of Sedna lies between 76 AU (perihelion) up to 100 AU (aphelion), which made it possible to attribute this object to the first observed celestial body from the Oort Cloud.

It should be noted that all planets and asteroids within the orbit of Neptune rotate in a plane close to the plane of the ecliptic. The Kuiper Belt is also close to it. At the same time, the Oort cloud can be represented as a sphere surrounding the Sun. It is assumed that between the Kuiper belt and the main Oort Cloud, there is a transition zone to the ecliptic plane. This region is called the Hills belt or the inner Oort Cloud. According to the models, the total mass of the inner Oort Cloud is tens (if not hundreds) of times larger than the outer one.

4.1.6. Possible relation of streaming meteoroids to parent bodies

The meteor complex includes both streaming meteoroids, that is, those belonging to the known meteor showers, and sporadic meteoroids that make up the "meteor background". Classification on this basis is to some extent conditional. More than twenty major meteor showers are known. They are called by the Latin names of the constellations where the radiant is located: Perseids, Lyrids, Orionids, Aquarids, Geminids, etc.

If two or more meteor showers operate in a given constellation at different times, they are designated by the nearest star: γ — Aquarids, γ — Aquarids, γ —

Table 4.1. **Annual meteor showers associated with comets**

Shower name	Date	α,°	δ,°	V, km/s	Parent body
Quadrantids	03.01	231°	+50°	41	Machholts 1986 VIII
Lyrids	22.04	271°	+34°	48	Thatcher 1861 I
η-Aquarids	03.05	336°	0°	66	Halley 1910 II
Diurnal Arietids	07.06	43°	+23°	39	Machholts 1986 VIII
ζ-Perseids	07.06	62°	+23°	27	Enke 1971 II
β-Taurides	29.06	86°	+19°	30	Enke 1971 II
Southern δ-Aquarids	29.07	333°	−16°	41	Machholts 1986 VIII
Northern. δ-Aquarids	12.08	339°	−5°	42	Machholts 1986 VIII
Perseids	12.08	46°	+57°	59	Swift-Tuttle 1862
Daily Sextantides	29.09	152°	0°	32	Phaeton (3200)
Draconids	09.10	262°	+54°	20	21P/ Giacobini-Zinner
Orionids	21.10	94°	+16°	66	Halley 1910 II
Southern Taurids	03.11	50°	+14°	27	Enke 1971 II
Northern Taurids	13.11	58°	+22°	29	Enke 1971 II
Leonids	17.11	152°	+22°	71	Tempel-Tuttle 1866
Andromedidae	27.11	25°	+44°	16	Biel 1846 II
Dec. Phenicides	05.12	15°	−55°	12	Blanpain 1819 IV
Geminids	14.12	112°	+32°	34	Phaeton (3200)
Ursids	22.12	217°	+76°	33	Machholts 1986 VIII

Table 4.2. **Main annual meteor showers associated with asteroids**

Shower name	Date	α,°	δ,°	V, km/s	Parent body
Virginides (complex)	20.03	185...208	–24...+28	14...24	Geographer (1620), 2002 FC, 2003 BD44, 1998 SJ70, 1998SH2
j-Bootids	30.04	224	+48	15	Geographer (1620), Aton (2062)
α-Scorpiids	16.05	243	–21	35	Adonis (2101) or minor planet 2004 BZ74?
χ-Scorpios	28.05...3.06	245	–12	12...14	Apollo (1862)
α-Capricornidae	30.07	307	–10	23	Adonis (2101)
Daily Sextantides	29.09...4.11	152	–2	32	Phaeton (3200)
Northern Taurids	30.10...7.11	54	+21		2004TG10
Geminids	14.12	112	+ 32	34	Phaeton (3200)

Perseids, etc. For some meteor showers, their genetic relationship with comets has been established. Some data on the possible relationship between annual meteor showers and their parent bodies, which are confirmed by different authors, are given in Table 4.1 and Table 4.2 (Babadzhanov, 1991; Hasegawa, 1993; Olsson-Steel, 1988; Porubcan 2004; Porubcan, 2005; Porubcan, 2006; Sekanina, 1970a; Sekanina, 1970b; Sekanina, 1973; Sekanina, 1976; Sokolova, 2016; McKinley, 1961; McKinlay, 1964).

The following designations are used in Table 4.1. Date — the day and month of manifestation of the shower's maximum activity, α — right ascension and δ — radiant declination (in degrees), V — geocentric speed of meteoroids (in km/s). In the column "Parent body", the name of the periodic comet and its symbol are given.

The column "Parent body" contains the name of the asteroid and (in brackets) its ordinal number by the catalog of minor planets.

The data given in the tables are not complete and will undoubtedly be corrected. The International Astronomical Union maintains a register of 713 meteor showers (http://www.astro.amu.edu.pl/~jopek/MDC2007/). Among them, 112 showers are distinguished and considered confirmed, but not all of them (~30) are associated with a possible parent body with a sufficient degree of reliability.

Knowledge of the genetic relationship of meteor showers with the parent body allows us to put forward reasonable assumptions concerning the geocentric velocity and physical and chemical properties of the meteoroid, the ATCH of which is recorded during radar observations (over the period of activity) of the corresponding meteor shower. Based on such information, ATCH catalogs can be created on the basis of signal reflections from meteor trails with a given radiant, which makes it possible to classify meteor trails according to ATCH and create appropriate databases for solving astronomical and telecommunication problems.

4.2. Model of a sporadic meteor complex

The report (Jones, 2004) presents a physics-based parametric model that allows predicting the spatial distribution of meteoroid occurrence frequency and the distribution of their velocities for a sporadic meteor complex. In this model, it is assumed that the main source of meteoroids are short-period comets with an aphelion of less than 7 AU and the contribution of long-period comets and asteroid meteoroids is also taken into account. It is based on radar observations of sporadic meteoroids and focuses on the main component, which is the meteoroid mass range of 10^{-5}—1 g.

Despite a number of assumptions, the model can be considered quite reliable, since it allows predicting the distributions of radiants and velocities that correspond quite well to the distributions of sporadic meteors observed from the Earth. Fig. 4.3 illustrates the results of modeling the predicted distribution of radiants and velocities (km/s) of meteoroids included in the sporadic meteor complex.

Based on the data presented in (Jones, 2004), it can be concluded that the model is essentially correct. However, the degree of agreement between the theory and the results of radar observations (after appropriate fitting of the model parameters) depends on many assumptions made.

The most comprehensive studies of the distribution of sporadic meteor complex (SMC) radiants have been carried out using:

- Canadian meteor orbital radar CMOR;
- specialized Australian orbital system SAAMER;
- Middle and Upper Atmosphere Radar MU, Kyoto University (Japan).

The results of radar measurements presented in Fig. 4.3 demonstrate the possibility of using the SMC model, which includes six main sources of sporadic meteoroids:

- north and south apex (NA and SA);
- northern and southern toroidal (NT and ST);
- helion (H);
- antihelion (AH).

A ring structure of radiants, weakly relative to other sources of the SMC, was also recorded as located approximately 55° around the apex, which varied in strength during the year.

To simplify the SMC model, a two-dimensional Gaussian approximation is often used. In this case, it is necessary to estimate the parameters of the radiant scattering ellipse for ecliptic longitude λ and ecliptic latitude β. Table 4.3 shows the results of estimates of the ecliptic coordinates of the main SMC sources and scattering parameters presented in (Campbell-Brown, 2006; Wiegert, 2009; Galligan, 2005; Chau, 2007; Brown, 1995; Jones, 2005).

Focusing on these data and combining with the results of mapping the annual distribution of SMC radiants (Fig. 4.4), Fig. 4.5 presents a map version of

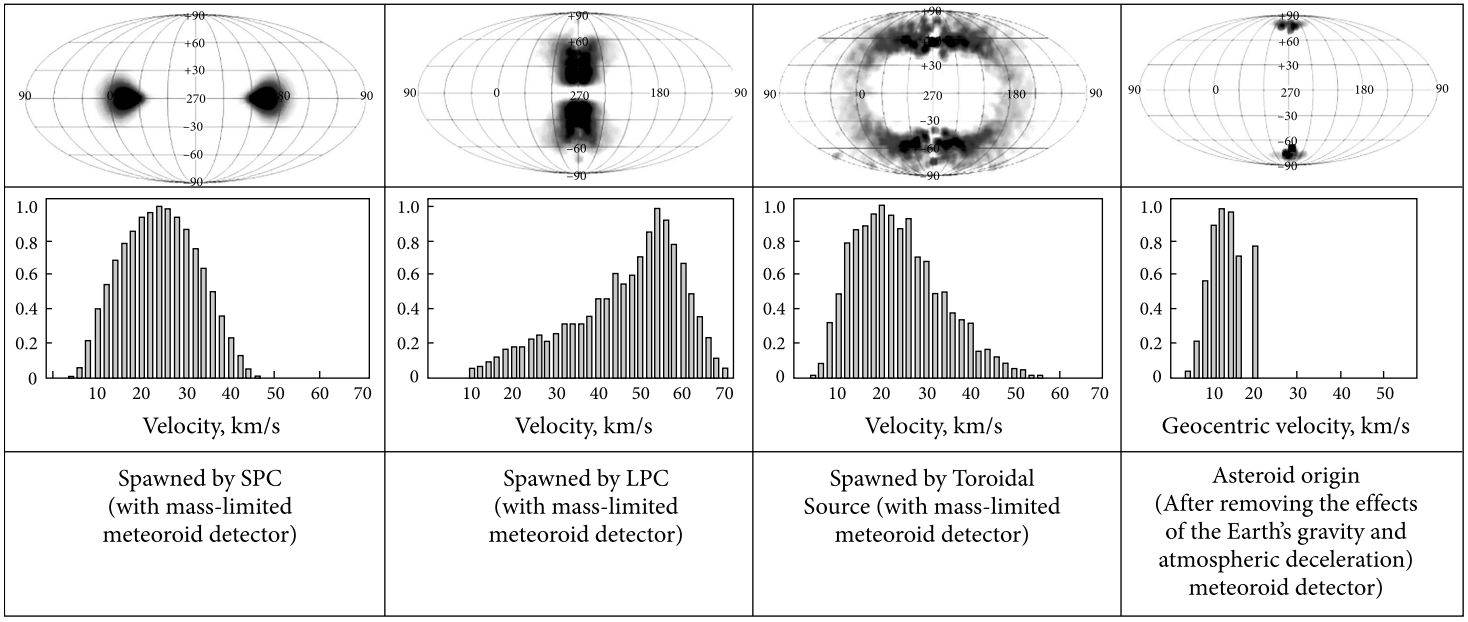

Fig. 4.3. Simulation results illustrating the predicted distribution of radiants and velocities of meteoroids included in the sporadic meteor complex. Designations used: SPC — Short-Period Comets; LPC — Long-Period Comets (taken from (Jones, 2004))

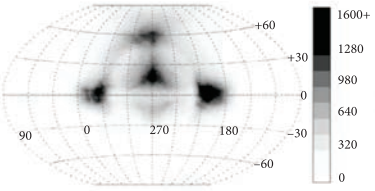

Raw Northern Hemisphere SMC radiant distribution from CMOR radar site (Campbell-Brown, 2008)

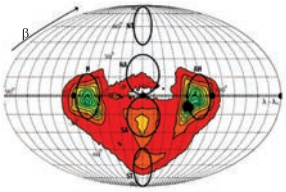

Southern hemisphere SMC radiant distribution obtained from the SAAMER-OS radar site (Janches, 2019)

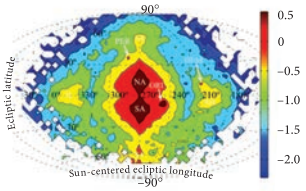

Distribution of SMC radiants of the Northern and Southern hemispheres obtained from the MU radar site (Kero, 2012)

Fig. 4.4. Results of radar measurements of SMC sources. When presenting the distribution of radiants obtained on the SAAMER-OS and MU sites, the wavelet transform was used

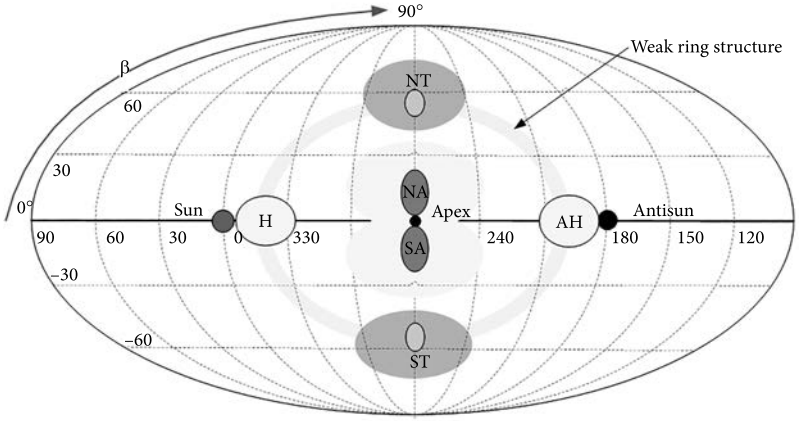

Fig. 4.5. A variant of the map of the annual distribution of radiants of six main sources and a weak ring structure of the sporadic meteor complex: H — Helion; AH — Anti–helion; NA, Northern Apex; SA, South Apex; NT — Northern Toroidal; ST — South Toroidal

Table 4.3. Results of estimates of the ecliptic coordinates of the main SMC sources

Source	$\lambda-\lambda_0$	β	Δλ	Δβ
North Apex	270	18	21	12
Apex	271	−10	19	16
South Apex	260	−32	19	12
Helion	340…342	0. 3…−15	15…19	10…24
Anti-helion	193…202	0. 2…−11	15…18	10…24
Northern Toroidal	275	56	13	9
Southern Toroidal	270…274	−55…−60	15…16	10…16

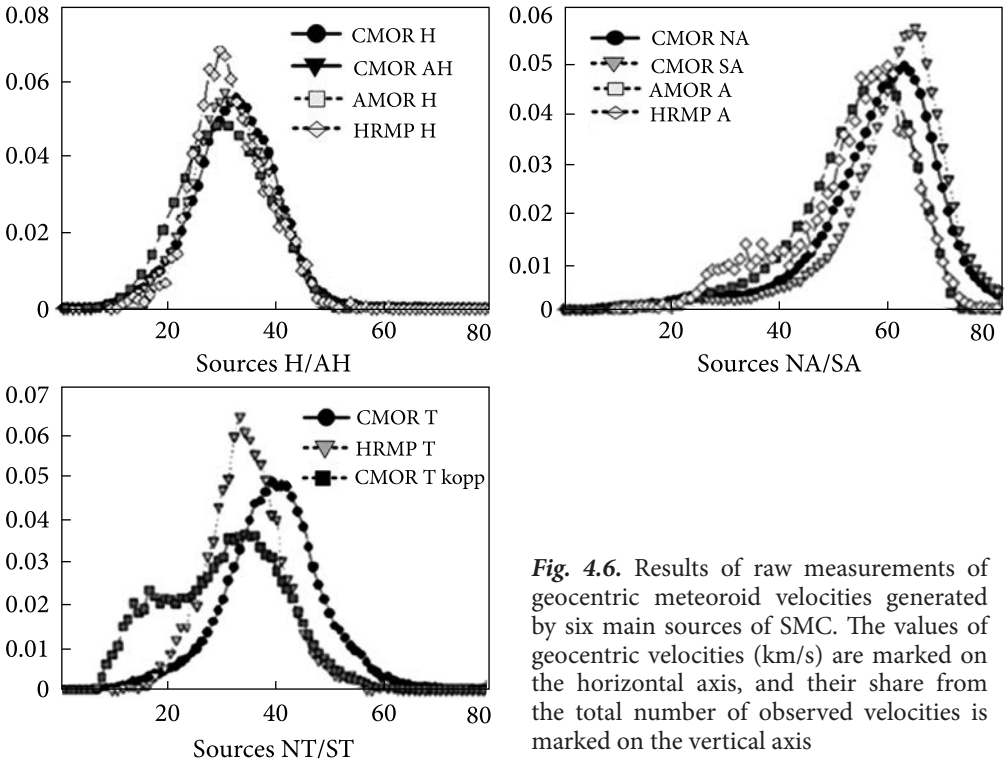

Fig. 4.6. Results of raw measurements of geocentric meteoroid velocities generated by six main sources of SMC. The values of geocentric velocities (km/s) are marked on the horizontal axis, and their share from the total number of observed velocities is marked on the vertical axis

the annual radiants distribution for six main sources and the ring structure of the SMC, where a two-dimensional Gaussian approximation is used.

Fig. 4.6 summarizes the results of raw measurements of geocentric velocities of meteoroids generated by six main sources of SMC presented in (Jenniskens, 2006).

Meteoroids from apex sources have velocities close to 70 km/s when the radiants are located near the ecliptic and about 45 km/s if they are at the northern and southern extreme points. The Helion and Anti-Helion sources show the greatest variation, from about 20 km/s to 45 km/s closer to the apex. The geocentric velocities of meteoroids from the northern and southern toroidal sources are almost uniformly distributed within the indicated zones and equal about 35 km/s.

The Apex sources (NA and SA) mainly consist of meteoroids in retrograde orbits from Halley's comets and long–period comets with orbital inclinations of ~15° above and below the ecliptic plane. From the side of the apex, the meteoroids of this source enter the atmosphere at velocities of ~60 km/s. The results of studies on the apex sources of SMC are presented in a number of works (Campbell-Brown, 2008; Jenniskens, 2006; Nesvorný, 2011; Taylor, 1997; Jones, 1993).

Sources of Helion (H) and Anti-Helion (AH). Meteoroids appearing in the Anti-Helion and Helion regions have orbits similar to those of short-period comets, as well as some Earth-crossing asteroids. They may have originated from comets of the JFm family with a period of below 20 years in prograde orbits. The

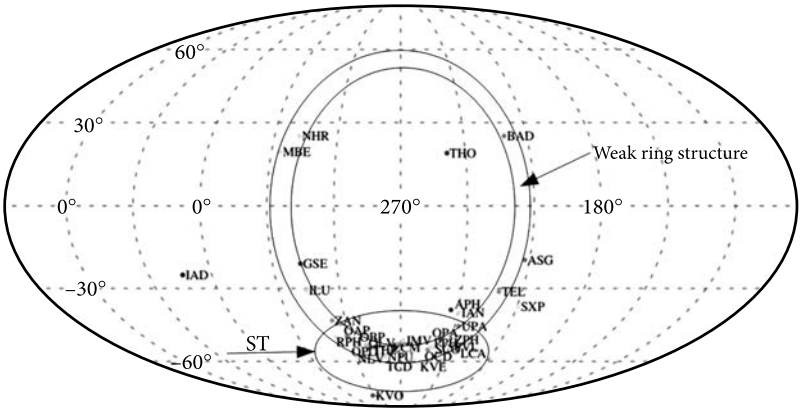

Fig. 4.7. Radiants of identified meteor showers detected by SAAMER-OS, confirmed by the data collected up to 2015

speeds of meteoroids from these sources are noticeably lower than those of apex meteoroids: most of them have velocities of ~12—45 km/s.

Toroidal sources (NT, ST) are observed at high latitudes (~60°) and are the least studied. Northern and southern toroidal meteoroids move in almost circular orbits at large angles relative to the ecliptic plane and have an average observed speed of ~35 km/s (Wiegert, 2009; Campbell-Brown, 2009).

In some papers, apex and toroidal sources are associated with long-period comets such as Halley-type comets and Oort cloud comets (eg (Wiegert, 2009)).

Sources of the SMC ring structure. When modeling the SMC (Campbell-Brown, 2008) and (Wiegert, 2009), it was concluded that the origin of the ring structure can be explained by cosmic dust (micrometeoroids) with a high inclination of orbits, whose radiants, under the influence of the Poynting-Robertson drag and the Kozai effect, grouped between 50 and 60°.

At the same time, the results of mapping meteor showers detected by an SAAMER-OS radar (Fig. 4.7) (Janches, 2019) demonstrate a clear relationship between the radiants of meteoroids of the ring structure and SMC toroidal sources with quite specific meteor showers with geocentric velocities in the range of 35—40 km s^{-1}. This confirms the need for further study of these SMC sources and the relationship between meteoroids generated by them and parent bodies.

4.3. Seasonal and diurnal variation in the count rates of meteor trails having a specular reflection point

The probability of the appearance of meteor trails with a specular reflection point depends on the time of year and day, as well as on the geographical location of the transmission and reception sites.

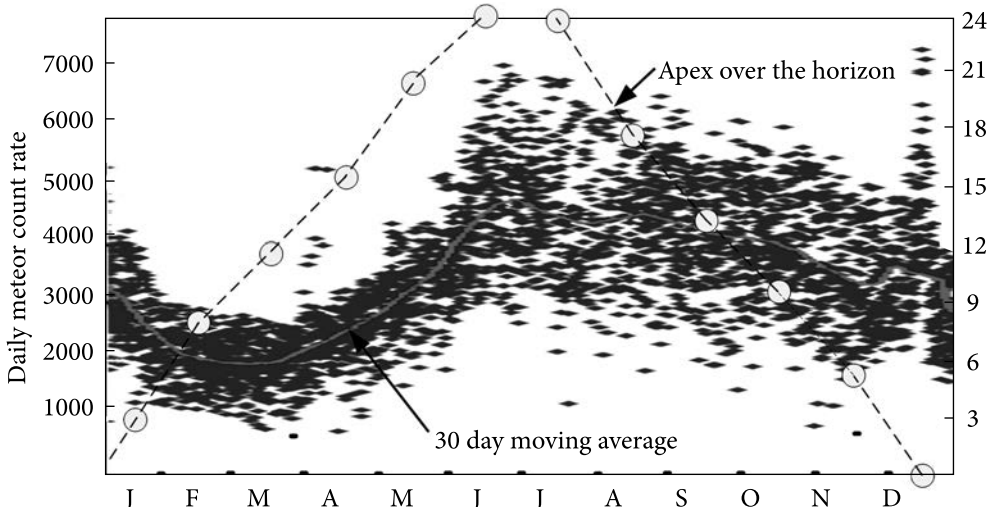

Fig. 4.8. Annual cycle of change in the daily meteor count rates at the Esrange point, observed in 1999—2008 (Pokorný, 2014). Months on the horizontal axis, daily meteor count rates on the vertical axis. The duration (in hours) of the Apex being above the horizon on the 15th day of each month is shown by a dashed line

The annual cycle of track count rates is the result of rising and setting visible sources of sporadic meteors, which depend on the geographic latitude. Fig. 4.8 shows the annual cycle of changes in the daily meteor count rates at the Esrange point, which has the coordinate 67.8°N (slightly above the Arctic Circle) observed in 1999—2008 (Younger, 2009). The same figure shows the duration (in hours) of the Apex being above the horizon on the 15th day of each month.

The contribution of the apex source of the SMC is significant; however, it is also necessary to consider other sources of the SMC. For example, in December, the apex is below the horizon, and the NA source can only be observed at very low elevation angles. This significantly reduces the daily count rates of meteors observed from this source. At the same time, the observed meteor count rates significantly exceed the average value.

A detailed analysis of the characteristics of the main sources of SMC, performed in (Younger, 2009), is illustrated by Fig. 4.9.

The figure shows the hourly meteor count rates observed at Esrange in January and July 2004 and the corresponding elevation angles of the six main SMC regions. Comparing these data, we can conclude that the high count rate is provided by SMC sources that have elevation angles from 20 to 40 degrees. The lowest count rates are observed when all sporadic sources are either below or close to the local horizon (at about 17:00 local time). Thus, the hourly meteor count rate is directly related to the elevation angles of the radiants, which determines their seasonal and daily dependence. It should also be noted that many of the meteoroids that have low elevation angles lose most of their mass before they are detected.

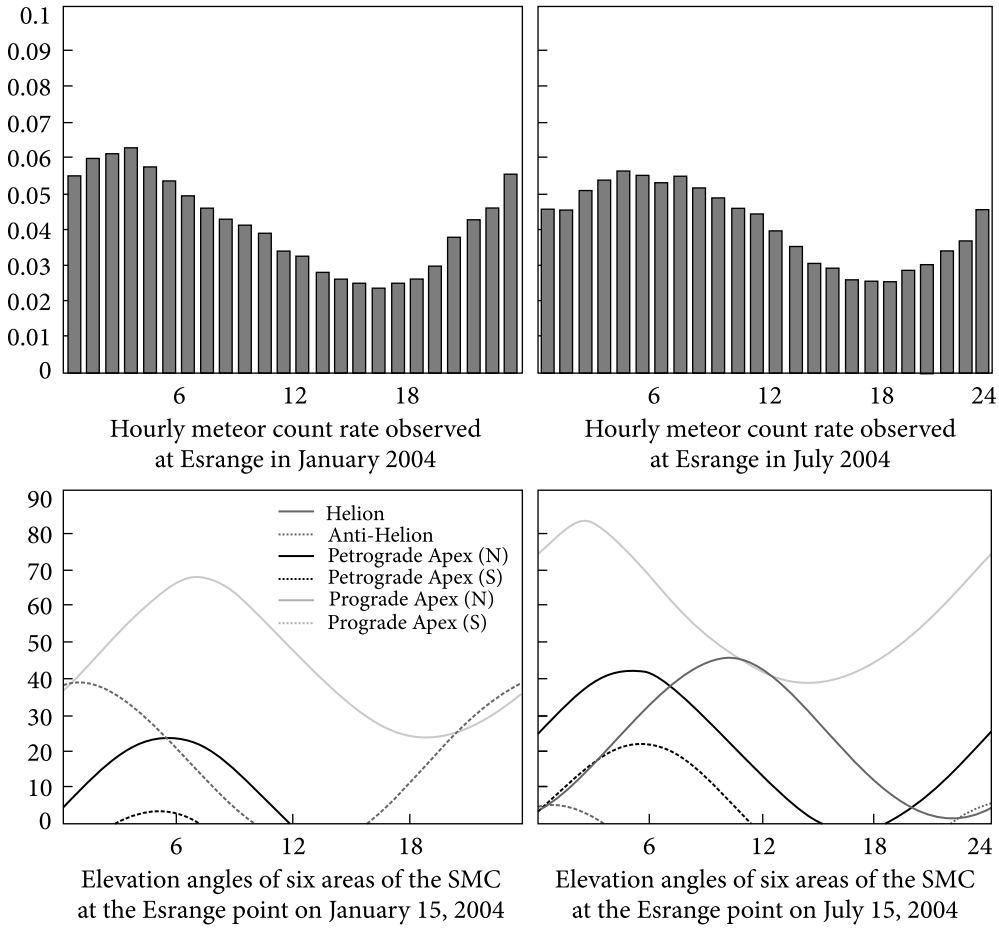

Fig. 4.9. Hourly meteor count rates observed at Esrange in January and July 2004 and corresponding elevation angles of six SMC regions. The horizontal axis shows universal time, and the vertical axis shows the height of the source h, expressed in angular measure ($h = 90^\circ - z$, where z is the zenith angle)

The radio visibility and elevation angles of the main SMC sources depend significantly on the coordinates of the observation points. Fig. 4.10, taken for illustration from (Younger, 2009), shows the seasonal change in the meteor count rates for observation points located at Esrange (67.88°N, 21.10°E), Ascension Island (7.9°S, 14.4°E), and Rothera (66.6°S, 68.1°E).

The presented results demonstrate a clear dependence of the meteor count rates on latitude (which is expected) since the elevation angles of the SMC radiants above the local horizon have a latitudinal dependence.

The distribution of SMC radiants obtained taking into account the position of the Earth as it moves along the ecliptic is very clear. For the northern and southern hemispheres, the average monthly distributions of SMC radiants are

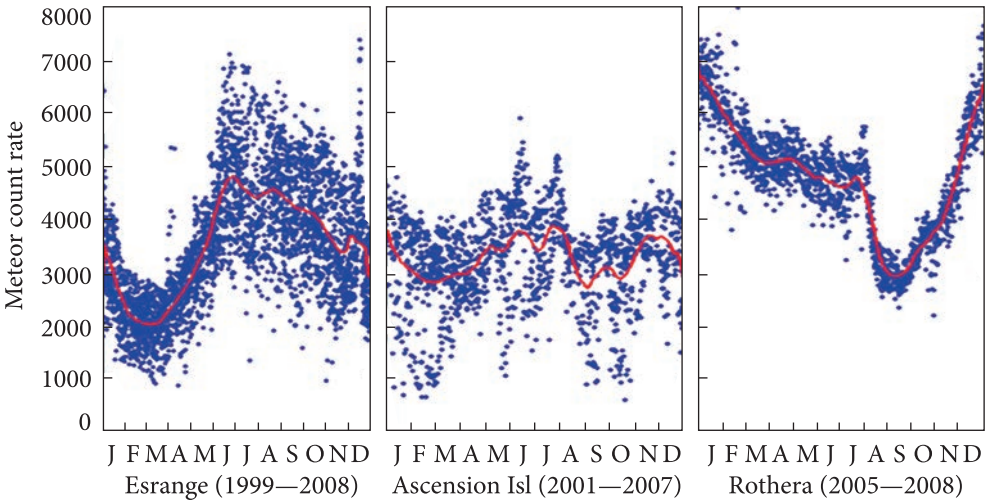

Fig. 4.10. Seasonal change in meteor count rates for observation points located at Esrange (67.88°N, 21.10°E), Ascension Island (7.9°S, 14.4°E), and Rothera (66.6°S, 68.1°E)

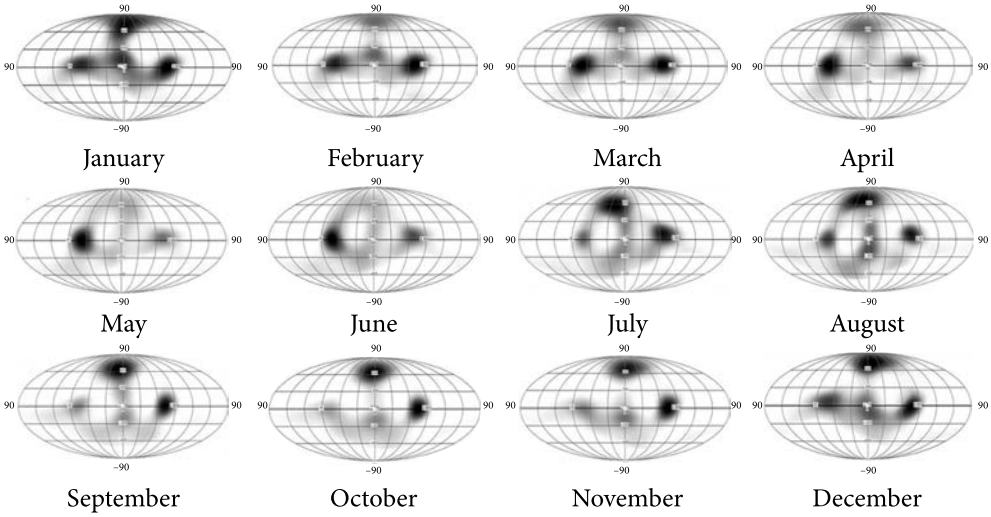

Fig. 4.11. Map of seasonal changes in the density of SMC radiants of the northern hemisphere in the apex plane of the geocentric ecliptic coordinate system (Campbell-Brown, 2006)

presented in (Campbell-Brown, 2006; Campbell-Brown, 2009; Galligan, 2005; Schult, 2018; Younger, 2009).

As an example, Fig. 4.11 shows a map of the seasonal variation of the SMC radiant density of the northern hemisphere in the apex plane of the geocentric ecliptic coordinate system, obtained as a result of observations using Canadian CMOR radar in the period from 2002 to 2005 (Campbell-Brown, 2009). Similar data are available for the southern hemisphere (Younger, 2009).

This figure clearly shows the seasonal change in the density of radiants, for which a specular reflection from the ionized trail is observed, which is confirmed by the results of radar measurements.

To predict the frequency of occurrence of IMTr belonging to the main sources of SMC or meteor showers and having a specular reflection point, it is necessary:

1. Use statistical data on the distribution of their radiants in the process of the Earth's movement in its orbit, which can be represented in the ecliptic geocentric coordinate system centered to the Sun.
2. Take into account the epoch (year, date, and time) of observation.
3. Take into account the geographical coordinates of observation points, and in the case of bistatic scattering of radio waves (two-position radar), to take into account the geometry of the path (coordinates of the path center, azimuth, and length).

The question of the influence of the state of the ionosphere in the meteor zone on the characteristics of trail detection remains open. Moreover, even less studied is the effect of seasonal and diurnal changes in the ionization and turbulence of the atmosphere in the meteor zone, as well as solar activity, which has an 11-year periodicity, on the observability of meteor trails.

4.4. Conclusions

The study of the main sources of SMC and meteor showers allows us to make reasonable assumptions about the genetic relation**shi**p of the meteoroid that created the ionized trail with the parent body and, as a result, assumptions about the physicochemical properties of the meteoroid. This is of interest both to astronomers and astrophysicists, as well as to specialists in the field of telecommunications.

The construction of a radiant density distribution map (for sporadic sources and meteor showers) is based on a physically and astronomically reasonable parametric model of the SMC, as well as the results of radar observations. The radiant density distribution map serves as the basis for developing a predictive (probabilistic) model for observing ionized trails, which takes into account the Earth's orbital motion and axial rotation. Such a model, with given coordinates of observation points and observation time, makes it possible to predict seasonal and diurnal variations in the frequency of occurrence of meteor trails with a specular reflection point belonging to the main SMC sources and meteor showers.

Due to the incompleteness of the initial data, the radiant density distribution map and the prognostic model need to be corrected when new observational data become available. To correctly interpret the results of observations, one should take into account the location and technical characteristics of the radar systems through which these data were obtained.

When developing a more precise map of the radiant density distribution of the main SMC sources, attention should be paid to supplementing it with data

on the distribution of meteoroid velocities, their density, and probable chemical composition.

The effect of seasonal and diurnal changes in atmospheric density, the degree of ionization and turbulence in the meteor zone, as well as solar activity on the trail detection characteristics, should also be taken into account.

The amount of computation required to implement a predictive model for the appearance of ISLMs associated with a given radiant is very large and requires the development of special software.

The possibilities of practical use of the predictive model by astronomers and specialists in the field of telecommunications are described above. We would like to draw attention to the possibility of using it to classify the observed ATCH signals reflected from the meteor trail. Reasonable assumptions about the SMC sources or the radiant of the meteor shower provide additional information for the development of a radiophysical model of signal scattering on the ionized meteoroid trail. This makes it possible to classify the meteor trail according to ATCH and create appropriate databases for solving astronomical and telecommunication problems.

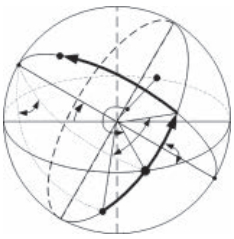

SECTION 5

BISTATIC SIGNAL SCATTERING ON IONIZED METEOROID TRAIL

In this section, the main attention will be paid to the study of the bistatic scattering of radio signals on an ionized meteoroid trail (IMTr). This is because the construction of networks for transmitting information via meteor radio channels is based on this principle. In addition, the ATCH of the signal scattered on the meteor trail implicitly contains information about both the genetic relationship of the meteoroid with the parent body and the physicochemical properties of the meteoroid that formed this trail, as well as information about the state of the atmosphere at the height of the trail formation. It should be taken into account that, depending on the path geometry, for meteoroids identical in all parameters, different ATCH and PTR of scattered signals can be observed.

Knowledge of the height of the specular reflection point and the velocity of the meteoroid, obtained as a result of measurements or predicts, opens up additional possibilities for extracting information about the meteoroid and the geophysical parameters of the atmosphere. The solution to this problem is complicated by the fact that it cannot be solved using only statistical processing of the results of observations due to the uncontrollability of the initial data. This implies the need to use predictive models that determine the probability of occurrence of meteor trails with a specular reflection point, as well as radiophysical scattering models that adequately describe the ATCH and PTR radio reflections from meteor trails.

Fig. 5.1 gives a fairly general geometric representation of bistatic scattering by IMTr in the flat Earth approximation. Here the XY plane is perpendicular to the radius of the Earth at the middle of the path and passes through the transmission and reception points. The meteoroid trail is in the plane tangent to the ellipsoid surface, and the specular reflection point coincides with the contact point. The sphe-

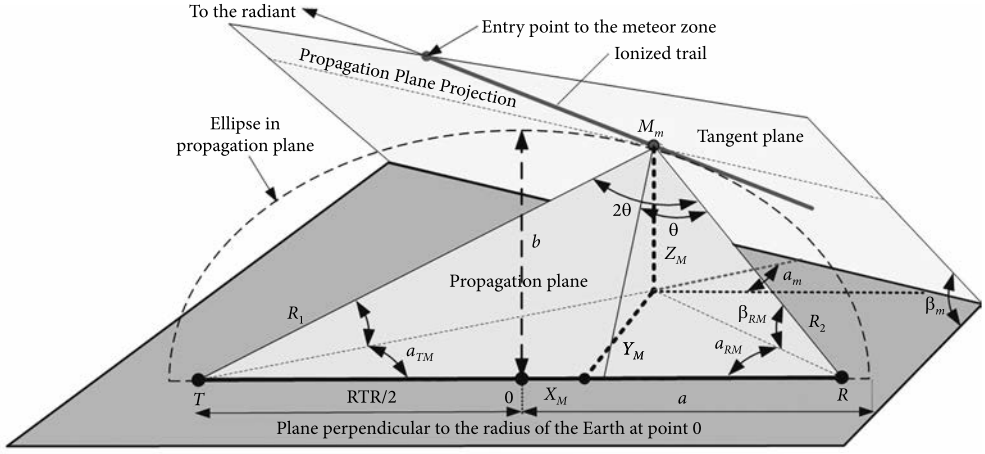

Fig. 5.1. Geometric representation of bistatic scattering on an ionized meteoroid trail

ricity of the Earth's surface was not taken into account, its influence will be considered below.

Fig. 5.1 uses the following notation: *T* and *R* are transmission and reception points, which are the foci of the ellipsoid determined by the corresponding geographical coordinates; R_{TR} is the distance between the transmitting and receiving antennas (interfocal distance for an ellipsoid, on the surface of which there is a specular reflection point); R_1 and R_2 are the distances between the transmitting antenna and specular reflection point Mm and the receiving antenna and specular reflection point, respectively; θ is the scattering angle depending on the position of M_m on the ellipsoid surface; *a* is the semi-major axis of the ellipsoid, on the surface of which there is a specular reflection point; *b* — semi-minor axis of the ellipsoid, on the surface of which there is a specular reflection point; β_{TM} and α_{TM} are the values of elevation and azimuth relative to the plane on which the specular reflection point is observed from point *T*; β_{RM} and α_{RM} are the values of elevation and azimuth relative to the plane on which the specular reflection point is observed from point *R*; X_M, Y_M, Z_M are the coordinates of the specular reflection point on the *XY* plane and the *Z* axis is perpendicular to it; αm is the azimuth angle of the meteor trail in the tangent plane perpendicular to the propagation plane, on which the dimensions of the first Fresnel zone depend.

H_M *is* the height of the specular reflection point above the Earth's surface, on which such important trail parameters as the initial radius r_0, linear electron density αe, and diffusion coefficient D of the ionized trail depend.

Obligatory conditions for observing radio reflection from the ionized trail of a meteoroid are:

- Presence of a SRP located within the meteor zone, which is usually taken to be 80...130 km from the Earth's surface.

- Finding the coordinates of the SRP within the radio visibility zone.
- Sufficiency of the energy potential of the radio link for reliable reception of the reflected signal.

5.1. Determination of the radio visibility zone of the meteor trail

Obviously, when observing meteor trails, it is necessary to take into account only that region of space that is simultaneously visible from the transmission and reception points (the radio visibility zone). It is a part of the sphere bounded by planes tangent to the Earth's surface at the points of transmission *T* and reception *R*. The intersection of these planes with the boundaries of the meteor zone form circles with a radius R_{RV}. Since the Earth is not a perfect sphere, its radius varies slightly depending on the geographic coordinates of the points. We will use the average value of the radius, which, by the WGS-84 standard (World Geodetic System 1984), is approximately equal to $R_{E\,WGS} = 6371$ km. This approximation allows an error in determining the value of R_E not exceeding 0.5%. If more accurate measurements are required, local values of the radius of curvature determined for the given coordinates of points *T* and *R* can be used (Yakimchik, 2019; NGA Standardization Document, 2014; International Civil Aviation Organization, 2002).

Fig. 5.2 for the XZ plane presents the data necessary to illustrate the calculation of the radio visibility zone and the height of the specular reflection point above the Earth's surface. In this case, the phenomena of refraction of radio waves at the entry into the troposphere and ionosphere, which affect the main characteristics of the radio visibility zone, are temporarily not taken into account. The distances R_{RV} to the upper and lower boundaries of the meteor zone (circle radii)

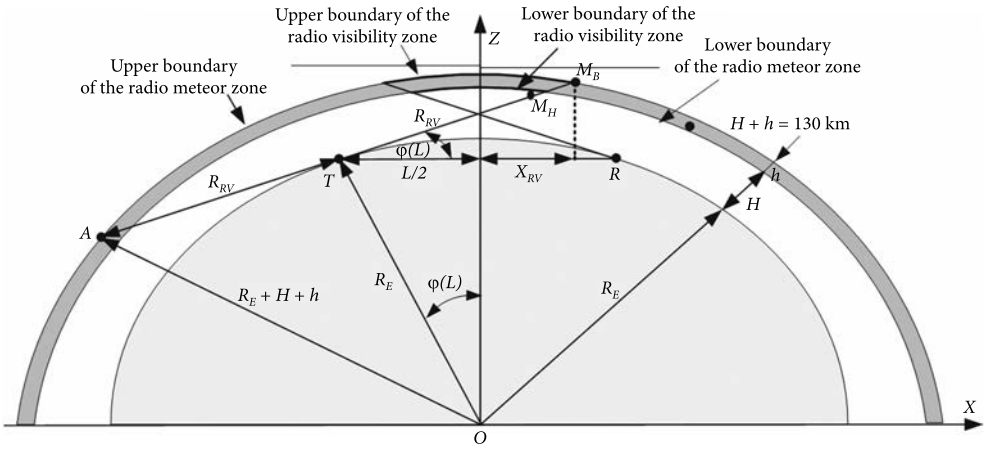

Fig. 5.2. Determination of the radio visibility zone of a meteor communication system without taking into account the refraction of radio waves in the troposphere and ionosphere

are determined by the expressions:

$$R_{RVH} = \sqrt{\left(R_{E\,WGS} + H + h\right)^2 - R_{E\,WGS}^2}\,, \tag{5.1}$$

$$R_{RVL} = \sqrt{\left(R_{E\,WGS} + H\right)^2 - R_{E\,WGS}^2}\,. \tag{5.2}$$

If the location of points T and R is given by geographical coordinates, the distance between them along the surface of the Earth can be determined using the formula:

$$L_{TR} = 2R_{E\,WGS}\arcsin\left(\sqrt{\sin^2\left(\frac{\varphi_2 - \varphi_1}{2}\right) + \cos(\varphi_1)\cos(\varphi_2)\sin^2\left(\frac{\lambda_2 - \lambda_1}{2}\right)}\right), \tag{5.3}$$

where φ_1 and λ_1 — the latitude and longitude of point T (with a plus sign for the north latitude and east longitude and a minus sign for the south latitude and west longitude), degrees; φ_2 and λ_2 — the latitude and longitude of point R, degrees.

With a known (calculated) distance along the Earth's surface, the shortest distance (the chord of a circular arc) between points T and R can be determined using the relationship:

$$R_{TR} = 2R_{E\,WGS}\sin\left(\frac{90L_{TR}}{\pi R_{E\,WGS}}\right). \tag{5.4}$$

From expresion (5.4) it follows that for L_{TR} = 1000 km, the difference between L_{TR} and R_{TR} is 1.026 km. In many cases this diference, is neglected.

The projection of the area of intersection of planes tangent to the Earth's surface at points T and R with the spherical surface of the upper boundary of the meteor zone on the XY plane is shown in Fig. 5.3, where X_{RV} and Y_{RV} are the extreme points of this area along the X and Y axes, respectively.

The extreme points of this area can be calculated by solving the system of equations

$$\begin{cases} \left(x - \dfrac{R_{TR}}{2}\right)^2 + y^2 = R_{RV}^2\,, \\ \left(x + \dfrac{R_{TR}}{2}\right)^2 + y^2 = R_{RV}^2\,. \end{cases} \tag{5.5}$$

from which it is easy to obtain

$$\pm X_{RV} = R_{RV} - \frac{R_{TR}}{2}, \tag{5.6}$$

$$\pm X_{RV} = R_{RC} - \frac{R_{TR}}{2}. \tag{5.7}$$

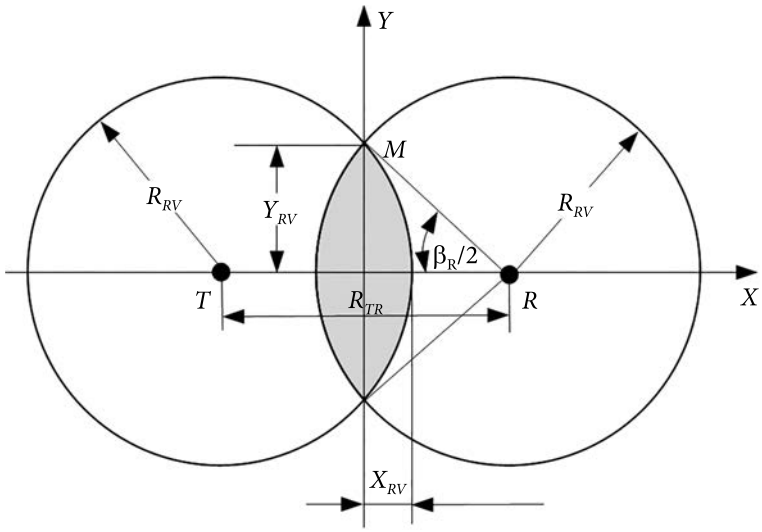

Fig. 5.3. Projection of the radio visibility zone on the XY plane

It is of interest to estimate the projection area of the radio visibility zone on the XY plane, in proportion to which the volume of the meteor zone changes, which is available for observing reflections from meteor trails. It can be shown that the area S_{PB} is equal to:

$$S_{RV} = R_{RV}^2 \left[2\arcsin\left(\sqrt{1-p^2}\right) - p\sqrt{1-p^2} \right], \tag{5.8}$$

where arcsin is calculated in radians and $p = R_{TR}/2R_{RV}$.

Table 5.1 presents data on the extreme points of the radio visibility zone and the area of its projection on the XY plane calculated by formulas (6.5), (6.6) and (6.7) for radio links of various RTR lengths under the condition that the upper boundary of the meteor zone is at an altitude of 130 km. The refraction

Table 5.1. **Data on the extreme points of the radio visibility zone and its areas for radio links of various lengths, obtained without taking into account the refraction of radio waves ($R_{E\,WGS}$ = 6371 km, R_{RV} = 1283.6 km).**

R_{TR}, km	Y_{RV}, km	X_{RV}, km	$S_{RV} \cdot 10^6$, km^2	R_{TR}, km	Y_{RV}, km	X_{RV}, km	$S_{RV} \cdot 10^6$, km^2
0	1293.6	1293.6	5.257	1500	1054.0	543.6	1.639
250	1287.5	1168.6	4.638	1750	952.8	418.6	1.085
500	1269.2	1043.6	4.022	2000	820.6	293.6	0.565
750	1238.0	918.6	3.411	2250	638.5	168.6	0.105
1000	1193.0	793.6	2.808	2500	333.0	43.6	0.001
1250	1132.6	668.6	2.215				

of radio waves at the entry into the troposphere and ionosphere was not taken into account.

The refraction of radio waves in the troposphere and, to a lesser extent, in the ionosphere leads to variations in the radio visibility zone. These changes have a seasonal and daily dependence, which must be taken into account when interpreting the results of observations. The standard refraction is the most common case, due to the average state of the troposphere, for which it is believed that the refractive index n varies with height by a linear law. In this case, the equivalent radius of the Earth ($R_{R\,EQV}$) is often used for calculations, which is determined by the ratio:

$$R_{R\,EQV} = \frac{R_{R\,WGS}}{1 + R_{R\,WGS}\, dn/dh}, \tag{5.9}$$

which for $dn/dh = -4 \cdot 10^{-5}$ km $^{-1}$ yields $R_{R\,EQV} \sim 8550$ km.

Refraction close to the standard is observed more often in the daytime. Increased refraction is most often noted in the evening, night, and morning hours of the summer months, and sometimes at the same hours in spring or autumn.

Calculations of the radio visibility zone taking into account refraction can be performed on the basis of formulas (5.1)—(5.7), where $R_{E\,WGS} = 6371$ km should be replaced by $R_{R\,E\,QV}$, calculated by expression (5.9). If it is necessary to calculate the equivalent radius of the Earth more accurately, one can use the results of (Handbook on Radiometeorology, 2013; Handbook on Radiometeorology, 2015), where refraction in the troposphere and ionosphere is taken into account.

5.2. Predictive model for observing ionized meteoroid trails

The value of the probability of the appearance of an ionized trail in the radio visibility zone with SRP and parameters that provide the possibility of transmitting information through a radio channel cannot be obtained using only statistical processing of the results of radar measurements because of the uncontrollability of the initial data. This determines the need to develop a predictive model that makes it possible to estimate the probability of the appearance of meteor trails with SRP and trail parameters that ensure the reception of the reflected radio signal with a required quality.

A predictive model of the frequency of IMTr observations belonging to the main sources of SMC or meteor showers will provide the ability to:

1. Calculate the coordinates and height of the SRP at given trail radiants, which makes it possible to predict the main trail characteristics used to estimate the energy potential of the radio link.

2. Make reasonable assumptions about the genetic relation of the meteoroid that generated the ionized trail to the parent body and, as a result, assumptions about the physicochemical properties of the meteoroid.

3. Obtain additional data necessary for the classification of the observed meteoroid by the ATCH of the signal scattered on the trail.

4. Optimize the pointing of transmitting and receiving antennas in the zones of the most probable occurrence of trails for a given set of meteoroid entry points into the meteor zone and the predicted zenith angle and azimuth of the trail and, thereby, ensuring the maximum throughput of meteor radio communication systems. Calculation of "hot zones" is especially relevant when choosing the location of base stations in the course of designing meteor radio communication networks and can also be used when choosing the observation time and points of transmission and reception for radio astronomy observations.

5. Optimize the information transfer protocol for meteor radio communication based on the data on the time of the trail appearance and the features of the initial segment of the scattered signal ATCH.

The initial data for building a predictive model are:

- The radiant coordinates of the supposed SMC source or meteor shower are given in the apex plane of the ecliptic geocentric coordinate system. The chosen radiant suggests the possibility, with some a priori probability, suppose the origin of the meteoroid, and, consequently, its velocity and chemical composition.
- The time of observation of the reflected signal (year, month, day, and local time) required for the subsequent coordinate transformation.
- The geocentric (geographical) coordinates of observation points, allowing the determination of the route center coordinates, azimuth, and the length of the radio link.

The calculation algorithm that implements the predictive model for the appearance of IMTr associated with a given radiant involves the following actions:

1. Based on the radiant $(\lambda - \lambda_0, \beta)$ specified in the apex plane of the ecliptic geocentric coordinate system and the date of observation, calculate its coordinates in the ecliptic geocentric coordinate system. To do this, it is necessary to add the longitude of the Sun $\boldsymbol{\lambda_0}$ on a given date to the centered longitude (see expressions (2.13—2.15)).

2. Perform the transition from the ecliptic geocentric coordinate system to the equatorial system (see expression (2.12)). In this case, we obtain the coordinates for a given radiant (α, δ).

3. Taking into account the geocentric coordinates of observation points, as well as the date and time of observation, perform the transition from the equatorial coordinate system to the horizontal one (see expression (2.10)). In this case, we obtain the value of the zenith angle and azimuth (z, A) for a given radiant at a given time.

4. By changing the observation time, obtain the dependence of the zenith angle and azimuth on the local time (z (t), A (t)) for the radiant of the supposed SMC source or meteor shower.

5. By setting the coordinates of the meteoroid entry point to the meteor zone, check the presence of the specular reflection point and its coordinates within the

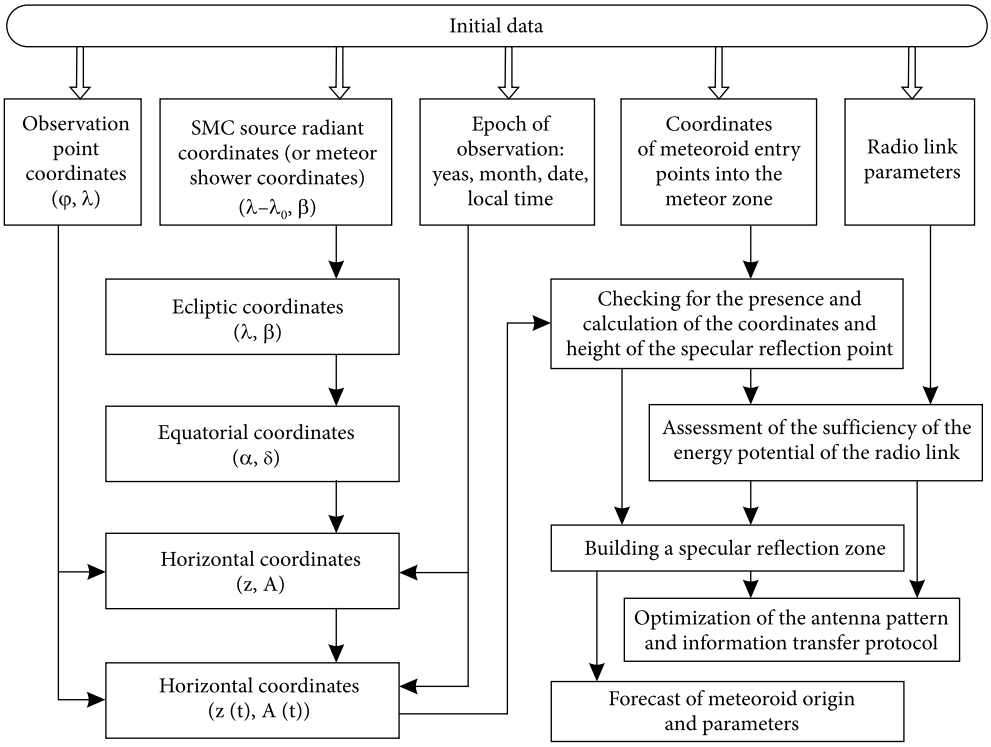

Fig. 5.4. Graphical representation of the calculation algorithm that implements the predictive model for IMTr with a given radiant

meteor zone. The conditions for observing the reflection and the expected height of the specular reflection point will be determined later.

6. Performing the above actions for a given set of meteoroid entry points into the meteor zone, obtain a geometric representation of the zone within which the reflection from IMTr with a given radiant is observed.

The geometric representation of the area within which the reflection from IMTr with a given radiant is observed makes it possible to determine the width of the RP antennas at the transmitting and receiving points and to point them to this area. The observation of a trail within a given zone suggests the possibility, with some a priori probability, to determine the origin of the meteoroid, and, consequently, its velocity and chemical composition.

The calculation algorithm that implements the predictive model is graphically presented in Fig. 5.4.

When choosing the entry points of a meteoroid into the meteor zone, it is necessary to conditionally divide the spherical surface limiting the radio visibility zone into surface elements with an equal area covering the surface in such a way that the distances between the centers of neighboring elements are the same. In this case, in an aggregate, they will represent the densest stacking of hexagonal ele-

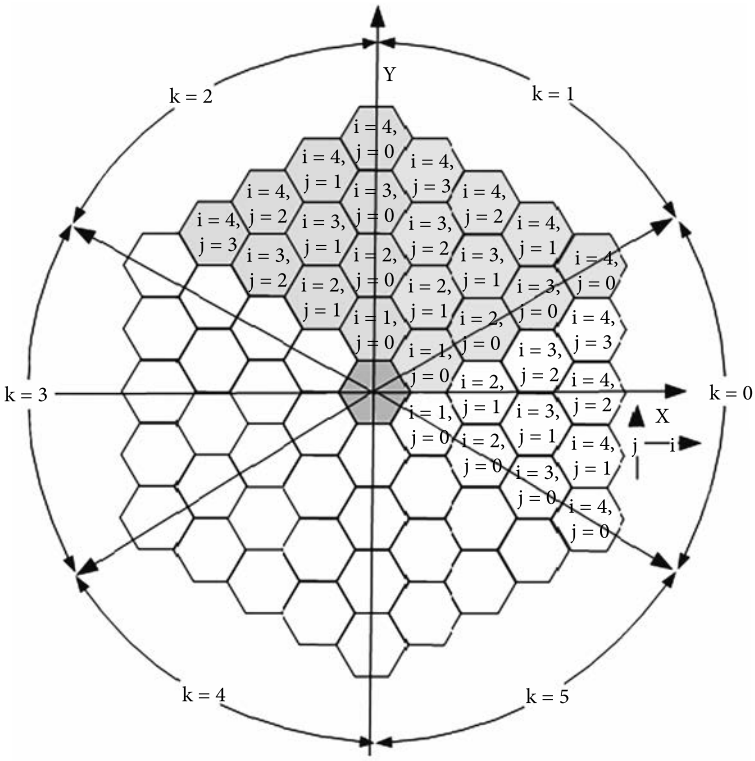

Fig. 5.5. The densest stacking of a set of regular hexagons on the XY plane aligned with the Earth center

ments on the spherical surface of the upper boundary of the radio visibility zone. This problem was solved in (Kharchenko, 2012a; Kharchenko, 2012b; Kharchenko, 2012c) by the method of projecting the densest stacking from a plane onto a sphere. Fig. 5.5 shows the densest stacking of a set of regular hexagons on the XY plane, aligned with the center of the Earth.

As a result of projection, the centers of each ji–th hexagon in the spherical coordinate system are determined by the relations:

$$\varphi_{ji} = arctg\frac{2\left(j-\frac{i}{2}\right)}{i\sqrt{3}} + k\cdot\frac{\pi}{3},\ i=1,2,...,N,\ j=0,1,2,...,(i-1),\ k=0,1,...,5, \tag{5.10}$$

$$\Psi_{ij} = \frac{\pi}{2}\left(1-\frac{R_{ij}}{\rho}\right), \tag{5.11}$$

$$R_{ij} = \sqrt{\left(i\frac{3}{2}r\right)^2 + \left(r\sqrt{3}\left(j-\frac{i}{2}\right)\right)^2}, \tag{5.12}$$

where $\rho = R_E + H$ is the distance from the center of the Earth to the upper boundary of the meteor zone, the selected value of r determines the required accuracy of specifying the coordinates of the entry point, the value of k determines the sector in which the angle j is determined (for $k = 0$, angle j can take values from minus p /3 to +p/3), and each i in the set from 1 to N corresponds to the value of j, which is less than the value of i.

The required radius for the coverage area is provided by choosing the appropriate values of r and N. In this case, the coverage radius for the upper boundary of the meteor zone can be defined as

$$R_{\text{cov}} = \rho \cdot \cos\psi_{\max} = \rho \cdot \cos\left[\frac{\pi}{2}\left(1 - \frac{r\sqrt{3}}{2\rho}\left(2N_{\max} + 1\right)\right)\right]. \tag{5.13}$$

To convert polar coordinates to Cartesian's, we can use the known relationships, where y_{ij} is the angle between the horizontal plane and the selected point

$$\begin{aligned} x_{entr\,ij} &= \rho\cos\left(\psi_{ij}\right)\cdot\cos\left(\varphi_{ij}\right), \\ y_{entr\,ij} &= \rho\cos\left(\psi_{ij}\right)\cdot\sin\left(\varphi_{ij}\right), \\ z_{entr\,ij} &= \rho\sin\left(\psi_{ij}\right). \end{aligned} \tag{5.14}$$

The singular point is the origin, for which the angle j is not defined. Pair $i = 0$ and $j = 0$ corresponds to the coordinates $x = 0$ and $y = 0$.

When the origin of coordinates is transferred from the center of the Earth to the center of the segment connecting the points of transmission and reception, the x and y coordinates remain unchanged, and the z coordinate becomes equal to

$$z^*_{entrij} = z_{entrij} - \sqrt{R_E^2 - \frac{R_{TR}^{\ 2}}{4}}, \tag{5.15}$$

where R_{TR} is the distance between the transmitting and receiving points.

5.2.1. Coordinates of the specular reflection point and its height above the Earth's surface

For radio links of various lengths SRP, given the coordinates of the meteoroid entry point into the meteor zone, and the known trail radiant, it is possible to determine the presence and coordinates of the specular reflection point (SRP), as well as its height above the Earth's surface. Reflection points in the meteor zone have only trails that are tangent to one of the ellipsoids of revolution included in the family of ellipsoids with foci at the receiving and transmitting points. An ellipsoid of revolution is a special case of an ellipsoid, two of three semiaxes of which are of the same length. For bistatic scattering, its canonical representation is:

$$\frac{x^2}{a^2}+\frac{y^2}{b^2}+\frac{z^2}{b^2}=1, \tag{5.16}$$

where $a^2 = b^2 + (R/2)^2$ is the square of the major semiaxis, and b is the minor semiaxis.

To find the coordinates of the points of intersection of the straight line describing the meteor trail with the ellipsoid, it is necessary to represent this straight line in a parametric form (Aleksandrov, 1968):

$$\begin{aligned} x &= mt + x_{entr}, \\ y &= nt + y_{entr}, \\ z &= pt + z_{entr}, \end{aligned} \tag{5.17}$$

where m, n, p are the coordinates of the directing vector of the straight line passing through the given meteoroid entry point into the meteor zone (x_{in}, y_{in}, z_{in}), and substitute (5.17) into equation (5.16).

If the direction to the radiant is given in the horizontal coordinate system

$$\begin{aligned} m &= \cos\alpha_R \sin z_R, \\ n &= \sin\alpha_R \sin z_R, \\ p &= \cos z_R, \end{aligned} \tag{5.18}$$

then the reduced azimuth angle (the angle about the x–axis) should be used, and the signs of the direction vectors of the straight line in equations (5.17) should be reversed. In this case, the parametric equation of the straight line takes the form:

$$\begin{aligned} x &= -mt + x_{entr}, \\ y &= -nt + y_{entr}, \\ z &= -pt + z_{entr}. \end{aligned} \tag{5.19}$$

After substituting (5.19) into (5.16) and a number of elementary but rather cumbersome transformations, we obtain an equation of the second degree with respect to the parameter t

$$At^2 + 2Bt + C = 0, \tag{5.20}$$

where

$$\begin{aligned} A &= b^2m^2 + \left[b^2 + \left(\frac{R_{TR}}{2}\right)^2\right]\cdot\left(n^2 + p^2\right), \\ B &= -b^2mx_{entr} - \left[b^2 + \left(\frac{R_{TR}}{2}\right)^2\right]\cdot\left(ny_{entr} + pz_{entr}\right), \\ C &= b^2x_{entr}^2 + \left[b^2 + \left(\frac{R_{TR}}{2}\right)^2\right]\cdot\left(y_{entr}^2 + z_{entr}^2 - b^2\right). \end{aligned} \tag{5.21}$$

The solution of equation (5.20) is known and has the form

$$t_{1,2} = -\frac{B}{A} \pm \frac{1}{A}\sqrt{D}, \tag{5.22}$$

where discriminant D is

$$D = B^2 - A \cdot C. \tag{5.23}$$

The point of contact can be observed if, for any value of the minor semiaxis b, the condition D = 0 (one intersection point) is satisfied. You can find this value by solving the equation

. $$B^2 - A \cdot C = 0. \tag{5.24}$$

The value of the minor ellipsoid axis that is touched by the straight line given by expression (5.18) remains undefined.

We represent the coefficients of expression (5.21) as an expansion in powers of the parameter b

$$\begin{aligned} A &= b^2 + R^2\left(n^2 + p^2\right), \\ B &= b^2\left(mx_{entr} + ny_{entr} + pz_{entr}\right) + R^2\left(ny_{entr} + pz_{entr}\right), \\ C &= -b^4 + b^2\left(x_{entr}^2 + y_{entr}^2 + z_{entr}^2 - R^2\right) + R^2\left(y_{entr}^2 + z_{entr}^2\right), \end{aligned} \tag{5.25}$$

where $R = RTP/2$.

Substituting the values of A, B and C from (5.25) into equation (5.24) leads to a sixth degree equation with respect to the unknown value of the ellipsoid minor semiaxis b. Having introduced the notation for the unknown $w = b^2$, we obtain the reduced equation of the third degree for the square of the minor semiaxis

$$w^3 + A_b w^2 + B_b w + C_b = 0, \tag{5.26}$$

where

$$\begin{aligned} A_b &= \left(mx_{entr} + ny_{entr} + pz_{entr}\right)^2 - (x_{entr}^2 + y_{entr}^2 + z_{entr}^2 - R^2) + R^2\left(n^2 + p^2\right), \\ B_b &= R^2\Big[2\left(mx_{entr} + ny_{entr} + pz_{entr}\right)\left(ny_{entr} + pz_{entr}\right) - \left(y_{entr}^2 + z_{entr}^2\right) - \\ &\quad - \left(x_{entr}^2 + y_{entr}^2 + z_{entr}^2 - R^2\right)\left(n^2 + p^2\right)\Big], \\ C_b &= R^4\left[\left(ny_{entr} + pz_{entr}\right)^2 - \left(n^2 + p^2\right)\left(y_{entr}^2 + z_{entr}^2\right)\right]. \end{aligned} \tag{5.27}$$

To solve equation (5.26), the Vieta method or the Cardano formulas (Korn, 2003; Boltyanskiy, 1967; Bronshteyn, 1986) can be used. When finding the roots of the reduced cubic equation (5.26), we prefer to use the Vieta method, for the implementation of which the following steps should be performed:

1. Calculate coefficients Q and P

$$Q = (A_b^2 - 3B_b)/9,\ P = (2A_b^3 - 9A_bB_b + 27C_b)/54. \tag{5.28}$$

2. Find the discriminant of an equation

$$\Delta = Q^3 - P^2. \tag{5.29}$$

3. If $\Delta > 0$, then the 3 real roots of equation (5.26) are defined by the formulas

$$\begin{gathered} w_1 = -2\sqrt{Q}\cos\varphi - A_b/3,\quad w_2 = -2\sqrt{Q}\cos(\varphi + 2\pi/3) - A_b/3, \\ w_3 = -2\sqrt{Q}\cos(\varphi - 2\pi/3) - A_b/3, \end{gathered} \tag{5.30a}$$

where *j* is

$$\varphi = \frac{1}{3}\arccos\left(\frac{P}{Q^{1.5}}\right).$$

4. If $\Delta = 0$, then the roots of equation (5.26) can be found based on simpler formulas

$$w_1 = -2\sqrt[3]{P} - A_b/3,\ w_2 = w_3 = -2\sqrt[3]{P} - A_b/3, \tag{5.30b}$$

Since $w = b^2$, the desired value of the minor semiaxis b of the ellipsoid of revolution is determined as the positive roots found on the basis of solutions (5.30a) and (5.31)

$$b = \sqrt{w_+}. \tag{5.31}$$

With the found value of b, the discriminant (5.24) is equal to zero, and the parameter t, which determines the coordinates of the touch point, is equal to

$$t_{touch} = -\frac{B}{A}, \tag{5.32}$$

where A and B are given by expression (5.21).

In this case, based on (5.19), (5.21) and (5.32), the coordinates of the touch point are determined by the values

$$x_M = -m\frac{b^2 m x_{entr} + \left[b^2 + \left(\frac{R_{TR}}{2}\right)^2\right] * \left(n y_{entr} + p z_{entr}\right)}{b^2 m^2 + \left[b^2 + \left(\frac{R_{TR}}{2}\right)^2\right] * \left(n^2 + p^2\right),} + x_{entr}, \tag{5.33}$$

$$y_M = -n\frac{b^2 m x_{entr} + \left[b^2 + \left(\frac{R_{TR}}{2}\right)^2\right] * \left(n y_{entr} + p z_{entr}\right)}{b^2 m^2 + \left[b^2 + \left(\frac{R_{TR}}{2}\right)^2\right] * \left(n^2 + p^2\right),} + y_{entr},$$

$$z_M = -p\frac{b^2 m x_{entr} + \left[b^2 + \left(\frac{R_{TR}}{2}\right)^2\right] * \left(n y_{entr} + p z_{entr}\right)}{b^2 m^2 + \left[b^2 + \left(\frac{R_{TR}}{2}\right)^2\right] * \left(n^2 + p^2\right),} + z_{entr}. \quad (5.33)$$

where the minor semiaxis of the ellipsoid is determined by the found expression (5.31).

After finding the coordinates of the touch point, it is necessary to make sure that this point is within the meteor zone. For this, we find HM, the height of SRP above the Earth's surface using the calculation formula

$$H_M = \sqrt{x_M^2 + y_M^2 + \left[z_M^2 + \sqrt{R_E^2 - \left(\frac{R_{TR}}{2}\right)^2}\right]^2} - R_E. \quad (5.34)$$

If 80 km < H_M < 130 km, we assume that the SRP is within the meteor zone.

Another method for determining the presence of SRP was described in (Antipov, 2006). It is based on determining the cosine of the angle between the direction to the radiant and the perpendicular to the plane tangent to one of the ellipsoids of the family with point *M*. In this case, the meteor trail is described by the equation

$$\frac{\mathrm{x\,x_M}}{b^2 + \left(\frac{\mathrm{R_{TR}}}{2}\right)^2} + \frac{\mathrm{y\,y_M}}{b^2} + \frac{\mathrm{z\,z_M}}{b^2} - 1 = 0, \quad (5.35)$$

where x_M, y_M, z_M are the coordinates of the point on the ionized meteoroid trail, and the direction cosines m, n, and p are

$$m = \cos\alpha_R \sin z_R, \quad n = \sin\alpha_R \sin z_R, \quad p = \cos z_R,$$

where α_R is the reduced azimuth of the radiant, and z_R is the zenith angle of the radiant.

The plane tangent at point M to the ellipsoid of revolution is described by the equation

$$\frac{\mathrm{x}\,\mathrm{x}_{\mathrm{M}}}{b^2+\left(\frac{\mathrm{R}_{\mathrm{TR}}}{2}\right)^2}+\frac{\mathrm{y}\,\mathrm{y}_{\mathrm{M}}}{b^2}+\frac{\mathrm{z}\,\mathrm{z}_{\mathrm{M}}}{b^2}-1=0, \tag{5.36}$$

and the perpendicular to the plane is described by the equation

$$\frac{\mathrm{x}\text{-}\mathrm{x}_{\mathrm{M}}}{A}=\frac{\mathrm{y}\text{-}\mathrm{y}_{\mathrm{M}}}{B}=\frac{\mathrm{z}\text{-}\mathrm{z}_{\mathrm{M}}}{C}, \tag{5.37}$$

where

$$A=\frac{\mathrm{x}_{\mathrm{M}}}{b^2+\left(\frac{\mathrm{R}_{\mathrm{TR}}}{2}\right)^2},\quad B=C=\frac{\mathrm{y}_{\mathrm{M}}}{b^2}.$$

Thereby, the cosine of the angle between the direction to the radiant and the perpendicular to the plane tangent to one of the ellipsoids of the family at point *M* is determined using expressions (Kharchenko, 2012a; Kharchenko, 2012b; Kharchenko, 2012c; Kharchenko, 2011; Kharchenko, 2010a; Kharchenko, 2010b)

$$\cos\lambda=\frac{\frac{mx_M}{b_e^2+(R_{TR}/2)^2}+\frac{ny_M}{b_e^2}+\frac{pz_M}{b_e^2}}{\sqrt{\left(m^2+n^2+p^2\right)\cdot\left[\left(\frac{x_M}{b_e^2+(R_{TR}/2)^2}\right)^2+\left(\frac{y_M}{b_e^2}\right)^2+\left(\frac{z_M}{b_e^2}\right)^2\right]}}. \tag{5.38}$$

After finding cos(γ) for the entry point of the meteor into the layer and the exit point from the layer, the condition for changing the cosine sign for these points is checked. If a sign change occurs, then the trail is tangent to one of the ellipsoids of the family and has specular reflection point, otherwise, the trail formed by a meteoroid with a given radiant has no mirror point and cannot be used to provide communication.

The method for determining the "hot zone" based on the analysis of the sign of the cosine is presented in (Kharchenko, 2012a; Kharchenko, 2012b; Kharchenko, 2012c; Kharchenko, 2011; Kharchenko, 2010a; Kharchenko, 2010b). It takes into account the statistical data on the most probable zenith angles of meteor trails for all SMC sources. Fig. 5.6*a* shows the region of the most probable occurrence of meteor trails suitable for communication formed by sporadic meteoroids for a radio link of 1000 km obtained on this basis. The obtained results are consistent with the qualitative assessment of this area given in the ITU-R Recommendations(Fig. 5.6*b*). In both cases, the radio visibility zone was not taken into account, which must be considered when long-distance radio links is using.

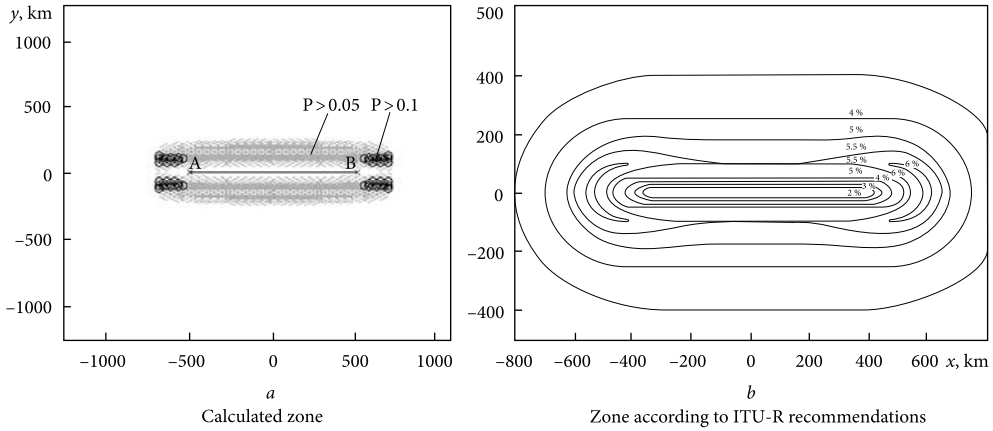

Fig. 5.6. The zone of the most probable occurrence of meteor trails suitable for communication formed by sporadic meteoroids for a radio link of 1000 km long

For meteor showers with a fixed zenith angle π/6 and reduced azimuths, which were taken as equal to π/2, 5π/4, and 3π, "hot zones" for radio links of various lengths have the form shown in Fig. 5.7.

These results can be used as test (indicative) results when compared to more correct calculations performed on the basis of the predictive model proposed above for the appearance of IMTr associated with a given radiant.

For the found SRP height, we estimate the sufficiency of the energy potential of the radio link for observing the reflected signal.

5.2.2. Estimation of the energy potential of a radio link with forward scattering

The energy potential of a meteor radio link determines the possibility of transmitting information with a given reliability and speed. It is characterized by the ratio of the energy of the reflected signal to the spectral density of the noise and depends on:

- geometric parameters of the radio link;
- radiated power of the transmitter P_T;
- carrier frequency f_c or, equivalently, operating wavelength λ_c;
- transmitting and receiving antenna gains at the operating frequency (G_T and G_R) in the SRP direction;
- peak power of the reflected signal that is formed within the first Fresnel zone and depends on the trail orientation relative to the radio wave propagation path;
- physical and chemical properties of the meteoroid that formed the trail;
- height H_M of the specular reflection point above the Earth's surface, on which such parameters of the ionized trail as the linear electron density q_e, the

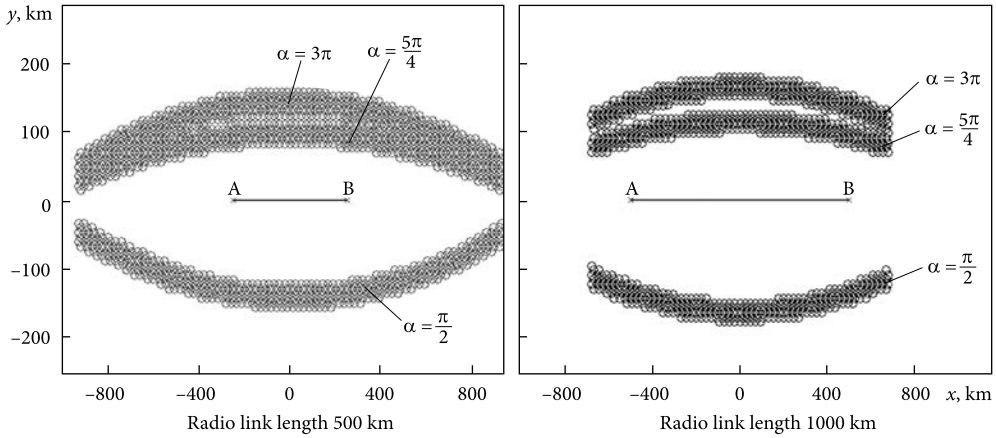

Fig. 5.7. Areas of the most probable occurrence of meteor trails suitable for communication formed by meteor showers with different reduced radiant azimuth angles

initial radius r_0, the radial distribution of the electron density, and the diffusion coefficient D depend;

• noise power in the frequency band Δf_s of the used signals at a given frequency of the carrier wave.

To estimate the power of the received signal during bistatic scattering on underdense and overdense trails, various simplified models are used, the degree of adequacy of which depends on the assumptions made at the model development stage. The analysis of simplified models was carried out in (McKinlay, 1961; McKinlay, 1964). To implement a prognostic model that makes it possible to estimate the probability of occurrence of meteor trails with SRP, it is sufficient to use known expressions for the power of the received signal reflected from an underdense meteor trail. Taking into account the geometry of the radio link and the direction of the polarization vector μ of the scattered signal, the received signal power can be described by expressions

$$P_R = \frac{P_T G_T G_R \lambda^3 \alpha_e^2 r_e^2 \sin^2 \mu \exp\left(-\dfrac{8\pi^2 r_0^2}{\lambda^2 \sec^2 \theta}\right)}{16\pi^2 R_1 R_2 (R_1 + R_2)(1 - \sin^2 \theta \cos^2 \beta_m)}. \quad (5.39)$$

Expressing the power of the received signal in terms of the effective electron scattering surface σ_e, we obtain

$$P_R = \frac{P_T G_T G_R \sigma_e \lambda^3 \alpha_e^2 \cos^2 \mu \exp\left(-\dfrac{8\pi^2 r_0^2}{\lambda^2 \sec^2 \theta}\right)}{64\pi^3 R_T R_R (R_T + R_R)(1 - \sin^2 \theta \cos^2 \beta_m)}, \quad (5.40)$$

where P_T is the transmitter power; G_T, G_R are transmitter and receiver antenna gains; λ is the wavelength; σ_e is the effective electron scattering surface; α_e is the linear electron density of the trail; r_e is the classical electron radius; μ is the angle between the electric field vector of the incident wave and the trail axis; θ is the angle of incidence of the transmitted wave on the trail; r_0 is the initial radius of the meteor trail; β_m is the angle between the meteor trail and the plane drawn through the receiving and transmitting points and the reflecting point of the meteor trail (propagation plane); R_1 and R_2 are the distances between the transmitting antenna and the reflecting area and between the receiving antenna and the reflecting area, respectively.

Although underdense tracks are more often observed, in some cases, it is necessary to determine the configuration of "hot zones" for overdense trails. This is especially relevant when operating in the upper part of the frequency range available for meteor radio communications. The duration of these trails is much longer, which significantly affects the operating cycle and the choice of the information transfer protocol in the MRS.

For an overdense meteor trail, the formula for calculating the received signal strength is (Wislez, 1995)

$$P_R = \frac{P_T G_T G_R \lambda^2 \sin^2 \mu}{32\pi^2 R_1 R_2 (R_1 + R_2)(1 - \sin^2 \theta \cos^2 \beta_m)} \cdot r_c(r_0, \alpha_e, r_e, \theta), \tag{5.41}$$

where r_c is the critical radius of the meteor trail, with a Gaussian distribution of electron density about the axis, which is given by

$$r_c(r_0, \alpha_e, r_e, \theta) = \sqrt{r_0^2 \cos^2 \theta \ln \frac{\alpha_e r_e \lambda^2 \sec^2 \theta}{\pi^2 r_0^2}}. \tag{5.42}$$

Noise power can be calculated using the well–known formula

$$P_s = k_B T_0 \cdot \left[N_F - 1 + \frac{T_A}{T_0} \right] \cdot \Delta F_s, \tag{5.43}$$

where $k_B = 1.38 \times 10^{-23}$ [J/K] — Boltzmann constant; $T_0 = 290$ K — standard temperature [K]; N_F — receiver noise Figure; T_A — noise temperature reduced to the antenna input [K]; ΔFs — the bandwidth of the receiving system, determined by the type of signals used and the rate of information transmission.

Noise power in a given band at frequencies exceeding 20 MHz is mainly determined by galactic noise and man-made noise.

Galactic noise is a function of frequency and in the range of 20...100 MHz can be calculated using formula (Schanker, 1990)

$$P_{\text{ø}}\,(dBW) = K - 27{,}7 \cdot \lg(f_{MHz}) + 10 \cdot \lg(\Delta F_{s,Hz}) \tag{5.44}$$

or calculated by the procedure given in Recommendation ITU-R P.372-13.

The power of industrial interference can be determined based on the expression

$$P_{ind}(dBW) = -154{,}5 - 22 \cdot \lg(f_{MHz}) + 10 \cdot \lg(\Delta F_{s,Hz}), \quad (5.45)$$

where the coefficient K depends on the location of the receiving station and can vary from 127.2 to 136.8.

The minimum power level at the receiver input can be determined by the formula

$$P_{R,\min}(dBW) = \left(\frac{P_s}{P_n}\right)_{\min}(dB) + P\ (dBW), \quad (5.46)$$

where $(P_s/P_n)_{min}$ is the minimum signal– noise power [dB] ratio at the input of the receiver decoder, which depends on the purpose of the meteor radio system, the parameters of the receiving and transmitting equipment and antennas, the type of signals used, and the information transfer protocol.

In (Miroshnikov, 2019), to apply effectively "complex" algorithms to the functioning of the meteor communication path, it is recommended to use methods that, for given parameters of the receiving–transmitting equipment (P_T, G_T, G_R) and the distance R_{TR} between the transmitting and receiving antennas, provide observation of reflected signals, for which (Ps/Pn) > 17...20 dB. For signals transmitted at an operating frequency of 30 MHz and having a spectrum width of 2400 Hz, based on (5.39) and (5.41), we obtain $P_{R,min}$ of minus (132.2...135.2) dBW or ($6.03\ 10^{-14}$...$3.02\ 10^{-14}$) W. Similar estimates were obtained in (Voronin, 2019; Solovev, 2000).

Depending on the purpose of MRS and the length of the radio link, it is necessary to optimize the parameters of the transceiver equipment and ensure that the antennas are pointed in the "hot zone". As one of the efficiency criteria, a minimum time for bringing an information packet of a given size with limited costs for its transmission can be used. It is possible to optimize construction and installation works by a set of quality indicators, the main of which are:

- Maximum throughput of the MRC network.
- Minimum time to deliver information of a given volume with a given reliability.
- Data line utilization.
- Increased secrecy of the operation, protection from natural interference, and resistance to electronic suppression.
- Minimum power consumption when placing stations at unattended sites.
- The minimum cost of production and operation of equipment.

Optimization allows for setting the minimum signal power level at the receiver input $P_{R,min}$, for which one should perform calculations of the "hot zone" and select the optimal antenna parameters, as well as the protocol and information transfer rate.

5.3. Measuring the height of the specular reflection point on a meteor trail

When performing research in the field of meteor astronomy, it is relevant to estimate the height of the specular reflection point with an unknown radiant of the meteoroid that generated the trail. When using the direction–finding–time radio method for measuring the velocities and radiants of individual meteors, the error in estimating the zenith angle is practically independent of its value. The MIR-2 complex made it possible to measure the angular coordinates of reflecting points with an accuracy of 1° and estimate the radiants of meteoroids with an accuracy of 2° (Narziev, 2017).

Let us show the possibility of using the radio direction finding method for measuring the height of the SRP during bistatic scattering, in which the specular reflection point M_m is located on the surface of an ellipsoid of revolution, the canonical representation of which is given by equation (5.16).

We assume that the distance R_{TR} between the points of transmission T and reception R, located in the foci and determined by the corresponding geographical coordinates, is known. The value of the minor semiaxis b depends on the coordinates of the specular reflection point M_m in the meteor zone, which determines the sum of the focal radii of the ellipsoid for a given value of R_{TR}. The sum of the focal radii of the ellipsoid can be estimated by measuring the propagation time τ_{TR} of the signal from point T to point R. Since the sum of the focal radii of the ellipsoid is twice the semi-major axis, the semi-major axis is given by the simple relation:

$$\alpha = \frac{\tau_{TR}}{2c}, \tag{5.47}$$

where c is the speed of light in the medium of radio wave propagation.

This allows us to determine the value of the minor semiaxis of the ellipsoid based on the expression

$$b = \sqrt{\left(\frac{\tau_{TR}}{2c}\right)^2 - \left(\frac{R_{TR}}{2}\right)^2}. \tag{5.48}$$

Thus, expressions (5.16, 5.47, and 5.48) completely describe the ellipsoid of revolution, on the surface of which there is a specular reflection point M_m.

We offer a simple and geometrically clear method for measuring the coordinates (x_M, y_M, z_M). It is based on a two-stage solution procedure and illustrated in Fig. 5.8, which uses the notations to Fig. 5.1.

Based on the presented figure, the following system of equations can be written

$$\begin{cases} Z_M^2 + Y_M^2 = b_M^2, \\ Z_M = C_M\, tg\beta_R, \\ Y_M = C_M\, tg\alpha_R. \end{cases} \tag{5.49}$$

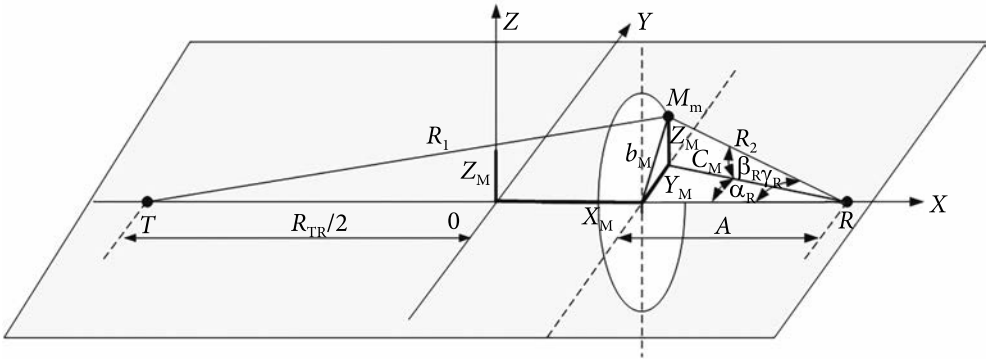

Fig. 5.8. Measurement of coordinates (X_M, Y_M, Z_M) of the specular reflection point

Substituting Z_M and Y_M into the first equation, we obtain the value of C_M expressed in terms of b_M — the radius of the section of the ellipsoid by the *YZ* plane at the point X_M, as well as the corresponding values of Z_M and Y_M

$$C_M = \frac{b_M}{\sqrt{tg^2\alpha_R + tg^2\beta_R}}, \quad Z_M = \frac{b_M}{\sqrt{tg^2\alpha_R + tg^2\beta_R}} tg\beta_R \,, Y_M = \frac{b_M}{\sqrt{tg^2\alpha_R + tg^2\beta_R}} tg\alpha_R \,. \quad (5.50)$$

To find the X_M coordinate and the b_M SRP parameter, we use the previously determined ellipsoid parameters, the equation of the straight line from point *R* to point M_m, and the relation connecting the angles α_R, β_R, and γ_R

$$\begin{cases} \dfrac{x^2}{\alpha^2} + \dfrac{z^2}{b^2} = 1, \\ z = tg\gamma_R\left(\dfrac{R_{TR}}{2} - x\right) \end{cases}, \quad (5.51)$$

$$\cos\gamma_R = \cos\alpha_R \cos\beta_R \,. \quad (5.52)$$

A graphical representation of the conditions of this task is illustrated in Fig. 5.9

The substitution method allows us to obtain a quadratic equation for *x* from system (5.51)

$$Ax^2 - Bx + C = 0 \,, \quad (5.53)$$

where $A = a^2tg^2\gamma_R + b^2$, $B = a^2tg^2\gamma_R R_{TR}$, $C = a^2tg^2\gamma_R\left(\dfrac{R_{TR}}{2}\right)^2 - a^2b^2$.

Using expression (5.51) and the well–known trigonometric identity, the value of $tg^2\gamma_R$ can be represented by an expression relating γ_R to the measured angles α_R and β_R

$$tg^2\gamma_R = \frac{1}{\cos^2\gamma_R} - 1 = \frac{1}{\cos^2\alpha_R \cos^2\beta_R} - 1 \,. \quad (5.54)$$

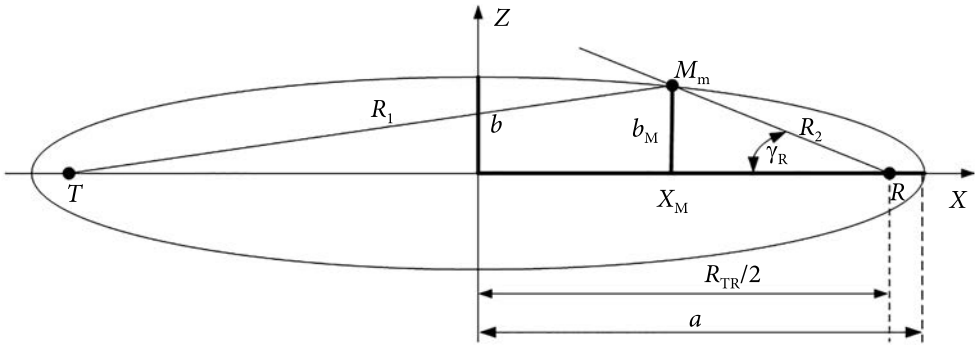

Fig. 5.9. To the task of determining the X_M coordinate and the b_M parameter of the specular reflection point M_m

The solution to equation (5.53) is the coordinate X_M

$$X_M = \frac{B + \sqrt{B^2 - 4AC}}{2A}. \tag{5.55}$$

With X_M calculated, the value of the parameter b_M is given by

$$b_M = \left(\frac{R_{TR}}{2} - X_M\right) tg\gamma_R = \left(\frac{R_{TR}}{2} - X_M\right)\sqrt{\frac{1}{\cos^2\alpha_R \cos^2\beta_R} - 1}. \tag{5.56}$$

Note that the angle β_R was determined relative to the *XY* plane and, if measured in degrees relative to the horizon, its value should be reduced by $\Delta\beta_R$

$$\Delta\beta_R = \arcsin\left(\frac{R_{TR}}{2R_{E\ WGS}}\frac{180}{\pi}\right), \tag{5.57}$$

where, in accordance with the WGS-84 standard, $R_{E\ WGS}$ = 6371 km. If it is necessary to perform more accurate calculations, instead of $R_{E\ WGS}$, the radius of curvature of the Earth's surface at the point of reception *R* can be used.

Example. Let the interfocal distance be R_{TR} = 1000 km, and the measured values τ_{TR} = 17.1 ms, α_R = 6°, $\beta_{R\ meas}$ = 8° (at the same time, based on (5.57), β_R = 12.5°). Performing calculations using formulas (5.47), (5.48), (5.49), and (5.52)—(5.56), we get:

$$X_M = 35.522 \text{ km and } b_M = 114.48 \text{ km};$$

$$Y_M = 49.038 \text{ km}; Z_M = 103.446 \text{ km}.$$

To calculate the height of the specular reflection point above the Earth's surface, let's transform the M_m point a coordinate system where the *XY* plane passes through center of the Earth's. In this case, the coordinates M_m in the new coordi-

nate system take the values:

$$X_{EM} = X_M, Y_{EM} = Y_M,$$
$$Z_{EM} = Z_M + \sqrt{R_{E\,WGS}{}^2 - \left(\frac{R_{TR}}{2}\right)^2} \tag{5.58}$$

and the height of the specular reflection point above the Earth's surface is equal to

$$H_M = \sqrt{X_{EM}{}^2 + Y_V{}^2 + Z_V{}^2} - R_{E\,WGS}\,. \tag{5.59}$$

For the above example, using (5.58) and (5.59), we get H_M = 84.08 km.

When estimating the influence of the measurement accuracy of the parameters τ_{TR}, α_R and β_R on the estimation error for H^*_M, it can be shown that for the example considered above, with a time measurement error of ~1 ms and an angular error of ~1°, the height estimation error ΔH_M is in the range from minus 1.3 km to plus 1.8 km. Consider an example in which the height of the specular reflection point is closer to the upper boundary of the meteor zone. Let the measured values be τ_{TR}=17.61 ms, α_R=10°, and β_R=15°. In this case, the calculated value H_M = 129.49 km. Similar calculations of the influence of measurement accuracy on the H_M estimate show that ΔH_M is in the range from minus 2.34 km to plus 2.52 km. An increase in the accuracy of measurements of angular coordinates leads to an approximately proportional decrease in the error in estimating the height of the specular reflection point (Slivinskiy, 2011).

5.4. Conclusions

The proposed predictive model for the observation frequency of IMTr belonging to the main SMC sources or meteor showers opens up additional possibilities for extracting information about the meteoroid and geophysical parameters of the atmosphere in the case of bistatic radio signal scattering.

Given the observation time, zenith angle, and azimuth of the trail, based on the prognostic model, an area where the SRP of the radio signal is observed with a given probability can be determined. This allows one to optimize the parameters of the transmitting and receiving antennas and the protocol for transmitting information for the maximum throughput of meteor radio communication systems while ensuring.

Analytical methods were used to calculate the coordinates and height of the SRP of the meteor trail, with a given radiant and entry point of the meteoroid into the meteor zone. This required solving a third–degree equation by the Vieta method. The possibility of using the direction-finding-time radio method for measuring the height of the SRP in bistatic scattering is shown. A simple and geometrically illustrative method is proposed for finding the SRP coordinates for an unknown radiant of the meteoroid that generated the trail.

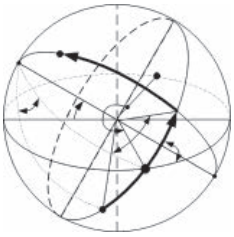

SECTION 6

PHYSICAL THEORY OF FORMATION AND TRANSFORMATION OF IONIZED METEOR TRAILS

The physical theory of the formation and transformation of ionized meteor trails is the basis for creating a generalized model of radio signal scattering on a meteor trail in the process of its formation and development. Many well-known researchers of meteor phenomena have been developing this theory for a long time. A historical review of the formation of the physical theory of meteor phenomena is given in (Levin, 1956; Bronshten, 1981; Bronshten, 1983). The fundamental works in this area can be considered in (Öpik, 1958; Verniani, 1964; Astapovich, 1958; Jacchia, 1955; Kascheev, 1967).

The ionized trail of a meteoroid available for radio engineering (radar or radio communication) observations implicitly contains information both about the meteoroid itself (mass, velocity, chemical composition, radiant) and about the state of the atmosphere at the height of the trail formation (density, chemical composition, ozone content, wind speed and direction, turbulence). By the displacement (drift) of trails, it is possible to reveal the regularities of the circulation of the upper atmosphere at different latitudes at different times of the year and day. This information can be used in solving tasks in various areas of research:

- astronomical and astrophysical;
- geophysical;
- radio engineering.

This determines the importance and necessity of constructing an adequate physical model of the formation and transformation of an ionized trail that takes into account many factors determining the trail characteristics during its observation. The construction of such a model involves taking into account the main physical processes that occur during the interaction of a meteoroid with atoms and molecules of the atmosphere.

During the formation and transformation of an ionized trail, a sequence of events occurs:

1. Preheating and, in certain cases, pulverization and crushing of the meteoroid.

2. Evaporation of the meteoroid and ionization of its atoms, and in certain cases, fragmentation (with own characteristics), which can continue throughout the flight interval of the meteoroid until its complete evaporation.

3. Formation of the head part of the ionized trail in the thermalization interval, which is detected on radars as a head echo, and then the trail itself, which has an initial radius corresponding to the formation conditions.

4. Trail expansion under the influence of ambipolar diffusion in the Earth's magnetic field.

5. Decrease in the linear electron density of the trail due to the effects of turbulent diffusion, recombination of positive ions with electrons, attachment of free electrons to oxygen molecules, as well as ionic reactions with ozone.

6. Destruction (curvature) of the ionized trail under the influence of wind shifts and atmospheric turbulence in the meteor zone.

Factors affecting the formation and lifetime of an ionized meteor trail depend on the properties of the meteoroid itself and the atmospheric parameters at the height of the trail formation. They are presented in Table 6.1.

The main characteristic of the ionized trail is the electron density, which is directly proportional to the number of evaporated meteoroid atoms per unit path length. Note that the meteor body atoms are ionized mainly because they have a lower ionization potential compared to the atoms of the atmosphere – the amount of energy necessary to transfer an electron of the atom's outer shell (optical electron) from the ground level to the excited one.

In the transition to intense evaporation, which occurs very quickly, the effect of "blocking" occurs. The stronger the evaporation, the smaller the proportion of incident molecules that can transfer to the body their energy necessary

Table 6.1. **Factors affecting the formation and lifetime of an ionized meteor trail.**

Meteoroid Parameters	Atmospheric parameters at the trail's formation height	Meteoroid Parameters	Atmospheric parameters at the trail's formation height
Mass	Density	Zenith angle *	Ozone concentration
Speed	Temperature	Physical Properties **	Electron density
Radiant	Chemical composition	Chemical composition	Wind speed and direction
			Turbulence

* The zenith angle is determined by the meteoroid radiant, path geometry, and local observation time. ** Physical properties — bulk density, structure (porosity), and thermophysical characteristics (heat transfer coefficient) of the meteoroid.

to maintain evaporation. On the contrary, if the evaporation weakens, the obstruction will also decrease, which means that more energy will begin to flow to the meteoric body, which will cause an increase in evaporation. Only at a certain rate of evaporation, the both processes can be in equilibrium. This equilibrium evaporation rate is determined by external conditions such as the velocity of the meteoroid, its dimensions (mass and midsection area), the density and chemical composition of the surrounding atmosphere, and the chemical composition and thermophysical properties of the body matter . The angle of the meteoroid's entry into the atmosphere and the body shape affect as well .

To calculate the number of free electrons produced per one evaporated atom of a meteor body, the ionization coefficient is used, which depends on the ratio of the probabilities of ionization (inelastic process) to momentum transfer (elastic process). Of all the collisions of meteoric atoms with incoming atmospheric molecules, the vast majority are elastic, leading to the transfer of momentum and energy to the atmosphere atoms. According to E. Öpik, only 3% of all collisions are inelastic, causing ionization of atoms.

Considering that each meteor atom can experience not one, but several collisions, the ionization coefficient can, under certain conditions, exceed unity.

Since atoms evaporating from the surface of a meteoroid have approximately the same velocities as the meteoroid itself, the initial period in the formation of an ionized trail is its rapid expansion until the end of thermalization, that is, the establishment of thermal equilibrium with the environment. This time interval depends on the height of the trail formation and varies from 1 ms at an altitude of 80 km to 150 ms at an altitude of 115 km (Baggaley, 1977).

It can be assumed that a kind of "ionization bunch" is formed in the thermalization interval, as Canadian astronomers P. Millman and D. McKinley called it, one of the first to discover this phenomenon, which is observed on radar screens as the head echo of a meteoroid.

To estimate the linear electron density after the completion of the thermalization process, a concept is introduced — the initial radius of the meteor trail, which in its physical essence characterizes the radius of the ionized trail, within which the bulk electron density is distributed according to a certain law.

The initial radius and electron density significantly depend on the presence and type of splitting (fragmentation) of the meteoroid, which manifests itself both at the initial stage of formation of the meteor trail (at the stage of preheating) and during the subsequent meteoroid movement in the atmosphere. The splitting effects are fixed during optical observations and are also distinguishable on the amplitude-time (ATCH) and phase-time (PTR) characteristics of radio reflections from meteor trails.

Various fragmentation mechanisms have been studied in many works, from which it follows that the nature and probability of fragmentation depend on the properties of the parent bodies, which are the true sources of meteoroids. Since meteoroids of cometary and asteroidal origin have significantly different geocen-

tric velocities, density, structure, and chemical composition, it can be expected that the mechanism of their fragmentation will also be significantly different.

As a result of fragmentation, the total midsection of the meteor body changes, and its mass is distributed among the fragments, which changes the linear electron density of the trail at a constant ionization coefficient. When estimating the ionization coefficient, it is necessary to apply various hypotheses regarding the origin of the meteoroid based on the actually observed height of the specular reflection point and the speed of the meteoroid.

The formation of the initial radius of the ionized trail can be influenced by the shock wave formed by fairly large meteoroids.

After the ionization coefficient is calculated and a decision is made on the initial radius of the meteor trail, the stage of evaluating its transformation up to complete destruction begins. The main transformation mechanism is the expansion of the trail radius under the influence of ambipolar diffusion. However, to obtain more reliable estimates of the trail parameters over the interval of its observation, it is necessary to take into account the factors listed above that affect its characteristics and lifetime.

Next, we consider the formation and transformation processes of ionized meteor trails in more detail.

6.1. Preheating and sputtering of meteoroids

Meteor bodies enter the Earth's atmosphere at speeds from 11 to 73 km/s. Their initial temperature is determined by the radiation of the Sun in the Earth's orbit and is equal to $T_C \approx 278$ K. The initial kinetic energy of meteoroids is much greater than the energy required for complete evaporation, and the initial speed is significantly greater than the thermal velocity of the medium molecules. If the size of meteoroid is much smaller than the mean free path of the molecules of the upper atmosphere, the interaction occurs due to the impacts of individual molecules on the surface of the meteoroid.

The incident molecule completely or partially transfers its momentum and kinetic energy to the meteoric body. At an altitude of 300—130 km, the collision energy leads to deceleration, heating, and dispersal of the meteoroid. Very small meteoroids with masses of the order of 10^{-9} g decelerate at altitudes of 110—130 km, without having time to heat up to the temperature at which intense evaporation begins, regardless of their chemical composition. Their kinetic energy is spent mainly on thermal radiation from the surface.

For meteoroids larger than 1 mm, the preheating process is controlled by thermal conductivity. When such bodies are heated to a certain temperature, when the surface tension (tangential compression) reaches the strength of the material, the process of crushing (fragmentation) can begin. For a homogeneous solid stone larger than a centimeter, this corresponds to a temperature of up to 900 K. For

smaller meteoroids, when the surface is heated to 500 K, the temperature gradient inside the meteoroid and internal compression can also cause fragmentation.

The physical dispersal of meteoroids of any size is an atomic cascade process in which the bombarding particles collide with the surface atoms of the meteoroid, displacing them from the lattice through a cascade of energy transfer. The energy required to overcome the potential barrier is called the surface binding energy (U_0). If the component of the velocity of atoms normal to the surface corresponds to an energy equal to or greater than U_0, they will leave this surface. The minimum kinetic energy of incoming atmospheric atoms ("projectiles") required to cause the meteor body ("target") to disperse is called the threshold energy ($E_{th)}$.

In (Rogers, 2005), for meteoroids in the mass range from 10^{-3} to 10^{-13} kg and in the velocity range from 11 to 71 km/s, a method for evaluating sputtering ablation was developed based on works (Tielens, 1994; Draine, 1979; Draine, 1977). It took into account the atmospheric pressure profiles and the molecular composition of the gas at different altitudes. In accordance with this technique, the rate of change in the meteoroid mass due to physical sputtering can be written as

$$\left(\frac{dm_m}{dt}\right)_{sp} = -2M_2 A v \left(\frac{m_m}{\rho_m}\right)^{2/3} \sum n_i Y_i(E), \qquad (6.1)$$

where M_2 is the mean molecular mass of meteoroid atoms; A is the shape factor of the meteoroid; v is the geocentric velocity of the meteoroid; m_m is the mass of the meteoroid; ρ_m is the bulk mass density of the meteoroid; i is an index indicating the type of molecule from the composition of the atmosphere; n_i is the number of particles of a given type i per unit volume; Y_i (E) is the sputtering yield averaged over all possible collision angles relative to the normal to the meteoroid surface. It represents the ratio of the average number of sprayed particles of the i–th type per one molecule of the atmosphere (one projectile).

Limited experimental data (Draine, 1979; Draine, 1977) indicate that the sputtering yield averaged over the encounter angle is determined by the relation

$$Y_i(E) \approx 2\, Y_i(E, \Theta = 0), \qquad (6.2)$$

where $Y_i(E, \Theta = 0)$ is the sputtering yield at a normal encounter angle, which in (Tielens, 1994) is determined by the expression

$$Y_i(E, \theta = 0) = \frac{3{,}56}{U(eV)} \frac{M_1}{M_1 + M_2} \frac{Z_1 Z_2}{\sqrt{Z_1^{2/3} + Z_2^{2/3}}} \alpha \frac{R_p}{R} s_n(\gamma) \times$$
$$\times \left[1 - \left(\frac{E_{th}}{E}\right)^{2/3}\right]\left(1 - \left(\frac{E_{th}}{E}\right)^2\right), \qquad (6.3)$$

where Y has the dimension of the number of atoms per projectile.

In this multicomponent theoretical relation, the notation is taken from (Rogers, 2005): *U(eV)* — surface binding energy; M_1 — mass of incoming particles of the atmosphere (projectile's mass); M_2 — mean molecular mass per atom of the target; β — maximum fractional energy transfer in head–on elastic collision; z_1 — projectile atomic number; z_2 — target atomic number; α — dimensionless function of the mass ratio; r_p/r — mean projected range to mean penetrated path length; $s_n(\gamma)$ — universal function; γ — reduced energy; e — energy of incoming particles of the atmosphere (incident projectile energy); e_{th} — minimum (threshold) kinetic energy of incoming atmosphere particles necessary to cause spraying.

The dimensionless function α depends on the ratio of atomic masses. For $0.5 < M_2/M_1 < 10$, it is approximated by

$$\alpha = 0,3\left(M_2/M_1\right)^{2/3}$$

and remains constant at approximately ~0.2 for $M_2/M_1 < 0.5$.

The correction factor R_p/R is the ratio of the mean projected range to the mean penetrated path length and can be approximated by

$$\frac{R_p}{R} = \left(K\frac{M_2}{M_1} + 1\right)^{-1},$$

where K is taken as a free parameter which depends on the target material (see (Tielens, 1994)).

The universal function $s_n(\gamma)$, which depends on the detailed form adopted for the screened Coulomb interaction (Tielens, 1994). It has a rather complicated form, but can be approximated by the expression (Matsunanmi, 1980)

$$s_n = \frac{3,441\sqrt{\gamma}\ln(\gamma + 2,718)}{1 + 6,35\sqrt{\gamma} + \gamma(-1,708 + 6,882\sqrt{\gamma})},$$

where γ is defined as

$$\gamma = \frac{M_2}{M_1 + M_2}\frac{\alpha}{Z_1 Z_2 e^2}E.$$

The screening length a for the interaction potential between nuclei is given by

$$\alpha = \frac{0,885\alpha_0}{\sqrt{Z_1^{2/3} + Z_2^{2/3}}},$$

where $a_0 = 0.529 \times 10^{-10}$ m is the Bohr radius.

The kinetic energy of the incident particles of the atmosphere E is determined by the known relation

$$E = M_1\frac{v^2}{2}.$$

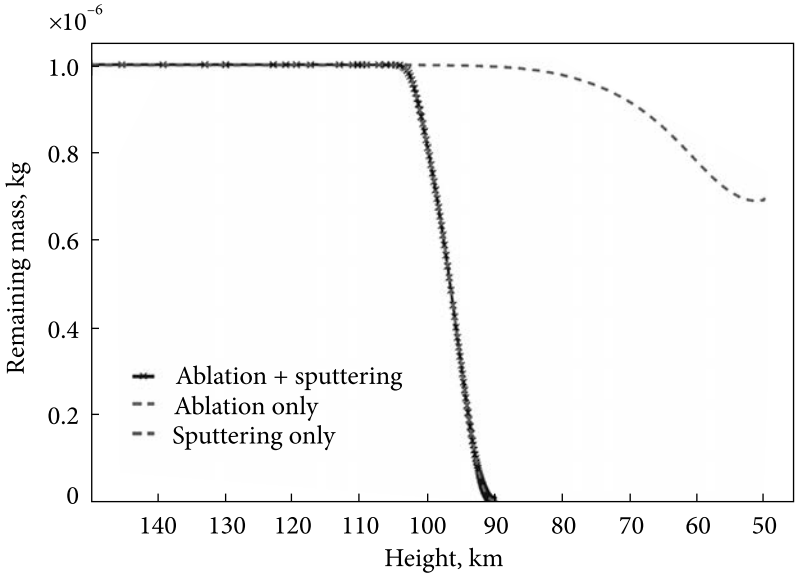

Fig. 6.1. Remaining meteoroid mass when only ablation (green curve), only sputtering (red curve), or both ablation and sputtering (black curve and crosses) are taken into account for a 1×10^{-6} kg test particle with a density of 3.3×10^3 kg/m^3. The velocity and zenith distance at the height of the common volume were set to 60 km/s and 35°, respectively (Kero, 2008)

The minimum (threshold) kinetic energy of incoming particles of the atmosphere E_{th}, necessary to cause spraying, is given by the expression (Bohdansky, 1980; Bohdansky, 1984; Anderson, 1981)

$$E_{th} = \frac{U_0}{\beta_{H-on}(1-\beta_{H-on})}, \quad \text{for } \frac{M_1}{M_2} \le 0{,}3,$$

$$E_{th} = 8U_0\left(M^1/M^2\right)^{1/3}, \quad \text{for } \frac{M_1}{M_2} \ge 0{,}3,$$

where the maximum partial energy E_{H-on} transferred in a frontal elastic collision is defined as

$$\beta_{H-on} = \frac{4M_1M_1}{M_1(M_1+M_2)^2}.$$

For consistency, U_0 and E_{th} are usually expressed in electron volts (eV).

In (Rogers, 2005), a numerical simulation of sputtering ablation was carried out for three models of meteoroids — asteroids, comets, and porous comets. Unfortunately, during the calculations, a technical error was made when estimating the number density of the atmosphere using the MSIS-E-90 model, which led to overestimations of the role of sputtering in the ablation process. This was pointed

Table 6.2. **Meteoroid material characteristics used in sputtering calculations (Kero, 2008)**

Meteoroid material	Composition	ρ_m, g cm^{-3}	M_2	Z_2	E_{th}, eV	K
Porous	C	0.3	12	6	4	0.65
Cometary	C	1.0	12	6	4	0.65
Asteroidal	SiO_2	3.3	20	10	6,4	0.1
Iron	Fe	7.8	56	26	4,1	0.35

Table 6.3. **Characteristics of the atmospheric constituents required for spray calculations**

Molecule	O	N_2	O_2	He	Ar	H	N
M_1	15.9994	14.007	15.999	4.0026	39.948	1.0079	14.007
Z_1	8	7	8	2	18	1	7

out in (Kero, 2008), where similar calculations using the method described above showed that sputtering is a much less important disintegration process than presented in (Rogers, 2005) and does not significantly affect the final meteoroid mass compared to thermal ablation. This fact is illustrated by Fig. 6.1, where the meteoroid parameters and characteristics of the atmospheric components given in Tables 6.2 and 6.3, respectively, were used in the sputtering calculations for porous, cometary, and asteroidal material.

Based on the foregoing, a reasonable conclusion can be made that, in the preheating interval, sputtering does not affect the total mass loss of the meteoroid. It may practically not be taken into account in the further motion of the meteoroid in the atmosphere.

At the same time, in the preheating interval, the process of crushing (fragmentation) can begin when the tangential compression reaches the strength limit of the material or the temperature gradient inside the meteoroid creates a corresponding internal compression. As a result of fragmentation, the midsection of the meteoroid changes, and this accordingly affects the luminosity and ionization coefficient and, thus, the linear electron density of the trail created by the meteoroid. In this regard, we first consider the possible mechanisms of meteoroid fragmentation, taking into account their possible origin, and then evaluate the effect of fragmentation on the electron density of the ionized trail.

6.2. Mechanisms of the meteoroids crushing

The fragmentation mechanisms of a meteoric body have been studied by many researchers (Bronshten, 1981; Levin, 1963; Simonenko, 1973; Babadzhanov, 1988a; Babadzhanov, 1988b; Babadzhanov, 1993; Ceplecha, 2005; Khanukaeva, 2002; Stokan, 2015). Observations reveal that 75 to 90% of meteoroids show fragmentation in some form, either as separate fragments or as a long trail of fragments with different deceleration rates (Weryk, 2013; Stokan, 2014; Subasinghe, 2016; Subasinghe, 2017). However, even those meteoroids that did not show evident fragmentation may be partially fragmented (Campbell-Brown, 2017).

Although the total mass of a meteoroid does not change significantly during fragmentation, some emerging effects must be considered when interpreting observations and conducting radiophysical measurements:

1. The total cross-section of the meteoroid fragments increases (hence, increases the evaporation surface area) and, accordingly, changes the linear electron density of the ionized trail.

2. The reduced mass of meteoroid fragments leads to a shortening of the time to the complete evaporation of the meteoroid.

3. The reduced mass of meteoroid fragments also leads to an increase in deceleration when they pass through the meteor zone and, accordingly, to a subsequent decrease in the ionization coefficient during the meteor trail formation .

4. There are fading of the received signal due to the interference of radio waves reflected from several meteoroid fragments located at distances commensurate with the wavelength.

Despite the fact that meteoroids' fragmentation during a flight in the atmosphere has long been recognized, there is still no unified model for the mechanism of this phenomenon. This is because, at hypersonic meteoroid speeds, aerodynamic braking and aerodynamic heating significantly interact. Therefore, a complex description of the motion in the atmosphere of a body with a variable mass and shape under the influence of aerodynamic resistance and heating, as well as under intense physical-chemical-mechanical interaction with the environment, is necessary. Obviously, such a task of aeroballistics is far from trivial.

The available meteoroid fragmentation models can be conditionally divided into the following characteristic groups:

1. Models of a single body (no fragmentation).

2. A model of progressive crushing into several fragments, a particular case of which is progressive fragmentation, when each subsequent fragment is divided into the same number of subsequent self-similar fragments (for example, into two self-similar parts).

3. Models of quasi-continuous crushing — destruction of the surface layer of the meteoroid by separating small fragments, dropping molten film drops, and crushing molten drops.

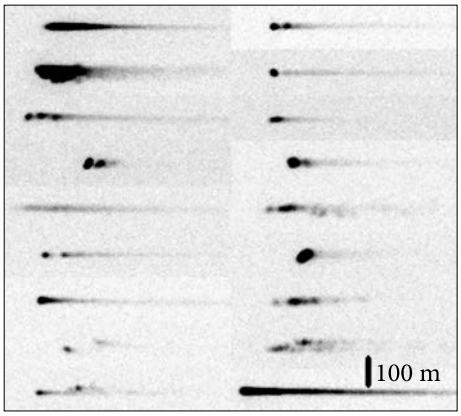

Fig. 6.2. Fragmentation states for 18 different meteoroids recorded by the CAMO narrow-field camera. A scale bar of 100 m for trail light width is shown for an average range of 130 km

4. Models of instantaneous fragmentation ("flash"), which can be considered as a limiting case of the progressive fragmentation model.

Since the real process of successive crushing is due to the inhomogeneity of the strength distribution of the original body material, and the meteoroid body itself has an unknown density and chemical composition, quantitative characteristics (such as mass, bulk density, grain structure, etc.) estimated based on known models can be obtained only using a probabilistic approach. At the same time, the qualitative estimates obtained from a model that determine the nature of the change in the fragmentation parameter, can be useful in assessing the reliability of assumptions regarding the true parent body of the meteoroid. Revealed features of fragmentation associated with the density of the meteoroid, the duration of its exposure to radiation and heating, which changes mineralogy, can give a hint in assessing the age and origin of the meteoroid. One should take into account that meteoroids generated by the same parent body may exhibit differences in the nature and features of the fragmentation process due to the inhomogeneity of the body itself.

To assess the reliability of any proposed fragmentation model, actual data are needed, which can only be obtained through observations. The most complete idea of the features and characteristics of crushing can be obtained through multi-position photometric studies. Such studies were carried out at the Canadian Automated Meteor Observatory (CAMO), which is a two-station video system with a baseline of ≈45 km, high resolution, and image enhancement.

Fig. 6.2 shows the fragmentation states (one frame captured by the narrow–field camera) for 18 different meteoroids presented in (Weryk, 2013).

Three types of fragmentation were observed — single, multiple, and complex fragmentation. With a single fragmentation, the meteoroid was fragmented once during the observation interval. With a multiple fragmentation, the meteoroid was fragmented several times. With a complex fragmentation, the original body and its fragments were continuously crushed.

For detailed studies at the CAMO, nine observations of the highest quality were selected, which made it possible to determine the speed of movement and acceleration of fragments, as well as to extrapolate the fragmentation height and calculate, using the well-known method (Ceplecha, 1987), the orbital parameters of each meteoroid.

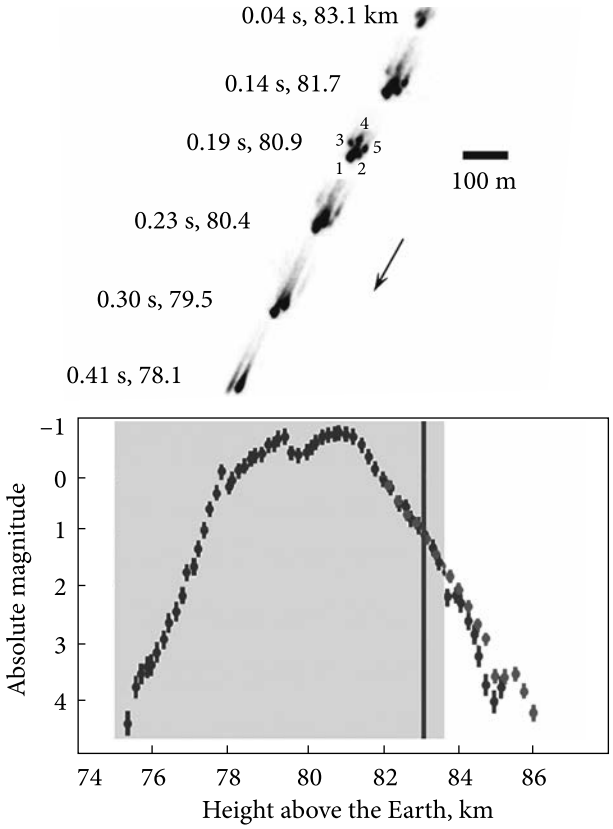

Fig. 6.3. Dynamic fragmentation and light curve for the meteoroid observed on October 16, 2010 at 07:00:52 UTC, where a 100 m light trail width scale bar is shown for an average range of 130 km, time is given relative to the first recorded frame, and the arrow indicates the meteoroid motion direction (initial data for the modified drawing are taken from (Stokan, 2014))

The fragmentation dynamics of a meteoroid can be clearly seen in the modified Fig. 6.3, which combines observations of progressive fragmentation and its light curve (light produced as a function of time or altitude). The snapshots for this figure were taken from (Stokan, 2014). They were obtained at the CAMO on October 16, 2010 at 07:00:52 UTC (meteor 20101016 070052) using a narrow-field camera with high light sensitivity and high spatial resolution, as well as with a wide-field camera. It is indicated that for this meteoroid, fragmentation apparently occurred before the first frame, in which the meteoroid was fixed at an altitude of 83.6 km. This follows from the presence of a maximum in the light curve shown in Fig. 6.3 at an altitude of approximately 85.5 km.

For the observed meteoroid, the orbital parameters and other characteristics were estimated (Table 6.4), allowing to draw a conclusion about its origin.

Five meteoroid fragments were identified, and their lateral displacement is tracked and displayed in Fig. 6.4. The obtained data do not contradict the existing models of meteoroid fragment expansion dynamics under conditions of supersonic flow around a system of bodies (Barry, 2005; Maksimov, 2013; Barry, 2010; Zhdan, 2007).

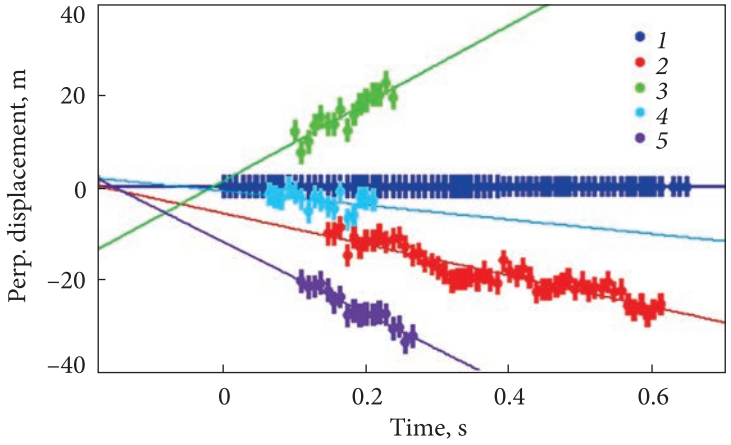

Fig. 6.4. Lateral displacement of five fragments of meteoroid 20101016 070052 (Stokan, 2014).

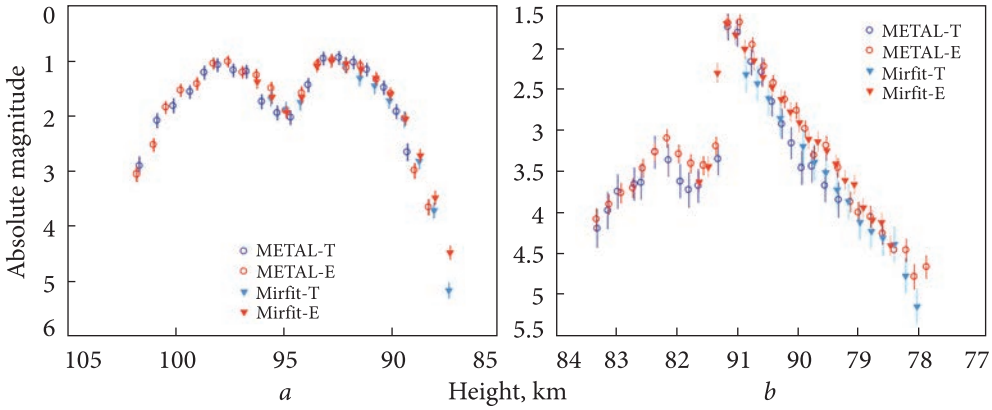

Fig. 6.5. *T*ypical light curve with a double peak (the event was recorded on September 20, 2010 at 08:46:08 UTC) — *a*; typical light curve with a "sudden peak" (the event was recorded on October 9, 2010 at 06:06:41 UTC) — *b*. Both events were observed at two sites, and photometric observations were processed using the METAL and "mirfit" software (Subasinghe, 2019)

The summary Table 6.4 presents the estimated parameters of the meteoroid 20101016 070052 given in (Stokan, 2014).

Based on the data in Table 6.4, we can conclude that the meteoroid is of asteroidal origin, although the Tisserand parameter does not unambiguously indicate this. The data can be used to approximate the correspondence of the proposed fragmentation models to the observational results.

Papers (Roberts, 2013; Subasinghe, 2019) present selective results of meteors observations obtained at CAMO, where 21 meteors (13% of events) were recorded with a pronounced bimodal light curve similar to that shown in Fig. 6.5*a*.

At the same time, in five of these meteor phenomena, "sudden peaks" similar to those shown in Figure 6.5*b* were observed.

Attempts to create a model explaining the physical reasons for the appearance of the observed bimodal light curves have been undertaken by many researchers (Campbell-Brown, 2017; Subasinghe, 2019; Jacchia 1955; Hawkes, 1975; Campbell-Brown, 2013).

However, even when fragmentation is included in the models and a good match is obtained for the light and deceleration curves, high–resolution observations by the CAMO system show the limitations of the models. The single–body ablation model was in many cases unable to reproduce the observed light curves.

Optical observations of meteor phenomena are very long and costly. This doed not allow for obtaining the necessary amount of factual material for any generalized conclusions based on statistical studies. It is possible to collect sufficient statistics to identify the fragmentation of meteoroids using radar and radio communications observations. In this case, it is important to get known how the light curves of meteors in optical observations correlate with the linear electron

Table 6.4. **Summary table of parameters for meteoroid 20101016 070052**

Orbital semi-major axis, AU	2.53 ± 0.08
Orbital inclination, degrees	14.5 ± 1.6
Orbital eccentricity	0 .663± 0.069
Argument of perihelion, degrees	230.5 ± 4.8
Perihelion distances, AU	0.853 ± 0.032
Tisserand parameter	3.07 ± 0.50
Geocentric velocity corrected for zenith attraction and diurnal aberration, km/s	28.0
Geocentric right ascension, degrees	348.2
Geocentric declination, degrees	32.7
Radiant uncertainty, degrees	0.7
Average observed meteoroid velocity, km/s	19.1 ± 1.0
Peak absolute magnitude	–7 ± 0.1
Total mass before fragmentation, kg	10^{-6}
Assumed meteoroid bulk density, kg/m^3	3300
Estimated meteoroid radius, m	2×10^{-3}
Fragment divergence interval, m	See Fig. 6.4
Fragment separation velocity, m/s	~100
Rotation speed (simulation results), Hz	7000
Pressure due to centrifugal forces, Pa	9×10^6
Initial height of observation by wide–field cameras, km	86.0 ± 0.9
Final height of observation by wide–field cameras, km	75.2 ± 0.9
Height at which fragmentation peaked, km	81.5 ± 1.3
Extrapolated fragmentation height, km	83,0

density and the initial radius of the ionized trail created by the meteoroid. It is also necessary to reveal the distinguishing signs of fragmentation based on the analysis of the observed amplitude–time and phase–time characteristics (ATCH and PTR) of radio signals mirrored from ionized meteor trails. Thus, depending on the path geometry, different ATCH and PTR can be observed for the same meteoroid. Knowing the height of the specular reflection point, obtained as a result of measurements, opens up additional possibilities for extracting information about the meteoroid and the geophysical parameters of the atmosphere.

6.3. Relationship between ionization and luminosity of a meteoroid trail

The general factors that determine the relationship between the level of ionization and the intensity of the glow of the trail created by a meteoroid are the kinetic energy and the area of the frontal section (middle) of the meteoroid, as well as the density and chemical composition of the atmosphere over the observation interval. In this case, the midsection depends on the number and relative position of the fragments currently participating in the creation of the meteor phenomenon. Further, we will use the model of a non-crushing body, in which the midsection is determined by the mass of the meteoroid and its bulk density. In the presence of crushing, for analysis, one can use the superposition of models of a non-crushing body, in which the midsection corresponds to the selected fragment.

Significant differences that determine the relationship between ionization and trail luminosity are the features of physical processes that determine the quantitative characteristics of the electron density and luminosity.

Luminosity is defined by the number of atoms and molecules of the meteoroid and atmosphere that have passed into an excited or metastable state as a result of collisions with the meteoroid and its evaporated atoms. The amount of energy (in eV) that must be expended to excite an atom or molecule of a gas is called the excitation potential . The excitation of atoms in collisions with ions and atoms is effective if the kinetic energy of the colliding particles (interaction energy) exceeds the threshold value. The excited state is unstable and, upon transition to the normal unexcited state, the excitation energy is transferred to the surrounding space in the form of light electromagnetic radiation. The average lifetime of excited molecules is about 10–10 s, and being in a metastable state can be much longer.

When interpreting the results of optical and radar observations of meteors, in the first approximation, the simplest physical theory of meteors (Bronshten, 1981; Bronshten, 1983; Öpik, 1937; Ŏpik, 1958; Fisher, 1934; Whipple 1938; Whipple 1943; Herlofson, 1948; McKinley, 1961; Evans, 1966) is usually used, which is based on the assumption that the main mechanism of ablation of meteoroids is the evaporation of non-crushing and not changing its shape form curing eveporation meteoroid. In this case, interaction of the meteoroid with the atmosphere is described by three basic equations.

The deceleration equation is the first basic equation of the physical theory of meteors, which is based on the assumption that the loss of momentum by the meteoroid $m_m\, dv$ is proportional to the momentum of the oncoming airflow:

$$m_m \, dv/dt = -\Gamma S \, \rho_a \, v^2, \tag{6.4}$$

where m_m is the mass of the meteoroid, v is the velocity, S is the area of the frontal section (midsection), ρ_a is the density of the atmosphere, Γ is the drag coefficient (the fraction of the momentum of the incident atoms and atmospheric molecules, which is converted into the deceleration of the body). The value of Γ can be both less than unity, when some of the oncoming molecules flow around the body, and greater than unity, when the reactive impulse of molecules rebounding from the meteoroid surface is noticeably manifested (Bronshten, 1981).

The mass loss equation is the second basic equation of the physical theory of meteors, which describes the mass loss of a meteoric body, provided that all the energy is spent on ablation (evaporation or melting and blowing off the molten film):

$$\frac{dm_m}{dt} = -\Lambda S \rho_a \frac{v^3}{2Q}, \tag{6.5}$$

where Q is the specific heat of evaporation of the meteoroid substance (J/kg), and Λ is the fraction of the kinetic energy of the oncoming flow of molecules spent on ablation during the time dt.

The third basic equation of the physical theory of meteors, the equation of luminosity, allows one to calculate the intensity of the glow of a meteor for a given moment in time. It is based on the assumption that the meteor radiation power, measured either bolometrically or in the bandwidth of a specific instrument, is proportional to the kinetic energy of the meteoroid mass dM_m evaporated over time dt:

$$I = -\tau_I \frac{dK_m}{dt} = -\tau_I \left(\frac{v^2}{2} \frac{dm_m}{dt} + mv \frac{dM_m}{dt} \right), \tag{6.6}$$

where τ_I is the radiation efficiency coefficient, or the luminosity coefficient, which depends on the velocity, mass, and chemical composition of the meteoroid, as well as on the density and chemical composition of the atmosphere at the observation altitude.

This equation can be represented as

$$I = -\tau_I \frac{v^2}{2} \frac{dm_m}{dt} \left(1 + \frac{m_m v \dfrac{dv}{dt}}{\dfrac{v^2}{2} \dfrac{dm_m}{dt}} \right) \tag{6.7}$$

or, using equations (6.4) and (6.5), converted to the form

$$I = -\tau_I \frac{v^2}{2} \frac{dm_m}{dt} \left(1 + 4 \frac{Q\Gamma}{v^2} \frac{\rho_a}{\rho_m} \right). \tag{6.8}$$

It is easy to show that the second term in parentheses of equation (6.8) is much less than unity, which agrees with the conclusion obtained in (Ceplecha, 1998) but was obtained without using the ablation coefficient introduced there. This allows us to represent the luminosity equation in the traditionally used form

$$I = -\tau_I \frac{v^2}{2} \frac{dm_m}{dt} . \tag{6.9}$$

In this equation, I is the radiant power (bolometric or in a specific bandwidth) and τ_1 is the luminous efficiency defined as the proportion of meteoroid kinetic energy loss converted into radiation. The luminous efficiency depends on the chemical compositions of the meteoroid and atmosphere (since different chemical elements are represented by different line intensities in the observed spectrum), on the speed of the meteoroid, and, possibly, on its mass.

The main part of the light energy is formed in the head part of the track when the evaporated atoms of the meteoroid and atmosphere are excited, which forms a coma. The density of the coma is such that it can be considered as a single body with the midsection interacting with the atmosphere. Some of the atoms and molecules of the atmosphere during impact ionization pass into a metastable state and, after returning to the normal state with some delay, emit a quantum of light, forming a "tail". A certain proportion of the light energy of the "tail" is created by the evaporated particles of the meteoroid and particles of the atmosphere, which have sufficient energy to excite, during repeated collisions.

In the case of fragmentation, each fragment of the meteoric body participates in the creation of light radiation, but their random mutual arrangement does not allow one to unambiguously determine the value of the total midsection (and, consequently, the light flux) over the observation interval.

The process of formation of an ionized trail is similar to the formation of a meteor characterized by a luminosity curve. The inelastic collision of the vaporized meteoroid atoms with air molecules leads to the formation of free electrons that create an ionized trail, the main characteristic of which is the linear electron density. It depends on the equilibrium evaporation rate and is proportional to the number of evaporated meteor body atoms colliding with atmospheric molecules and atoms per unit path length.

To calculate the number of free electrons produced per one evaporated atom of a meteor body, the ionization coefficient is used, which depends on the ratio of the probabilities of ionization (inelastic process) and momentum transfer (elastic process). Taking into account that each meteor atom may experience not one but

several collisions as a result of the cascade ionization process, the ionization coefficient may, under certain conditions, exceed unity.

The ionization produced by meteoroids is described on the basis of the same deceleration and mass loss equations and, without taking into account fragmentation, leads to the well–known expression for the linear electron density.

$$q = -\frac{\beta}{\mu_m v}\frac{dm_m}{dt}. \tag{6.10}$$

Here q is the linear electron density along the path of the meteoroid, μ_m is the atomic mass of a typical meteor atom, β is the ionization coefficient, which determines the number of electrons produced by one ablated atom, and dm_m/dt is given by equation (6.5).

To interpret radar measurements, it is necessary to know the ionization coefficient β, defined as the probability of formation of an ion-electron pair due to collision of a meteoroid atom with an atmospheric molecule. It depends on the ratio of the effective cross-sections of two processes: ionization and momentum transfer. Since the effective cross-section is a quantity that determines the probability of a given process (it got its name because it has the dimension of area), the above is equivalent to saying that the ionization coefficient depends on the ratio of the probabilities of ionization (inelastic process) and momentum transfer (elastic process). In this case, the collision of atmospheric particles with the meteoroid midsection at a unit length occurs with a probability close to unity. The probability of subsequent collisions and ionization due to the cascade process of interaction of atoms and ions of a meteoric body and the atmosphere over a time interval of flight is determined by their residual kinetic energy, atomic radii, and threshold ionization energy. Obviously, the number of collisions with the meteoroid midsection and the number of subsequent collisions outside the midsection depend on the density and chemical composition of the atmosphere at the observation altitude.

In the equations that determine the luminosity and linear electron density, the most uncertain parameter is the meteoroid mass change dm_m/dt, which cannot be measured directly. Perhaps, the most important physical parameter that can be obtained from meteor observations is the meteoroid mass. It can be determined by summing either all the light emitted during the meteor lifetime (photometric mass) or all the electrons generated during ablation (ionization mass), but only if the efficiency of electron and photon generation by each unit of ablated mass is known.

Unfortunately, β and τ_I cannot be directly measured as separate quantities based on video and radar observations. Laboratory studies (Thomas, 2016; Friichtenicht, 1967; Jones, 1997; Friichtenicht, 1971; Friichtenicht, 1973) are very effective and are the basis of many theoretical studies, but they do not cover the entire range of meteoroid velocities and cannot provide real conditions for observing meteors and ionized trails. The uncertainty of laboratory estimates of β

and τ_I is exacerbated by the lack of a priori data on the physical and chemical properties of the meteoroid, as well as the nature of the fragmentation of the meteoroid during the observation interval and before it.

Since q and I are proportional to dm_m/dt, equations (6.9) and (6.10) can be combined to give the relation β/τ_I independent of the rate of mass loss:

$$\frac{\beta}{\tau_I} = \frac{\mu_m v^3}{2}\frac{q}{I}. \tag{6.11}$$

This relation can be considered true only if q and I correspond to the same trail segment. It can be determined from simultaneous radar and photometric measurements. If β or τ_I are known or assumed to be known, then knowing one of the values, one can estimate the other.

There are good reasons to believe that β has fewer uncertainties than τ_I (Weryk, 2012; Weryk, 2013), which is due to the instrumental features of video measurements and calibration methods, when they are performed.

In (Bronshten, 1981; Thomas, 2016; Jones, 1997; Weryk, 2012; Weryk, 2013; Moorhead, 2017) the integral equation (6.12), which can be solved numerically, and the expressions (6.13—6.14) are used to estimate β

$$\beta(v) = \beta_0(v) + (1-\beta_0(v))\frac{1+\chi^2}{2v^2\chi}\int_{v_0}^{v}\beta(v')v'dv', \tag{6.12}$$

$$\beta_0(v) = \frac{\sigma_{ion}}{\sigma_{ela}+\sigma_{ion}} = \frac{c(v-v_0)^2 v^{0,8}}{1+c(v-v_0)^2 v^{0,8}}, \tag{6.13}$$

$$v_0^{\,2} = \frac{2(1+\chi)E_{ion1}}{\chi\mu_a} = \frac{2(1+\chi)e\varphi_{ion1}}{\chi\mu_a}, \tag{6.14}$$

where β_0 is the ionization coefficient in the primary (single) collision; $\chi = \mu_m/\mu_a$ is the ratio of the average atomic mass of meteoroid atoms to the average atomic mass of atmospheric atoms at the observation height; σ_{ela} is the elastic collision cross-section; σ_{ion} is the ionization cross-section (inelastic collision); v_0 is the minimum velocity of an atom at which the kinetic energy is sufficient for ionization during a collision with an atmospheric molecule; E_{ion1} is the first ionization energy per mole, which determines the amount of energy required to detach the electron most weakly bound to the nucleus from an isolated unexcited atom of an element in the gas phase (it refers to 1 mole of electrons, i.e., measured in kJ/mol); e is the electron charge; Φ_{ion1} is the first ionization potential; c is a free parameter used to fit the values of β_0 obtained from experimental studies.

Note that the above formulas imply the possibility of obtaining estimates for β(v) under various assumptions regarding the physical and chemical properties of meteoroids (PCPMet) and the atmosphere (PCPAtm). For a meteoroid with

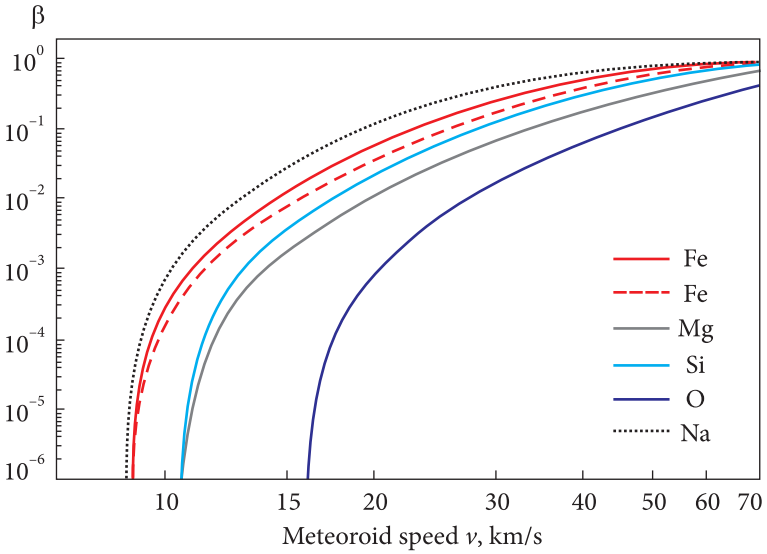

Fig. 6.6. Ionization efficiency β as a function of the meteoroid velocity for iron (Fe), magnesium (Mg), silicon (Si), oxygen (O), and sodium (Na), calculated using formulas (6.12)—(6.14) and the parameters listed in Table 6.5. The exception is the dashed red line, which corresponds to the iron parameters (Thomas, 2016)

a complex chemical composition, the integral estimate β_{total} will be a linear combination, where each element is taken with a weight p_j proportional to its share in the total number of meteoroid atoms (Moorhead, 2017)

$$\beta_{total} = \sum_j p_j \beta_j . \qquad (6.15)$$

Based on expressions (6.12—6.14) and the data given in Table 6.5, the ionization efficiency β was calculated as a function of the meteoroid velocity for iron (Fe), magnesium (Mg), silicon (Si), oxygen (O) and sodium (Na). The calculation results taken from (Moorhead, 2017) are presented in Fig. 6.6.

Table 6.5. **Atomic weight (μ_m), first ionization energy (E_{ion1}), minimum ionization rate (v_0), free parameter (c) for five types of meteor particles. When calculating v_0, it is assumed that μ_a = 28.966 g/mol**

Element	μ_m, g/mol	E_{ion1}, kJ/mol	v_0, km/s	c, × 10^6
O	15.9994	1313.9	15.97	4.31
Fe	55.845	762.5	8.94	32.8
Mg	24.305	737.7	10.57	8.94
Si	28.055	786.5	10.50	17.6
Na	22.989	495.8	8.80	69.5

Note that the calculations used the first-order ionization energy and did not consider the possibility of higher-order ionization, which is accompanied by the formation of an additional number of free electrons, which should lead to an increas in the estimate of the ionization efficiency coefficient β.

In calculations, instead of the ionization energy expressed in *kJ/mol*, the ionization potential $I_{ion\,i}$ is often used, expressed in electron volts (eV), which is numerically equal to the ionization energy of one atom. The relationship between ionization energy (*kJ/mol*) and ionization potential (eV) is determined by a simple expression (Glinka, 2010)

$$E_{ioni}\left(kJ/mol\right) = 96.5 \times I_{ion\,i}(eV) \tag{6.16}$$

An electron volt is a convenient unit for measuring the energy of molecules and elementary particles, but it does not belong to the SI system. Therefore, when calculating, one should convert electron volts to joules using the coefficient given above.

Table 6.6, as an example, shows the values of the 1st and three subsequent ionization potentials of the elements presented in Table 6.5.

For other elements that may be part of the atmosphere at the selected altitude, as well as the composition of the meteoroid model, the ionization potential values can be found in reference books (for example, (Glinka, 2010; Mak–Daniel, 1967; Popkov, 2010; Mishenina, 2007)).

In (Whipple 1938), a power-law approximation of the ionization coefficient was used, which was refined based on experimental data (Thomas, 2016)

$$\beta(v) = bv^a, \tag{6.16}$$

where v is the velocity measured in km/s, $b = 1.629 \times 10^{-4}$, $a = 2.068$.

It can be used in the range of meteoroid velocities of 20—90 km/s for an approximate estimate of the value of $\beta\,(v)$.

Given that the meteoroids are H-chondrite and the atomic mass of a typical meteor atom is $\mu_m = 0.0241$ kg/mol, an approximation of $\beta(v)$ by the expression Weryk, 2012)

$$\log_{10}\beta\left(v\right) = 5{,}84\ldots0{,}09\,v^{0{,}5} - 9{,}56/\log_{10} v \tag{6.17}$$

where v is measured in km/s.

Table 6.6. **Values of the ionization potentials of the elements**

Element	E_{ion1}, kJ/mol	$I_{ion\,1}$, eV	$I_{ion\,2}$, eV	$I_{ion\,3}$, eV	$I_{ion\,4}$, eV
O	1313.9	13.6	35.1	54.9	77.4
Fe	762.5	8.23	16.2	30.6	54.8
Mg	737.7	7.64	15.0	—	—
Si	786.5	8.15	16.3	33.5	45.1
Na	495.8	5.14	—	—	—

There are other expressions for estimating $\beta(v)$, obtained by fitting to the results of radar observations (Gorelov, 2005), where the comparison of calculations based on methods similar to those described above was also carried out.

In (Bronshten, 1981), the dependence of the ionization coefficient on the velocity β (v) is based on experimental data for a number of chemical elements' characteristics of meteoric matter (Friichtenicht, 1967; Kaiser, 1955; Lindblad, 1967; McCrosky, 1955; McCrosky, 1958). The average data for these elements are presented in Table 6.7.

As a result, an approximating calculation formula for β (v) was obtained

$$\beta(v) = 4{,}36 \times 10^{-24} \times v^{3{,}42}, \tag{6.18}$$

where the meteoroid velocity v is measured in cm/s. If v is measured in km/s, then (6.18) is converted to the form

$$\beta(v) = 5{,}4889 \times 10^{-7} \times v^{3{,}42}. \tag{6.19}$$

Formulas (6.16) and (6.19) were obtained for a given meteoroid chemical composition (indicated in Tables 6.5 and 6.7) and can be used as a guide when calculating the ionization coefficient $\beta(v)$ for meteoroids of various origins.

To determine the value of the luminous efficiency τ_I based on expression (6.11), in addition to $\beta(v)$, it is necessary to estimate the linear electron density q of the ionized trail of a meteoroid.

However, direct measurement of q by radar methods is not feasible. To estimate it, the power of the reflected signal is used, measured within the first Fresnel zone (~2 km), which essentially depends on the radial distribution of the electron density and the accepted value of the initial trail radius, which are not determined accurately enough. In addition, the effects of meteoroid fragmentation and the dependence of the ionization coefficient β on the chemical composition of the observed meteoroids can affect the estimate of the peak power of the reflected signal.

Linear electron density measurements using the ALTAIR system, based on radar observations of echoes from the meteoroid head, have been described in (Campbell-Brown, 2007). Each echo was modeled using code developed at the European Space Research and Technology Center (ESTEC) of the European

Table 6.7. **Values of the ionization coefficien**t

Element	Fraction, %	Meteoroid velocity v, km/s			Element	Fraction, %	Meteoroid velocity v, km/s		
		20	40	70			20	40	70
O	56.0	0.00016	0.043	0.554	Ca	0.9	0.082	0.619	1.98
Fe	11.4	0.068	0.595	3.41	Si	14.4	0.023	0.300	1.70
Mg	15.4	0.020	0.151	0.81	***β (v)***	**100.1**	**0.0154**	**0.170**	**1.12**

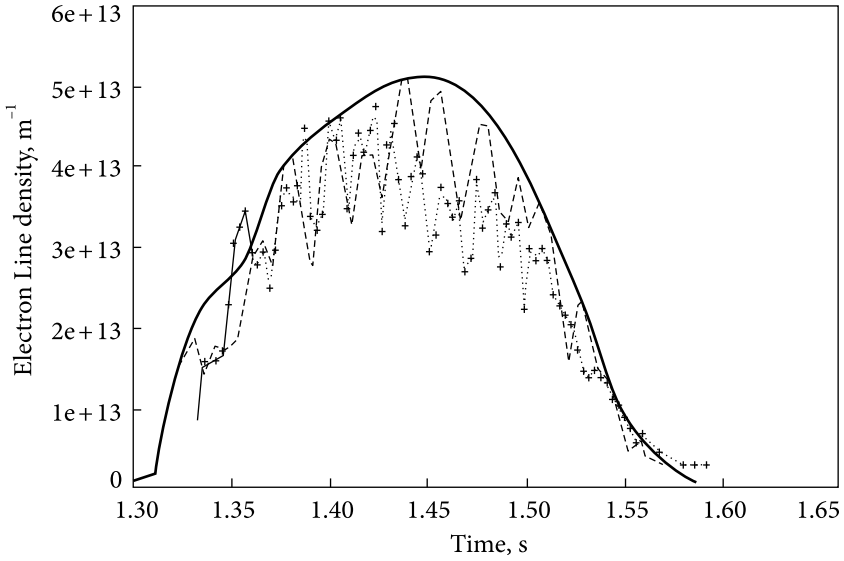

Fig. 6.7. Linear electron density versus time for the meteor 982100_53. The dotted line shows the measured values, the solid line is the theoretically predicted total ionization, and the dashed line is the predicted ionization that can be obtained taking into account interference between fragments (Campbell-Brown, 2007)

Space Agency (Campbell-Brown, 2004), which was modified to calculate the ionization density. The radar cross-section (RCS) of an equivalent point source was found for each individual pulse echo along the meteor trail and converted to the linear electron density using a three-dimensional scattering model (Close, 2004). An example of the measured linear electron density along with the simulation results is shown in Fig. 6.7 (Campbell-Brown, 2007).

Obviously, the nature of the change in the linear electron density $q(t)$ in time is the same as for the change in luminosity (see Figure 6.3) and contains signs of meteoroid fragmentation.

Since the luminous efficiency τ_I and the ionization coefficient β depend on the respective fractions of the kinetic energy of the interaction between meteoroid atoms and atmospheric atoms, it can be assumed that the optical radius of the meteor head and the initial radius of the ionized trail are in a certain relationship . In this case, the optical radii will be larger than the electronic radii, since the energy of atom's excitation is less than the energy of its ionization, and the probability of repeated collisions leading to the excitation of atoms is higher. This can give a "hint" for developing a model for the distribution of electron density in the head of a meteor and determining the initial radius of the ionized meteoroid trail.

6.4. Model of the electron density of the trail created by a meteoroid at the point of observation

The main characteristics of the ionized trail created by a meteoroid are the value of the linear electron density and the shape of its two-dimensional probability density of the distribution of electrons relative to the trail axis. The characteristics of IMTr over the observation interval determine the amplitude–time and phase–time characteristics of the reflected radio signals, which are necessary for the design of telecommunication systems and allow us to make assumptions about the features and origin of the meteoroid, as well as about the characteristics of the atmosphere at altitudes of 80—130 km.

6.4.1. The estimating model for the linear electron density of meteor trail

When developing an LEDTr model, we will use the results of the integral estimate of the ionization coefficient $\beta_{total}(v)$ presented in section 6.3 and take into account that the number of collisions per one meter of the meteoroid path is proportional to the concentration of atmospheric particles and the midsection of the meteoroid head $S_{MH}(v, m_m, h_M, PCPMet)$ in the SRP region

$$q\left(v, m_m, h_{\text{i}}, PCPMet\right) = \beta_{total}\left(v, PCPMet\right) \times$$
$$\times S_{MH}\left(v, m_m, h_{\text{i}}, PCPMet\right) \times N\left(h_{\text{i}}\right) \times l^{-1}, \qquad (6.20)$$

where $\beta_{total}(v, PCPMet)$ is the integral estimate of the ionization coefficient presented in subsection 6.3, $N_a(h_M)$ is the number density of the atmosphere at the observation height h_M, which can be determined from data given in various standard atmosphere models, and $l = \Delta h_M / \cos \gamma_m = 1$m is the length of the path along which the electron density was calculated.

The most difficult task is to estimate $S_{MH}(v, m_m, h_M, PCPMet)$. The value of this midsection depends on the initial mass and density of the meteoroid, the intensity of evaporation, which depends on the physicochemical characteristics of the meteoroid, its kinetic energy, and the atmospheric density $\rho_{atm}.(h_M)$ at the observation altitude, as well as the presence and parameters of fragmentation and differential ablation.

The value of the meteoroid midsection at the entry to the meteor zone without taking into account fragmentation and differential ablation is determined by the expression

$$S_{m0} = A_0 \left(\frac{m_{m0}}{\rho_m} \right)^{\frac{2}{3}}, \qquad (6.21)$$

where A_0 is a shape factor, m_{m0} and ρ_m are the initial mass and density of the meteoroid, respectively. It is easy to show that $A_0 \approx 1.2$ for a sphere and $A_0 = 1$ for

a cube. Mass and density differ for asteroidal and cometary meteoroids. With fragmentation and differential ablation, the value of A_0 can be significantly greater than unity.

The midsection S_{mM} at the observation point is determined by its residual mass m_{mM}, and expression (6.21) is converted to the form

$$S_{m\mathrm{M}} = A_0 \left(\frac{m_{m\mathrm{M}}}{\rho_m} \right)^{\frac{2}{3}}, \tag{6.22}$$

Particles that have evaporated within a given interval $\Delta l = \Delta h / \cos \gamma$ of the motion trajectory form a "cushion" of vapor in front of the meteoroid, which leads to a change in the midsection. In this case, the midsection of the head part at a height h_M can be represented by the expression

$$S_{HM}\left(h_M\right) = A_0 \left(\frac{m_{in}}{\rho_m} \right)^{\frac{2}{3}} + N_{\mathrm{evep}}\left(h_M\right) \cdot \sigma_{m\,\mathrm{av}}, \tag{6.23}$$

where $\sigma_{m\,av}$ is the average cross-section for the collision of evaporated particles, and N_{evep} (h_M) is the number of particles evaporated at height h_M, which can be represented by the expression

$$N_{e\,vep}\left(h_M\right) = \frac{\Delta m_m\left(h\right)}{\mu_{m\,av}} = \frac{\left[m_m\left(h_M + \Delta h\right) - m_m\left(h_M\right) \right] \cdot N_A}{M_{m\,mol}} = \frac{\Delta m_m\left(h_M\right) \cdot N_A}{M_{m\,mol}}, \tag{6.24}$$

where Δ_{mm} (h_M) is the mass loss at height h_M when it changes by Δh, $\mu_{m\,ev}$ is the average absolute mass of evaporated particles defined as the ratio of the molar mass $M_{m\,mol}$ to the Avogadro number $N_A = 6.02214082 \cdot 10^{23}$ mol^{-1}. The molar mass of any substance, expressed in grams per mole, is numerically equal to the relative mass of the molecule of this substance and can be found from the periodic table. Neglecting the mass defect, the relative atomic mass of a molecule is equal to the sum of the relative atomic masses of its constituent elements. It should be noted that if Δ_{mm} (h_M) was calculated in kg (SI system), the molar mass in g/mol should be converted to that in kg/mol, i.e., divided by 1000.

Based on expressions (6.23) and (6.24), the midsection area S_{MH} (h_M) at the observation point can be represented by the expression

$$S_{HM}\left(h_M\right) = A_0 \left(\frac{m_{in}}{\rho_m} \right)^{\frac{2}{3}} + A_1 \frac{\Delta m_m\left(h\right) \cdot N_A}{M_{m\,mol}} \cdot \sigma_{m\,\mathrm{av}}, \tag{6.25}$$

where A_1 is the coefficient correcting the increase in the midsection S_{MH} due to evaporation, and $\sigma_{m\,av}$ is the average value of the cross-sections of the molecules (atoms) of the meteoroid, which depends on its chemical composition. The minimum distance at which the centers of two molecules approach during a collision

is called the effective diameter d of the molecule, and the value $\sigma = \pi d^2$ is usually called the effective cross–section of the molecule.

The average value of the effective cross–section of molecules (atoms) of meteoroids may differ for meteoroids of various types, depending on their physicochemical properties, which are largely determined by their origin. By origin, asteroidal and cometary meteoroids are distinguished. A more complete classification according to the chemical composition of meteoroids is given, for example, in (Ivanov, 2019) and a number of other works.

The volume of a mole of a substance X can be estimated by calculating its molar mass and dividing it by the density of this substance

$$V\left(X_{mole}\right) = \frac{M\left(X_{mole}\right)}{\rho\left(X\right)}. \tag{6.26}$$

The molar mass of a substance $M(X_{mole})$ in kg/mol is numerically equal to the relative molecular mass of the given substance $\mu_m(X)$ divided by 1000, and its density $\rho(X)$ is selected from the appropriate reference books. An approximate estimate of the volume of one molecule of a substance $V(X_1)$ can be performed, assuming that the molecules are located as close as possible to each other and dividing $V(X_{mol})$ by the Avogadro number N_A

$$V\left(X_1\right) = \frac{M\left(X_{mole}\right)}{\rho\left(X\right)\cdot N_A} = \frac{\mu_m\left(X\right)}{1000\cdot\rho\left(X\right)\cdot N_A}. \tag{6.27}$$

In this case, the diameter of the molecule d_X is equal to

$$d_X = \sqrt[3]{\frac{6V\left(X_1\right)}{\pi}}, \tag{6.28}$$

and the effective cross–section of a molecule (atom) of a meteoroid σ_{X1} is defined by the expression

$$\sigma_{X1} = \pi d_{X1}^2 = \frac{\pi}{100}\cdot\left[\frac{6\,\mu_m\left(X\right)}{\pi\,\rho\left(X\right)\cdot N_A}\right]^{2/3}. \tag{6.29}$$

Taking into account expressions (6.24) and (6.29), the total average cross–section of particles $\sigma_{\Sigma m\,av}$ evaporated at height h_M is equal to

$$\sigma_{\Sigma m\,av} = \frac{\Delta m_m\left(h_M\right)\cdot N_A}{M_{m\,mol\,av}}\cdot\sigma_{X1av}, \tag{6.30}$$

where

$$M_{m\,mol\,av} = \sum_{j=1}^{L} p_j M_{mj}\,,\ \sigma_{X1\mathrm{cp}} = \sum_{j=1}^{L} p_j \sigma_{\mathbf{X}\mathrm{j}}\,,\ X1_{\mathrm{av}}$$

and p_j is the proportion of the *j-th* evaporated substance.

To implement the midsection calculations based on expression (6.25), it is necessary to obtain the dependence of the meteoroid mass on the height of the observation point h_M, which will allow estimating the amount of evaporated matter in a given interval Δh.

The mass of the meteoroid at the observation point m_{mM} depends on the initial mass m_{m0}, its velocity at the observation point v_M, and the zenith angle γ_m, which is determined by the radiant of the meteoroid. Let us estimate m_{mM} based on equations (6.4) and (6.5). We relate the change in time to the change in altitude using the expression from (Chernogor, 2018)

$$dt = -\frac{dz}{v\cos\gamma}. \tag{6.31}$$

Then expressions (6.4) and (6.5) can be transformed to the form

$$m_m \frac{dv}{dz} = -\frac{\tilde{A}}{Q_m \cos\gamma} S_m \rho_a v, \tag{6.32}$$

$$\frac{dm_m}{dz} = -\frac{\Lambda}{\cos\gamma} S_m \rho_a v^2, \tag{6.33}$$

where the previously used notation is applied.

Dividing (6.33) by (6.32), we obtain a relation relating the mass m_m and the velocity v of the meteoroid

$$\frac{1}{m_m} dm_m = \frac{\Lambda}{2Q_m \Gamma} v\, dv. \tag{6.34}$$

Integrating the left side of (6.34) from the value of the initial meteoroid mass m_{m0} to its mass m_{mM} in SRP, and the right side from the value of the initial meteoroid velocity v_{m0} to its value at the observation point M, v_{mM}, we obtain the equation

$$\int_{m_{m0}}^{m_{mM}} \frac{1}{m_m} dm_m = \frac{\Lambda}{2Q_m \Gamma} \int_{v_{m0}}^{v_{mM}} v\, dv. \tag{6.35}$$

As a result of integration, we obtain the value of the meteoroid mass at point M depending on the velocity at this point v_{mM} for a given initial velocity v_{m0}

$$m_{mM} = m_{m0} \exp\left[-\frac{\Lambda}{2Q\Gamma} \frac{\left(v_{m0}^{\,2} - v_{mM}^{\,2} \right)}{2} \right] \tag{6.36}$$

or, using the value of the ablation parameter $\sigma_a = \Lambda/2Q\Gamma$ (Bronshten, 1981)

$$m_{mM} = m_{m0} \exp\left[-\sigma_a \frac{\left(v_{m0}{}^2 - v_{mM}{}^2 \right)}{2} \right]. \tag{6.37}$$

To calculate the mass of a meteoroid at an observation point, it is necessary to estimate its velocity at this point, which depends on the midsection of the meteoroid, and the density of the atmosphere. In the first approximation, which is usually sufficient for many purposes of meteor astronomy, from the equation of state and the equation of hydrostatic equilibrium of the atmosphere, we obtain the exponential distribution of the atmospheric density $\rho_a(h)$ with respect to height h:

$$\rho_a(h) = \rho_b \exp\left[-\frac{g_b m_{ab} (h - h_b)}{R T_b} \right], \tag{6.38}$$

where ρ_b, g_b, and T_b are the atmospheric density, gravitational acceleration, and absolute temperature at h_b selected (base) altitude, m_{ab} is the average molar mass (kg/kmol) of atmosphere particles at base altitude, and R = 8314.46 (J/kmol · K) is the universal gas constant.

If we choose h_b = 95,000 m as the base height and use the data from (State Standard 4401-73), formula (6.38) is converted to the form

$$\rho_a(h) = 1{,}4051 \cdot 10^{-6} \exp\left[-0{,}17768 \cdot 10^{-3} (h - 95000) \right]. \tag{6.39}$$

Table 6.8 and Fig. 6.8 presents the results of calculating the change in atmospheric density depending on the height h, performed according to formula (6.32), and the corresponding data given in (State Standard 4401-73) for the northern latitude 45°32'33". The discrepancy between the calculated and experimental data

Table 6.8. **Change in the atmosphere density depending on the height**

h, km	ρ kg/m³, (calculated)	ρ kg/m³, (GOST)	Deviation, %
80	2.019E-05	1.8458E-05	9.40
85	8.305E-06	8.2200E-06	1.04
90	3.416E-06	3.4182E-06	–0.06
95	1.405E-06	1.4051E-06	0.00
100	5.779E-07	5.5495E-07	4.14
105	2.377E-07	2.2617E-07	5.11
110	9.777E-08	9.3404E-08	4.68
115	4.022E-08	4.5181E-08	–10.99
120	1.654E-08	2.4494E-08	–32.47

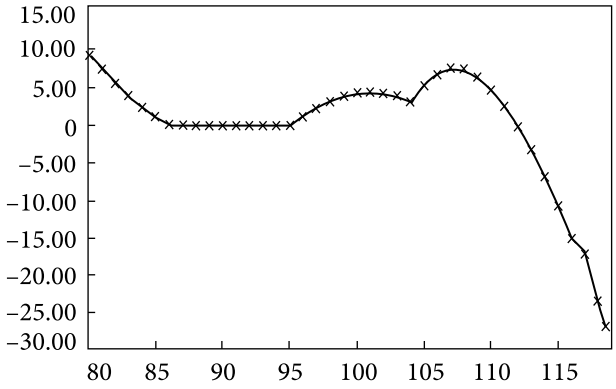

Fig. 6.8. Deviation of the calculated values of the density of the atmosphere from the reference values

is relatively small and can be reduced for the required height range by choosing the appropriate base height and parameters in formula (6.39).

In (Tirskiy, 2000), when calculating the meteoroid velocity, it was assumed that its mass m_m and midsection S_m did not change when moving with an initial velocity v_{m0} in a medium with a density ρ_m, and the force of gravity was negligibly small compared to the force of resistance to the motion. This made it possible to obtain an approximate estimate of the meteoroid velocity at the observation point represented by the expression

$$v_{mM}(h) = v_{m0} \exp\left(-\rho^*/2\right). \tag{6.40}$$

where $\rho^* = \rho_a(h)/\rho_\beta(h)$, $\rho_\beta(h) = \beta \cos\gamma /h$, $\beta = m_m/S_m$ — ballistic coefficient, and S_m — meteoroid midsection.

Taking into account the accepted notation, the expression (6.40) is transformed to the form

$$v_{mM}\left(h_{aM}, m_{mM}, \gamma_m\right) = v_{m0} \exp\left[-\frac{\rho\left(h_{aM}\right) h_{aM} S_{mM} C_D}{2 m_{mM} \cos\gamma_m}\right], \tag{6.41}$$

where γ_m is the zenith angle of the meteoroid radiant; C_D is a dimensionless aerodynamic drag coefficient, which, when a meteoroid moves in the range of meteor heights, can take values from 2 to 0.5 (depending on the shape of the body and the Reynolds number for it). If at the height of observation, the mean free path of molecules is greater than the characteristic size of the body, the coefficient C_D can be taken equal to 2.

Expressing the midsection of the meteoroid in terms of its mass m_{mM} and density ρ_m using formula (6.22), we obtain

$$v_{mM}\left(h_{aM}, m_{mM}, \gamma_m\right) = v_{m0} \exp\left[-\frac{\rho_a\left(h_{aM}\right) h_{aM} C_D A_0}{2\left(m_{mM} \rho_m^2\right)^{\frac{1}{3}} \cos\gamma_m}\right]. \tag{6.42}$$

The algorithm for calculating the values of m_{mM} and v_{mM} can be implemented based on the calculation formulas (6.42) and (6.36) using the recurrent method, in which each next member of the sequence is calculated using the result of calculating the velocity and mass at the previous step. This approach makes it possible to partially remove the restrictions on the requirement that the mass and midsection of the meteoroid be constant during its motion and velocity calculation at the observation point.

To implement the recurrent method of calculating m_{mM} and v_{mM}, one must perform the following steps:

1. Calculate, using expression (6.42), the value of the velocity v_{mM} at a point close to the upper boundary of the meteor zone at a height $h_{max} - \Delta h$. At the same time, the velocity of the meteoroid at the entry to the meteor zone v_{m0}, its initial mass m_{m0}, density ρ_m, and radiant zenith angle γ_m are assumed to be known, and the height of the upper boundary of the meteor zone h_{max}, the coefficients C_D and A_0 are also considered given. The value of atmospheric density at height $h_{max} - \Delta h$ can be calculated using expression (6.39).
2. Calculate the meteoroid mass value at height $h_{max} - \Delta h$ using expression (6.36).
3. Calculate, using expression (6.42), the value of the velocity v_{mM} at the height $h_{max} - i\Delta h$, where $i = 2$. In this case, use the value of the meteoroid mass obtained at the previous step (at the height $h_{max} - \Delta h$).
4. Calculate the value of the meteoroid mass at the height $h_{max} - 2\Delta h$ using expression (6.36).
5. Calculate the value of the velocity v_{mM} at the height $h_{max} - i\Delta h$, where $i = 3$. In this case, use the value of the meteoroid mass obtained at the previous step (at the height $h_{max} - 2\Delta h$).
6. Repeat the calculations of v_{mM} and m_{mM} for $i = 4 \ldots N$, where N is determined from the condition $(h_{max} - N\Delta h) \geq h_{min}$.

As a simple example, Table 6.9 and Figure 6.9 present the results of m_{mM} and v_{mM} calculations for an iron meteoroid with the following initial data:

- meteoroid velocity at the entry to the meteor zone $v_{m0} = 40\,000$ m/s;
- meteroid initial mass $m_{m0} = 0.001$ kg;
- meteoroid density $\rho_m = 7874$ kg/m^3;
- relative molar mass of an iron meteoroid μ_m (Fe) = 29.4387;
- ionization coefficient for iron $\beta_{Fe}(v = 40$ km/s) ≈ 0.8;
- specific heat of evaporation of a meteoric body $Q = 6.3 \cdot 106$ J/kg;
- zenith angle of the meteoroid radiant $\gamma_m = 60°$;
- shape factor $A_0 = 1.21$;
- drag coefficient $C_D = 2$;
- correction factor $A_1 = 1$.

The obtained dependences allow, on the basis of the previous and subsequent values of expression (6.36), calculation of the mass loss of the meteoroid on the path length $l = 1$ km, on which the LEDTr is determined. The calculation results are presented in Table 6.10 and Fig. 6.10.

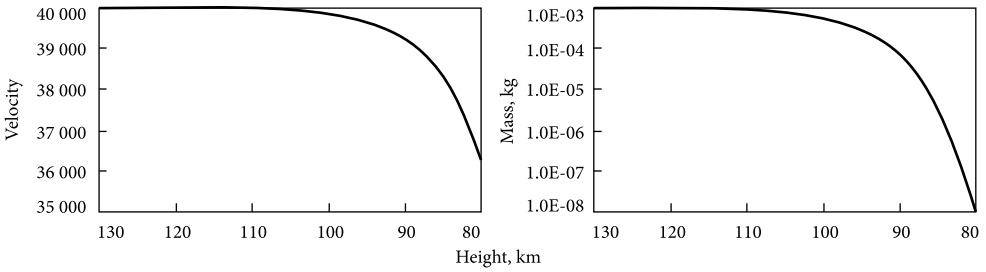

Fig. 6.9. Velocity and mass of the meteoroid depending on the height of observation

Table 6.9. **Velocity and mass of an iron meteoroid depending on the height of observation**

Height, km	Velocity, m/s	Mass, kg	Height, km	Velocity, m/s	Mass, kg
130	39999.1	9.97E-04	104	39928.4	7.97E-04
128	39998.8	9.96E-04	102	39899.9	7.28E-04
126	39998.3	9.94E-04	100	39860.1	6.42E-04
124	39997.6	9.92E-04	98	39804.5	5.38E-04
122	39996.6	9.89E-04	96	39727.0	4.22E-04
120	39995.2	9.85E-04	94	39619.2	3.00E-04
118	39993.2	9.79E-04	92	39469.2	1.88E-04
116	39990.5	9.70E-04	90	39261.2	9.79E-05
114	39986.7	9.59E-04	88	38973.1	4.00E-05
112	39981.4	9.43E-04	86	38575.5	1.18E-05
110	39973.9	9.21E-04	84	38029.0	2.24E-06
108	39963,5	8.91E-04	82	37281.8	2.40E-07
106	39948.9	8.50E-04	80	36267.6	1.24E-08

Now, based on formulas (6.25), (6.29), and (6.30), we can calculate the mid-section of the meteor head $S_{MHM}(h_M)$ at different heights. The calculation results are presented in Table 6.11 and Fig. 6.11.

To calculate the LEDTr using formula (6.20), it is necessary to determine the particle number density of the atmosphere $N_a(h_M)$ (particle concentration) at a given altitude. This can be done on the basis of the reference data (State Standard 4401-73) or by using the approximate relation ship

$$N_{\grave{a}}\left(h_{\mathrm{M}}\right)=\frac{\rho_a\left(h_{\mathrm{M}}\right)N_A}{\mu_{a\,av}}, \tag{6.43}$$

where $\mu_{a\,ev}$ is the average molar mass of atmospheric particles (kg/kmol), which in the interval of 80...130 km can be approximated by the expression

$$\mu_{a\,av}\left(h_{\mathrm{M}}\right)=\begin{cases}28{,}964, & \text{when } 95 \text{ km} \geq h_M \geq 80 \text{ km},\\ 28{,}964-0{,}14056\left(95-h_{\mathrm{M}}\right), & \text{when } h_M > 95 \text{ km}.\end{cases} \tag{6.44}$$

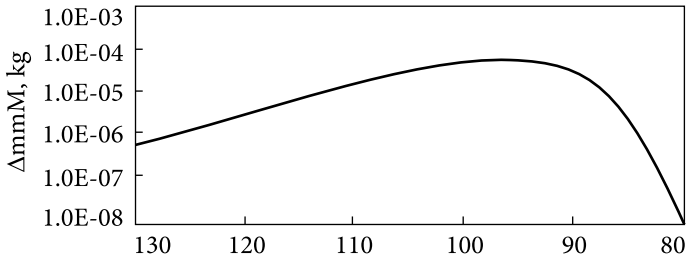

Fig. 6.10. Mass loss of the meteoroid on the path length l = 1km

Table 6.10. **Mass loss of an iron meteoroid on a path length of l = 1 km**

Height, km	Δ_{mmM}, kg	Height, km	Δ_{mmM}, kg	Height, km	Δ_{mmM}, kg
130	5.1734E-07	110	1.3871E-05	90	3.3046E-05
125	1.2020E-06	105	2.8443E-05	85	3.2268E-06
120	2.7724E-06	100	4.9698E-05	80	1.2421E-08
115	6.3008E-06	95	6.0528E-05		

Based on expression (6.20), using relations (6.25), (6.29), (6.30), (6.39), (6.43) and (6.44), we obtain a formula that allows us to calculate the LEDTr

$$q\left(v,m_m,h,\gamma\right)=\beta_{total}\left(v\right)\times\left[A_0\left(\frac{m_{\text{in}}}{\rho_m}\right)^{\frac{2}{3}}+A_1\frac{\Delta m_m\left(h,v,\gamma\right)\cdot N_A}{\mu_{m\,av}}\sigma_{X1av}\right]\times$$

$$\times\left[\frac{\rho_a\left(h_1\right)N_A}{\mu_{a\,av}}\right]\times\frac{\cos\gamma}{\Delta h_1}. \qquad (6.45)$$

To determine the ionization coefficient $\beta_{total}(v, PCPMet)$, we will use its integral estimate, represented by expression (6.19), which was obtained for a given chemical composition of the meteoroid and can be used as an approximate one, and the effective cross-section of the molecule (atom) of the meteoroid σ_{X1} is determined by the expression (6.29).

The results of calculation by formula (6.45) for the above initial data are presented in Table 6.12 and Fig. 6.12.

Since stony meteorites with a chondritic structure are the most common, we assume that the observed meteoroid is close in composition to the Chelyabinsk meteorite, which mainly consists of silicates: olivines $(Mg, Fe)_2[SiO_4]$ and pyroxenes $(Mg, Fe)_2[Si_2O_6]$. Knowing the chemical formula of olivine and the atomic mass of the elements, which we take from the Periodic table of elements, we determine its molar mass M_{oliv} = 252. Since the olivine molecule contains (2 Fe atoms = 2 × 55.847, 2 Mg atoms = 2 × 24.305, 1 atom Si = 28.085, and 4 atoms O = 4 × 15.9994, it is easy to show that the average value of the relative atom mass for the olivine molecule $\mu_{m\,av}$ = 28,0042).

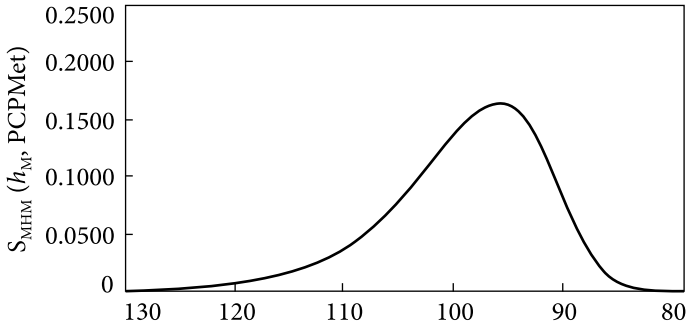

Fig. 6.11. Dependence of the midsection of the iron meteoroid head on the observation point height

Table 6.11. **Dependence of the midsection of the iron meteoroid head on the height of the observation**

Height, km	$S_{MHM}(h_M)$, m²	Height, km	$S_{MHM}(h_M)$, m²	Height, km	$S_{MHM}(h_M)$, m²
130	0. 0065299	110	0.1674635	90	0.1528023
125	0.0150743	105	0.3267676	85	0.0051255
120	0.0345603	100	0.5099290	80	0.0000035
115	0.0777517	95	0.4822221		

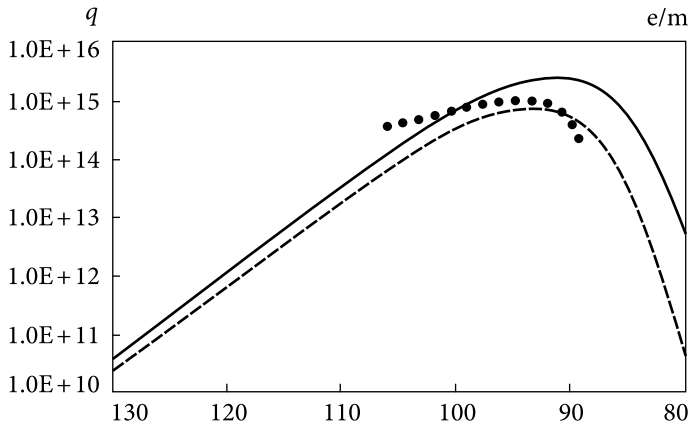

Fig. 6.12. Dependence of the LEDTr of an iron meteoroid on the height of the observation point — a solid line. The dashed? line shows the LEDTr for a meteoroid close in composition to the Chelyabinsk meteorite, and the dots show the result of calculation using semi-empirical formula (6.46)

Table 6.12. **Dependence of LEDTr on the height of the observation**

Height, km	LEDTr , e/m	Height, km	LEDTr , e/m	Height, km	LEDTr , e/m
130	4. 0002E+10	110	3.2863E+13	90	2.5346E+15
125	2.1689E+11	105	1.5959E+14	85	6.0171E+14
120	1.1764E+12	100	6.6098E+14	80	5.6310E+12
115	6.3113E+12	95	1.9095E+15		

The density of olivine is usually close to 3300 kg/m^3, and the integral ionization coefficient β_{total} *(v, PCPMet)* is chosen in accordance with formula (6.19). The results of the LEDTr calculation according to the method described earlier are shown in Fig. 6.12 by a dotted line.

In work (Belkovich 2008), based on the previously obtained results (Eshleman, 1957; Belkovich, 1971; Tokhtasev, 1975), it was proposed to calculate the linear electron density (in e/m) using a semi-empirical formula, which is valid only in the region of maximum ionization and obtained through fitting to the results of radar measurements:

$$q(h_M) = 4{,}03\times10^{14}\cdot\frac{m(v_{m0}-8{,}15)^3}{H_M}\cdot\cos\chi\cdot Z(t), \tag{6.46}$$

where h_M — height above the Earth's surface at the considered trail point; v_{m0} — velocity (in km/s) of the meteoroid at the entry to the meteor region; m — mass (in kg) of the meteoroid at the entry to the meteor region; χ — zenith angle of the meteoroid; $Z(t)$ — function defined by the expression

$$Z(t) = \begin{cases} \dfrac{9}{4}e^{-t}\left(1-\dfrac{1}{3}e^{-t}\right)^2 & \text{when } -\ln 3 \le t \le 1.7, \\ 0 & t < -\ln 3, \text{ or } t > 1.7, \end{cases} \tag{6.47}$$

where relative height t is defined as

$$t = \frac{h_M - h_{\max}}{H_M}, \tag{6.48}$$

where H_M is the reduced height of the atmosphere H_M (in km), calculated by the formula

$$H_M(h_M) = 6{,}4 + 0{,}09\left(h_M - 95\right), \tag{6.49}$$

h_{max} is the height of maximum ionization (in km), determined by the empirical relation:

$$h_{\max} = 47.4 + 12.76\ln v_{m0}. \tag{6.50}$$

The results of calculations by formulas (6.46—6.50) are presented in Fig. 6.12 by a line of dots. They show a fairly good agreement with the corresponding calculations of the LEDTr by the proposed method for a meteoroid with a chondrite structure.

In contrast to the classical formula (6.10) and the semiempirical formula (6.46), expression (6.45) allows taking into account the main factors influencing the value and change of LEDTr and performing calculations for the given parameters of the meteor body. It should be noted that the LEDTr estimation model described in this section can be modified since it does not consider the decrease

in electron density due to the recombination of positive ions with electrons, attachment of free electrons to oxygen molecules, and ionic reactions with ozone.

The proposed model for estimating the electron density of the trail created by a meteoroid at the observation point can be adapted for the fragmentation of a meteoroid at a given height. In this case, the initial conditions for calculations are data on the velocity and mass of the meteoroid at the fragmentation point, as well as a given number of fission fragments. For each fragment, one should calculate LEDTr according to the method described above, and then use the principle of superposition, that is, the assumption that the effect of several independent events can be represented by the sum of the effects caused by each event separately.

6.4.2. Distribution model of the bulk electron density concerning to the trail axis

The radar scattering from meteor trails depends on several insufficiently well-defined quantities, such as the bulk electron density of the trail, its initial radius r_0, and the ambipolar diffusion coefficient D_a.

As a model for describing the radial profile of the bulk electron density outside the thermalization interval, the Gaussian function is usually used, which leads to the well–known expression

$$n(r,t) = \frac{q}{\pi(r_0^2 + 4D_a t)} \cdot \exp\left(-\frac{r^2}{r_0^2 + 4D_a t}\right), \tag{6.51}$$

where $n(r, t)$ is the number of electrons per unit volume at time t from the onset of ambipolar diffusion at the meteor trail point at a distance r from the trail axis with initial radius r_0, and q is the linear electron density at the trail point being considered.

Other models have been explored but have not shown significant benefits.

At the moment of completion of thermalization, we can accept a similar model for the distribution of the volume electron density of the trail

$$n(r) = \frac{q}{\pi r_0^2} \cdot \exp\left(-\frac{r^2}{r_0^2}\right). \tag{6.52}$$

The physical validation of representation (6.52) is confirmed by the modeling of the distribution of vapor removed from the surface of a meteoroid, which is ionized due to collisions with atmospheric particles, performed in (Boyd, 2000). In this study, the direct statistical modeling (DSM) Monte Carlo method was used for the case of an unfragmented spherical meteoroid with a diameter of 1 cm, which enters the Earth's atmosphere at an altitude of 95 km at a speed of 72 km/s in the regime of a strong nonequilibrium flow state.

The simulations used standard atmospheric conditions at this altitude: number density $N_2 = 2.8 \times 10^{19}$ m^{-3}, $O_2 = 7.0 \times 10^{18}$ m^{-3}, $O = 4.9 \times 10^{17}$ m^{-3}, and the temperature 176 K. H-chondrite and cometary meteoroids with specific heats of vapor-

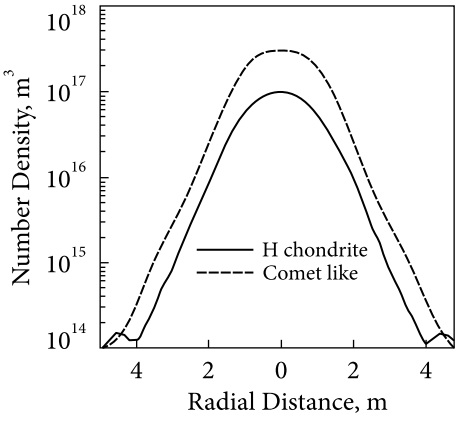

Fig. 6.13. Radial ablated vapor density profiles for H–chondrite and cometary meteoroids at a distance of 20 m from the head (Boyd, 2000)

ization Q_H = 6.3 kJ/g and Q_K = 3.8 kJ/g, respectively, were considered. No chemical reactions between meteoroid particles and the atmosphere were considered.

As a result of the simulation, the radial density profiles of the ablated vapor at a distance of 20 m from the meteoroid head were obtained, which are presented in Fig. 6.13.

The obtained radial density profiles of the ablated vapor are well approximated by the Gaussian function, and there is a reason to believe that the collisions of the evaporated meteoroid atoms (dissociated molecules) with atmospheric particles result in the formation of an ionized trail with the corresponding density distribution.

Undefined in expressions (6.51) and (6.52) is the initial radius of the track r_0, and in expression (6.51) the coefficient of ambipolar diffusion D. To determine the linear electron density of the trail, we will use the previously given method.

It should be noted that the used concept of "initial radius" has no physical meaning and is used as a parameter to describe the volume electron density profile of the meteoroid trail. However, it is directly related to the geometric and physicochemical properties of the meteoroid and atmosphere. The parameter r_0 becomes valid after the completion of the thermalization process when the trail expansion is mainly determined by ambipolar diffusion. Apparently, this is the reason for its name.

For a graphical representation, instead of r_o, you can use the concept of "equivalent radius" r_{eq}, which characterizes the radius of a cylinder with a uniformly distributed bulk electron density, which has similar LEDT.

For the distribution of bulk electron density, represented by expression (6.52), the value of r_{eqv} can be determined from the condition of equality of areas

$$\frac{1}{\pi r_0^2}\int_0^\infty \exp\left[-\left(\frac{x^2}{r_0^2}\right)\right]dx = \frac{1}{\pi r_0^2} r_{\text{ýêâ}},$$

whence it follows r_{eqv}

$$r_{eqv} = \int_0^\infty \exp\left[-\left(\frac{x^2}{r_0^2}\right)\right]dx = \frac{\sqrt{\pi}}{2} r_0 \approx 0{,}866 r_0 \cdot \qquad (6.53)$$

In some works, the deviation from the axis is taken as the initial radius, at which the electron density decreases by half compared to the maximum observed value. In this case, using the equation

$$\exp\left[-\left(\frac{r_{0,5}^2}{r_0^2}\right)\right]=\frac{1}{2}$$

and taking the natural logarithm of both sides of the equation, we get the relationship for r_0 and $r_{0.5}$

$$r_{0,5}=r_0\sqrt{\ln 2}\approx 0,833 r_0, \tag{6.54}$$

which differs little from the value of r_{eqv}.

This interpretation of the initial radius makes it possible to estimate its value using the method of two–frequency radar measurements. In some works where the Gaussian approximation of the electron density is used, the root-mean-square deviation (RMS) from the trail axis is taken as the initial radius. In this case, the relationship between r_0 and r_{RMS} is determined by the expression

$$r_{0\ RMS}=r_0/\sqrt{2}\approx 0,707 r_0. \tag{6.55}$$

In the presence of fragmentation of a meteoric body, the distribution of electron density is not symmetrical, and the concept of "effective initial radius" (Jones, 1995) can be used to harmonize theoretical calculations with the results of observations. It is assumed that the non-Gaussian trail scatters radio waves as if it had a Gaussian radial ionization distribution at the corresponding initial radius.

For a quantitative comparison of the results of direct statistical modeling with the results of calculations of r_o using formulas obtained both taking into account physical considerations and fitting to observed values, we use the expression (Bronshten, 1981)

$$r_0=2,58\times 10^{10} v^{0,8}/N, \tag{6.56}$$

where v is the initial velocity of the meteoroid (m/s), and N is the number of atmospheric molecules per unit volume (1/cm^3). For the velocity used in the simulation, 72 km/s, and $N = 5.4 \times 10^{13}$ 1/cm^3 (typical for a height of 95 km), the calculation by formula (6.27) gives r_o = 3.7 m, which does not contradict the results shown in Fig. 6.13.

There are other expressions for calculating the initial radius, obtained by different authors, a review of which is presented in (Bronshten, 1981; Gorelov, 2005; Belkovich 2008).

In a generalized form, the expression for calculating the initial radius can be represented by the formula (Bronshten, 1981)

$$r_0=C\rho^a v^b, \tag{6.57}$$

Table 6.13. **Calculation formulas for the initial radius of the ionized trail of a meteoroid**

Information source	Calculation formula for the initial radius, m		Units of measurement
(Jones, 1995)	$r_0 = 2,845 \times 10^{18}\, v^{0,8}/N$	(6.58)	v, km/s; N, 1/m^3
(Jones, 2005)	$\log_{10} r_0 = a_1 + b_1(h-90) + c_1 \log_{10}(v/40)$ $a_1 = -0.0802 \pm 0.0027$ $b_1 = +0.0238 \pm 0.0006$ $c_1 = -0.200 \pm 0.0132$	(6.59)	v, km/s; h, km
(Kascheev, 1961)	$r_0 = 0,109\, v^{0,65} \exp\left(\frac{h-95}{H}\right)$, $H = 46,8273 - 0,95h + 0,0055h^2$	(6.60)	v, km/s; h, km; H, km
(Tokhtasev, 1975)	$r_0 = 1,65\sqrt{\frac{v}{40}\exp\left(\frac{h-95}{H}\right)}$, $H = 46,8273 - 0,95h + 0,0055h^2$	(6.61)	v, km/s; H, km

where ρ is the density of the atmosphere at the height of the trail observation, a and b are coefficients that researchers determine from various physical considerations or by fitting to the results of radar measurements.

Table 6.13 shows several calculation formulas for the initial radius along with the source of information. When calculating the reduced height H(h) and the numerical density of the atmosphere N(h), the standard atmosphere models CIRA-2012, MSIS-86 or MSIS-E-90, or other reference books (for example, GOST R. 53460-2009) can be used to obtain the corresponding values at the given height h and the geographical latitude of the observation. It should be taken into account that these parameters depend on the time of year and day, as well as on geomagnetic activity, which is not taken into account in the above formulas.

A common flaw of the calculation formulas presented in Table 6.13 is the lack of connection between the initial radius and the physicochemical characteristics of the meteoroid and atmosphere, as well as the lack of reference to the latitude and time of observation, which will inevitably lead to the complexity of interpreting radar measurements.

In (Marshall, 2017; Silber, 2018; Sugar, 2019; Dimant, 2017), as an alternative to the Gaussian, a distribution of the form

$$n_e = n_{e0} \frac{1}{1 + \left(r / r_0\right)^2}, \qquad (6.62)$$

which seems to correspond to the unwrapped sinusoidal curve of Agnesi ("The Witch of Agnesi") (Vyigodskiy, 1976) and, according to the authors, provides the possibility of a better fit to the observational results and a more accurate quantitative interpretation of radar measurements. This distribution is confirmed by the results of direct statistical modeling taking into account multiple collisions.

Having reduced expression (6.62) to a form similar to the two–dimensional distribution density (6.52), we obtain

$$W(x)=\frac{1}{\pi^2 r_0^{\,2}}\times\left[1+\left(\frac{x}{r_0}\right)^2\right]^{-1}. \tag{6.63}$$

The value of r_{eqv} can be determined from the condition of equality of areas

$$\frac{1}{\pi^2 r_0^{\,2}}\int_0^{\infty}\left[1+\left(\frac{x}{r_0}\right)^2\right]^{-1} dx=\frac{1}{\pi^2 r_0^{\,2}} r_{eqv},$$

whence it follows

$$r_{eqv}=\int_0^{\infty}\left[1+\left(\frac{x}{r_0}\right)^2\right]^{-1} dx=\frac{\pi}{2} r_0 \approx 1{,}57 r_0. \tag{6.64}$$

If the initial radius is taken to be the deviation from the trail axis, at which the electron density decreases by half compared to the maximum observed value, then using the equation

$$\left[1+\left(\frac{r_{0,5}}{r_0}\right)^2\right]^{-1}=\frac{1}{2},$$

we get that r_0 and $r_{0.5}$ coincide

$$r_{0,5}=r_0. \tag{6.65}$$

Thus, it can be argued that both analytical representations (6.52) and (6.63) can be used as a model of the two-dimensional axisymmetric electron density of the ionized trail of a meteoroid. The main uncertainty in the models is the value of the initial trail radius, which depends on the velocity and physicochemical composition of meteoroids, as well as the physicochemical composition of the atmosphere at the height of the specular reflection point of radio signals.

Issues related to the influence of the shock wave and hydrodynamic shielding, which are characteristic of meteoroids of sufficiently large sizes, are beyond the scope of consideration in this subsection. Complex reactions of multiple ionization of atoms, as well as recombination of free electrons with ions at the initial stage of an ionized trail formation in a high-temperature shock layer, are partially considered in (Silber, 2017; Menees, 1976; Berezhnoy, 2010).

The influence of hyperthermal chemistry and mesospheric ozone on the formation of the initial radius has not been considered. All this suggests that, despite the presence of a fairly large number of studies aimed at estimating the initial radius of the trail, work on creating an adequate model should be continued.

When using existing models, one should pay attention to how the author defines the concept of "initial radius" in the proposed formula.

After the completion of the thermalization process and the formation of the initial radius, an equally complex process of transformation of the ionized trail begins, which carries information about the state of the atmosphere in the meteor zone and determines the lifetime of the trail suitable for transmitting information via meteor radio channels. The main process leading to a change in the trail characteristics is ambipolar diffusion, during which the trail expands, its bulk electron density decreases, but the linear density remains constant. In this case, the bulk electron concentration is determined by expression (6.51).

The diffusion coefficient D_a increases approximately exponentially with height. It significantly depends on the geographical location of the observation site, experiences daily and seasonal changes, and also depends on local atmospheric conditions.

The effective diffusion coefficient for electrons in the meteor trail (provided that the geomagnetic field is not taken into account) can be written as in (Ceplecha, 1998; Bryunelli, 1979)

$$D = D_i\left(1 + T_e/T_i\right), \tag{6.66}$$

where D_i is the diffusion coefficient for positive ions, and T_e and T_i are the electron and ion temperatures, respectively. Since the ambipolar diffusion coefficient is applicable for electron density calculations only after the completion of the thermalization process, T_e can be equated to T_i, and the known relation can be obtained

$$D = 2D_i. \tag{6.67}$$

The diffusion coefficient D_i can be described in terms of the mobility in the zero field K of a group of ions using the Einstein relation

$$D_i = kT_i K/e, \tag{6.68}$$

where k is Boltzmann's constant and e is the electronic charge. Laboratory measurements have yielded values of K for a significant number of ions in various common gases. A typical value is 2.2×10^{-4} m^2 s^{-1} V^{-1}, and it changes by less than 20% for a 100 K change in ambient temperature. Since K is inversely proportional to the molecular concentration of the surrounding gas, the expression for the ambipolar diffusion coefficient D (m^2 s^{-1}) becomes

$$D = 2D_i = 6{,}390 \times 10^{-2} KT^2 / p = 1{,}41 \times 10^{-5} T^2 / p, \tag{6.69}$$

where p is the atmospheric pressure in pascals.

Table 6.14 shows D values in the meteor region for mid-summer and mid-winter at some representative latitudes, calculated by formula (6.43), where pressure and temperature data are taken from CIRA-1986, the value of K is taken equal to 2.2×10^{-4} (Ceplecha, 1998).

Previously, it was believed that the most reliable results in determining D are given in (Greenhow, 1955), where for altitudes between h = 80 km and h =110 km, the diffusion coefficient is described by the relation

$$\lg D = 0.067h - 5{,}6\,, \tag{6.70}$$

where D is in m^2/s and h is in km.

Based on this formula, for a height h = 80 km, we have $D(80)$ = 0.576 m, which is approximately the June/December average for 40°N given in Table 6.8. For a height h = 110 km, calculation using formula (6.44) gives the value D (110) = 58.9 m, which differs significantly from the data in Table 6.14.

There are also other calculation formulas for estimating the value of the ambipolar diffusion coefficient. Some of them are shown in Table 6.15 with the source of the information.

The formulas given in the table are approximate, obtained through fitting to the results of observations, do not take into account the real atmospheric parameters characteristic of a given geographical area and season, and can only be used as a guideline for a qualitative analysis of the results of observations at altitudes up to 95 km.

Above 95 km, the influence of the Earth's magnetic field can no longer be ignored, as diffusion becomes substantially anisotropic. The values of the ambipolar diffusion coefficient given in Table 6.9 for heights above 95 km are maximum and are limited to a specific radial direction.

Table 6.14. **Ambipolar diffusion coefficient**

Height, km	Ambipolar diffusion coefficient, $m^2\ s^{-1}$							
	60°S		60°N		40°S		40°N	
	June	December	June	December	June	December	June	December
70	0. 24	0. 09	0. 10	0.22	0.17	0.11	0.11	0.16
75	0. 45	0.17	0.17	0.44	0.35	0.21	0.22	0.34
80	0.90	0.31	0.33	0.89	0.72	0.42	0.43	0.71
85	2.20	0.65	0.56	1.94	1.62	0.79	0.90	1.42
90	4.53	1.35	1.55	3.82	3.30	1.83	2.12	2.81
95	9.12	4.43	5.14	7.76	7.16	4.93	5.73	6.15
100	21.0	15.9	18.5	18.0	16.9	14.6	17.0	14.5
105	51.6	53.2	61.9	44.5	42.0	43.3	50.2	36.2
110	132.4	143.5	167.7	114.3	115.7	122.7	142.4	99.8
115	357.2	318.3	369.2	308.6	356.5	317.9	373.8	307.8
120	913.1	745.3	869.1	789.9	908.3	751.6	890.5	784.7

For electrons moving parallel to the magnetic field in the absence of positive ions, the diffusion coefficient is

$$D_{\text{ex}} = kT/m_e \nu, \tag{6.74}$$

where ν is the collision frequency, and m_e is the mass of the electron.

For electrons moving across the magnetic field, the diffusion coefficient is (Jones, 1991a)

$$D_{ey} = D_{\text{ex}} \frac{\nu^2}{\left(\nu^2 + \omega^2\right)}, \tag{6.75}$$

where ω is the angular gyroscopic frequency.

The value of D_{ey} is equal to D_{ex} at about 95 km and becomes much smaller at higher altitudes, due to which the trail becomes elliptical in cross–section. This situation with a trail formed at an arbitrary angle to the magnetic field was analyzed in (Jones, 1991a; Cervera, 2000), and the results are presented in Fig. 6.14.

Diffusion in the radial direction defines the major axis of the elliptical cross-section. It steadily decreases as the field tilt angle changes from 90° to ~5°, where the trail cross-section becomes almost circular at all heights, and the diffusion coefficient takes on its ambipolar value.

Thus, the lifetime of ionized trails formed above 95 km and oriented within ~2° relative to the direction of the magnetic field can be many times longer than the typical lifetime of other trails at the same altitude.

Immediately after formation, the meteor trail has a circular cross-section determined by the initial radius, and the development of significant ellipticity at altitudes above 95 km will take some time before reaching the values presented in Fig. 6.14. However, it is likely that at altitudes above 110 km, the initial cylindrical ionization column at the moment of observation may have an elliptical cross-section, which will affect the characteristics of the reflected signal.

In addition to ambipolar diffusion, the electron density of the ionized trail of a meteoroid is affected by other processes, which are reviewed in (Bronshten,

Table 6.15. **Calculation formulas for estimating the value of the ambipolar diffusion coefficient**

Information source	Calculation formula for the ambipolar diffusion coefficient	Units
(Jones, 1990)	$\lg D = 0.06h - 4,74$ (6.71)	v, km/s; h, km
(Kascheev, 1961)	$D = \exp\left(0,108\ h - 7,842\right)$ (6.72)	h, km
(Tokhtasev, 1975)	$D = 13.2 \cdot \exp\left(\frac{h-95}{H}\right)$, (6.73) where $H = 46,8273 - 0,95h + 0,0055h^2$	h, km; H, km

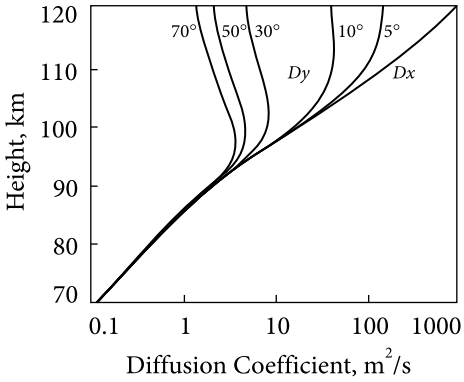

Fig. 6.14. Diffusion coefficient *versus* the height and angle between trail and direction of the magnetic field. D_x refers to diffusion in the plane containing the Earth's wake and magnetic field, and D_y refers to diffusion in the orthogonal direction

1981; McKinley, 1961; Evans, 1966). They include a decrease in the linear electron density of the trail as a result of the recombination of positive ions with electrons, the attachment of free electrons to neutral molecules and atoms, the destruction of the ionized trail under atmospheric turbulence in the meteor zone, and its curvature due to wind shifts.

In a number of works (Baggaley, 1980; Jones, 1990b; Sukara, 2013; Dyrud, 2011), the influence of hyperthermal chemistry, as well as ionic reactions with mesospheric ozone, has been studied. A study of various meteor ionization depletion processes was given in (Baggaley, 1980), where it was shown that the electron density is determined mainly by ambipolar diffusion at altitudes above 93 km and by chemical destruction below 93 km. The main chemical process is the reaction of meteoric ions with ozone yielding oxide ions, which quickly dissociate with free electrons. It was shown in (Jones, 1990b) that the distribution of the duration of echo signals from overdense trails at a given height has a "characteristic time" corresponding to the transition from "diffusion-limited" to "chemically-limited" durations. Based on the known rate constants for the production of oxide ions, the values of "characteristic time " can be converted into ozone concentrations. Thus, by observing the duration distribution at several altitudes, one can determine the ozone concentration profile between 80 and 100 km.

In (Sukara, 2013), the mechanism of ozone participation in hyperthermal chemistry was analyzed. It is shown that singlet oxygen formed during photodissociation and thermal decomposition of O_3 under the action of ultraviolet radiation and a high-temperature layer behind the shock wavefront reacts with metal ions and subsequently removes electrons from the expanding ionized trail. The results obtained for chemically removed electrons are in good agreement with the vertical density profile of mesospheric ozone.

The physical interpretation of the depletion of the trail electron density as a result of the recombination of positive ions with electrons, as well as the attachment of free electrons to neutral molecules and atoms, is given in the above works and is not considered further. At the same time, the decrease in the dura-

tion of the reflected signal associated with these processes should be taken into account when analyzing the results of modeling the scattering of radio signals on the meteor trail.

Important factors affecting the reflected signal duration are the turbulence of the meteor zone medium, as well as the trail turbulence (Bronshten, 1983; Dyrud, 2011; Ayers, 1970; Kharchenko, 2012). This is due to the fact that when a meteoroid of a sufficiently large size enters a meteor region at a hypersonic velocity, the resulting trail is turbulent, and, along with ambipolar diffusion, turbulent diffusion can play an important role. The influence of turbulent diffusion on the parameters of the scattered signal has not been sufficiently studied and requires additional research.

6.5. Conclusions

The physical theory of the formation and transformation of ionized meteor trails is the basis for creating a generalized model of radio signal scattering on a meteor trail in the process of its formation and development, which makes it possible to calculate the amplitude-time and phase-time characteristics of specularly reflected and incoherently scattered radio signals.

The main parameters characterizing the ionized trail of a meteoroid are:

1. Accepted model of two–dimensional axisymmetric electron trail density.
2. The initial radius of the meteor trail r_0, which becomes valid after the completion of the thermalization process.
3. Ionization coefficient β, which depends on the speed of the meteoroid and its physical and chemical properties. It determines the number of electrons produced by one ablated atom of the meteoric body and, accordingly, the linear electron density of the trail.
4. Ambipolar diffusion coefficient D_a, which determines the rate of the trail expansion process, during which the bulk electron density decreases. In this case, D_a determines the trail lifetime suitable for transmitting information via meteor radio channels.

These parameters depend on the physicochemical characteristics of the meteoroid, as well as the physicochemical characteristics of the atmosphere, which, in turn, depend on the height of the specular reflection point, time of year and day, latitude of the observation point, and solar activity. The complex dependence allows us to assert that it is impossible to obtain universal calculation ratios for the coefficients r_0, β, and D_a, taking into account all the characteristics of the meteoroid and the atmosphere. Calculations should be performed separately for asteroidal and cometary meteoroids of a given composition, which is determined a priori. It is also necessary to estimate the speed of the meteoroid and measure the height of the specular reflection point. At reflection heights of more than 95 km, to estimate D_a and interpret radar observations, it is necessary to take into account the impact of the geomagnetic field, the degree of influence of which de-

pends on the geographical parameters of the radio wave propagation path. This is a difficult but fundamentally feasible task.

The chosen fragmentation model, which determines the observed midsection of the meteoroid, and the analytical model of the electron density of the trail have a significant impact on the reliability of calculations of the main parameters of the trail. The fragmentation model must be consistent with the chosen physicochemical properties of the meteoroid. In the case of quasi-continuous fragmentation, expression (6.62) can be used as a model for the two-dimensional electron density of the trail, but this assumption needs additional research. In the case of successive fragmentation into several fragments, a single body model can be used with subsequent superposition of the results of parameter estimates. In this case, expression (6.51) can be used as a model for the two-dimensional electron density of the trail. This approach will be used in the development of a radiophysical model of signal scattering on an ionized meteoroid trail, which is the subject of the next section.

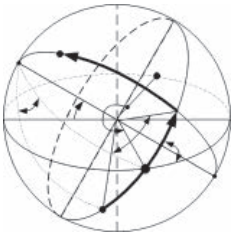

SECTION 7

A RADIOPHYSICAL MODEL OF SIGNAL SCATTERING ON A METEOR TRAIL

A radiophysical model of signal scattering on a meteor trail makes it possible to create a model image of a scattered signal in the process of its formation and development for given parameters of the meteoroid and atmosphere at the height of observation of the ionized trail. The most complete data on the meteoroid and its surrounding atmosphere at the SRP altitude are contained in ATCH, which implicitly contains information on the mass, chemical composition, velocity, and radiant of a meteoroid. This information allows us to make reasonable assumptions about the genetic relationship of the meteoroid with its parent body, which is necessary for developing the theory of the origin and evolution of meteoric matter. The estimation of ATCH parameters at the initial stage of the trail formation (20—100 ms) can be used to predict the reflectivity of the trail in the process of its further transformation. It makes it possible to optimize the protocol and transfer rate of information, on which the throughput of meteor radio channels depends.

7.1. The concept of constructing a radiophysical model of signal scattering on a meteor trail with bistatic location

Bistatic (two-position) location opens up additional possibilities for studying meteor phenomena. It determined by the fact that the level of the scattered signal can be significantly higher than with a monostatic location due to the increase in the first Fresnel zone.

When constructing models of a signal scattered by the meteor trail, methods based on the diffraction theory (stationary phase method, phase plane method) (Landau, 1973; Rytove, 1978; Bryunelli, 1979) were used.

In all cases, while constructing models based only on the first Fresnel zone, a number of assumptions were made to

simplify the calculations, which were not always well-founded. For example, the assumption of scattering by free plasma electrons was used. It will be shown below that such an assumption cannot be applied even for underdense meteor trails.

Within the framework of existing models, it is difficult to explain the observed dependences of the scattered signal intensity on the wavelength, the presence of diffraction oscillations of the signal power, and the possibility of the signal observed at a considerable distance from the receiving point, where the reflection has a specular character.

The conditional division of meteor trails into trails of underdense and overdense types does not allow one to obtain an adequate description of real observed trails within the framework of existing models. This is due to the fact that the scattered signal is formed both by the overdense part of the trail (represented by the model of a metal cylinder) and the simultaneously existing underdense part (plasma shell with a bulk electron density less than $2 \cdot 10^{14}$ e/m^3), which significantly changes the parameters of the observed signal.

Existing models of meteor trails were built only for a certain type of meteor trails — underdense or overdense, the division between which is very arbitrary and depends on both electron density and frequency. At the same time, it should be noted that IMTr is characterized by several phases of development, during which the trail passes from an overdense state to an underdense one:

- An initial phase during which a trail forms within the first Fresnel zone and several neighboring zones.
- The phase during which the meteor trail is fully formed and expands, and its bulk electron density may exceed a critical value at which the permittivity within the trail is less than or equal to zero.
- The phase of expansion due to diffusion, within which the electron density decreases and becomes less than the critical value, and the signal scattering is determined by the differential cross-section of plasma electrons through accounting for their collective interaction.

It is practically impossible to formulate and solve the diffraction problem of radio wave scattering on a meteor trail at all phases of its development in a strict formulation, and it is problematic to obtain reliable empirical calculation formulas directly from the observation results due to the uncontrollability of the initial data. From this, it follows that to construct a radiophysical model of a meteor trail, it is necessary to use heuristic methods for solving the diffraction problem.

The models used practically do not take into account the fact that when a meteoroid enters a meteor region at a hypersonic speed, the trail formed is turbulent, as well as the medium in the meteor zone. Trail turbulence and the presence of a specular reflection point suggest the simultaneous existence of the incoherent (Close, 2008) and coherent components of the scattered field, which is not taken into account in any of the known models and calculation methods.

Proceeding from the above, an urgent task is to develop a new radiophysical model of signal scattering, which makes it possible to evaluate both the coherent

and incoherent components of the signals scattered on the IMTr in the process of its transformation. In this case, it will be taken into account that in different phases of development, the trail may contain both overcompacted and undercompacted (i.e., overdense and underdense) parts.

7.1.1. Generalized meteor trail scattering model

We will assume that the scattered signal at the receiving point contains a coherent component, which is formed mainly in the region of the first Fresnel zone and in several adjacent regions, and an incoherent component, which is formed when the signal is scattered by the permittivity inhomogeneities of turbulent origin in the entire trail. In this case, the total power of the scattered signal can be represented by the generalized model (Kharchenko, 2012; Kharchenko, 2011)

$$P_{\Sigma}(t) = a(t)P_{coh}\left(\lambda, \sqrt{S(\tau,t)}, N_1, N_2, N_3, N_4\right) + \\ + b(t)P_{incoh}\left(\lambda, \Phi(q), S(\tau,t), N_1, N_2, N_3, N_4\right), \quad (7.1)$$

where $a(t)$ and $b(t)$ are the weight contributions of the coherent P_{coh} and incoherent P_{incoh} components in expression (7.1), where $a(t) + b(t) = 1$; λ — wavelength corresponding to the carrier frequency; $S(\tau)$ — time (range) scatter-function (Ishimaru, 1978; Van Tris, 1977; Kennedy, 1973), calculated for a meteor trail with a specular reflection point; $\Phi(q)$ — generalized energy spectrum of turbulent inhomogeneities (Tatarsky, 1967; Kravtsov, 1983); q — modulus of the scattering vector; N_1 — set describing the physicochemical parameters of the meteoroid: mass m, velocity v, and chemical composition; N_2 — set describing the parameters of the meteor trail (direction to the radiant, linear electron density α and initial radius r_0 of the meteor trail, ambipolar diffusion coefficient D, distribution of the bulk electron density $N(t)$ of the meteor trail as a function of time, and σ — the effective scattering surface (Thomson cross-section) of an electron); N_3 — set describing the relative position in space of a radio link, a meteor trail with a specular reflection point, the geographical coordinates of the transmitter and receiver, as well as the distances between the transmitter, receiver, and the specular reflection point; N_4 — set describing the energy parameters of the radio link: the transmitter power P_T, the antenna gain of the receiver G_R and the transmitter G_T in the direction of the trail.

Model (7.1) is focused on using a scatter-function of a meteor trail to calculate the power of the coherent and incoherent components of the reradiated signal. It should be noted that this model can be generalized to the case of the presence of several specular reflection points on the trail by introducing the corresponding terms characterizing the coherent components of the scattered signal.

7.1.2. Scattering on an underdense meteor trail for bistatic location

We will calculate the intensity of the scattered signal for bistatic location on an underdense meteor trail, assuming that the operating frequency of the signal ω exceeds the Langmuir frequency ω_0 of the natural longitudinal oscillations of the space charge in the trail plasma in the absence of a magnetic field:

$$\omega > \omega_0 = \sqrt{\frac{Ne^2}{m_e \varepsilon_0}}, \tag{7.2}$$

where N is the bulk electron density of the trail, e and m_e are the electron charge and mass, and ε_0 is the vacuum permittivity. The limiting value of the electron density, which characterizes an underdense trail, according to various estimates, has different values (Kravtsov, 1983) and is of the order of 10^{14} e/m^3. In this case, we can assume that the field inside the trail coincides with the field of the incident wave.

When the condition (7.2) is satisfied, the intensity of the scattered signal can be generally represented by the integral (Ishimaru, 1978)

$$I(t) = \int \frac{\lambda^2 G_T(\hat{i}) G_R(\hat{o})}{(4\pi)^3 R_1^2 R_2^2} \sigma(\hat{o}, \hat{i}) \rho_v \exp(-\gamma_1 - \gamma_2) \left| \tilde{U}(t) \left(t - \frac{R_1 + R_2}{c} \right) \right|^2 dV, \tag{7.3}$$

where $G_T(\hat{i})$ — power gain of the transmitting antenna in the direction towards the scattering particle; $G_R(\hat{o})$ — power gain of the receiving antenna in the direction towards the scattering particle; $\sigma(\hat{o}, \hat{i})$ — differential cross-section of a scattering particle; ρ_v — the bulk density of scattering particles; $\tilde{U}(t)$ — the complex envelope of the input signal; $\exp(-\gamma_1 - \gamma_2)$ — the attenuation multiplier; γ_1 — optical path from the transmitter to the scattering particle; γ_2 — optical path from the scattering particle to the receiver, which are calculated by the formula

$$\gamma_i = \int_0^{R_i} \rho_v \sigma_t ds, \tag{7.4}$$

where σ_t is the total scattering cross-section of the particle.

It can be seen from expression (7.3) that waves scattered from points for which the value of $R_1 + R_2$ is constant arrive at the receiving point at the same time. The scattering volume is limited by the dimensions of the trail, which change in time due to diffusion, and elementary particles are free electrons with a differential cross-section (Landau, 1973)

$$\frac{d\sigma}{\Omega} = r_e^2 \cos^2 \gamma, \tag{7.5}$$

for a linearly polarized wave, or

$$\frac{d\sigma}{\Omega} = \frac{r_e^2}{2}\left(1+\cos^2\gamma\right), \tag{7.6}$$

for a circularly polarized wave.

Depending on the value of the bulk electron density, the collective properties of cold plasma manifest themselves to one degree or another, affecting the magnitude of the differential scattering cross-section (Landau, 1973; Rytove, 1978; Bryunelli, 1979). Let's evaluate this effect.

For cold plasma in the absence of a magnetic field, the relative permittivity is given by the relation (Alpert, 1972; Chernyiy, 1962)

$$\varepsilon = 1 - \frac{e^2}{\varepsilon_0 m_e}\frac{N_e}{\nu_{eff}^2 + \omega^2}, \tag{7.7}$$

where $e = 1.602 \times 10^{-19}$ [C] — electron charge; $m_e = 9.106 \times 10^{-31}$ [kg] — electron mass; $\varepsilon_0 = 8.854 \times 10^{-12}$ [F m^{-1}] — vacuum electric permittivity; N_e = bulk free electron density [el/m^3]; ν_{eff} — the number of collisions of an electron with ions, atoms, and gas molecules per unit time [s^{-1}]; $\omega = 2\pi c/\lambda$ — circular frequency; λ — emitted wavelength [m]; c — speed of light in free space [m/s].

Taking into account that in the meter range of waves $\omega >> \nu_{eff}$ and setting $\varepsilon = 0$ in expression (7.7), we obtain an estimate of the critical value of the bulk electron density depending on the wavelength

$$N_{e\,cr}\left(\lambda\right) = \frac{4\pi^2\varepsilon_0 \tilde{m}_e{}^2}{e^2}\frac{1}{\lambda^2}. \tag{7.8}$$

Substituting the known values of the parameters into expression (7.8), we obtain

$$N_{e\,cr}\left(\lambda\right) = 1.115\cdot 10^{15}\frac{1}{\lambda^2}. \tag{7.9}$$

For $\lambda = 7.5$ m, the value of the critical bulk electron density $N_{e\,cr}(\lambda = 7.5\text{ m}) = 1.98 \times 10^{13}$ el/m^3.

Let us estimate the value of the Debye radius R_D for the critical electron density in accordance with expression (Bryunelli, 1979)

$$R_D = \sqrt{\frac{\varepsilon_0 k_B T_{abs}}{N_e e^2}}, \tag{7.10}$$

where k_B=1.38 × 10^{-23} [J/K] — Boltzmann constant; T_{abs} — absolute temperature [K] corresponding to the most probable height (h = 93 km) of the meteor trail reflection point ($T_{abs} \approx 240$ K).Substituting the value of the critical electron density in expression (7.10), we obtain $R_D[N_{e\,cr}(\lambda = 7.5)] = 2.4 \times 10^{-6}$ m.

In the case of incoherent scattering for a wave with circular polarization, taking into account the collective properties of cold plasma, the scattering cross-section in the general form is determined by the approximate relation (Bryunelli, 1979)

$$\sigma_\varepsilon = \frac{r_e^2\left(1+\cos^2\left(\frac{\theta}{2}\right)\right)}{2} N_e \left[\frac{q^2R_D^2}{1+q^2R_D^2} + \frac{1}{\left(1+q^2R_D^2\right)\left(1+\frac{T_e}{T_i}+q^2R_D^2\right)}\right], \quad (7.11)$$

where T_e and T_i are the temperatures of electrons and ions, respectively.

For a thermal equilibrium plasma, expression (7.11) takes the form (Rytove, 1978; Bryunelli, 1979)

$$\sigma_\varepsilon = \frac{1}{2} r_e^2\left(1+\cos^2\left(\frac{\theta}{2}\right)\right) N_e \frac{1+q^2R_D^2}{2+q^2R_D^2}, \quad (7.12)$$

where $q = \frac{2\pi}{\lambda}\cos\left(\frac{\theta}{2}\right)$ — scattering vector modulus.

With coherent scattering, the wave amplitudes are added, but not the powers, and in expressions (7.11, 7.12), N_e is squared. Thus, since in the meter wavelength range at values of θ/2 characteristic of the meteor region $R_D << 1$, the collective properties of the plasma manifest themselves, and the scattering cross-section should be taken four times smaller than for scattering by free electrons.

It is possible to simplify calculations based on expression (7.3) by applying the scatter-function, which allows one to go from three-dimensional integration within the scattering volume to one-dimensional integration over the delay parameter and evaluate both the coherent and incoherent components of the scattered signal power.

The number of particles that determine the same delays in bistatic scattering determines the time-varying random complex impulse response of scattering $\tilde{b}(\tau,t)$. By analogy with (Ishimaru, 1978; Van Tris, 1977; Kennedy, 1973), we call the averaged impulse response the scatter-function by delay (below — the scatter-function).

$$S_t(\tau) \underline{\Delta} \left\langle \tilde{b}(\tau,t) \right\rangle, \quad (7.13)$$

where $\langle\ \rangle$ denotes the operation of averaging over a set.

The coherent component of the received signal will be determined by the convolution integral

$$\tilde{U}_{coh}(t)\cdot e^{-i\omega_0 t} = \int_{\tau_{\min}}^{\tau_{\max}} S_t(\tau)\cdot\tilde{U}(t-\tau)e^{-i\omega_0(t-\tau)}d\tau, \quad (7.14)$$

where $(\tau_{\min}, \tau_{\max})$ is the delay interval during scattering, $\tilde{U}(t)$ is the complex envelope of the signal emitted at frequency ω_0.

Using the scatter-function $S_t(\tau)$ and assuming that the antenna gains do not change within the meteor trail and the attenuation factor $\exp(-\gamma_1-\gamma_2)$ for an un-

derdense meteor trail can be neglected, the power of the coherent component of signal at the receiving point will be equal to

$$P_{coh}(t)=\frac{\lambda^2 P_T G_T G_R \sigma_\varepsilon}{(4\pi)^3 R_1^2 R_2^2}\int_0^{\tau_{\max}} S_t(\tau)\tilde{U}(t-\tau)d\tau\int_0^{\tau_{\max}} S_t(\tau)\tilde{U}^*(t-\tau)d\tau, \qquad (7.15)$$

or, for a real signal,

$$P_{coh}(t)=\frac{\lambda^2 P_T G_T G_R \sigma_\varepsilon}{(4\pi)^3 R_1^2 R_2^2}\left[\int_0^{\tau_{\max}} S_t(\tau)U(t-\tau)d\tau\right]^2. \qquad (7.16)$$

Note that each value of τ_i corresponds to a pair of values R_{1i} and R_{2i} and, in a more strict formulation of the problem, it would be necessary to calculate the multiplier for each τ and include it in the scatter-function (which is possible in principle), but the complication of calculations does not significantly increase the accuracy of the power estimate and are not suitable for engineering applications. Therefore, in formulas (7.15) and (7.16), it seems reasonable to calculate R_1 and R_2 for the specular reflection point.

Based on (7.16) and (7.12), we obtain an expression for the power of the received signal scattered by IMTr in which the bulk electron density of the formed trail does not exceed $N_{e\,cr}(\lambda)$

$$P_{coh}\left(t,N_e\le N_{ekr}\right)=\frac{P_T G_T G_R \lambda^2 r_e^2\left(1+\cos^2(\theta/2)\right)\dfrac{1+q^2R_D^2}{2+q^2R_D^2}}{128\pi^3 R_1^2 R_2^2}\times$$
$$\times\left[\int_0^{\tau_{\max}} S_t(\tau)U(t-\tau)d\tau\right]^2. \qquad (7.17)$$

The scatter–function can also be used to estimate the power of an incoherently scattered signal. We can offer the following expression for calculating the incoherent component of the scattered field

$$P_{incoh}(t)=\frac{P_T G_T G_R \lambda^2 \sigma_\varepsilon}{(4\pi)^3 R_1^2 R_2^2}\Phi_\varepsilon^n(q)\int_{\tau_{\min}}^{\tau_{\max}} S_t(\tau,t)d\tau, \qquad (7.18)$$

where $\Phi_\varepsilon^n(q,)$ is the normalized value of the energy spectrum of turbulent inhomogeneities. Since there are currently no reliable data on the spectral density of fluctuations (energy spectrum of turbulent inhomogeneities $\Phi_\varepsilon^n(q))$ generated by the turbulence of a meteoroid moving at the hypersonic velocity in a turbulent medium, it is proposed to use an energy spectrum model, the parameters of which can vary over a fairly wide range limits. The generalized expression for the class of correlation functions of isotropic turbulence is the expression

(Vvedensky, 1965)

$$B(\rho) = (\Delta\varepsilon)^2 \frac{2^{(1-p)}}{\tilde{A}(p)} \left(\frac{\rho_t}{l}\right)^p K_p\left(\frac{\rho_t}{l}\right), \tag{7.19}$$

where $(\Delta\varepsilon)^2$ — average fluctuation of intensity ε, p — generalized function index, l — characteristic scale of turbulent inhomogeneities, Γ — gamma function, K_p — Macdonald function, and ρ_t — the distance between two points in a turbulent flow within which pulsations ε are considered.

In this case, the generalized spectrum of fluctuations can be represented as

$$\Phi(q) = \frac{2\tilde{A}(p+0.5)}{\pi^{1/2}\tilde{A}(p)} (\Delta\varepsilon)^2 \frac{l}{\left(1+q^2l^2\right)^{(p+1)/2}}, \tag{7.20}$$

where $q = 2k \sin(\theta/2)$ is the scattering vector, and θ is the scattering angle.

The representation of the spectrum in a generalized form, as well as the choice of weight coefficients $a(t)$ and $b(t)$ in expression (7.1), make it possible to match the calculated data on the frequency dependence of the scattered field with the results of experimental observations.

The initial phase of the trail formation within the limits has features that should be taken into account when building a signal scattering model. When a meteor body enters the first Fresnel zone, a head echo can be observed in the thermalization interval, which is a consequence of the rapid expansion of the IMTr . This time interval depends on the height of the trail formation, changing from 1 ms at an altitude of 80 km to 150 ms at an altitude of 115 km (see Section 6) and ends with the formation of the initial radius r_0 of the meteor trail, within which the bulk electron density is distributed according to a certain law. The parameter r_0 is necessary to perform calculations of the power of reflected radio signals for certain values of the linear electron density of the trail.

If $N_e(\lambda) \geq N_{e\,cr}(\lambda)$, it is necessary to use other signal scattering models based on some approximations. One of such approximations is the assumption that up to a certain point in time, the trail can be considered as a thin cylinder with a high conductivity (metal cylinder) and a given initial radius. In the process of further expansion, it can be represented as a metal cylinder in a plasma shell. These models will be discussed next.

7.2. Scattering function of an underdense meteor trail

The number of free electrons that lead to the same delays in the received signal during bistatic scattering is determined by the surface area of the ellipsoid located within IMTr with a given radius.

The mutual arrangement of the transmitter A, the scatterer (a trail in the form of a cylinder with a radius $r = r_{eq}$) and the receiver B, which registers the scattered

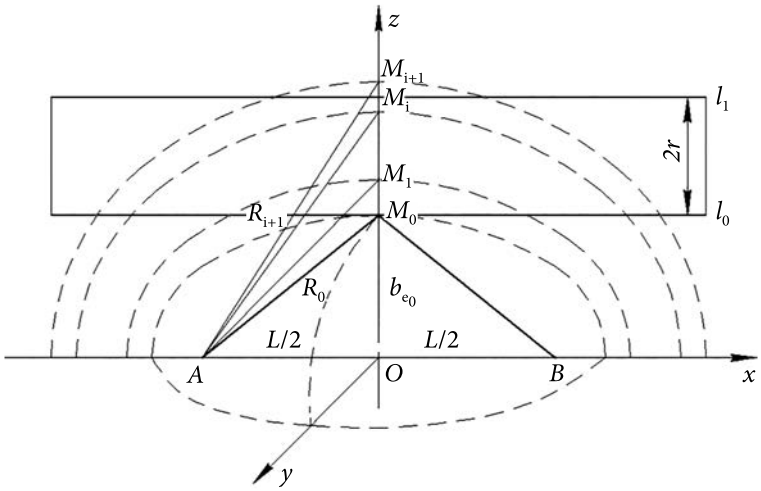

Fig. 7.1. Mutual arrangement of the transmitter, scatterer, and receiver that registers the scattered signal (the figure is schematic, not to scale)

signal, is shown in Fig. 7.1, which shows surfaces of equal delay, which are ellipsoids of revolution with foci at the points of transmission *A* and reception *B*.

The semi-minor axis of the ellipsoid b_{e0} and the distance AB make it possible to determine the sum of focal radii, which is constant for the chosen ellipsoid and determines the propagation delay τ_i of the signal. Giving the delay increment $\Delta\tau_i$, we obtain the corresponding increment Δb_i and then can calculate the elementary volume ΔV_i bounded by the diffuser surface and ellipsoids with parameters τ_i and $\tau_i + \Delta\tau_i$.

As a result, the entire volume of the diffuser will be divided into a large number of layers containing different numbers of particles. It is obvious that the number of particles in an elementary volume may differ from the average value $N_{av}(\tau_i)$ determined by the elementary volume and the volumetric particle distribution density by some random value $\Delta N(\tau_i)$ for different delays, i.e.,

$$N(\tau_i) = N_{\text{av}}(\tau_i) + \Delta N(\tau_i)\,. \tag{7.21}$$

Since $\Delta N(\tau_i) << N_{av}(\tau_i)$, the value of the random variable can be ignored. Knowing the volumetric density distribution of homogeneous particles within the scatterer, it is possible to calculate the average number of particles $N_{av}(\tau_i)$ within the elementary volume ΔV_i. The waves scattered by each particle arrive at the receiving point practically in the same phase and are added coherently; as a result, the signal power at the receiving point will be proportional to $N^2_{av}(\tau_i)$.

If the trail radius in the process of diffusion expansion exceeds the wavelength, and the average number of particles in each of the layers is approximately the same, then almost all phases will be present within the scattering volume, and the coherent component of the scattered field will approach zero. At the same

time, the number of scattering particles remains unchanged, and the signal power at the observation point will be determined by the incoherent component, which is proportional to the total number of particles in the scattering volume N_{Σ}.

The scatter-function of the meteor channel is proposed to be calculated in the following order (Kharchenko, 2010; Kharchenko, 2012):

1. Using the prognostic model presented in subsection 5.2, for a radio link of a given length, select one of the SRPs in the radio visibility zone and, based on the calculated coordinates, determine its height above the Earth's surface.

2. Calculate the linear electron density, the initial radius of the meteor trail, and the diffusion coefficient based on the given parameters of the meteoroid and the height of the SRP above the Earth's surface.

3. Determine the values of the equivalent radius $r_{eq}(t)$ of the meteor trail at different times. (The introduction of the equivalent trail radius allows us to consider the bulk electron density of the meteor trail to be constant inside the cylinder with radius r_{eq}).

4. Determine the delay of the signal that passed from the transmission point to the reception point through the point M_0 (Fig. 7.1).

5. Increase the value of the minor semiaxis of the ellipsoid in such a way that the delay of the signals reflected from the points M_1, M_2 …, M_i increase uniformly with a step $\Delta\tau$.

6. Determine the surface area of the intersection of the ellipsoid with the meteor trail S_i and calculate the scattering volume $\Delta V_i = S_i \cdot \Delta b_e$ on the interval Δb_e corresponding to $\Delta\tau$.

7. Estimate the number of electrons K in a given volume.

8. Determine the intensity of the scattered signal.

Using the method described in subsection 6.4, we determine the linear electron density of IMTr in the SRP region. For given SRP height, physicochemical properties of the meteoroid, and atmospheric parameters determined at the SRP height, we calculate the trail linear electron density, its equivalent radius, and ionization coefficient β.

Based on the calculated scatter-function, using formula (7.17), we obtain an estimate of the coherent component of the scattered signal power.

As a model for describing the change in time of the radial profile of the bulk electron density, we convert expression (6.51) to the form

$$n(r,t_i) = \frac{q}{\pi(r_0^2 + 4D_a t_i)} \cdot \exp\left(-\frac{r^2}{r_0^2 + 4D_a t_i}\right). \tag{7.22}$$

Since the boundaries of the meteor trail are conditional in the Gaussian approximation of the electron density, we use the concept of the time-varying equivalent radius of the trail

$$r_{eqv}(t_i) = \sqrt{r_0^2 + 4Dt_i}\ . \tag{7.23}$$

The introduction of the equivalent trail radius makes it possible to consider the bulk electron density of the meteor trail to be constant inside a cylinder of radius r_{eq} and equal to

$$N_{eqv}(t) = \frac{q}{\pi r_{eqv}^2(t)}, \tag{7.24}$$

and at the initial moment of time (after the completion of thermalization)

$$N_{eqv}(t) = \frac{q}{\pi r_{eqv}^2(t)}. \tag{7.25}$$

The ambipolar diffusion coefficient and the initial radius of the meteor trail can be found using the method described in section 6. Without losing the generality of the reasoning, we use empirical formulas (Tokhtas'ev, 1975) (see subsection 6.4)

$$q(h_M) = 4{,}03\times10^{14}\cdot\frac{m(v_{m0}-8{,}15)^3}{H_M}\cdot\cos\chi\cdot Z(t), \tag{7.26}$$

$$D_a = 13.2\cdot\exp\left(\frac{h_i - 95}{H_i}\right), \text{ [m}^2\text{/s]}, \tag{7.27}$$

$$r_0 = 1.65\sqrt{\frac{\nu}{40}\exp\left(\frac{h_M - 95}{2H_i}\right)}, \text{ [m]} \tag{7.28}$$

where m is the meteoroid mass at the considered point; v_{m0} is the velocity (in km/s) of the meteoroid at the entry to the meteor region; h_M is the height above the Earth's surface at the considered point on the track, km; H_p is the reduced height of the atmosphere, km.

The dependence of the bulk electron density on the trail radius calculated by formula (6.51) at the given time points 0.01 s, 0.05 s, 0.1 s, and 0.5 s for a meteoroid with a mass of 0.2 g entering the atmosphere at a speed of 40 km/s is shown in Fig. 7.2.

The minimum delay during signal propagation is determined by the point of contact $M_0(x_0,y_0,z_0)$ of the lower boundary of the meteor trail with one of the ellipsoids of the family with a given size of the minor semiaxis b_{e0} (see Fig. 7.1) and is calculated by the expression

$$\tau_{M_0} = \frac{1}{c}(AM_0 + M_0B), \tag{7.29}$$

where

$$AM_0 = R_1 = \sqrt{(x_a - x_0)^2 + (y_a - y_0)^2 + (z_a - z_0)^2},$$

$$M_0B = R_2 = \sqrt{(x_0 - x_a)^2 + (y_0 - y_a)^2 + (z_0 - z_a)^2}.$$

AM_0 and M_0B are the distances from the transmitter to the touch point and from the touch point to the receiver, respectively.

It is known that the sum of the focal radii of an ellipsoid is constant and equals

$$AM_0 + M_0B = 2\sqrt{b_e^2 + \left(\frac{L}{2}\right)^2}\,. \quad (7.30)$$

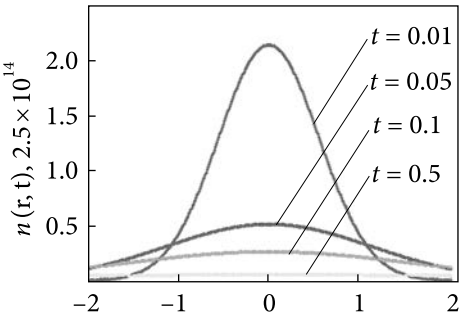

Fig. 7.2. Bulk electron density as a function of meteor trail radius

With an increase in the minor axis of the ellipsoid b_e, the delay of the scattered signal, determined by the position of point M_i, increases accordingly. When constructing the scatter-function, the value of b_i should be increased in such a way that the delay of the signal reflected from points M_1, M_2, …, M_i increases with a uniform step $\Delta\tau$. To do this, it is necessary to choose the increment of the value of the minor semiaxis in accordance with the expression

$$\Delta b_{e_{i+1}} = b_{e_{i+1}} - b_{e_i} = \sqrt{\left(R_0 + (i+1)\Delta R\right)^2 - \left(\frac{L}{2}\right)^2} - \sqrt{\left(R_0 + i\Delta R\right)^2 - \left(\frac{L}{2}\right)^2}\,. \quad (7.31)$$

Let us find the surface area of the intersection of ellipsoids having foci at the points of reception and transmission with a meteor trail as a cylinder of radius r_{eq}.

To do this, the value of the minor semiaxis b_y of the ellipsoid be will be increased step by step by Δb_{ei}

$$b_{e_i} = b_{e_0} + \sum_0^i \Delta b_{e_i}\,. \quad (7.32)$$

The boundary of the intersection of the ellipsoid and the cylinder is an ellipse, the major and minor axes of which are designated as P_1P_2 and P_3P_4 in Fig. 7.3.

The area of an ellipsoid bounded by a cylinder of radius r_{eq} is approximately determined by the well-known formula for the area of an ellipse

$$S_{ell} = \pi \cdot P_1P_2 \cdot P_3P_4\,, \quad (7.33)$$

where

$$P_1P_2 = \left(t_1 - t_2\right)\sqrt{m^2 + n^2 + p^2}\,; \quad (7.34)$$

$$P_3P_4 = 2\sqrt{r_{eqv}{}^2 - \left(\sum_{k=0}^{i} \Delta b_{e_k}\right)^2} = 2\sqrt{r_{eqv}{}^2 - \left(b_{e_i} - b_{e_0}\right)^2}\,; \quad (7.35)$$

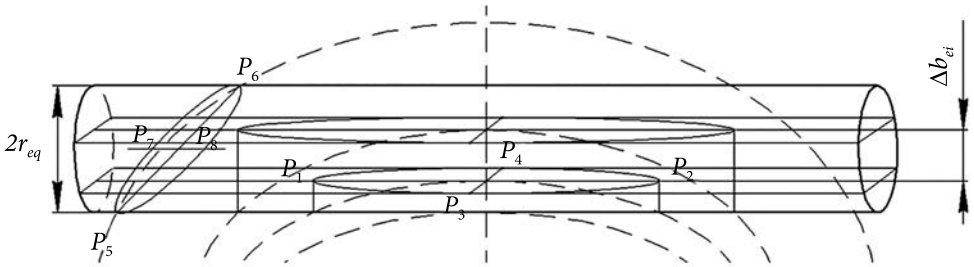

Fig. 7.3. Intersection of ellipsoids and a cylinder

m, n, and *p* are the direction vectors of the meteor trail, and t_1, t_2 are the roots of the equation

$$\left(b_e^2 \cdot c_e^2\right)\left(mt + x_0\right)^2 + \left(a_e^2 \cdot c_e^2\right)\left(nt + y_0\right)^2 + \\ + \left(a_e^2 \cdot b_e^2\right)\left(pt + z_0\right)^2 - \left(a_e^2 \cdot b_e^2 \cdot c_e^2\right) = 0. \quad (7.36)$$

When exceeds the trail diameter $2r_{eq}$, the area of the ellipses of the section is equal to

$$S_{ell} = 2\pi \cdot P_5P_6 \cdot P_7P_8, \quad (7.37)$$

where

$$P_5P_6 = \sqrt{\left(x_0 - x_1\right)^2 + \left(y_0 - y_1\right)^2 + \left(z_0 - z_1\right)^2}, \quad (7.38)$$

$$P_7P_8 = 2r_{eqv}. \quad (7.39)$$

The derivation of formulas (7.34)—(7.39) is given in the Appendix to (Kharchenko, 2012).

The elementary volume bounded by two ellipses is

$$\Delta V_i = S_{elli} \cdot \Delta b_{e_i}. \quad (7.40)$$

Since the bulk electron density inside a cylinder with an equivalent radius is assumed to be constant, the number of coherently scattering electrons in an elementary volume and, therefore, the differential scatter-function is

$$dS\left(\tau\right) = n(r_{eqv})V\left(\tau\right)d\tau, \quad (7.41)$$

and the meteor trail scatter-function has the form

$$S\left(\tau\right) = n(r_{eqv})V\left(\tau\right). \quad (7.42)$$

It determines the intensity of the scattered signal in the time interval from 0 to τ_{max}.

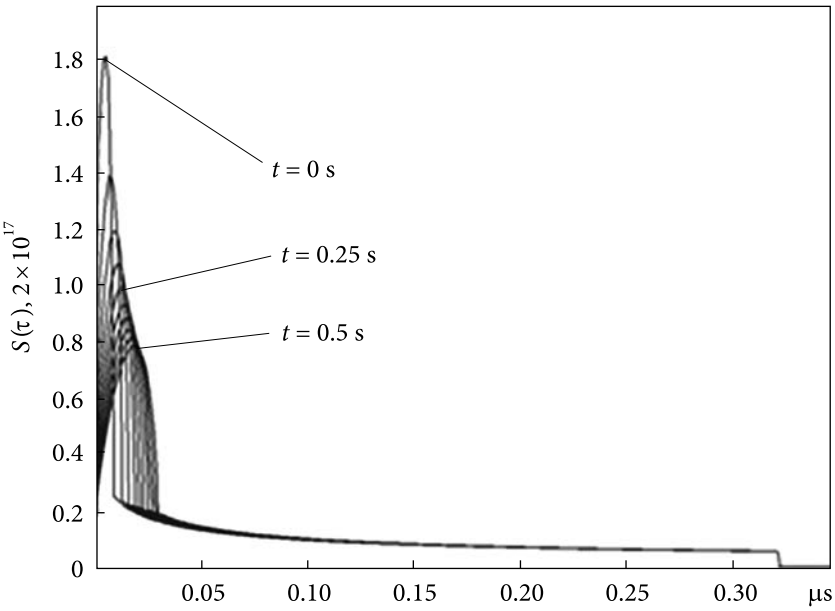

Fig. 7.4. Scatter-functions of a meteor trail expanding under the action of ambipolar diffusion

Fig. 7.4 shows the scatter-functions of the meteor trail expanding under the action of ambipolar diffusion at different times calculated for the following parameters of the meteor trail and radio link: meteoroid mass m = 0.1 g, velocity v = 40 km/s, wavelength λ = 10 m, and the length of the radio link L = 1000 km.

To estimate the influence of the operating frequency on the change in time of the received signal power scattered by a meteoroid with a mass of 0.1 g and a velocity of 40 km/s, numerical calculations were performed for operating frequencies f_1 = 30 MHz, f_2 = 45 MHz, f_3 = 60 MHz, and also for a linear frequency modulated (LFM) signal with a center frequency f_s = 45 MHz and a frequency change from 30 to 60 MHz, represented by the expression

$$U(t) = \cos\left(2\pi f_s t + \frac{\mu}{2}t^2\right), \tag{7.43}$$

where $\mu = 2\pi\dfrac{\Delta F_c}{T_c}$ is the frequency deviation; f_s is the frequency of the carrier wave; ΔF_s is the width of the LFM signal spectrum; T_s is the signal duration.

The calculation results obtained using expressions (7.17), (7.43) and the scatter-function calculated by the proposed method are shown in Fig. 7.5.

We assume that in the band 30—60 MHz, the effective area of the antennas is determined by the average frequency of the operating range. The results of

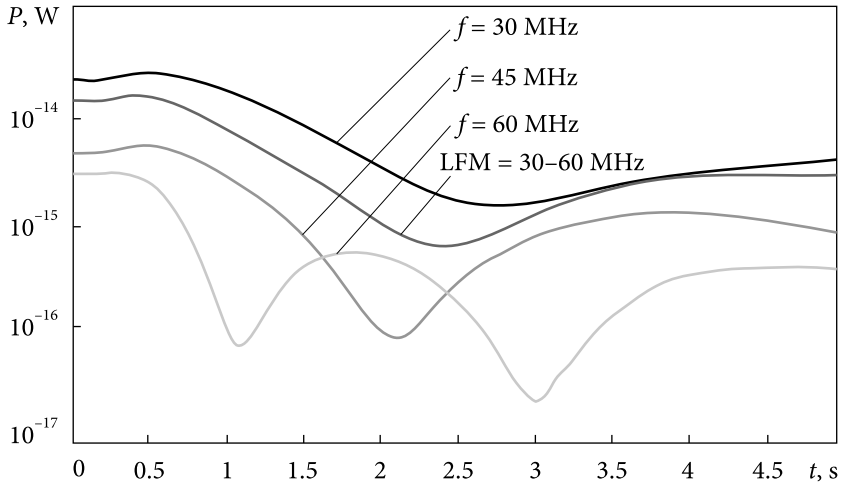

Fig. 7.5. Change in power of received quasi-harmonic and LFM signals over time

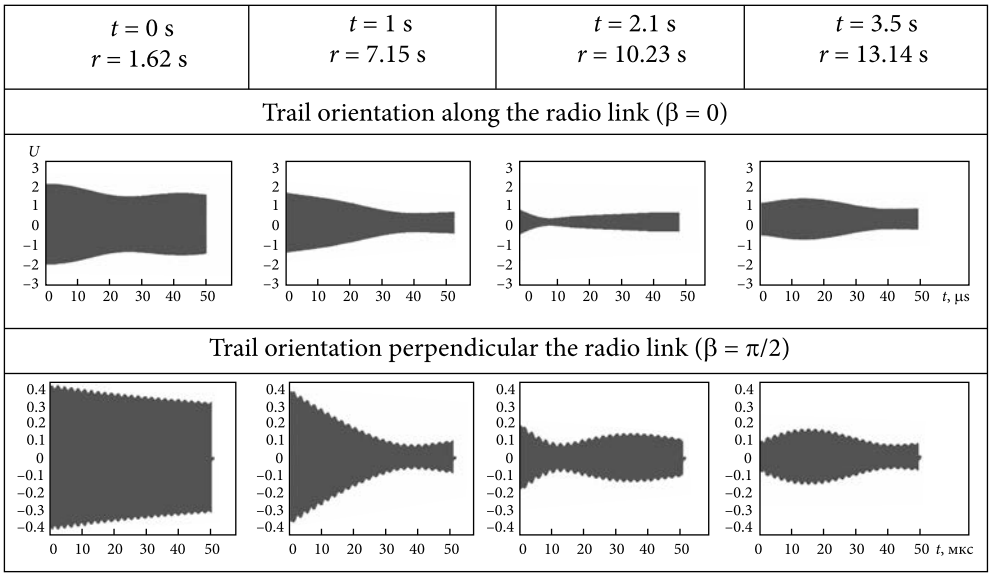

Fig. 7.6. Changing in the form of the LFM signal at the receiver input at different times

the numerical simulation presented in the figure showed that with increasing the radius of the meteor trail due to diffusion, at certain points in time, the power of quasi-harmonic signals changes significantly. At the same time, there are no significant power fluctuations for the LFM signal, and the average power changes smoothly and remains higher in relation to the power scattered on the meteor trail at the middle frequency of the range.

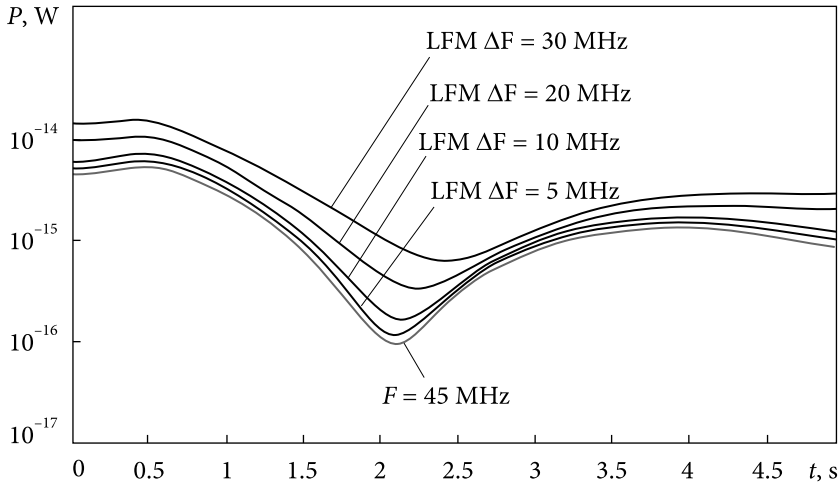

Fig. 7.7. The power changing for the LFM signal scattered on an underdense meteor trail at the selected value of the spectrum width

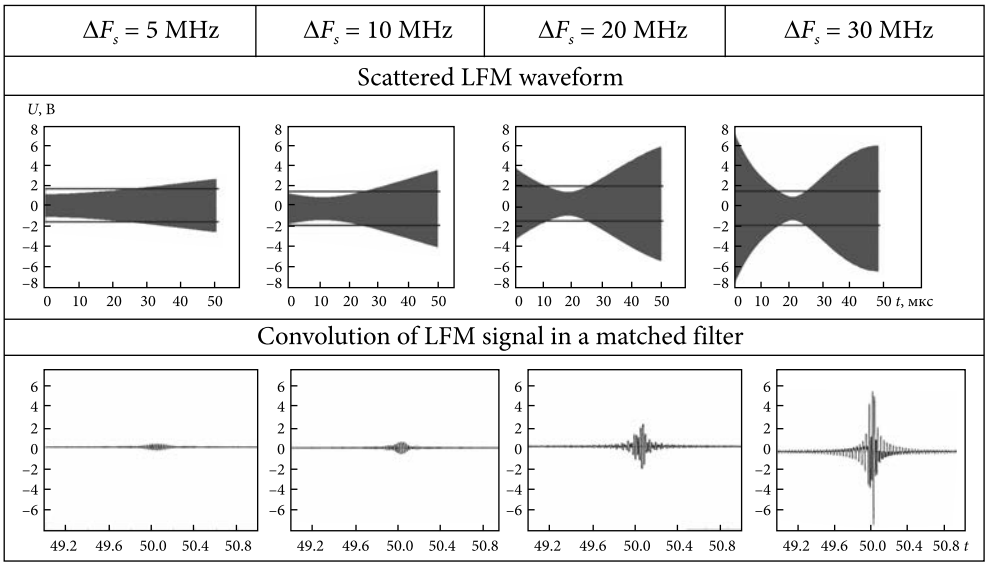

Fig. 7.8. Changing in the waveform of the scattered chirp signal and its convolution in a matched filter for different values of the signal spectrum width

Fig. 7.6 shows changing in the waveform of the LFM signal at the receiver input at different times when the trail is oriented along the radio link ($\beta = 0$) and perpendicular to the radio link ($\beta = \pi/2$) for the carrier frequency $f_0 = 45$ MHz with the signal spectrum width $\Delta F = 30$ MHz.

To justify the choice of the WNLS spectrum width, the influence of the LFM signal spectrum width on the change in the received signal power due to diffrac-

tion oscillations was estimated. Fig. 7.7 shows the results of calculations obtained using a computer model that implements the proposed method for calculating the power dissipated within an underdense meteor trail.

For the characteristic time t = 2.1 s, the waveform of the scattered LFM signal and its convolution in the matched filter was calculated. The calculation results for the carrier frequency f_c = 45 MHz and different values of the signal spectrum width ΔF_s = 5, 10, 20, and 30 MHz are shown in Fig. 7.8. The same figure, for comparison, shows the amplitude of quasi-harmonic oscillations (a line against the background of the LFM signal) and the convolution of an unscattered LFM signal with an indicated spectrum width.

An analysis of the above results suggests that the use of code division of channels and ensembles of broadband signals with good cross-correlation properties in meteor radio communication systems (Varakin, 1985; Kuznetsov, 2007) will increase the throughput of these systems. In this case, to reduce the effect of diffraction oscillations, it is necessary to use signals with a spectrum width exceeding 10 MHz.

It should be noted that the results based on expressions (7.15—7.17) are obtained under the assumption that the meteor trail is completely formed. The time interval in which the meteoroid head crosses the first and neighboring Fresnel zones was not taken into account. Further, a model will be proposed that takes into account this phase of the trail evolution.

7.3. Scattering by an expanding plasma ball

Let us estimate the reliability and accuracy of the representation of the scattered signal using the scatter-function calculated by the method proposed in subsection 7.2. To do this, we set a plasma ball as a scatterer, the radius of which varies from some initial value a_0 to a_{max}. Assume that the number of free electrons within the sphere remains constant (that is, the bulk electron density changes). The calculations will be carried out in the single-scattering approximation.

A feature of the selected scatterer is that it has an exact solution obtained by other methods (Alpert, 1972; Menzer, 1958; Van de Hulst, 1961; Mie, 1908; Boren, 1986; Pascale, 2017).

Fig. 7.9*a* shows the location of a ball with a radius *a* relative to the transmission and reception points, which are the foci of the ellipsoid of revolution, and Fig. 7.9*b* shows the sections of the ball with ellipsoids.

Figure 7.10 shows a view of the plasma ball scatter-function obtained by the section method described in subsection 7.2.

The effective scattering cross-section of a dielectric ball was previously independently calculated by several authors using different methods, which gave

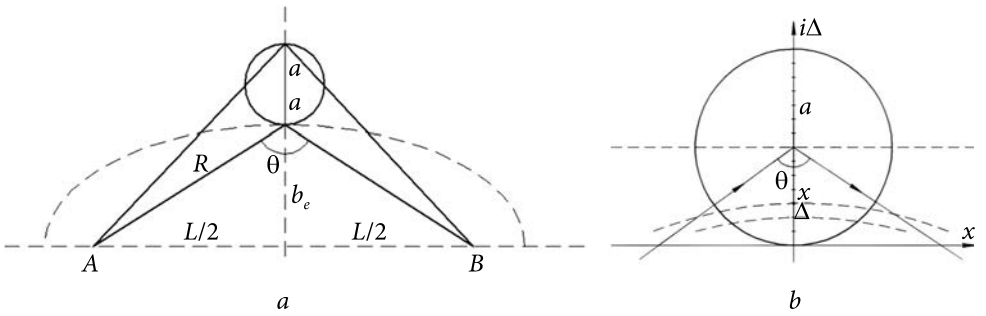

Fig. 7.9. Scattering on the plasma ball: *a* — location of the ball with a radius *a* relative to the points of transmission and reception; *b* — sections of the ball by ellipsoids

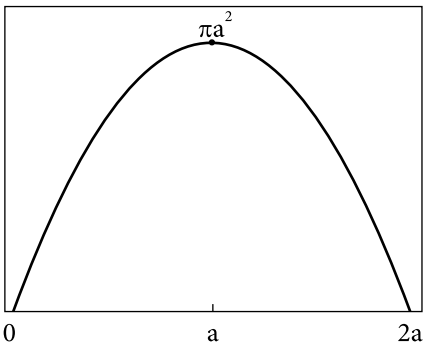

Fig. 7.10. Ball scatter-function

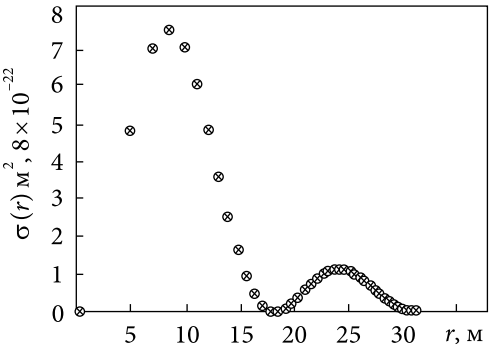

Fig. 7.11. Effective scattering cross-section of an expanding plasma

practically the same results. The expression for the effective scattering cross-section of a plasma ball obtained in (Alpert, 1972) has the form

$$\sigma(a) = \frac{\pi^3 e^4 c^2 N_e^2}{m_e^2 \omega^6 \sin^6\left(\frac{\theta}{2}\right)} \left[\sin\left(2ka\sin\left(\frac{\theta}{2}\right)\right) - 2ka\sin\left(\frac{\theta}{2}\right)\cos\left(2ka\sin\left(\frac{\theta}{2}\right)\right)\right]^2. \quad (7.44)$$

Fig. 7.11 shows the results of calculating the effective scattering cross-section of an expanding plasma ball by formula (7.44) as well as the results of calculating the scattered power for a plasma ball, performed using the calculated ball scatter-function and a method similar to that used in calculating the scattering on a meteor trail (subsections 7.1 and 7.2).

For a sphere, the effective scattering cross-section calculated using the scatter-function is in full agreement with the formula (7.44) and other results obtained using various methods of diffraction theory. This confirms the correctness of the proposed method for determining the power scattered by a meteor trail and

the possibility of using the bistatic scatter-function to find the effective scattering cross-section for objects of complex form under the introduced restrictions.

7.4. Bistatic scattering on overdense meteor trail

The calculation of the effective scattering surface of an overdense meteor trail when the transmission and reception points are separated (bistatic version) is a rather complicated diffraction problem. To solve it, one has to use approximations that need to be verified. At the initial moment of trail formation, its radius $r_0 < \lambda/2$, and the length $l >> \lambda$, and the trail can be considered as a thin cylinder with a high degree of conductivity (metal cylinder). In the resonant region, for cylinders whose radius lies within (0.01—0.5) λ and the length exceeds 0.5 λ, the scattering characteristics when the field is polarized perpendicular to the cylinder axis can be determined based on a strict solution for an infinite cylinder, or, under certain assumptions and simplifications, obtain an approximate solution (Hönl, 1964; Nikolskij, 1989; Wait, 1955; Leavens, 1965; Liou, 1972). It should be taken into account that approximate methods for solving the diffraction problem do not imply the possibility of determining resonant frequencies with sufficient accuracy.

As the trail expands, its bulk electron density, distributed relative to the trail axis according to a specific law (the Gaussian distribution usually used), decreases, and the meteor trail must be considered as a metal cylinder in a plasma shell (Kharchenko, 2012; Kharchenko, 2011; Neganov, 2000; Zouros, 2011; Azarenkov, 2008; Azarenkov, 2011; Naishadham, 2010). With further expansion of the trail, its bulk electron density becomes less than the critical value for a given frequency, and it becomes possible to consider it as scattering on fluctuations in the permittivity, i.e., to use the calculation method described in subsections 7.2 and 7.3.

Methods for solving diffraction problems are divided into strict and approximate (heuristic). Strict methods involve solving Maxwell's equations, taking into account the corresponding boundary conditions on the surface of the scattering body. With a harmonic dependence of the electromagnetic field strength on time and in the absence of other sources except for the acting electromagnetic field, Maxwell's equations are reduced to the Helmholtz equations for complex amplitudes.

The strict methods of the theory of diffraction differ from each other in the mathematical means used in solving the initial equations. The name "strict methods" does not mean that their application necessarily gives accurate results. Solutions can be approximate or asymptotic. The rigor of the methods lies in the fact that, within the limits of the imposed restrictions, the error of the obtained solutions can always be accurately estimated using strict mathematical methods at all stages of solving the problem up to obtaining numerical results. This is the main distinguishing feature of strict methods in comparison with heuristic ones, where mathematical difficulties are bypassed with the help of one or another physical

hypothesis. The field of application of strict methods, generally speaking, is not limited by either the shape or the size of the scattering bodies. However, practically up to now, only a very small number of problems have been solved by strict methods either for bodies of the simplest shape (sphere, spheroid, and disk) or for bodies with some or all dimensions small compared to the wavelength.

In contrast to strict methods, approximate or heuristic methods for solving diffraction problems make it possible to obtain approximate solutions in a closed form by relatively simple means. Each heuristic method is based on a physical hypothesis, which allows one to either completely eliminate or significantly simplify purely mathematical problems that are insurmountable with a strict formulation of the problem. However, when using approximate methods, uncontrollable errors occur, which depend on specific conditions and may be different in each individual case. Any heuristic method is usually applicable only under certain predetermined conditions. The error of the heuristic method is estimated by comparing the approximate and strict solutions under equal conditions. If a strict solution is not found, there is only one way left — comparison with experimental data.

7.4.1. Analysis of strict methods for solving the diffraction problem on scattering by a dielectric cylinder

The calculation of the effective scattering surface (ESS) in the vast majority of cases reduces to solving the corresponding diffraction problem, determining the necessary polarization components of the scattered field, and then calculating the ESS.

The problem of scattering an electromagnetic wave by a cylinder occupies the first place in the number of works published to date, ahead of even the problem of scattering by a sphere. With an oblique incidence of an electromagnetic wave on a cylinder with an arbitrary but constant permittivity in a strict formulation, the problem was formulated in many works (Menzer, 1958; Nikolskij, 1989; Wait, 1955; Leavens, 1965; Liou, 1972; Potekhin, 1948). Its solution was obtained in the form of an infinite series, but it was not brought to the point of obtaining numerical results. Numerical results have been obtained for the case of normal wave incidence relative to the axis of the cylinder, in which the Maxwell equations are reduced to the form of differential equations with separable variables. Even with the above formulation of the problem, the computational complexity of obtaining a solution is very high and, in addition, it becomes even more complicated when taking into account the time-varying radius of the cylinder and its dielectric constant. Even having overcome computational problems, it is difficult to assess the degree of adequacy of such a representation for describing an expanding meteor trail with a non-uniform distribution of electron density relative to the axis.

Making certain assumptions and applying the technique of solving differential equations used in (Landau, 1973; Menzer, 1958; Van de Hulst, 1961; Hönl, 1964; Brysk, 1965; Senior, 1965; Volman, 1971), the solution of the scattering problem on a cylinder with oblique wave incidence can be obtained under the conditions that the electric field is parallel to the axis of the cylinder, there is no magnetic field surrounding the cylinder, and the electron density of the cylinder has a symmetric distribution about the axis. Thanks to this symmetry, and in the case the electric field strength vector E is parallel to the z-axis, the Maxwell equations, when passing to cylindrical coordinates, are reduced to the form of Bessel differential equations, which in the CGS system have the following form (Brysk, 1965; Volman, 1971; Jones, 1974):

$$\frac{\partial^2 E_z}{\partial r^2}+\frac{1}{r}\frac{\partial E_z}{\partial r}+\frac{1}{r^2}\frac{\partial^2 E_z}{\partial \phi^2}+\varepsilon\frac{\omega^2}{c^2}E_z=0, \tag{7.45}$$

$$\frac{\partial^2 H_z}{\partial r^2}+\left(\frac{1}{r}-\frac{1}{\varepsilon}\frac{\partial \varepsilon}{\partial r}\right)\frac{\partial H_z}{\partial r}+\frac{1}{r^2}\frac{\partial^2 H_z}{\partial \phi^2}+\varepsilon\frac{\omega^2}{c^2}H_z=0, \tag{7.46}$$

where E_z is the electric field strength along the z-axis; Hz is the magnetic field strength along the z-axis; ε is the relative permittivity; ω is the angular frequency of the radio wave; c is the speed of light; r, φ, and z are cylindrical coordinates.

The solution of equations (7.45) and (7.46) was found under the assumption that the term $\frac{1}{\varepsilon}\frac{\partial \varepsilon}{\partial r}\frac{\partial H_z}{\partial r}$ in equation (7.47) can be neglected (Jones, 1974). In this case, the solution of equation (7.46) tends asymptotically to the solution of equation (7.45).

After the usual procedure of separation of variables, equation (7.45) is transformed to the form

$$\frac{\partial^2 E_z}{\partial r^2}+\frac{1}{r}\frac{\partial E_z}{\partial r}+\left(\varepsilon k^2-\frac{m_n^{\,2}}{r^2}\right)E_z=0, \tag{7.47}$$

where m_n is zero or a positive integer. The solution to this equation can be represented as

$$E_z=\sum_0^\infty P_m \cos m_n\theta, \tag{7.48}$$

where θ is the scattering angle. Using as an approximation for the incident wave the identity

$$E_{inc}=\exp\left(jkx\right)=\sum_{m-0}^{\infty}\mu_n j^m J_m\left(kr\right)\cos m\phi, \tag{7.49}$$

where μ_n is the Neumann factor, the scattered wave in the far zone takes the form

$$E_{refl}=\sum_{m=0}^{\infty}\varepsilon t_m j^m H_m^{(1)}\left(kr\right)\cos m\phi, \tag{7.50}$$

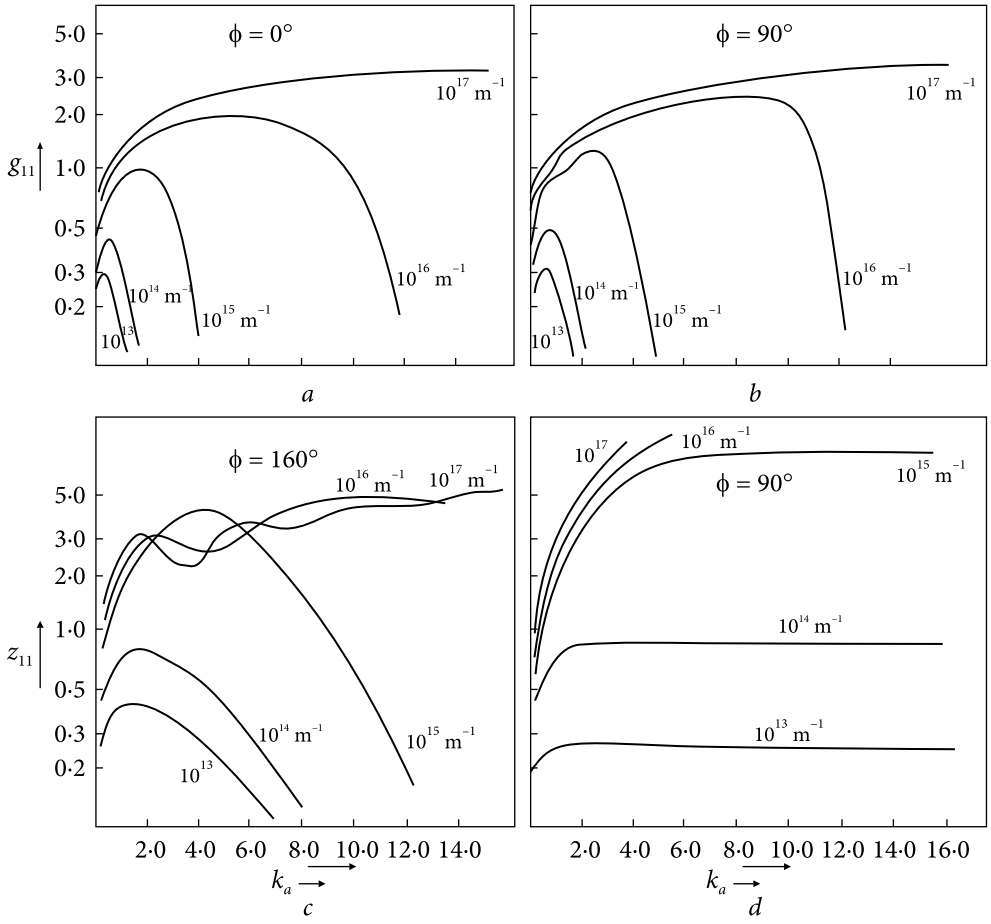

Fig. 7.12. Reflection coefficient g_{11} depending on the normalized radius k_a for different values of linear electron density: *a* — backscattering, *b* — orthogonal scattering; *c* — 160° forward scattering; *d* — 180° forward scattering (Brysk, 1965)

where t_m is the reflection coefficient and $H^{(1)}_m$ is the Hankel function of the first kind and m-th order. The reflection coefficient t_m is found from the solution of the system of equations

$$J_m(kr) + t_m H_m^{(1)}(kr) = A_m P_m(kr), \tag{7.51}$$

$$J_m'(kr) + t_m H_m'^{(1)}(kr) = A_m P_m'(kr), \tag{7.52}$$

where the primes (') denote differentiation to the radial coordinate.

It follows from the linear nature of the differential equation that if P_m is a solution, then $A_m P_m$ is a solution as well. Moreover, from (7.51) and (7.52) we

obtain

$$t_m = \frac{J_m(kr)P_m'(kr) - J_m'(kr)P_m(kr)}{P_m(kr)H_m^{(1)}(kr) - H_m'^{(1)}(kr)P_m'(kr)}. \quad (7.53)$$

Thus, the total reflection coefficient g_{11} at the oblique incidence of the wave takes the form

$$g_{11} = \sum_{m=0}^{\infty} \mu t_m \cos m\phi. \quad (7.54)$$

Fig. 7.12 shows the results of calculating the modulus of the reflection coefficient, which determines the wave amplitude at the receiving point for various values of the linear electron density of the trail and four values of φ: φ = 0, 90°, 160°, and 180°, covering the range from backscattering to forward scattering (Brysk, 1965).

The presented solution is strict, but the assumptions made do not allow us to consider it exact. For example, neglecting the equation term $\frac{1}{\varepsilon}\frac{\partial\varepsilon}{\partial r}\frac{\partial H_z}{\partial r}$ does not allow us to take into account resonance phenomena, while using the Bessel, Hankel, and endless rows to apply the obtained solution for $k_a < 0.4$ (Van de Hulst, 1961). However, the above results can be used to assess the adequacy of the heuristic solution, at least qualitatively.

7.4.2. Heuristic scattering model for an overdense meteor trail

Let us consider the main phases of the formation of the scattered signal and the allowable approximations in calculating the scattering in each phase. The initial moment is the moment when the meteoroid enters the trajectory section corresponding to the first Fresnel zone, and the first phase is the time interval at which the head part crosses the first and subsequent Fresnel zones. In this phase, fluctuations in the scattered signal power arise, which we will call diffraction oscillations of the first type (Fresnel oscillations). Then, the trail radius can be considered equal to the initial radius r_0, which is much smaller than the wavelength, and the electron density of the trail makes it possible to use a metal cylinder as a model. The dimensions of the first Fresnel zone l_{F1} in bistatic scattering are determined by the wavelength and radio link geometry, in particular, by the distance between the transmitter, receiver, and specular reflection point, as well as by angle β between the plane of the incident wavefront and the trail axis. Following (McKinley, 1961; McKinlay, 1964) and Recommendations ITU-R P.843-1 the dimensions of this zone can be estimated by the expression

$$l_{F1} = \sqrt{\frac{\lambda R_1 R_2}{(R_1 + R_2)} \frac{1}{1 - \sin^2\left(\frac{\theta}{2}\right)\cos^2\beta}}. \quad (7.55)$$

If we assume that the effective trail length is determined by the first Fresnel zone, and the initial trail radius $r_0 << \lambda$, then in the physical optics approximation, the median value of the trail RCS in the direction of the receiver is

$$\sigma_m = kr_0 l_{F1}^2 = \frac{2\pi r_0 R_1 R_2}{\left(R_1 + R_2\right)\left[1 - \sin^2\left(\frac{\theta}{2}\right)\cos^2\beta\right]}. \tag{7.56}$$

In this case, the square of the field strength at the receiving point will be equal to

$$\left|E_r\right|^2 = \left|E_0\right|^2 \frac{\sigma_m}{4\pi R_2^2}\frac{G_T\lambda^2}{4\pi}, \tag{7.57}$$

where

$$\left|E_0\right|^2 = \frac{P_T G_T}{4\pi R_1^2}. \tag{7.58}$$

Substituting (7.56) into (7.57) and simplifying it, in the approximation of physical optics, we obtain an expression for the power of the scattered signal at the reception point

$$P_r = \frac{\left|E_r\right|^2}{2} = \frac{P_T G_T G_R \lambda^2}{64\pi^2 R_1 R_2 (R_1 + R_2)} \cdot \frac{r_0}{1 - \sin^2\left(\frac{\theta}{2}\right)\cos^2\beta} =$$

$$= A \cdot \frac{r_0}{1 - \sin^2\left(\frac{\theta}{2}\right)\cos^2\beta}, \tag{7.59}$$

where

$$A = \frac{P_T G_T G_R \lambda^2}{64\pi^2 R_1 R_2 (R_1 + R_2)}. \tag{7.60}$$

The power of the scattered signal significantly depends on angle β. When $\beta = 0$

$$P_r = A\frac{r_0}{\cos^2\left(\frac{\theta}{2}\right)} = Ar_0 \sec^2\left(\frac{\theta}{2}\right), \tag{7.61}$$

and for $\beta = \pi/2$

$$P_r = Ar_0. \tag{7.62}$$

Thus, for a given scattering angle, the relative value of the power at the receiving point depends on the orientation angle of the meteor trail and is determined

by the expression

$$\frac{P_r(\theta,\beta=0)}{P_r(\theta,\beta=\frac{\pi}{2})}=\frac{1}{\cos^2\left(\frac{\theta}{2}\right)}=\sec^2\left(\frac{\theta}{2}\right). \tag{7.63}$$

Note that angle θ depends on the length of the radio link, the location of the specular point relative to the middle of the radio link, and the height of the specular point within the meteor region.

While the trail expands, its equivalent radius increases in accordance with expression (7.28), and the power changes in proportion to the radius and can be calculated based on expression (7.60) by replacing r_0 with the time–varying critical radius $r_{cr}(t, \lambda)$, which is determined from expression (7.24) for $N(t) = N_{e\,cr}(\lambda)$

$$r_{cr}\left(t,\lambda\right)=\sqrt{-\left(r_0^2+4Dt\right)\ln\left(\frac{\pi N_{ekr}\left(\lambda\right)\left(r_0^2+4Dt\right)}{\alpha}\right)}, \tag{7.64}$$

where $N_{e\,cr}(\lambda)$ is calculated by the formula (7.8).

For cylinders whose radius lies within (0.01...0.5) λ and the length exceeds 0.5 λ, a strict solution for an infinite cylinder based on Maxwell's equations (Menzer, 1958) can be used to calculate the RCS. For normal incidence on the track axis, the effective scattering surface is equal to

$$\sigma=\sigma_m U\left(kr_{cr},kl_{eff}\right), \tag{7.65}$$

where σ_m is the asymptotic value of the EPR, which is determined by expression (7.57), and $U(kr_{cr},kl_{eff})$ is the energy scatter-function. At $l > 0.5\ \lambda$, one can take $U(kr_{cr},kl_{eff}) \approx U(kr_{cr})$. This allows using a strict solution for an infinite cylinder and representing the scatter-function as a series (Menzer, 1958):

$$U\left(kr_{cr}\right)=\frac{4}{\pi kr_{kr}}\left|\sum_{n=-\infty}^{\infty}\left(-1\right)^n\frac{\frac{d}{dkr_{kr}}\left[J_n\left(kr_{kr}\right)\right]}{\frac{d}{dkr_{kr}}\left[H_n^{(1)}\left(kr_{kr}\right)\right]}\right|^2, \tag{7.66}$$

where $J_n(kr_{cr})$ is the Bessel function and $H^{(1)}_n$ is the Hankel function.

Fig. 7.13 shows the results of calculating the normalized RCS obtained using a strict solution in the infinite cylinder approximation at a fixed wavelength and a monotonically increasing radius r_{eq}.

The results of calculating the normalized RCS determined by the overdense part of the meteor trail, the critical radius $r_{cr}(t, \lambda)$ of which does not change monotonically in time (see Fig. 7.14), are shown in Fig.7.15.

In bistatic scattering, the effective scattering surface depends on the angle between the direction of wave incidence and the direction of scattering and is

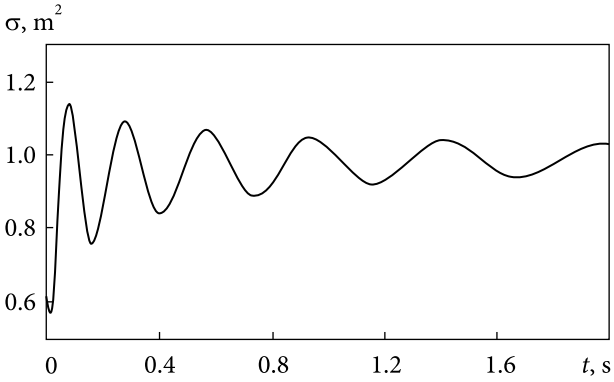

Fig. 7.13. Change in the normalized RCS of the meteor trail over time with increasing equivalent radius r_{eq} and initial radius $r_0 = 1.61$ m

determined by expression (7.57). Thus, in the approximation of physical optics, the power of the scattered signal $P_r(t)$ is determined by an expression that takes into account the expansion of the critical trail radius due to diffusion

$$P_r(t) = \frac{P_T G_T G_R \lambda^2}{64\pi^2 R_1 R_2 (R_1 + R_2)} \frac{r_{kr}(t)}{1 - \sin^2\left(\frac{\theta}{2}\right)\cos^2\beta} U\left[kr_{cr}(t)\sec(\theta/2)\right], \quad (7.67)$$

where $U[kr_{cr}(t)sec\theta/2]$ is determined by relation (7.66).

Substituting (7.66) into (7.67) and taking into account that $k = 2\pi/\lambda$, we obtain

$$P_r(t) = \frac{P_T G_T G_R \lambda^3}{32\pi^4 R_1 R_2 (R_1 + R_2)} \frac{1}{1 - \sin^2\left(\frac{\theta}{2}\right)\cos^2\beta} \times$$

$$\times \left| \sum_{n=-\infty}^{\infty} (-1)^n \frac{\frac{d}{dkr_{cr}}\left[J_n\left(kr_{cr}(t)\right)\right]}{\frac{d}{dkr_{cr}}\left[H_n^{(1)}\left(kr_{kr}(t)\right)\right]} \right|^2, \quad (7.68)$$

Based on this expression, we can speak about the presence of diffraction oscillations of the second type, determined by the wavelength and the time–varying critical radius of the overdense meteor trail. Expression (7.68) was obtained under the assumption that the meteor trail was completely formed, and the influence of the transition region on the meteoroid flight interval was not taken into account.

To describe scattering on an overdense meteor trail, we divide the scattering process into two parts. The first part, which characterizes the transition region, will be described assuming that scattering occurs on an overdense meteor trail with a critical radius $r_{cr}(t, \lambda) = r_0$ in the metal cylinder approximation, taking into

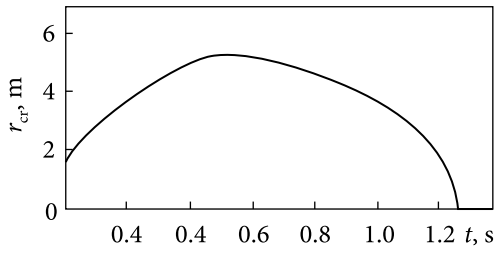

Fig. 7.14. Change in the critical radius r_{cr} in time

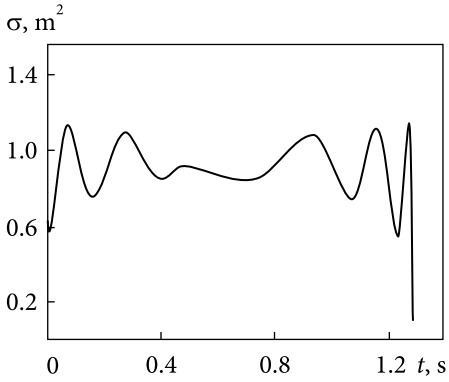

Fig. 7.15. Change in the normalized RCS of an overdense meteor trail in time depending on the critical radius r_{cr} at the initial radius r_0 = 1.61 m

account the first type of diffraction oscillations caused by the successive passage of the meteoroid through the Fresnel zones

$$P_{cr1}(t)=\frac{P_T G_T G_R \lambda^2}{64\pi^2 R_1 R_2 (R_1+R_2)}\frac{r_{cr}(t)}{\left[1-\sin^2\left(\frac{\theta}{2}\right)\cos^2\beta\right]}\cdot\left[\frac{C^2(x)+S^2(x)}{2}\right], \qquad (7.69)$$

where $C=\int_{x_1}^{x}\cos\frac{\pi x^2}{2}dx$ and $S=\int_{x_1}^{x}\sin\frac{\pi x^2}{2}dx$ differ from the usual Fresnel integrals, which are used in the optical diffraction theory, in the limits of integration, and the parameter x, which relates to the phase of the scattered oscillation, is determined by the expression

$$x=vt\left(1-\sin^2(\theta/2)\cos^2\beta\right). \qquad (7.70)$$

From expression (7.70), it is easy to obtain the corresponding value of the parameter t

$$t=\frac{x}{v}\frac{r_{cr}(t)}{1-\sin^2\left(\frac{\theta}{2}\right)\cos^2\beta}. \qquad (7.71)$$

The second part of the process of coherent scattering on the overdense part of the meteor trail in the approximation of a metal cylinder with a changing radius is described by expression (7.68), and we denote this part by $P_{cr2}(t)$. To conjugate these two parts, we use the Heaviside function H(x), defined by expression:

$$H(x)=\begin{cases}0, & \text{when} \quad x<0,\\ 1, & \text{when} \quad x\geq 0,\end{cases} \qquad (7.72)$$

and we find the conjugation point t_0 as the minimum non-trivial root of the equation obtained from the condition of equality of expressions (7.68) and (7.69), which, after simplifying and substituting the parameter x from expression (7.70), takes the form

$$\frac{r_{kr}(t)}{4}\cdot\left[C^2\left(vt\left(1-\sin^2(\theta/2)\cos^2\beta\right)\right)+S^2\left(vt\left(1-\sin^2(\theta/2)\cos^2\beta\right)\right)\right]=$$

$$=\frac{\lambda}{\pi^2}\left|\sum_{n=-\infty}^{\infty}(-1)^n\frac{\frac{d}{dkr_{kr}}\left[J_n\left(kr_{cr}(t)\right)\right]}{\frac{d}{dkr_{kr}}\left[H_n^{(1)}\left(kr_{cr}(t)\right)\right]}\right|^2. \qquad (7.73)$$

It is obvious that the solution of this equation can be obtained only by numerical methods; however, such a solution is quite rigorous. As an approximate solution, we can use the condition of equality of the median value of scattering on the overdense trail (7.60) and the power determined by expression (7.64). In this case, we obtain the equation

$$C^2\left[vt\left(1-\sin^2(\theta/2)\cos^2\beta\right)\right]+S^2\left[vt\left(1-\sin^2(\theta/2)\cos^2\beta\right)\right]=1, \qquad (7.74)$$

whose minimal nontrivial solution determines the approximate value of the conjugation point t_0.

Based on the foregoing, the expression for the coherent component of the scattering power on the overdense part of the meteor trail, including the transition region, can be represented as

$$P_{coh}^{(1)}(t)=P_{cr1}(t=t_0)\left[1-H(x-x_0)\right]\left[\frac{C^2(x)+S^2(x)}{2}\right]+$$

$$+P_{cr1}(t=t_0)H(x-x_0)\left[\frac{C^2(x)+S^2(x)}{2}-1\right]+P_{cr2}(t)H(x-x_0), \qquad (7.75)$$

where $P_{cr1}(t)$, $P_{cr2}(t)$; t_0, and x_0 are defined by expressions (7.69), (7.68), (7.71), and (7.70) respectively.

It should be taken into account that the meteor trail, in addition to the overdense part characterized by the critic al radius $r_{cr}(t, \lambda)$, contains an underdense part, where the electron concentration is below the critical value. Such a model can be represented by a metal cylinder in a plasma shell, the electron density of which is below the critical value. Based on the above, a rigorous solution of the diffraction problem shows (Azarenkov, 2008; Azarenkov, 2011) that the

dissipated power is much higher than when scattered by a metal cylinder with a given critical radius.

As a result of diffusion, after some time, an overdensed trail becomes underdensed, and its electron concentration provides a high scattering power for a sufficiently long time.

A model of coherent scattering of a wave on an overdense meteor trail is proposed, which takes into account the above scattering mechanisms and is described by the expression

$$P_{coh}^{\Sigma}(t) = P_{coh}^{(1)}(t) + \rho(t) P_{coh}^{(2)}(t), \tag{7.76}$$

where $P^{(1)}_{coh}$ is the coherent component of the overdense part of the trail, determined by expression (7.75), and $P^{(2)}_{coh}$ is the coherent component of the underdense part of the trail, which takes into account (7.11) and (7.75) and has the form

$$P_{coh}^{(2)}(t) = \frac{P_T G_T G_R \lambda^2 r_e^2 \left(1+\cos^2(\theta/2)\right)}{64\pi^3 R_1^2 R_2^2} \frac{1+q^2R_D^2}{2+q^2R_D^2} \left[\int_0^{\tau_{\max}} S_t(\tau) U(t-\tau) d\tau \right]^2, \tag{7.77}$$

where $\rho(t)$ is a weight function that determines the degree of influence of the overdense and underdense parts of the meteor trail on the amount of dissipated power.

As was shown in subsection 7.2, scattering on an underdense meteor trail causes scattered power fluctuations due to the increasing equivalent radius of the trail, which we will call diffraction oscillations of the third type.

The type and parameters of the weight function are determined based on the following physical assumptions:

- scattering on the overdense part of the trail in the metal cylinder approximation is determined by the time-varying critical radius $r_{cr}(t, \lambda)$;
- when reflected from the overdense part of the trail, scattering effects on fluctuations of the permittivity are simultaneously present, increasing the scattering intensity by several times;
- with time, the volume electron density becomes less than the critical value, at which the permittivity becomes zero, and scattering on the underdense part of the meteor trail becomes dominant;
- in the case of scattering on the underdense part of the trail and sufficiently high bulk electron density that corresponds to the vicinity of the zero permittivity, attenuation effects appear, dependent on the changing equivalent radius and electron density of the meteor trail;
- the ratio between the effects of the formation of scattered power at the reception point due to the influence of the overdense and underdense parts of the trail is difficult to determine analytically, which leads to the need to use empirical coefficients that ensure agreement with the observation results.

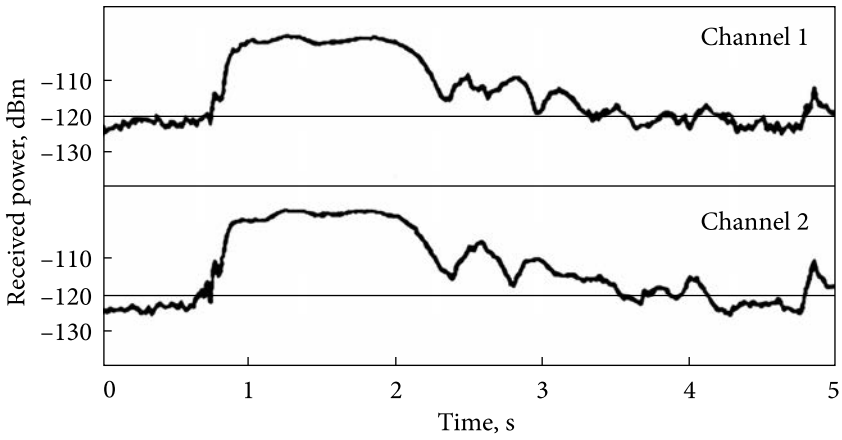

Fig. 7.16. The power changing during scattering on an overdense meteor trail, observed during experimental research (Cannon, 1991)

These physical considerations allow us to represent the weight function in the form

$$\rho(t)=\begin{cases}\mu_{emp}\exp\left\{-\gamma_{emp}\left[\dfrac{N_{ekv}(t)}{N_{cr}(\lambda)}\right]\right\} & \text{when } N_{ekv}(t)\geq N_{cr}(\lambda),\\ 1-\left(1-\mu_{emp}\right)\exp\left\{-\gamma_{emp}\left[\dfrac{N_{ekv}(t)}{N_{kr}(\lambda)}\right]\right\} & \text{when } N_{ekv}(t)<N_{kr}(\lambda),\end{cases} \tag{7.78}$$

where γ_{emp} and μ_{emp} are empirical coefficients that are set based on statistical processing of the results of observations of scattering on meteor trails.

A feature of the proposed model is that it allows one to take into account and display three types of diffraction oscillations:

- diffraction oscillations caused by the meteoroid passing through the Fresnel zones (diffraction oscillations of the first type);
- diffraction oscillations arising from scattering on the overdense part of the trail, which depends on the wavelength and time-varying critical radius of the meteor trail (diffraction oscillations of the second type);
- diffraction oscillations arising from the expansion of an underdense trail (diffraction oscillations of the third type).

To assess the reliability of the proposed heuristic calculation model, calculations of the change in power were performed with the following initial data:

- length of the radio link 800 km;
- transmitter power 400 W;
- transmission frequency 37 MHz;
- type of transmitting/receiving antennas — 4-element Yagi antenna.

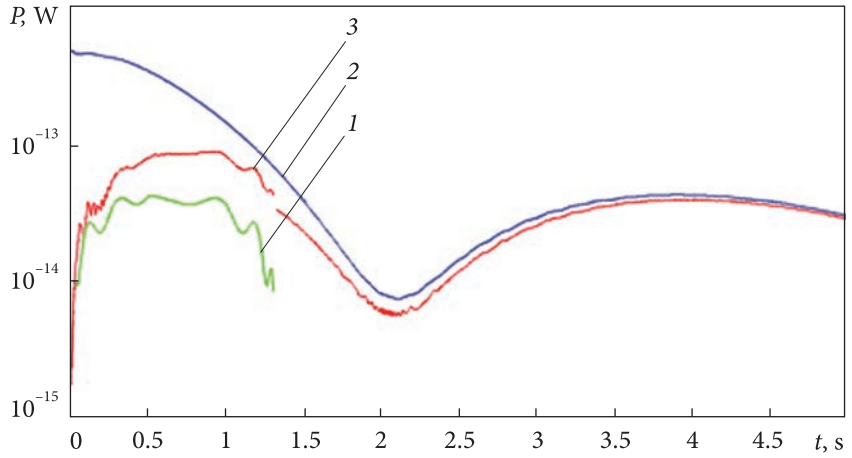

Fig. 7.17. The result of calculating the change in power over time during scattering of a quasi-harmonic signal on an overdense meteor trail, performed in accordance with the proposed model: *1* — power of the coherent component determined by the model of a metal cylinder; *2* — power of the coherent component determined by the model of scattering on the permittivity inhomogeneities ; *3* — total power

For a radio link with such parameters, there are experimental data on the scattering of signals on an overdense meteor trail (Cannon, 1991) presented in Fig. 7.16.

When estimating the power of the received signal scattered on an overdense meteor trail, the calculations were performed for a meteoroid with a mass of m = 2 g and a velocity of v = 40 km/s, which creates a linear electron density of $\alpha = 4.1 \cdot 10^{15}$ el/m^3. The calculation results (for the selected coefficients of the weight function ρ (t): $\mu_{emp} = 0.5$ and $\gamma_{emp} = 1.5$) are shown in Fig. 7.17.

A comparison of the results of calculations and experimental observations is shown in Fig. 7.18. The solid line shows the results of calculations performed using the proposed heuristic scattering model on the meteor trail (Fig. 7.17), and the dotted line shows the results of experimental observations (Cannon, 1991) (Fig. 7.16).

The results of numerical calculations are in good agreement with the results of experimental observations of scattered signals, which allows us to speak about the adequacy of the proposed model and the possibility of its use in carrying out the corresponding calculations. A quantitative analysis of the results of calculating the power dissipated on an overdense meteor trail shows that in the time interval from 0 to 2 s, the agreement between the calculated data and the experimental data (Cannon, 1991) (obtained using a 2-channel measuring receiver with diversity antennas) is very high. With a longer observation time, the calculation results slightly exceed the observed power of the scattered signal, and the measurement results show the presence of interference fading. These differences may

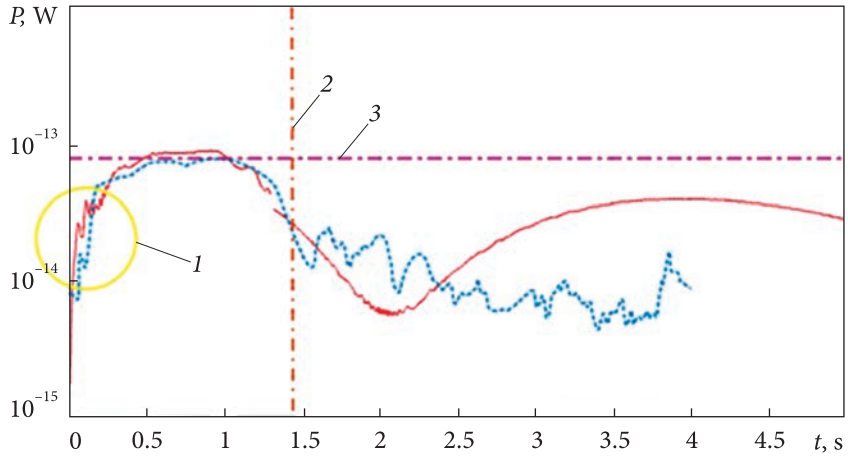

Fig. 7.18. Power changing during scattering on an overdense meteor trail observed in experimental studies and performed by the proposed model: *1* — diffraction oscillations at the stage of meteor trail formation, *2* — coincidence of time at which a high level of scattered power is observed, *3* — coincidence of received signal levels

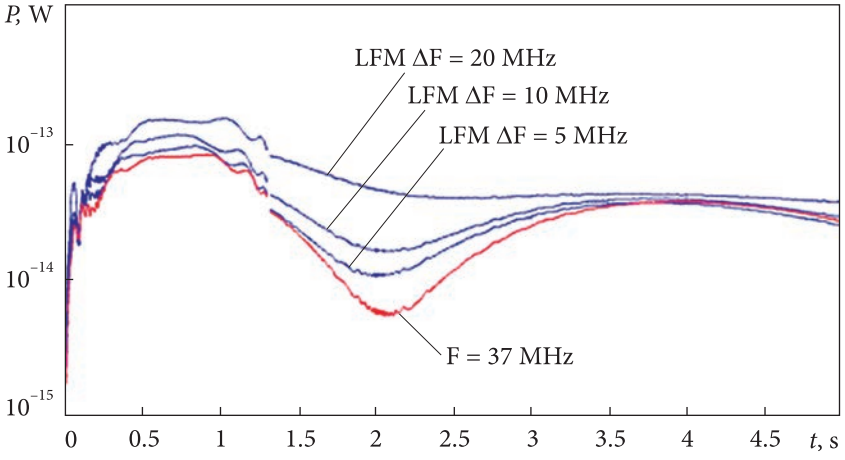

Fig. 7.19. Change in the power of LFM signal scattered on an overdense meteor trail at the selected value of the spectrum width

be due to the influence of turbulent diffusion, fragmentation of the meteor body, and trail deformation caused by large-scale wind shears characteristic for the meteor zone, which were not taken into account in the calculations.

It is known (Varakin, 1985; Pestryakov, 1969; Tuzov, 1985) that an effective way to deal with interference fading is to use wideband noise-like signals (direct spread signals). To assess the influence of the type and parameters of the signal on the power of the signal scattered on an overdense trail, calculations

were performed for the frequency of the carrier wave f = 45 MHz with the previously selected parameters of the meteoroid and radio link. The results of calculating the signal power at the receiver input for a sinusoidal signal and chirp signals with a spectrum width ΔF_s = 5, 10, and 20 MHz and a duration T_c = 50 μs are shown in Fig. 7.19.

Calculations show that, with LFM signal spectrum width exceeding 10 MHz, the minimum signal power due to diffraction oscillations decreases significantly. It can be assumed that the indicated spectrum width will also be sufficient to effectively combat interference fading.

7.5. Conclusions

The proposed generalized scattering model describes both coherent and incoherent components of the average power of a signal scattered on an ionized meteoroid trail.

The heuristic radiophysical model of radio signal scattering on a meteor trail made it possible to obtain an analytical expression for calculating the power of the coherent component of the scattered signal on meteor trails of both underdense and overdense types.

The MRCh scatter-function obtained by numerical methods for a time-varying meteor trail equivalent radius makes it possible to estimate the signal shape at the receiver input at characteristic times. This allows one to set the type and parameters of the signal used, which provide resistantce to fading and an increase in the reliability of information transmission over the meteor radio channel. The scatter-function also makes it possible to calculate the change in the average signal power over the observation interval of the trail.

The results of numerical calculations performed using the heuristic model show good agreement with the results of experimental observations of scattered signals over a time interval from 0 to 3 s and confirm the presence of diffraction oscillations for meteor trails of any type. Outside this interval, the calculated values of the power of the scattered signal somewhat exceed the observed values. Decreasing the signal level may be due to the interferences caused by the fragmentation of the meteoric body and the additional influence of turbulent diffusion, which were not considered by the scattering model. The effects of recombination and attachment of free trail electrons, the influence of hyperthermal chemistry and ionic reactions with mesospheric ozone, as well as the possible influence of wind displacement, were not taken into account. This indicates the need for further improvement of the radiophysical model of signal scattering on meteor trails of various types.

The joint consideration of the influence of the overdense and underdense parts of the meteor trail, the presence of which is typical for almost all trails, makes it possible to explain the difference in estimates of the dependence of the scattered power on the operating wavelength. This dependence can vary with a

change in the mass and velocity of the meteoroid, as well as with a change in the orientation of the meteor trail relative to the radio line.

The use of a generalized representation of the spectral density of permittivity fluctuations, as well as the choice of weight coefficients, makes it possible to reconcile the calculated data on the frequency dependence of the scattered field with the results of experimental observations, and the presence of an incoherent component of the signal scattered by inhomogeneities of the dielectric permittivity of turbulent origin, that is, to substantiate the possibility of its observation at a distance from the point reception over a considerable distance.

Using for an example LFM signals showed that the use of broadband noise-like signals with a large base makes it possible to reduce the effect of diffraction oscillations caused by the change in time of the meteor trail equivalent radius. This suggests that the use of code division channels and ensembles of complex signals with good cross-correlation properties and a spectrum width exceeding 10 MHz in meteor radio communication systems will increase their throughputs of these systems.

The analytical expression obtained using the scatter-function for the change in the power of the scattered signal makes it possible, based on a comparison of its shape with the results of observations, to make reasonable assumptions about the characteristics of the meteoroid and its genetic relation to the parent body. Based on the classification of meteor trails according to the features of signals scattered on them, the mass, density, velocity, and radiant of the meteoroid that formed the trail can be indirectly estimated.

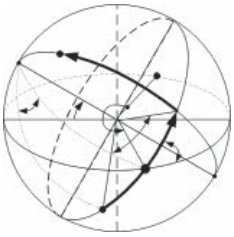

SECTION 8

CLASSIFICATION BASED ON ANALYSIS OF SIGNALS SCATTERED BY IONIZED METEOROID TRAILS

By the term "classification", we mean the division of objects and phenomena into classes (groups, aggregates) that differ from each other in certain characteristics, to obtain information about them. In our case, the objects under study are small celestial bodies — meteoroids and the characteristics of radio signals scattered on ionized trails formed during the interaction of meteoroids with the Earth's atmosphere. Observational data and the degree of their correspondence to the selected models can be used as features. The classification is a deployed system where each object can be divided into new objects, which may be divided into some classes as well. But none of the classifications can be approached as complete.

The main objectives of our classification are:

- Estimation whether the meteoroid that formed the observed IMTr with SRP belongs to the cometary or asteroidal classes.
- Determination the meteoroid's genetic connection with the parent body or meteor shower, which allows for reasonable assumptions about the geocentric velocity and physicochemical composition of the meteoroid, as well as using the results to develop a theory of the origin and evolution of the meteor matter.
- Estimation of mass of the meteoroid that formed the IMTr, based on the characteristics of the radio signal scattered on it, which makes it possible to clarify the effect of the meteoric matter influx on the atmospheric parameters and the risks of spacecraft damage.
- Prediction the duration and amplitude of the reflected radio signal according to its characteristics at the initial observation site. This is necessary for solving telecommunication problems such as choosing the type and parameters of the radio signals used, the speed and protocol for transmitting information, on which the throughput of meteor radio channels depends.

Characteristics of the scattered radio signal, as well as the measured or predicted radiant, velocity, and height of the meteoroid's SRP, can be used as features for classification.

The radiophysical model of signal scattering on a meteor trail makes it possible to create a model image of the scattered signal in the process of its formation and evolution for given parameters of the meteoroid and atmosphere at the observation height of the IMTr. By specifying the physicochemical characteristics of a meteoroid of cometary or asteroidal origin (see Section 6), as well as the height of the SRP, one can create appropriate databases (images of scattered signals with different radiants and velocities) for solving astronomical and telecommunication problems. Such databases must be created taking into account the geographical coordinates of the points of transmission and reception, as well as the epoch — the time of year and day (see Subsection 5.2).

Classification using the radiophysical model can be performed by comparing the normalized images stored in the database with the normalized images of the observed radio signals scattered on the IMTr. When normalizing, one should take into account the radio link length, the equivalent isotropically radiated power (EIRP) EIRP = $P_T \times G_T \times G_R$, the operating frequency (wavelength), and the noise power at this frequency.

The set of features used in predicting should reflect the greatest extent of those properties of objects that are important for the fulfillment of the task. The computational complexity of decision-making procedures, the reliability of predicting, and the time spent on the corresponding calculations largely depend on the dimension of the feature space.

When predicting the duration of the reflected radio signal based on the obtained characteristics in the initial observation section, as the main features, the amplitude of the signal at the end of the observation interval and the rate of its rising can be considered. The time of amplitude rise to the maximum value is determined by both the meteoroid velocity and the length of the first Fresnel zone, which depend on the trail orientation relative to the radio wave propagation path (see Subsection 5.2.2). At the same time, the power of the measured signal depends on the orientation of the trail: the greater the first Fresnel zone length, the greater the measured amplitude. Thus, a large amplitude can also predict a long signal duration, but its value must be corrected (decreased) in view of the duration of the rising interval and the meteoroid velocity. A possible option for determining the correction factor is using artificial neural networks (ANNs). Their ability to predict directly follows the ability to generalize and highlight hidden dependences between input and output data. The ability to learn is one of the main advantages of ANNs over traditional classification algorithms. Testing the quality of ANN training should be carried out on examples that did not participate in its training. The number of test examples should be the greater, the higher the required quality of training.

All estimates made during the classification and prediction are probabilistic, and their reliability can be determined based on comparison with the results of

observations of meteor showers, the genetic relationship between which and the parent body is considered established (see Subsection 4.1.6).

8.1. Classification of meteoroids based on observations of reflections from meteor trails

Traditionally, there are two types of meteor trails — "underdense" and "overdense", the names of which are used to evaluate the characteristics of the reflected signal. At the same time, at least twenty-eight different types of reflections from the trail have been identified, which are quite common, differing in shape, duration, and amplitude (Ostergaard, 1985; Melville, 1989; Melville, 1993; Melville, 1996).

In (Melville, 1989; Melville, 1993; Melville, 1996), classification was carried out using the TrailStar expert system, based mainly on rules, including conditions and actions . Data were collected on reflections from meteor trails on radio links of 550 km and 1100 km, which can be considered typical meteor radio systems. To normalize the observation results, the measured scattered signal power was compared to the noise power in the 2 kHz band, which was taken to be — 120 dB_m (see Subsection 5.2.2). Therefore, patterns can be described by changing the ratio of signal power to noise power, expressed in decibels (dB).

Recording began when the signal received from the transmitter reached a certain signal–to–noise power ratio (10 dB) for at least 20 ms. After that, every 5 ms, samples of the signal amplitude were taken until the signal fell below the cut–off threshold. At the same time, the system continued monitoring the signal level for 400 ms to make sure that the shutdown was not premature and the decrease in signal level was not caused by interference.

Based on neural network technology, the TrailStar system is both flexible and highly user-friendly thanks to its design. This allows experts involved in the recognition of reflections from ionized meteoroid trails to easily change or expand the classification scheme by introducing appropriate rules and observation results.

As an example, Fig. 8.1*a* and 8.1*b* show two types of reflections from trails, which are interpreted in (Melville, 1996) as "underdense" and "overdense", respectively.

One can disagree with this classification, since duration of 400 ms is not typical for underdense trails. With greater certainty, the reflection presented in Fig. 8.1*a* should be attributed to trails of the transitional type, as underdense trails have a significantly shorter duration and can have the shape of ATCH and PTR shown in Fig. 8.2.

There is a connection between classified objects and phenomena and the theory of their formation and development . Therefore, when choosing classification criteria, it is necessary to know which features are the most significant for differentiating the objects. The features may be heterogeneous but should characterize the internal commonality of the objects of each class.

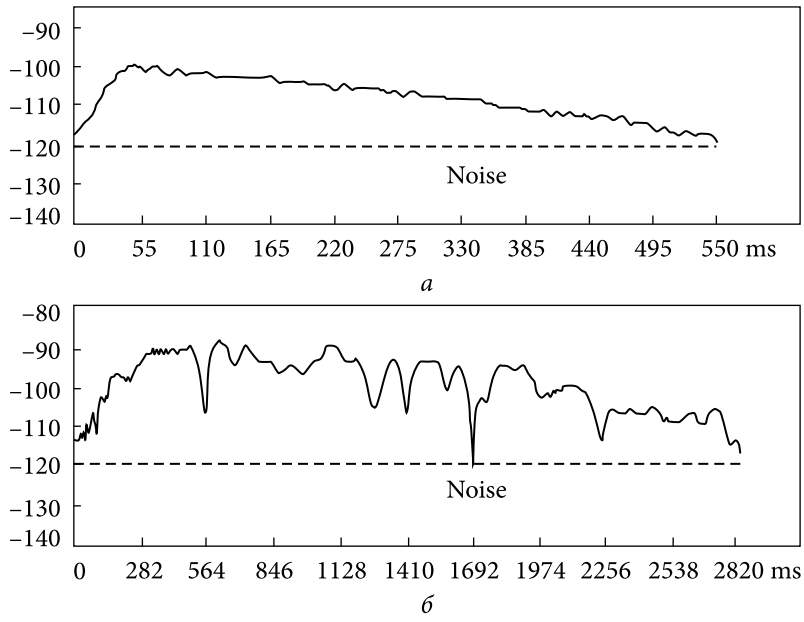

Fig. 8.1. Example of signals observed on the 1100 km path between Arniston and Pretoria in South Africa (Melville, 1996)

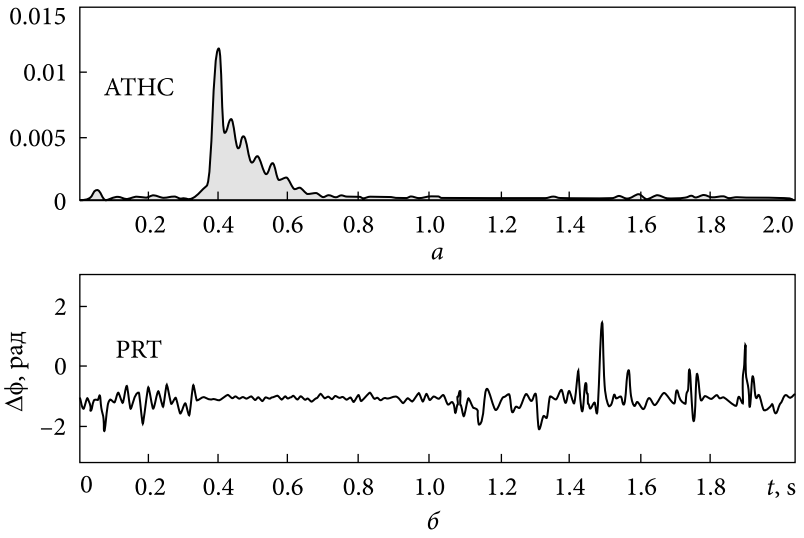

Fig. 8.2. Example of a signal reflected from an underdense trail (Lykov, 2010)

In addition to the amplitude and duration, important features for classification are the time of rising the reflected signal amplitude to the maximum value and the features of the ATCH diffraction oscillations. The rise time τ_{Φ} depends on the length of the first Fresnel zone, which, in turn, is determined by the operating

wavelength and orientation of IMTr relative to the radio wave propagation path, as well as the meteoroid velocity v_m.

$$\tau_F = \frac{1}{v_m}\sqrt{\frac{\lambda R_1 R_2}{\left(R_1 + R_2\right)}\frac{1}{1-\sin^2\left(\frac{\theta}{2}\right)\cos^2\beta}}. \qquad (8.1)$$

The three types of diffraction oscillations (discussed in subsection 7.5.2) also can be included in the list of features for classification. Their absence is also a sign of the presence of meteoroid fragments (see subsection 6.2). Interference fading of the observed signal can also be a sign of fragmentation other than progressive.

The essential feature used in classification is the SRP height, which can be measured or calculated at a given radiant (see subsections 5.2 and 5.3). Depending on the SRP height formation, one can make assumptions about the meteoroid's velocity, density, and chemical composition. The SRP height can be used to estimate the ionospheric plasma density, which can significantly affect duration of the trail.

The preliminary simulation results (Galindo, 2014) show that for non-specular reflection, the trail duration depends linearly on changes (up to one order) in the density of the ionospheric plasma. They are supported by the meteor data collected from the University of Illinois Portable Radar located at Fort Macon, North Carolina (34°N, 65°W).

Can be used , additional data to improve the classification quality if they are recorded during the observation process. Such data include the measured or predicted meteoroid velocity and orbital parameters, which allow us to calculate the Tisserand constant. This constant allows a dynamic separation between comets and asteroids with respect to Jupiter and is given by the following expression (Jewitt, 2012):

$$T_J = \frac{1}{v_m} + 2\left[\frac{a}{a_J}\left(1-e^2\right)\right]^{0,5}\cos i,$$

where a, e, and i are the semi–major axis, eccentricity, and inclination of the object's orbit, respectively; a_J = 5.2 AU is the semi–major axis of Jupiter's orbit. For comets, T_J ranges from 2.08 to 3.12, and for asteroids, it is over 3.12.

It should be taken into account that too large and too small features (dimensions) usually worsen the accuracy of identification. The computational complexity of training and decision–making procedures, the reliability of recognition, and the time spent on the corresponding calculations largely depend on the dimension of the feature space. A large number of features, in addition, significantly complicate the formation of decision rules.

It is reasonable to use as significant features for classification:

- normalized ATCH amplitude and its features;

- duration of the signal being observed;
- interval of rising signal amplitude up to the maximum value;
- rate of rising signal amplitude in the initial observation section of the reflected signal;
- diffraction oscillations of various types or their absence in the observation interval of the reflected signal;
- interference fading of signals.

When predicting the mass of a meteoroid, the product of the amplitude of the observed signal and its duration can be used as an integral feature.

As additional features that simplify decision-making and improve the quality of classification, the following can be used:

- predicted or measured the height of the specular reflection point;
- predicted ionospheric plasma density at SRP;
- given (predicted) or measured meteoroid radiant;
- orbital parameters allowing for calculation of Tisserand's constant.

The results of training and testing of the neural network, performed for a radio link of a given length, significantly depend on the geographical location of the transmission and reception points, as well as the epoch, that is, the time of year and day. This significantly complicates the interpretation of the observation results and does not answer the questions of the origin and estimation of the meteoroid mass based on the classification performed in (Melville, 1989; Melville, 1993; Melville, 1996).

8.2. Classification of meteoroids based on the results of modeling reflections from meteor trails

Meteoroid classification may use a different technology than that used in artificial neural networks. It is based on the creation of model images of the signals scattered on the IMTr. To create them, the radiophysical model of IMTr can be used. It allows one to create a model image of a scattered signal in the process of its formation and evolution for given parameters of the meteoroid and atmosphere in the SRP, presented in the form of ATCH (see Section 7). For practical use, the model image must be normalized to provide the ability to transform the observed data to a single scale.

Creation of a database containing images of normalized ATCH scattered signals for different geographic latitudes, observation time and SRP height, which determines the properties of the atmosphere, as well as given masses and physicochemical properties of the meteoroid is theoretically possible but computationally very difficult.

The classification should be performed by comparing the normalized images stored in the database (DB) with the normalized images of the observed scattered radio signals. The normalization should take into account the equivalent

isotropically radiated power (EIRP), the operating frequency (wavelength), and the noise power at this frequency at the observation site (see subsection 5.2.2). The closeness criterion of the observed and model images can be the minimum of the mean squared deviation (MSD) or a weighted average when the ATCH values in one of the sections (for example, the initial one) of the observation interval are considered more significant than the others. The parameters of the weight function are determined by the features of the problem being solved.

Other parametric metrics can also be used to estimate the proximity of the observed and reference images. The Minkowski metric is defined as:

$$\rho_p(x,y) = \left(\sum_{i=1}^{d} \left| x_i - y_i \right|^p \right)^{1/p}, \tag{8.2}$$

where x_i and y_i are the parameters of the observed and reference images, respectively. For $p \in (0, 1)$, this function is not a metric but can still be used as a distance measure. Particular cases of this metric are:

- Euclidean metric (p = 2), which defines the distance as the length of a straight line connecting the given points.
- Manhattan distance (p = 1) — the minimum length of the path from x to y, provided that the movement can be only parallel to the coordinate axes.

In radar observations, the necessary initial data for constructing a fairly complete model of meteor phenomena are the mass, velocity, density, and chemical composition of the meteoroid, as well as the height of the SRP formation, the chemical composition of the ionosphere, pressure, and turbulence at a given height.

The ATCH of the meteor trail reflected from the trail depends on all the above initial data and implicitly contains information about them. At the same time, only the height of the meteor trail formation, the radiant and velocity of the meteoroid, as well as, in some cases, its chemical composition (according to the results of spectral analysis of the luminosity of the trail) are available for direct measurements.

At hypersonic meteoroid velocities, aerodynamic drag and aerodynamic heating in a real (nonisothermal) atmosphere significantly interact with each other, which, in some cases, leads to fragmentation of the meteoroid. The splitting effect leads to a change in the characteristics of the IMTr and, accordingly, in the ATCH of the reflected signal.

A generalized classification algorithm based on the use of reference images is shown in Fig. 8.3.

The full enumeration of comparisons with images stored in the database can be reduced by building this database hierarchically. It is quite obvious that for a given radio link length at a given latitude and a given observation time, it is necessary to use a well-defined DB area that is significantly smaller than its total size. Another solution is also possible — the creation of a database of standards for well-defined observation sites using the appropriate software. This simplifies the construction of the database and does not require normalization of the ATCH of the received signal.

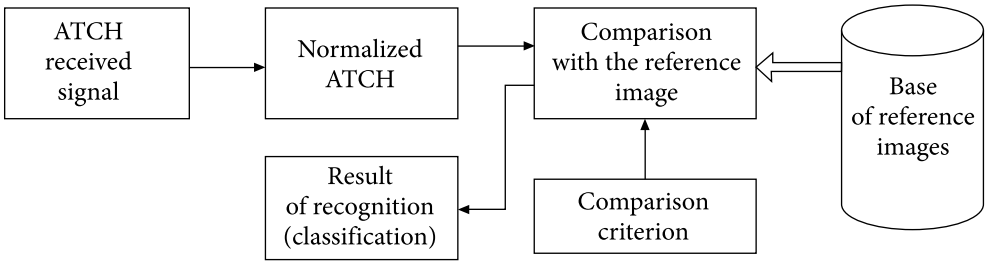

Fig. 8.3. Generalized classification algorithm based on the use of reference images

Table 8.1. **Manhattan distance Δ_i between the image and the reference images, taken as on example**

i	1	2	3	4	5	6	7	8	9	10	11	12
ModΔ	0.00	0.22	0.14	0.19	0.00	0.00	0.02	0.03	0.00	0.07	0.17	0.04
i	13	14	15	16	17	18	19	20	21	22	23	24
ModΔ	0.18	0.09	0.33	0.37	0.35	0.30	0.24	0.18	0.13	0.09	0.05	0.00

As an example, consider a classification mechanism based on a comparison of a conditional normalized observed image with a conditional normalized reference image (Fig. 8.4). To assess the proximity of the images, we will use the minimum standard deviation criterion and evaluate the influence of the weight function.

The measured Manhattan distance Δ_i between the observable and reference images taken as an example is presented in Table 8.1.

The *RMS* value calculated using formula (8.3) and data from Table 8.1 is 0.031557.

$$RMS(x,y)=\frac{1}{N}\sum_{i=1}^{N}(x_i-y_i)^2=\frac{1}{N}\sum_{i=1}^{N}\Delta_i^2\ . \qquad (8.3)$$

It is assumed that it is minimal for the set of images stored in the database.

Model ATCH images for cometary and asteroidal meteoroids can be created and stored in separate databases. Since they are created taking into account the physicochemical properties of the meteoroid for a given SRP height, reasonable assumptions can be made about the origin of the meteoroid based on the minimum standard deviation in the corresponding image database.

The reliability of the classification is largely determined by the used image model, which depends on the adequacy of the used radiophysical model IMTr and the scatter-function of the meteor radio channel (see Subsections 7.2 and 7.5).

When developing the radiophysical model of IMTr, many effects were not taken into account (meteoroid fragmentation, recombination and attachment of free trail electrons, the influence of hyperthermal chemistry and ionic reactions with mesospheric ozone, as well as turbulent diffusion and the possible influence

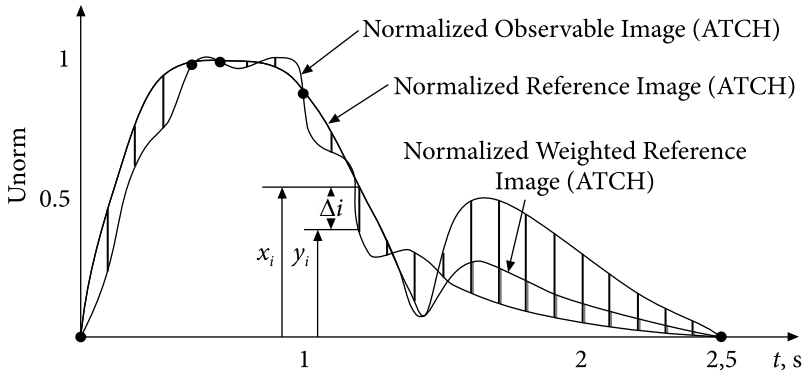

Fig. 8.4. Comparison of conditional normalized observablable images with the reference ones

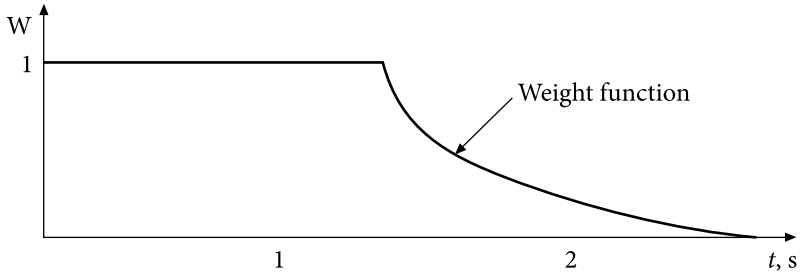

Fig. 8.5. Example of a weight function, the parameters of which are chosen experimentally

of large-scale wind shears). Outside the observation interval exceeding 1—2 seconds, these effects usually lead to a decrease in the received signal compared to that calculated without taking into account these factors. This indicates the need for further improvement of the radiophysical scattering model, which requires significant efforts. An alternative is to use the weight function *W(t)*, the parameters of which are chosen experimentally when normalizing the reference image or calculating the weighted standard deviation. The form of the function *W(t)* is shown in Fig. 8.3, and the result of its application to the reference image is shown in Fig. 8.5.

The scatter-function MRCh significantly affects the reliability of the model image, the method and calculation results of which are presented in Subsection 7.3. When developing the methodology for calculating $S(\tau)$, the concept of the equivalent trail radius r_{eq} for given instants of time was used while the two-dimensional radial distribution of the electron density relative to the trail axis was not taken into account. Such an allowance is possible in principle but complicates the calculations and cannot guarantee an improvement in the accuracy of the estimate of $S(\tau)$ in the presence of meteoroid fragmentation (see Subsection 6.2).

The reliability of the model image is affected by the initial radius of the meteor trail, the ionization coefficient and the ambipolar diffusion coefficient, which depend on the physicochemical characteristics of the meteoroid, as well as the physicochemical characteristics of the atmosphere. They, in turn, depend on the height of the specular reflection point, time of year and day, the latitude of the observation site, and solar activity (see Section 6). In the ATCH calculations performed in Subsection 7.3, semi-empirical formulas were used to estimate them, but the data on the physical characteristics of meteoroids given in Section 6 allow the use of physically more reasonable values. When calculating the necessary parameters, one can take into account the expected origin of the meteoroid, which will allow one to form independent databases of model images for cometary and asteroidal meteoroids.

8.3. Prediction of reflected signal characteristics

Estimation of the ATCH parameters for the initial section of the trail formation (20—100 ms) can be used to predict the trail reflectivity in the process of further transformation. The prediction of the change in the amplitude and duration of the reflection from IMTr based on measurements in the initial section (first phase) of its existence provides a fundamental opportunity to adapt the protocol and information transfer rate without feedback to ensure the maximum throughput of the MRCh. Available for measurements are the rate and rise time of the signal amplitude, as well as the maximum value of the amplitude in the observation interval. Instead of amplitude, a more informative sign can be used — the ratio of signal power to the noise power in a given frequency band (or signal energy to noise spectral density). It follows from formula (8.1) that the slew rate depends on the meteoroid velocity, and the slew duration is determined by the size of the first Fresnel zone. A short rise time may indicate that the meteoroid velocity is high or that the trail is located perpendicular to the propagation plane and the Fresnel zone is minimal. At high velocity, the SRP height usually exceeds 95 km, and at low velocity, it is below 90 km. The slew rate, rise time, the observed maximum amplitude of the reflected signal, and the SRP height are related, in a rather complex way, to the meteoroid mass, which determines the amplitude and duration of the reflection from the meteor trail.

To predict the duration of the reflection from the meteor trail, you can use the technology of artificial neural networks described in sufficient detail in (Fraser, 1994).

In the same work, the expediency of using early fast Doppler information, which precedes many overdense trails providing a large signal-to-noise ratio as a reflection duration predictor, is shown. This is because the atoms evaporating from the meteoroid surface have approximately the same velocity as the meteoroid itself, and the initial period of formation of the ionized trail consists in its

rapid expansion until the end of thermalization — the establishment of thermal equilibrium with the environment. This time interval depends on the trail formation height and varies from 1 ms at the height of 80 km to 150 ms at the height of 115 km (Baggaley, 1977).

When radio waves are reflected from a rapidly expanding to the initial radius of IMTr, scattered signal features and Doppler effects are observed, which

Table 8.2. **Results of comparing predicted and measured fast Doppler values**

Geometrical parameters for medium mean? length of radio link for testing bistatic scattering		
Receiver position	Durban, South Africa	29.5°S 31. 0°E
Transmitter position	Pretoria, South Africa	25.6°S 28. 0°E
Mean Normal Distance from Tx to SRP — R1		256 km (mid-path)
Mean Normal Distance from Rx to SRP — R2		256 km (mid-path))
Mean half internal angle between Rx & Tx to meteor — φ		71°
Mean angle between trail axis and plane containing Tx Rx & trail — β		56°
Mean meteoroid velocity — v_m		35 km/s
Mean SRP height — h_m		95 km/s
Radio wavelenth — λ		6 m

Measured and predicted early fast Doppler for a *medium mean*? length bistatic scattering test line			
	Meaning	Measured	Predicted
Peak early fast Doppler deviation	Mean	38.7 Hz	33.9 Hz
	Std. dev.	17.6	—
Early fast Doppler duration	Mean	89.3 ms	76.4 ms
	Std. dev.	51.4	—
Early fast Doppler slope	Mean	433.3 Hz /s	—
	Std. dev.	292.3	
Peak signal amplitude of trails exhibiting early fast Doppler	Mean	103.9	
	Std. dev.	5.9 dBm	
Total duration of trails exhibiting early fast Doppler	Mean	1597.6 ms	
	Std. dev.	961.4	
Early fast Doppler duration as a mean total trail duration in trails exhibiting early fast Doppler	Mean	5.6%	
Percent of trails per hour exhibiting early fast Doppler		9.04%	
Percent of long trails with early fast Doppler (>500 ms)		30.2%	

can be used to predict not only the duration of the reflection but also the initial radius of the trail and the observed SRP height. Unfortunately, little attention has been paid to research these effects, and much work remains to be done to study them.

Some radiophysical effects that manifest themselves in the initial period of the formation of an ionized trail were presented in (Fraser, 1994), where there is bibliography of information sources on which the results were based. As an illustration, Table 8.2 shows the results of comparing the predicted and measured fast Doppler values taken from (Fraser, 1994).

The results of predicting based on the use of ANNs confirmed the possibility of using early fast Doppler as an indicator of reflections with large amplitude and duration (Fraser, 1994). The relatively low statistical significance of the prediction based on measurements of early fast Doppler duration and frequency dispersion is related to the chosen decision rule and can be increased. Sufficiently high significance for predicting the Doppler duration was shown by the maximum amplitude of the reflected signal over the observation interval. It can be expected that the joint consideration of the measured amplitude and the duration of its rise, as well as the frequency dispersion of the reflection in the formation of the decision rule, will significantly improve the prediction quality. An assessment of the quality of the decision made can be made by comparing the predicted ATCH with the actually observed one.

8.4. Conclusions

1. For the classification of reflections from IMTr during long–term observations, an expert system based on the use of ANN can be applied. Based on the significant features defined in subsection 8.1 and the corresponding decision rules and training of ANN, the expert system allows making reasonable assumptions about the geocentric velocity, physicochemical composition, and mass of the meteoroid. These results can be used to determine the genetic relationship of the meteoroid with the parent body, as well as to develop the theory of the origin and evolution of the meteoric matter. To assess the effectiveness of the selected features and decision rules, one can use a comparison of the classification results with observations of meteor showers, the genetic relationship of which is assumed to be known (see Subsection 4.1.6).

When estimating the mass of a meteoroid, the main significant feature is the product of the reflection amplitude and duration, and the necessary additional data are the velocity, SRP height, and the expected physicochemical characteristics of the meteoroid. Forming the decision rules and learning methods of ANN is not an easy task. The prediction results are probabilistic, require statistical processing, and their quality is difficult to evaluate numerically.

2. A new meteoroid classification technology based on the use of model images of signals scattered by IMTr is proposed. The IMTr radiophysical model

makes it possible to create a model image of a signal in the process of its formation and development for given meteoroid and atmospheric parameters in SRP, presented in the form of ATCH (see Section 7).

To perform the classification of meteoroids, a single database is needed in which pre-calculated normalized ATCH models should be stored. When calculating them, it is necessary to take into account the length and orientation of radio lines, as well as the physicochemical characteristics of meteoroids and the atmosphere. Obviously, the creation and usage of such a database, even when it is built according to a hierarchical principle, is extremely difficult.

An easier way is to use the appropriate software to create a database of standards for well-defined observation sites. This does not require ATCH normalization of the received signal. Such a database can store ATCHs calculated for meteoroids with different FHSs, radiants, and velocities, as well as the corresponding SRP heights and initial trail radius values. The decision on whether the observed ATCH belongs to a meteoroid with well-defined parameters is made by comparing the images stored in the database with the images of scattered radio signals observed by ATCH. The minimum standard deviation can be used as a proximity criterion. When classifying, it is possible to form a certain set of solutions with weight coefficients corresponding to the proximity criterion. This increases the reliability of the conclusions obtained as a result of statistical processing of the results of observations. The decision made provides information on the mass of the meteoroid and its PCP, which makes it possible to clarify the influence of the influx of meteoric matter on the atmosphere parameters and the risks of damage to spacecraft.

A similar classification method can be applied to study the characteristics of meteor showers and their genetic relationship with the parent body, as well as to develop a theory of the origin and evolution of meteoric matter.

The quality of the classification based on the use of model signal images is largely determined by the adequacy of the used radiophysical scattering model for IMTr. The model developed in section 7 is approximate, but its construction technology can be used to create more advanced models.

3. Prediction of the duration and amplitude of the reflected radio signal according to its characteristics at the initial observation site is necessary for solving telecommunication problems — choosing the speed and protocol for transmitting information, on which the throughput of meteor radio channels depends. This prediction can be made using ANN technology. In this case, the measured signal amplitude and the time of its rise to the maximum value, as well as the frequency dispersion of the reflection due to fast Doppler, should be used as significant features. It can be expected that the decision rule built on the basis of these features will provide a classification quality sufficient to make a decision on the advisability of adaptively changing the speed and transfer protocol of information. This is an important result, which is of direct importance for the design of advanced meteor radio communication systems.

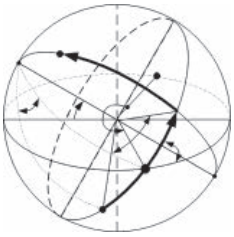

SECTION 9

CONCEPT AND TECHNOLOGY FOR BUILDING ADVANCED METEOR-BURST RADIO COMMUNICATION SYSTEMS

By the term "concept", we understand the set of principles that determine the ways of development of the MRS, depending on its purpose. Speaking about technology, we will keep in mind the techniques and methods for obtaining the required results, determined by the concept of constructing MRS.

In the publications (Holovan, 2020a; Holovan, 2020b), attention was focused on the use of code division channels (CDCh) for information transmission over meteor radio channels (MRCh), which, as shown in Section 7.3, is effective, but limits the possibilities of using MRS. In this section, the material of these articles is expanded, supplemented, and some inaccuracies are eliminated.

In a broader sense, in MRS, along with CDCh, it is possible to simultaneously use signal-code structures of various types and corresponding multiple access methods to separate them. It is possible to increase the efficiency of using MRS by linking base stations (BS) with satellite or other channels with a sufficiently high bandwidth. When solving some problems, it may be appropriate to use asymmetric MRCh. In this case, information from BS is transmitted by using one type of signals, and when do that from subscriber stations (SS), signals of other types are used.

The main technologies used in the implementation of the concept include the use of software-controlled smart antennas (SMART antennas), software-defined radio technology (SDR), and the algorithms for adapting to the conditions of information transmission via MRCh.

9.1. The concept of building advanced meteor radio communication systems

The proposed concept of building advanced meteor radio communication systems involves increasing the throughput, noise immunity, and secrecy of the system, as well as reducing the connection waiting time.

To increase the bandwidth of the MRS, reduce the connection waiting time, increase the number of subscribers served by the system (SS of the network), and increase the noise immunity and secrecy of the system operation, it is necessary:

• By choosing the network topology, to provide the necessary coverage and the possibility of simultaneous access of MRS SS to several BS of the network, which reduces the waiting time for the appearance of the IMTr with a specular reflection point and, accordingly, increases the system throughput.

• Provide for the possibility of additional protection against intentional and unintentional interference for the BS, since it is the most critical element of the meteor radio network. This possibility can be implemented based on the use of program–controlled antennas that provide the necessary coverage and adaptation to changing operating conditions of the system.

• To use at SS antennas with a controlled (or switched) radiation pattern (RP) for pointing at the space areas where the appearance of suitable meteor trails is most likely — the so-called "hot zones", the position of which depends on the geographical location of the BS and MS, as well as time of year and day. This will reduce the connection latency and increase the throughput of the MRS.

• Apply signals and their processing methods to resist interference fading that occurs in the observation interval during meteoroid defragmentation and diffuse expansion of the meteor trail, as well as the impact of interference concentrated over the spectrum, which will improve noise immunity and, as a result, the throughput of the communication channel.

• Reduce the time of detection of a meteor trail suitable for communication and estimate (predict) the time interval available for message transmission, as well as the change in the energy potential of the non-stationary meteor radio channel over this interval, using its initial section. This will allow the use of adaptation for the transmission rate and duration of the transmitted packets, which will increase the throughput of the MRS.

Since any properly designed modern system must allow subsequent upgrades at the life cycle interval without changing the circuit design, system management, transmission protocols, as well as signal generation and processing methods, must be oriented toward the use of SDR technologies.

9.1.1. Topology of the meteor radio network

Recommendation ITU-R F. 1113 gives as an example of MRS with a star network topology with a central (base) station designed to serve up to 1000 remote (subscriber) stations in a coverage area with a radius of up to

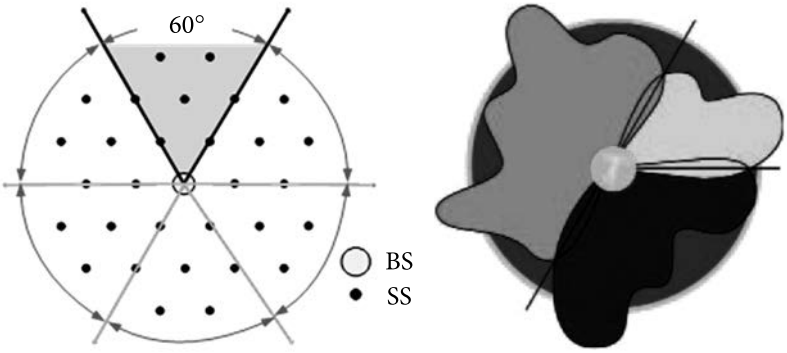

Fig. 9.1. MRS with a star topology for SS evenly distributed over the area

Fig. 9.2. MRS with a star topology for SSs unevenly distributed over area with three RP formation sectors (taken from (Slyusar, 2004))

2000 km. Each of the remote stations can communicate with any number of other remote stations via the central station using a half-duplex packet protocol with single-segment automatic retransmissions if the errors presence. It is indicated that larger networks can be built using several intermediate stations, between which a connection is established. Such a network can be reconfigured for any given number of subscriber stations.

Fig. 9.1 shows an MRS with a star topology, including one BS and 30 SSs, evenly distributed in a circle of a given radius ("dense stacking"). To cover the SS location area, the BS antenna system must form a circular radiation pattern (RP) in the azimuthal plane, which, at a given transmitter power, is capable of providing the necessary energy potential of the meteor radio link for information exchange with the SS. Such a radiation pattern (RP), in principle, can be created using a complex phased array antenna (PAA) at the BS (Monzingo, 1986).

Structurally, the PAA can be somewhat simplified if it is built from several simpler arrays, each of which serves its own sector of the SS location area. In Fig. 9.1, such a sector is equal to 60º and, therefore, it is necessary to have 6 corresponding FAAs on the BS.

With an uneven distribution of SS over the territory of their deployment, SMART antennas with digital RP formation can be used. Fig. 9.2 shows an MRS with a star topology, where in three sectors, RP with given shape is formed. The required directivity coefficients are determined by the number of PAA elements and the type of elementary antennas used (Slyusar, 2004; Widrow, 1989). The sector construction provides an additional advantage — the ability to use its form of the probing signal in each of them. This makes it possible to increase the number of SSs in the network.

It is necessary to allow an SS to access multiple BS network. This reduces the waiting time for the appearance of an ionized meteor trail with SRP and, accord-

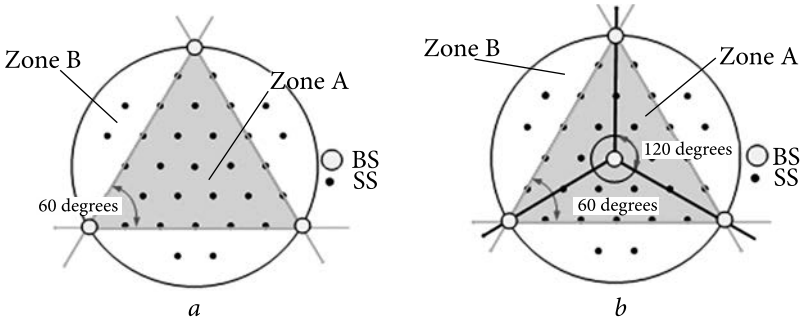

Fig. 9.3. MRS with three (*a*) and four (*b*) base stations

ingly, increases the throughput of the system. The placement topology for 3 BSs with 30 SSs and 4 BSs with 30 SSs is shown in Fig. 9.3.

With three BSs, SSs located in "zone A" have the fundamental ability to simultaneously receive three probing signals, and in three "zones B" — two or three probing signals, which, with an appropriate routing strategy, significantly reduces the meteor trail waiting time and, accordingly, increases the throughput MRS ability.

Obviously, with four BSs, the waiting time is further reduced and, in addition, the requirements for the terminal equipment of a significant number of subscribers can be reduced.

Communication between BSs can be provided via a meteor radio channel, but its bandwidth may not be enough to collect all the information at one point. It is advisable to use additional communication channels between BSs — for example, satellite radio channels. This will allow access to information at any BS location and increase network connectivity.

9.1.2. The base station anti-jamming protection

Since BS is the most critical element of the meteor radio communication network, it is necessary to provide for the possibility of additional protection against intentional and unintentional interference. When using adaptive PAA (APAA), there is a possibility of programmatic formation of "zeros" of the RP pattern in the direction of jamming sources (Monzingo, 1986; Widrow, 1989; Mawrey, 1995).

For the automatic formation of "zeros" in the direction of the interference source, a software-controlled auto-jamming canceller (which is an automatic control device with correlation feedback) and additional (compensation) antennas with an RP width of about 80—90°, located near the main BS antenna, are used. The control voltage (feedback signal) ensures the adjustment of the transmission coefficients of the compensation channels in such a way that when the outputs of all channels are summed, the interference power is minimal. The gains

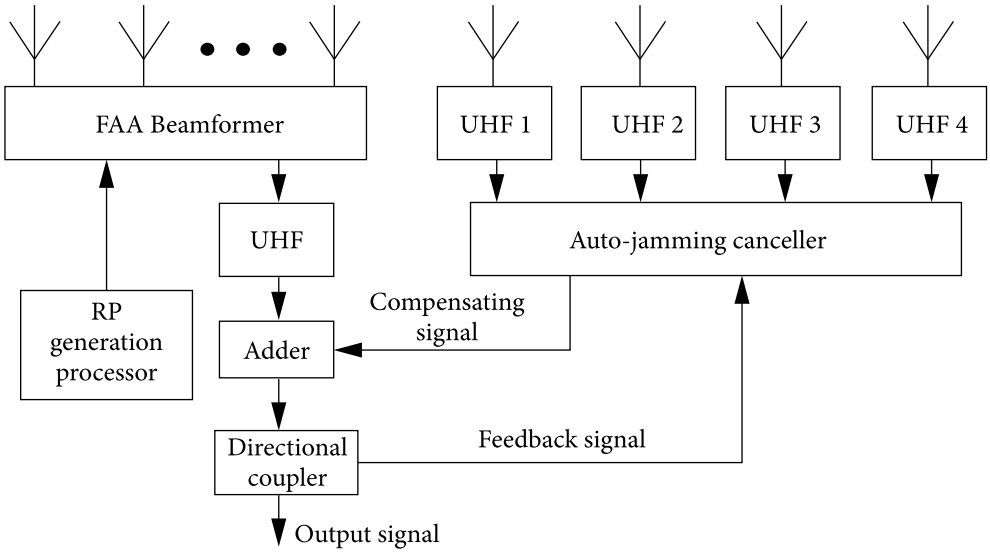

Fig. 9.4. Structural diagram of the system for automatic formation of "zeros" RP in the direction of the jamming source

of the compensation antennas must be the same and not less than 2 dB higher than the level of the side lobes of the RP of the main antenna.

A block diagram of the system for the automatic formation of "zeros" RP in the direction of the interference source is shown in Fig. 9.4.

9.1.3. Subscriber station antenna control

It is possible to significantly reduce the connection latency and increase the MRS throughput via using an antenna with a controlled (or switched) radiation pattern at SSs (Larsen, 1992; Mawrey, 1995; Vendik, 2002) (see Fig. 9.5).

For an MRS subscriber station, it may be sufficient to use 2 horizontally arranged elementary antennas. Uda-Yagi antennas (directional antennas), cross-vibrators, and log-periodic or helical antennas can be used as such antennas. It should be borne in mind that under the influence of the Faraday effect, the plane of polarization rotates when radio waves pass through the D region and the lower part of the E region of the ionosphere. This makes using circular polarized antennas more preferable, especially during the daytime.

When developing a program for pointing SS antennas at "hot zones", the maximum throughput can be achieved taking into account the seasonal change in the distribution of density and radiant values, their daily variation, as well as the geographical location of BS and SS (see Subection 5.2 and (Kozin, 2002; Eshleman, 1961)). For temperate latitudes of the northern hemisphere, a positive effect of pointing SS antennas is observed if the following recommendations are followed:

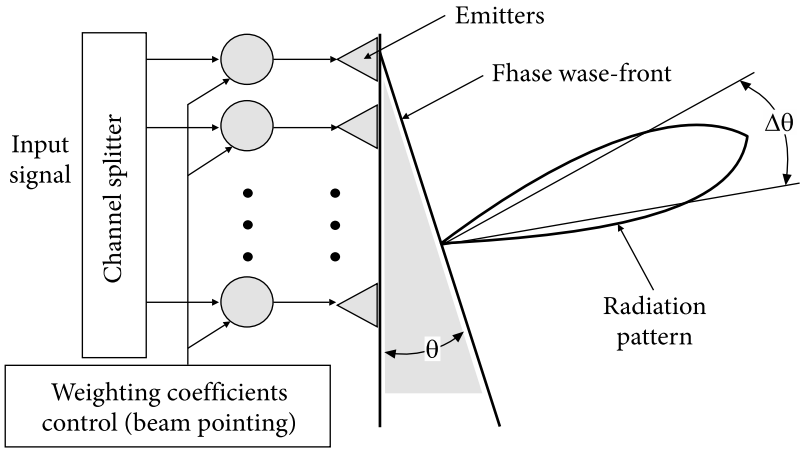

Fig. 9.5. Phased array antenna with the beam pointing

• on predominantly east-west paths, the BS and SS antennas should be directed so that the major axes of the RP intersect north of the path from 00:00 to 12:00 local time and south from 12:00 to 24:00 local time hours;

• on predominantly north-south paths, the BS and SS antennas should be pointed west of the path direction from 18:00 to 06:00 local time and east from 06:00 to 18:00.

The largest daily variations are observed at the equator, the smallest — at the poles. The greatest seasonal variations are at the poles and the smallest — at the equator.

Optimal antenna pointing methods for short paths were studied in the monograph (Antipov, 2006).

Given the geographic location of BS, the optimal pointing of the SS antennas and the development of appropriate software require taking into account the seasonal and daily distribution of sporadic meteoroid radiants for each SS with specified coordinates.

In Fig. 4.11, as an example, a map of the seasonal variation in the radiant density of a sporadic meteor complex in the apex plane of the geocentric ecliptic coordinate system, obtained using the Canadian meteor orbit radar CMOR, is presented. The measurements were made at 29.85 MHz for five sporadic sources visible in the northern hemisphere. Detailed information about CMOR can be found in subsection 3.3 as well as in publications (Jones, 2005; Webster, 2004).

Similar maps of the seasonal variation of the radiant density of a sporadic meteor complex for the southern hemisphere, obtained using the SAAMER radar, are shown in Fig. 9.6 (Younger, 2009).

For optimal pointing of the SS antenna at the "hot zone", it is necessary to establish which sources of radiants for the coordinates of the center of the SS — BS radio link were dominant on the date of the communication session and de-

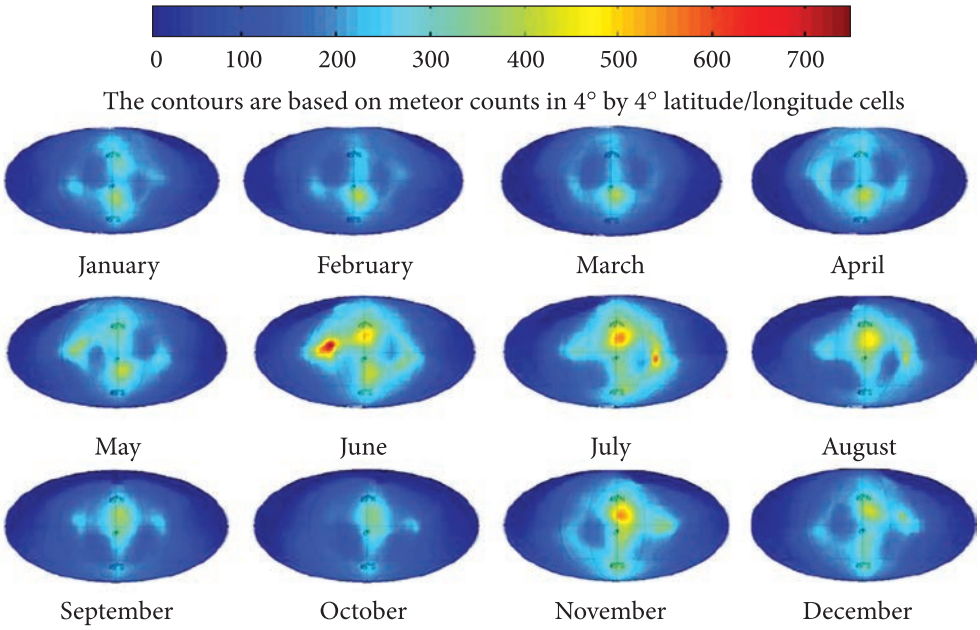

Fig. 9.6. Map of seasonal variation of the sporadic meteor complex radiant density in the apex plane of the geocentric ecliptic coordinate system for the southern hemisphere (Younger, 2009)

termine the prevailing values of meteoroid radiants, taking into account local time (see subsections 4.3 and 5.2, as well as works (Kazantsev, 1961; Kharchenko, 2012; Kharchenko, 2011)).

The calculation of the prevailing radiants of sporadic meteoroids can be performed by successively transforming the coordinates from the geocentric ecliptic system to the topocentric one. During the functioning of the SMS and the collection of relevant statistics, the initial data for software pointing of antennas can be refined.

9.1.4. Application of wideband noise-like signals to meteor radio links

To increase the throughput, noise immunity and secrecy of the functioning of SMS allow the use of wideband noise-like signals (WNLS) along with methods for their processing that are optimal under the influence of non-Gaussian interference (Tuzov, 1985; Varakin, 1985).

Section 7.3 shows that the use of WNLS with a spectrum width more than 10 MHz is attenuate the effect of interference fading that occurs during meteoroid fragmentation and diffuse expansion of the meteor trail and its curvature under the influence of wind. Frequency redundancy provides the ability to notch filtering narrow-band noise in the signal spectrum (Tuzov, 1985; Varakin, 1985; Turin, 1980; Torrieri, 2022).

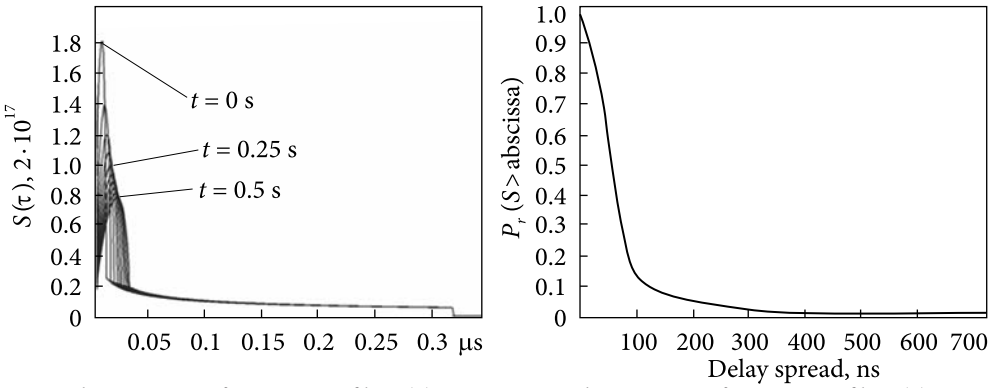

The scattering function profile S (τ) of the meteor trail at different times for a radio link length of 1000 km (subsection 7.2)

The scattering function profile S (τ) of the meteor trail for a radio link length of 500 km (Recommendations ITU-R P.843-1)

Fig. 9.7. Comparison of the calculated scatter-function S (τ) of the meteor trail with the data given in Recommendations ITU–R P. 843–1

To evaluate the effectiveness of the WNLS application, let us consider the influence of the signal scatter-function on IMTr on the reliability of information transmission. As known, in radio channels with signal delay scattering, it is possible to implement implicit diversity, which provides an equivalent diversity multiplicity N, determined by the relation (Turin, 1980; Torrieri, 2022; Kennedy, 1973; Van Tris, 1977)

$$N = 1 + \Delta\tau \cdot \Delta F_S, \tag{9.1}$$

where $\Delta\tau$ is the interval of effective delay scattering, and ΔF_s is the spectrum width of the complex signal.

Fig. 9.7 shows the scatter-function S(τ) of a meteor trail expanding under the action of ambipolar diffusion at different times, calculated on the basis of a radiophysical model of signal scattering on a meteor trail. For comparison, the same figure shows the scatter-function profile of the meteor radio channel given in Recommendations ITU-R P. 843-1 for a 500 km long meteor radio link.

An analysis of the impulse response profiles (given in Recommendations ITU-R P. 843-1) shows that 12% of all underdense trails and 71% of all overdense trails exhibited multipath (scattering) effects. In 90% of cases, the RMS delay, ΔS, is less than 100 ns, and in 99% of cases, the delay spread is less than 400 ns. At the same time, infrequently, there was a spread in delays in the range from 1.0 to 7.0 μs, which can significantly affect the quality of communication.

If we assume that ΔS = 100 ns, and the signal spectrum width = 10 MHz, then, based on formula (9.1), we obtain the equivalent separation factor N = 2, and for ΔS = 1 ms — the equivalent separation factor N = 10.

It is difficult to obtain a quantitative estimate of the gain in the throughput of the meteor radio channel by analytical methods, due to the lack of the necessary statistical data, but the existence of the gain is beyond doubt.

9.1.5. Code separation of complex signals in meteor radio networks

With code division of channels, which involves the use of complex signals, in order to increase subscriber capacity (servicing a large number of SS), it is necessary to have large ensembles of signals with good auto and cross-correlation properties (Varakin, 1985; Sklyar, 2016).

Currently, Walsh sequences, linear and non-linear recurrent sequences, derived orthogonal sequences, Gold and Kassami sequences, which are quite well studied, are used as signals with the necessary characteristics. At the same time, methods for synthesizing large ensembles of weakly correlated discrete signals have not been sufficiently developed. Most of the known methods are based on the use of enumeration procedures and do not provide a guaranteed result for the synthesis of signals with given ensemble and correlation properties. Noteworthy are sequences formed by a pseudo-random permutation of elements of code words of a register code of maximum length (for example, M — sequences) (Kuznetsov, 2007; Stasev, 2008). Permutation transformations, which are a special case of affine transformations, make it possible to increase the volume of any ensemble of signals by many times over that without changing the distance between signals in the signal space.

9.1.6. Combining signals and signaling protocols in meteor radio networks

The frequency resources of the meteor radio channel are limited, and its use is regulated by the recommendations of the International Telecommunication Union (ITU), international agreements and decisions adopted by authorized bodies at the national level (Handbook, 2015). For example, the frequency subbands allocated by the US Government in the 40—50 MHz band for meteor radio communications are 40—42 MHz, 46.6—47 MHz, and 49.6—50 MHz, and their use governed by relevant legislation (Cohen, 1989).

The structure and principles of MRS operation are determined by its purpose. If the main purpose is transmitting notifications and receiving acknowledgment of their receipt, then wide-band signals and addressing based on code division channels can be used at BSs, while frequency division channels (CDCh — FDCh) — at SSs.

At the same time, the SS operating ranges are to correspond to the legislations of the country in which they are located.

If the main purpose of an MRS is voice announcement without feedback, it becomes necessary to transmit sufficiently long information packets, and the use of CDCh is justified.

In SNOTEL-type MRSs focused on collecting geophysical information, as well as dispatching ground and air vehicles and collecting information about the

location of moving objects (icebergs, buoys, etc.), the BS functions are limited to the transmission of a sounding signal, and the transmission of the required information is performed by SS.

If the main indicators of the effectiveness of an MRS are low cost and ease of maintenance, then its implementation can use frequency division multiple access (FDCh — FDCh) and use discrete frequency modulation with minimum shift (MSK) or its varieties with limited spectrum.

In the case of information exchange within a single country, especially if the secrecy and noise immunity of an MRS are a priority, the CDCh-CDCh multistation mode can be used for data transmission. In this case, at both BS and SS, a matched filtering of complex signals should be applied.

9.1.7. Adaptation in rate and length of transmitted packets in meteor radio communication networks

An increase in the MRS throughput is possible based on the predict of the time interval available for message transmission and changes in the energy potential of the non-stationary MRCh in this interval. Such a prediction can be made on the SS using the ATCH of the received probing signal at the initial part of the meteor trail in the MRS with feedback (see Section 8.3). In this case, the SS is transmits signals at a rate and length of the information packet that provide the maximum throughput of the MRCh.

To increase the throughput of the BS based on the assessment of the state of the MRCh performed at the initial section of the meteor trail by the subscriber station SS_j can transmit a short message indicating the level of the received probing signal, the level of interference at the receiving point, and the predicted duration of the message transmission interval, allowing optimizing the information transmission protocol on BS. In this mode, it is possible to collect statistical information about the change in the throughput of the radio link BS — SS_j depending on the time of year and day and introduce it into the database. The processing of statistical information allows us to propose a transmission protocol for BS — SS radio links that maximize the throughput of the meteor communication network.

9.2. Building technologies for advanced meteor radio communication systems

While implementing meteor communication systems with CDCh following the above principles, it is necessary to solve the following main technical problems:

1. Form the radiation patterns of the BS antennas, providing the necessary coverage of the service area and compensation for interference entering the receiving path of the main channel through the side lobes of the phased array design.

2. Manage the directional patterns of the AC antennas, ensuring their guidance to the "hot zones."

3. Set the required operation frequency and generate signals corresponding to the selected MRS operation mode.

4. Generate large ensembles of complex signals with improved cross-correlation properties.

5. Perform coordinated filtering of complex signals and rejection of narrowband interference in their spectrum.

6. Ensure optimal reception along with a short detection and synchronization time for received scattered signals of various intensities when exposed to non-stationary and non-Gaussian interference.

7. Implement multi-standard protocols for information transmission in the network, including the adaptation of the transmission rate and duration of the transmitted packets to the characteristics of the meteor communication channel, which are oriented toward increasing the MRS throughput and reducing the delivery time of a message of a given length.

The solution to these problems is possible with the use of the SDR technology, the presence of significant computing resources, and a multitasking mode of operation. These conditions correspond to programmable logic devices (PLD) (integrated circuits) and multi-core personal computers (PC) of general use, operating in real-time. PLDs can be used in the implementation of SS software since transmission and reception are performed in a single-channel mode. For BS operating in a multi-channel control mode and with digital signal processing, it is necessary to use sufficiently powerful PCs.

The first two tasks go beyond the issues considered in this monograph. Let's take a closer look at the last four tasks.

9.2.1. Generation of large ensembles of complex signals with improved cross-correlation properties

To implement code division of channels with a large number of SS, it is necessary to have large ensembles of signals with good auto and cross–correlation properties (Varakin, 1985; Sklyar, 2016; Kuznetsov, 2007; Stasev, 2008; Gorbenko, 2015).

Permutation transformations, which are a special case of affine transformations, make it possible to increase the volume of an ensemble of signals many times over that without changing the distance between signals in the signal space. The algorithm for generating large ensembles of equidistant signals with improved cross-correlation properties is illustrated by the block diagram shown in Fig. 9.8.

The generator of orthogonal equidistant signals generates N cyclic shifts M — sequences that are written to N shift registers. The permutation block, in accordance with the program generated by the Key Source, performs a coordinated permutation of code elements simultaneously in all registers. In accordance with the given permutation, which provides strong mixing, an ensemble of N weakly correlated signals is formed. The number of signals in the ensemble is determined

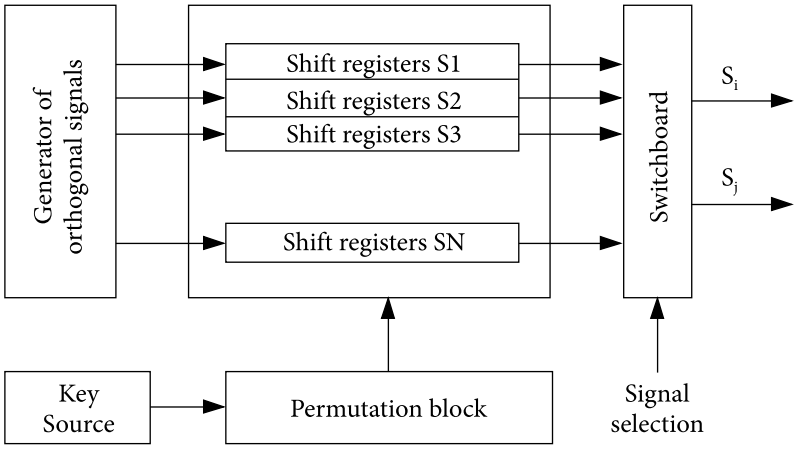

Fig. 9.8. Structural diagram illustrating the algorithm for generating large ensembles of equidistant signals with improved cross-correlation properties

by the number of elements of the source code. Each permutation provides the formation of its own ensemble of signals, and there can be a very large number of such ensembles (of the order of N factorial). However, it should be noted that signals from different ensembles may not have sufficiently good cross-correlation properties, which suggests the need for proper planning of SS location and assignment of signals from ensembles to them.

From the results of a comparative analysis of the ensemble and correlation properties of discrete signals (Stasev, 2008), it follows that sequences formed by a pseudo–random permutation of elements of code words of a register code of maximum length have improved properties. The corresponding synthesis method is one of the most promising from the viewpoint of further development and practical application to solving the problem of constructing meteor radio communication systems and networks with code division of channels. Its computational complexity is not great and the method is quite simply implemented on the basis of software methods using microcontrollers or PLDs.

9.2.2. Matched filtering of complex signals and rejection of narrowband noise in their spectrum

Detection and discrimination of large baseband signals can be performed using a multi-channel correlator or an analog matched filter (for example, tapped delay lines, surface acoustic wave filters, convolvers, etc.). However, the use of large ensembles of complex signals and the need to change them programmatically excludes the possibility of using analog processing and leaves the only alternative — digital matched filtering. The implementation of programmable digital matched filters (PDMF) is based on the use of Fast Direct Fourier

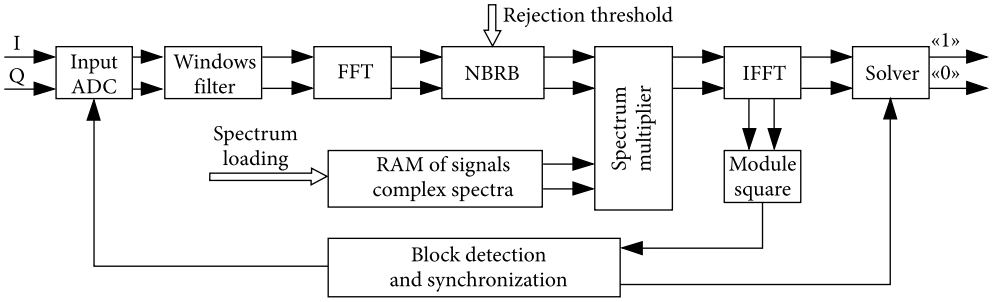

Fig. 9.9. Structural diagram of the programmable digital method of non-threshold synchronization of matched filter with narrowband rejection

Transform and Inverse Fast Fourier Transform (FFT and IFFT). The convolution can be carried out by the algorithm "FFT-multiplication-IFFT". When processing signals with a base above 100, frequency domain convolution has the advantage of computational operations number required (Handbook, 2015; Cohen, 1989; Gorbenko, 2015; Kuzmin, 2000; Lyons, 2006; Nussbaumer, 1981).

For tuning PDMF to a given signal in the alphabet used, it is enough to load the complex conjugate spectrum of the corresponding signal. In addition, frequency domain convolution naturally provides additional protection against the effects of narrowband interference (NBI) falling within the received band.

Fig. 9.9 shows a block diagram of a PDMF with an additional window filter and a narrowband rejection block (NBRB). The window filter is necessary to reduce the effect of the spreading of the narrowband interference (NBI) after the FFT (Harris, 1978), and the principle of operation of the BRUP is based on zeroing the complex spectral FFT coefficients, the square of the modulus of which exceeds the set threshold. The rejection threshold for narrowband interference may be adaptive.

To tune PDMF to a given waveform from an external control device (computer or specialized control panel) via a standard interface (for example, via SPI interface), the mirror forms of the processed signals are loaded into the RAM of the waveforms, supplemented with a sequence of zeros to obtain a linear convolution. After that, in the FFT block, their complex spectra are calculated and the result is recorded in the RAM of the signal spectra. It is also possible to prior calculate the complex conjugate spectra and directly load them into the RAM of the signal spectra via the SPI interface.

When constructing the circuit, it was taken into account that the recording of information from the ADC to the RAM input is carried out block by block in the 2^N format to implement the FFT.

The studies required bit depth of the ADC, described in (Kharchenko, 2008), showed that (6—8) quantization levels per peak-to-peak of the combinated signal, noise, and narrow-band interference is sufficient to significantly reduce the

level of intermodulation interference. In some cases, this number of quantization levels reduced the power loss by up to 6 dB compared to a two-sided ideal bandpass limiter.

The proposed PDMF algorithm implementation is focused on using PLDs from different manufacturers, such as ALTERA (Steshenko, 2000), XILINX (Zotov, 2003), and others. The proposed implementation of PDMF allows the processing of any kind of signal, including pre-recorded and digitized noise implementations, TV signal sync sequences, chirp signals, or signals with improved autocorrelation properties. It can be used both in communication systems and for corresponding measurements of meteor trail parameters.

9.2.3. Optimal signal reception and synchronization when transmitting digital information via meteor radio channels

For channels with scattered signals, which include MRCh, based on the formation of sufficient statistics (Van Tris, 1977) and the solution of the inhomogeneous Fredholm integral equation of the second kind, an expression for the optimal detector has been obtained (Kharchenko V., 1988). It is implemented by the circuit shown in Fig. 9.10, where r(t) is the noisy input signal, N_0 is the noise spectral density, MF is the matched filter, C1 and C2 are the calculated coefficients, and l is the solution.

Note that in the case of a non-scattering channel, $S(\tau)$ degenerates into a δ function, the output effect of the lower branch of the circuit becomes zero, and the upper branch is transformed into the well-known optimal incoherent detector.

One of the most difficult problems that arise in the design of communication systems with broadband noise-like signals is the problem of synchronization. It includes the detection of signal phase, determination of the moment of decision on the transmitted signal (clock synchronization), and determination of the moment of the beginning of the information packet transmission (frame synchronization). The less time allocated for synchronization, the more efficient its MRCh operation is.

For a non-stationary MRCh, when exposed to a complex of interference with rapidly changing characteristics, the existing methods for synchronizing signals with direct spread spectrum are either inoperative, or requiring for significant acquisition time, up to several seconds. This is unacceptable for meteor radio channels, since the lifetime of an ionized trail is measured in tenths of a second, and the change in the maximum value of the intensity of the scattered signal over a wide range makes it problematic to use detection algorithms based on the use of adaptive signal detection thresholds (Gharmonov, 2000).

The non-threshold synchronization method described in (Kharchenko V., 2006) consists in detecting *m* multiple repetitions in a row of the subtact addresses, in which the maximum convolution value of the complex signal is observed

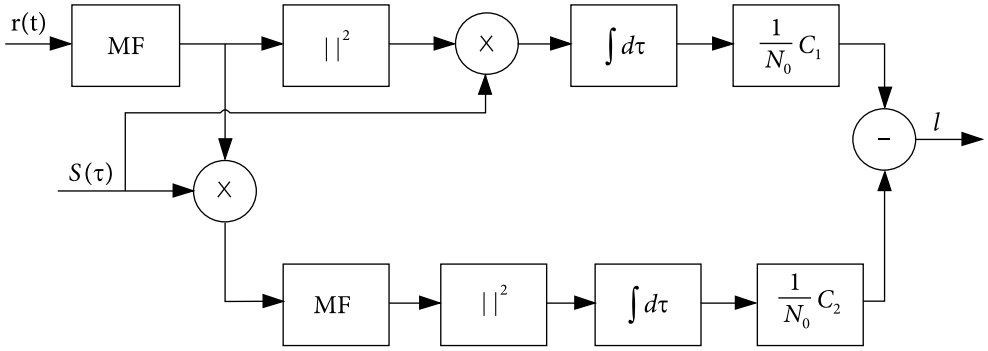

Fig. 9.10. Optimal detector for time-dispersed signals

("*m* in a row" criterion), or the repetition of the subtact address with the maximum convolution value of at least *k* times in *n* consecutive observation intervals (cycles) ("*k* out of *n*" criterion). These algorithms can be represented as a synthesized, parameterized, and structured VHDL model, focused on the use of FPGAs from verious manufacturers (Kharchenko, 2009).

A patent (Khachaturov, 2014) has been obtained for such a system, but for MRCh the proposed synchronization method can be improved by using a combination of the threshold and non–threshold methods. The essence of the proposed method is that the current threshold value is set at a level sufficient to receive information with a given reliability (the noise level is measured at signal absence intervals), and the decision is made for the condition "k out of n" and exceeding the specified threshold level. This makes it possible, with the false alarm probability set, to reduce the value of *m* (or *n*), which means reducing the time allocated for synchronization. For example, set m = 2 ("*m* in a row" criterion) and set the condition that the threshold is exceeded during the second observation of the convolution. Or set k = 2, n = 3 ("k out of n" criterion) and set the condition that on three cycles the observed convolution value exceeds the threshold at least once.

Based on several received and stored values of the WNLS convolution, it is possible to estimate the intensity of the reflected signal and predict the type and characteristics of the trail. This, in turn, makes it possible to indicate the initial information transfer rate in the header of the transmitted frame and, based on the current estimates of the probing signal intensity, to change the instructions by transmitting the appropriate markers.

Note that multi-channel signal processing and code division of channels at the BS can be provided not in real-time but by recording the signal to the RAM after detecting the fact of transmission, followed by demodulation of the received message. This will significantly reduce hardware costs and computing resources.

SDR technology allows one to optimize the information transfer rate by changing the number of elements (bases) of the signals used and programming

the PDMF accordingly. In this case, the duration of the element does not change, which means that the parameters of the high-frequency paths of transmitter and receiver remain unchanged.

SDR technology makes it possible to implement multistandard protocols for information transfer in a network, including an adaptation of the transmission rate and duration of transmitted packets to the characteristics of a meteor communication channel, which are focused on increasing the MRS bandwidth and reducing the delivery time of a message of a given length.

A detailed description of the information exchange protocol between SS and BS depends on the purpose of the MRS and is beyond the scope of this monograph. Variants for the transmission protocols used, the efficiency of which depends on the characteristics of the MRCS, are given in (Recommendation ITU-R F. 1113; Schilling, 1993; Schanker, 1990; Kascheev, 1996; Weitzen, 1993; Miroshnikov, 2019) and many other publications.

9.3. Conclusions

The use of software-controlled smart antennas, large ensembles of complex signals, and adaptation to changing operating conditions open up new prospects for the creation of MRS. It can be expected that the new generation of meteor radio communication networks will have a significantly higher bandwidth, lower connection latency, increased noise immunity, and secrecy of the operation.

An increase in the MRS bandwidth, reduction in the connection latency, increase in the number of subscribers served by the system, and increase in the noise immunity and secrecy of the system operation can provide:

1. Choosing a network topology that allows one to provide the necessary coverage and the possibility of simultaneous access of MRS subscriber stations to several base stations, which reduces the waiting time for the appearance of IMTr with a specular reflection point and, accordingly, increases the system throughput.

2. Additional protection of the base station against intentional and unintentional interference, which is the most critical element of the meteor radio communication network. It can be implemented based on the use of software-controlled antennas that provide the necessary coverage and adaptation to changing operating conditions of the system.

3. The use of an antenna with a controlled (or switched) radiation pattern at subscriber stations for pointing at areas of space where the appearance of suitable meteor trails is most likely. This will reduce connection latency and increase MRS throughput.

4. Application of signals and methods of their processing, which allow resisting interference fading and the effects of interference concentrated in the spectrum, which will increase the noise immunity and, as a result, the throughput of the communication channel.

5. Implementation of multi-station access with CDCh, which will increase the number of subscribers served by MRS. The use of large signal ensembles with a direct spread spectrum also provides an increase in jamming and secrecy of the MRS operation.

6. Selection of the types of signals used, operating frequencies and methods of multiple access, determined by the purpose of the MRS and the corresponding performance indicators. When appointing them, it is necessary to take into account the recommendations of the International Telecommunication Union, international agreements, and decisions on the allocation of frequencies, wich are taken by authorized bodies at the national level.

7. Adaptation of the MRS in terms of the transmission rate and duration of the transmitted packets, for the implementation of which a predict based on the analysis of the reflected signal at the initial stage of its formation along with the corresponding protocol for the interaction of the SS and the BS can be used.

8. Reducing the detection time of a meteor trail suitable for communication at the synchronization stage, which requires the use of a combination of non-threshold and threshold detection methods.

Many questions related to MRS network and system architectures, as well as optimal control strategies, need to be answered before cost-effective meteor communication systems can be developed.

The construction and subsequent modernization of the system will be facilitated by the use of SDR technologies that allow the introduction of new signal processing methods and information transfer protocols along with the unification and subsequent modernization of almost all elements of the MRS without a significant change in circuit solutions.

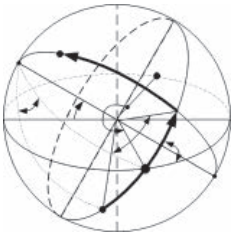

GENERAL CONCLUSIONS

The original researches and a system analysis of published works in the field of meteor physics provides an opportunity for further improvement of methods necessary for astrophysical and geophysical research, as well as for transmitting information via meteor radio channels.

Observational data on meteoroids obtained through the use of meteor trail radars can provide insight into the genetic relationship of meteor showers and sporadic meteoroids with the parent body (comet or asteroid) and their chemical composition, mineralogical and bulk density. They are necessary for the development of the theory of the origin and evolution of meteoric matter and prognostic models of signal scattering on a meteor trail.

When interpreting the results of observations, it is necessary to take into account the features of the systems through which the corresponding data were obtained. In this regard, the technical characteristics and geographical position of radars were presented, which were used to study atmospheric physics, radiant mapping of the sporadic meteor complex (SMC) and meteor showers, as well as to estimate the parameters of the orbits and speed of meteoroids.

Bistatic scattering from ionized meteoroid trails can be used to study the dynamics of the lower ionosphere and the influx of meteor matter to the Earth and to build maps of the distribution density of SMC and meteor showers radiants across the celestial sphere. It opens up new opportunities for ionospheric and geophysical studies at the height of the trail formation – wind and temperature fields, turbulence, ambipolar diffusion, processes of generation and propagation of acoustic gravity waves, as well as ozone concentration in the meteor zone at different latitudes and different times of the year and day.

The system for transmitting information on SRPs can be used for telecommunication and synchronization of time

scales. For communication systems with low traffic, it can be a low-budget alternative to satellite communication systems used in the interests of the Ministry of Defense of Ukraine and diplomatic missions to organize radio communications in disaster areas, as well as in hard-to-reach and remote areas.

The proposed prognostic model makes it possible to estimate the seasonal and diurnal change in the frequency of the appearance of ionized meteoroid trails — IMTRr with a specular reflection poi a SRP, belonging to the main SMC sources and meteor showers, in a bistatic radar. Based on the prognostic model, the zone where the SRP of the radio signal is observed with a higher probability is determined. Calculation of the coordinates and height of the meteor trail SRP with given radiant and point of entry of the meteoroid into the meteor zone was performed analytically. This required solving a third-degree equation. When solving the equation, the Vieta method was used. The possibility of using a direction-finding-time radar for estimating the height of the SRP under bistatic scattering is shown. A simple and geometrically illustrative method is proposed for measuring the SRP coordinates with an unknown radiant of the meteoroid that generated the trail. This makes it possible to compare the results of calculations and measurements.

When developing a more advanced prognostic model, attention should be paid to the need to supplement it with data on the distribution of meteoroid velocities, its density and probable chemical composition, to take into account the effect on the trail detection characteristics of seasonal and daily changes in atmospheric density, the degree of ionization and turbulence in the meteor zone, as well as solar activity. Due to the incompleteness of the initial data, the radiant density distribution map and the prognostic model need correcting as new observational data become available. It should be noted that the number of calculations required for the practical use of the predictive model is very large and requires the development of special software.

The physical theory of the formation and transformation of ionized meteor trails (IMTr) is the basis for calculating the electron density of the trail and creating a generalized model for the scattering of radio signals on a meteor trail during its formation and development.

A model and an algorithm for estimating the height-dependent linear electron trail density (LEDTr) created by a meteoroid with predictable (given) physical and chemical characteristics are proposed. The simulation results correspond to the LEDTr estimates according to the well-known semi-empirical formula, which is valid only in the region of the ionization maximum and obtained as a result of fitting to the results of radar measurements. It is shown that the height dependence of LEDTr qualitatively coincides with the luminosity curve. A feature of the proposed model is the possibility of its adaptation for the case of fragmentation of a meteoric body at a given height. For each fragment, it is necessary to calculate the LEDTr by the proposed algorithm and then use the superposition principle, that is, the assumption according to which the resulting effect of several

independent events can be represented by the sum of the effects caused by each event separately.

The studies carried out made it possible to estimate the bulk electron density and propose a model of a two-dimensional axisymmetric trace electron density. Such a model is necessary for the development of a radiophysical model of the bistatic scattering of signals on the IMTr in the process of its transformation.

It is almost impossible to formulate and solve the diffraction problem of radio wave scattering on a meteor trail for all phases of its development in a rigorous formulation, and it is problematic to obtain reliable empirical calculation formulas directly from the observation results since the initial data are unknown. In this regard, heuristic methods for solving the diffraction problem were used to construct a radiophysical model of signal scattering on a meteor trail.

The heuristic radiophysical model of radio signal scattering on a meteor trail made it possible to obtain an analytical expression for calculating the change in the power of the coherent component of the scattered signal on meteor trails of both underdense and overdense types. The analytical expression is based on the use of the MRCh scattering function. It allows one to calculate not only the power of the scattered signal but also to estimate the time of existence of a meteor trail suitable for transmitting information and describe the features of the observed diffraction oscillations of the received signal amplitude.

The joint consideration of the influence of the overdense and underdense parts of the meteor trail, the presence of which is typical for almost all trails, makes it possible to explain the difference in estimates of the dependence of the scattered power on the operating wavelength. This dependence can vary with a change in the mass and velocity of the meteoroid, as well as with a change in the orientation of the meteor trail relative to the radio line.

The results of numerical calculations performed using the heuristic radiophysical scattering model show good agreement with the results of experimental observations of scattered signals over a time interval from 0 to 3 s and confirm the presence of diffraction oscillations in meteor trails of any type. Outside this interval, the calculated values of the scattered signal power somewhat exceed the observed values. Dcreasing the signal level may be due to the interferences caused by the fragmentation of the meteoric body, by the additional influence of turbulent diffusion, which were not considered by the scattering model. The effects of recombination and attachment of free trail electrons, the influence of hyperthermal chemistry and ionic reactions with mesospheric ozone, as well as the possible influence of wind displacement were not taken into account. This indicates the need for further improvement of the radiophysical model of signal scattering on meteor trails of various types.

The resulting MRC scattering function allows one to estimate the signal shape at the receiver input at characteristic times. This made it possible to propose the type and parameters of a radio signal providing resistance to fading and an increase in the reliability of information transmission through a meteor radio channel.

Using the example of LEM signals, it is shown that the use of direct spread spectrum signals makes it possible to reduce the effect of diffraction oscillations caused by the change in time of the equivalent radius of the underdense part of the meteor trail. This suggests that the use of code division channels (CDCh) and ensembles of complex signals with good cross-correlation properties and a sufficiently large spectrum width in meteor radio communication systems will increase their throughput of thes systems.

The radiophysical models of signal scattering on a meteor trail make it possible to calculate the amplitude-time (ATCH) and phase-time characteristics of the signal and create a model image of the scattered signal in the process of its formation and development for given parameters of the meteoroid and atmosphere at the height of the ionized trail observation.

Comparison of the amplitude-time ATCH characteristics of the received signal with the calculated model images allows one to make reasonable assumptions about the characteristics of the meteoroid that generated the ionized trail. Based on the classification of meteor trails by the features of signals scattered on them, the mass, density, velocity, and radiant of the meteoroid that formed the corresponding trail can be indirectly estimated.

By setting the physicochemical parameters characteristic of a meteoroid of cometary or asteroidal origin, as well as the height of the SRP, it is possible to create appropriate databases (images of scattered signals for different radiants and velocities) for solving astronomical and telecommunication problems. Such databases must be created taking into account the geographical coordinates of the points of transmission and reception as well as the epoch — the time of year and day. When normalizing, one should take into account the length of the radio link, the equivalent isotropically radiated power, the operating frequency, and the noise power at this frequency.

The classification of meteoroids based on the use of the radiophysical model can be performed by comparing the normalized images stored in the database with the normalized images of the observed radio signals scattered on the IMTr.

The set of features used in predicting should reflect the greatest extent of those properties of objects that are important for solving the problem. The computational complexity of the decision-making procedures, the reliability of predicting, and the time spent on the corresponding calculations largely depend on the dimension of the feature space.

When predicting the duration of the reflected radio signal based on the results of measurements of its characteristics in the initial observation area, such main features can be considered as the signal amplitude measured at the end of the initial observation interval and the rate of its increase. It should be taken into account that the time of amplitude rise to the maximum value is determined both by the meteoroid velocity and by the length of the first Fresnel zone, which depends on the trail orientation relative to the radio wave propagation path. The power of the measured signal depends on the trace orientation as well: the greater

the length of the first Fresnel zone, the greater the measured amplitude. Thus, on the basis of large amplitude, one can also predict a long signal duration, but its value must be corrected (decreased) taking into account the duration of the rise interval and the meteoroid velocity. A possible option for determining the correction factor is the use of artificial neural networks (ANNs). The ability of a neural network to predict directly follows its ability to generalize and highlight hidden dependencies between input and output data. The ability to learn is one of the main ANNs advantages over traditional classification algorithms.

Prediction of the duration and amplitude of the reflected radio signal based on its characteristics at the initial observation site is necessary for solving telecommunication problems such as choosing the rate and protocol for transmitting information, on which the throughput of meteor radio channels depends. Such a prediction can be made using ANN technology as well. In this case, the measured signal amplitude and the time of its rise to a maximum, as well as the frequency dispersion of the reflection due to fast Doppler, should be used as main features. It can be expected that the decision rule based on these features will provide a classification quality sufficient to decide on the advisability of adaptively changing the rate and protocol of information transfer. This is an important result, which is of direct importance for the design of advanced meteor radio communication systems.

The proposed concept of building a promising system of meteor radio communication involves increasing the throughput, noise immunity, and secrecy of the system, as well as reducing the connection waiting time. This can be achieved through:

- choice of network topology;
- additional protection of the base station against intentional and unintentional interference using software-controlled antennas;
- use at subscriber stations of antennas with a controlled (or switched) directivity pattern for pointing at the areas of space where the appearance of suitable meteor trails is most likely;
- application of signals and methods for their processing, allowing to resist interference fading and the impact of interference concentrated over the spectrum;
- introduction of multiple access with CDCh, which will increase the number of subscribers served by meteor radio communication systems (MRCS);
- use of large ensembles of signals with direct spread spectrum and good cross-correlation properties, which provides increased noise immunity and secrecy of the MRCS functioning;
- selection of the types of signals, operating frequencies, and methods for multiple access, which are determined by the purpose of the MRCS and the corresponding performance indicators;
- assignment of operating frequencies, taking into account the Recommendations of the International Telecommunication Union, international agreements, and decisions on the allocation of frequencies made by authorized bodies at the national level;

- adaptation of MRCS in terms of transmission rate and duration of transmitted packets, for the implementation of which a prediction based on the analysis of the reflected signal at the initial stage of its formation, and the corresponding protocol for the SS-BS interaction can be used;
- optimal signal reception based on matched filtering using fast Fourier transform and suppression of narrow-band interference in the signal spectrum;
- reducing the time of detection of a meteor trail suitable for communication at the synchronization stage.

For a given geographical position of the BS, the optimal pointing of the SS antennas and the development of appropriate software require taking into account the seasonal and daily distribution of radiants of sporadic meteoroids for each SS with the specified coordinates.

The choice of information transfer protocol depends on the purpose of the MRCS, the chosen criterion for its optimality, the length of the radio link, and the characteristics of the receiving and transmitting equipment. A detailed description of the protocol for the information exchange between the SS and the BS depends on the purpose of the MRCS and is beyond the scope of this monograph.

The construction and subsequent modernization of the system will be facilitated by the use of SDR technologies, which allow the introduction of new signal processing methods and information transfer protocols, as well as the unification and modernization of almost all elements of the MRCS without significant changes in the circuitry.

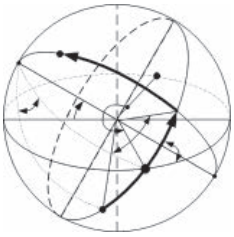

REFERENCES IN ALPHABETICAL ORDER

Abalakin, V.K. (1979). Osnovy efemeridnoy astronomii [Fundamentals of Ephemeris Astronomy]. Moscow: Nauka. (in Russian). URL: http://ikfia.ysn.ru/wp-content/uploads/2018/01/Abalakin1979ru.pdf

Aleksandrov, P.S. (1968). Lektsii po analiticheskoy geometrii [Lectures on Analytical Geometry]. Moscow: Nauka. (in Russian).

Allen, B.B. (1989). Meteor Burst Communications For The U.S. Marine Corps Expeditionary Force (Accession Number: ADA207831) [Master Thesis, Naval Post Graduate School Montery, CA]. URL: https://apps.dtic.mil/sti/citations/ADA207831

Alpert, Y.L. (1972). Rasprostranenie elektromagnitnykh voln i ionosfera [Propagation of Electromagnetic Waves and Ionosphere]. Moscow: Nauka. (in Russian).

Anderson, H.H., & Bay, H. L. (1981). Sputtering yield measurements. In J. E. Ehrstein & G.C. Riach (Eds.). Sputtering by Particle Bombardment, 157—171. Springer-Verlag. URL: https://link.springer.com/chapter/10.1007/3540105212_9

Antipov, I.E., Koval, Y.A., & Obedlchenko, V.V. (2006). Razvitie teorii i sovershenstvovanie radiometeornykh sistem svyazi i sinkhronizatsii [Development of the theory and improvement of radio meteor communication and synchronization systems]. Kharkiv: Kollegium. (in Russian).

Antipov, I.E., Kostyrya, A.A., & Shkarlet, A.I. (2010). Modern means and methods of radar meteor studies. Radiotekhnika, 160, 39—46. (in Russian).

Arnold, N.F., Cook, P.A., Robinson, T.R., Lester, M., Chapman, P.J. & Mitchell, N. (2003). Comparison of D-region Doppler drift winds measured by the SuperDARN Finland HF radar over an annual cycle using the Kiruna VHF meteor radar. Ann. Geophys., 21, 2073—2082. http: // doi.org: 10.5194/angeo-21-2073-2003

Asher, D.J., Bailey, M.E., Hahn, G., & Steel, D. (1994) Asteroid 5335 Damocles and Its Implications for Cometary Dynamics. Monthly Notices of the Royal Astronomical Society, 267, 195—221. URL: https://adsabs.harvard.edu/full/1994MNRAS.267...26A

Astapovich, I.S. (1958). Meteornye yavleniya v atmosfere Zemli [Meteor Phenomena in the Earth's Atmosphere]. Moscow: Fizmatgiz. (in Russian).

Asteroidy [Asteroids]. URL: http://galspace.spb.ru/asteroid.html

Ayers, W.G., McCrosky, R.E., & Shao, C.-Y. (1970). Photographic Observations of 10 Artificial Meteors. SAO Special Report No. 317. URL: https://ntrs.nasa.gov/api/citations/19700023536/downloads/19700023536.pdf

Azarenkov, N.A., & Galaydych, V.K. (2008). Electromagnetic diffraction by metal cylinder coated with inhomogeneous magnetoactive plasma sheath. Journal of Kharkiv University, No. 808 (2), 73—76. URL: http://dspace.univer.kharkov.ua/bitstream/123456789/4868/2/808_2%2838%29_08_p73-76.pdf

Azarenkov, N.A., Galaydych, V.K., & Leleko, Yu.Ja. (2011). Electromagnetic wave diffraction by metal cylinder coated with inhomogeneous magnetoactive plasma sheath. Journal of Kharkiv University, No. 979 (4), 98—102.

Babadzhanov, P. B., Novikov, G. G., Lebedinets, V. N., & Blokhin, A. V. (1988). Kvazinineprey-vnoye drobleniye meteorikh tel s uchetom tormozheniya [Quasi-continuous fragmentation of meteor bodies taking into account deceleration]. Astronomicheskiy Vestnik [Astronomical Bulletin], 22, 71—78. (in Russian).

Babadzhanov, P.B., Novikov, G.G., Lebedinets, V.N., & Blokhin, A.V. (1988). Techiques for interpreting meteor observations with an account of fragmentation. Solar System Research 22, 71—78.

Babadzhanov, P.B., & Obrubov, Y.V. (1991). Meteoroidnye roi: Obrazovanie, evolyutsiya, svyaz' s kometami i asteroidami [Meteoroid Swarms: Formation, Evolution, Connection with Comets and Asteroids]. Astronomicheskiy vestnik [Astronomical Bulletin], 25 (4), 387—407. (in Russian).

Babadzhanov, P.B. (1993). Quasi–continuous fragmentation and meteoroid density. Solar System Research, 26 (5), 488—491.

Baggaley, W. J. & Webb, T. H. (1977). The thermalization of meteoric ionization, Journal of Atmospheric and Terrestrial Physics, 39, 1399—1403. http://doi.org/10.1016/0021-9169(77)90094-0

Baggaley, W. J. (1980). Meteors and atmospheres. In Symposium — International Astronomical Union, Volume 90: Solid Particles in the Solar System, 85—100. http://doi.org/10.1017/S0074180900066535

Baggaley, W. J., Bennet, R. G. T., Steel, D. I. & Taylor A. D. (1994). The advanced meteor orbit radar facility: Quarterly Journal of the Royal Astronomical Society, 35 (3), 293—320. URL: https://adsabs.harvard.edu/full/1994QJRAS..35..293B

Baggaley, W. J., Marsh, S. H., Bennett, R. G. T., & Galligan, D. P. (2001). Features of the enhanced AMOR facility: The advanced meteor orbit radar. In Proceedings of the Meteoroids 2001 Conference, 6—10 August 2001, Kiruna, Sweden, 387—391. URL: https://adsabs.harvard.edu/full/2001ESASP.495..387B

Baggaley, W.J., Bennett, R.G.T., Marsh, S.H., Plank, G.E. & Galligan D.P. (2002). Update on new developments of the Advanced Meteor Orbit Radar AMOR. COSPAR Colloquia Series 15, 38—41. http: //doi.org/10.1016/S0964-2749(02)80321-3

Barabash, V. (2004). Investigation of Polar Mesosphere Summer Echoes in Northern Scandinavia (IRF Scientific Report 283). URL: https: //www.irf.se/publications/SciReports/IRFreport283.pdf

Barry, N.G. (2005). Model razleta fragmentov razrushennogo meteoroida [Model of the Spread of Fragments of a Disintegrated Meteoroid]. Vestnik Moskovskogo universiteta. Seriya 1. Matematika. Mekhanika [Bulletin of Moscow University. Series 1. Mathematics. Mechanics], 4, 56—59. (in Russian).

Barry, N.G. (2010). Aerodinamika fragmentov meteornogo tela. Effekt kollimatsii [Aerodynamics of Meteoroid Body Fragments. Collimation Effect]. Astronomicheskiy vestnik [Astronomical Bulletin], 44 (1), 59—64. (in Russian).

Beldon, C.L. (2008). VHF radar studies of the mesosphere and thermosphere [A thesis submitted for the degree of Doctor of Philosophy] University of Bath Department of Electronic and Electrical Engineering. URL: https://researchportal.bath.ac.uk/en/studentTheses/vhf-radar-studies-of-mesosphere-and-thermosphere

Belkovich, O.I. (1971). Statisticheskaya teoriya radiolokatsii meteorov [Statistical theory of meteor radio location]. Izdatelstvo Kazanskogo gosudarstvennogo universiteta [Publishing house of Kazan State University]. (in Russian).

Belkovich, O.I. (2008). Meteornoe rasprostranenie radiovoln [Meteor propagation of radio waves]. Zelenodolsk: Izdatelstvo Kazanskogo gosudarstvennogo universiteta [Publishing house of Kazan State University]. (in Russian).

Berezhnoy, A.A., & Borovicka, J. (2010). Formation of molecules in bright meteors. Icarus, 210 (1), 150—157. http: //doi.org: 10.1016/j.icarus.2010.06.036

Biryukov, E.E. (2007). Zahvat komet iz oblaka Oorta na orbityi galleevskogo tipa i orbityi semeystva Yupitera [Capture of Comets from the Oort Cloud to Galilean-Type and Jupiter–Family Orbits]. Astronomicheskiy vestnik [Astronomical Bulletin], 41 (3), 232—240. (in Russian).

Blazhko, S.N. (1954). Kurs sfericheskoy astronomii [Course on Spherical Astronomy]. Moscow: Gostekhizdat. (in Russian).

Bohdansky, J. (1984). A universal relation for the sputtering yield of monoatomic solids at normal incidence. Nuclear Instruments and Methods in Physics Research Section B, 2 (5), 587—591. http://doi.org: 10.1016/0168–583X(84)90271–4

Bohdansky, J. (1980). Important sputtering yield data for tokamaks: A comparison of measurements and estimates. Journal of Nuclear Materials, Vol. 93—94, 44—60. http://doi.org/10.1016/0022–3115(80)90302–5

Boltyanskiy, V.G., & Vilenkin, N.Ya. (1967). Simmetriya v algebre [Symmetry in Algebra]. Moscow: Nauka. (in Russian).

Boren, K., & Huffman, D. (1986). Poglozhenie i rasseyanie sveta malyimi chastitsami [Absorption and Scattering of Light by Small Particles]. Moscow: Publishing house Mir. (in Russian).

Boyd, I.D. (2000). Computation of atmospheric entry flow about a Leonid meteoroid. In: Leonid Storm Research, 93—108. Springer.

Bronshten, V.A. (1981). Fizika meteorovykh yavleniy [Physics of Meteor Phenomena]. Moscow: Nauka. (in Russian).

Bronshten, V.A. (1983). Physics of Meteoric Phenomena. [Translated from Russian (Fizika meteornykh iavlenii, Moscow: Nauka, 1981)]. Dordrecht: Springer. http://doi.org/10.1007/978–94–009–7222–3

Bronshteyn, I.N., & Semendyaev, K.A. (1986). Spravochnik po matematike dlya inzhenerov i uchaschihsya VTUZ-ov [Handbook of Mathematics for Engineers and Students of Higher Technical Schools]. Moscow: Nauka. (in Russian).

Brown, P., & Jones, J. (1995). A determination of the strengths of sporadic radiometeor sources. Earth, Moon, and Planets, 68, 223—245. URL: https://adsabs.harvard.edu/full/1995EM%26P...68..223B

Brown, P., Simek, M., Jones, J., Arlt, R., Hocking, W.K., & Beech, M. (1998). Observations of the 1996 Leonid meteor shower by radar, visual and video techniques. Monthly Notices of the Royal Astronomical Society 300 (1), 244—250. http://doi.org/10.1046/j.1365—8711.1998.01901.x

Brown, P., Jones, J., Weryk, R.J., & Campbell–Brown, M.D. (2004). The Velocity Distribution of Meteoroids at the Earth as Measured by the Canadian Meteor Orbit Radar (CMOR). Earth, Moon, and Planets, 95 (1—4), 617—626. http://doi.org: 10.1007/s11038–005–5041–1

Brown, P., Weryk, R. J., Wong, D.K., & Jones, J. (2008). The Canadian Meteor Orbit Radar Meteor Stream Catalogue. Earth, Moon, and Planets, 102, 209—219. URL: https://aquarid.physics.uwo.ca/research/radar/cmor_pub/cmor_wavelet_EMP.pdf

Brown, P., Wong, D.K., Weryk, R.J., & Wiegert, P. (2010). A Meteoroid Stream Survey Using the Canadian Meteor Orbit Radar-II: Identification of minor showers using a 3D wavelet transform. Icarus, 207, 66—81. URL: https://aquarid.physics.uwo.ca/research/radar/cmor_pub/cmor2.pdf

Brysk, H., & Buchanan, M.L. (1965). Scattering by a cylindrical Gaussian potential: exact solution. Canadian Journal of Physics, 43, 28—37. http://doi.org: 10.1139/p65–003

Bryunelli, B.E., Kochkin, M.I., Presnyakov, I.N., Tereschenko, E.D., & Tereschenko, V.D. (1979). Metod nekogerentnogo rasseyaniya radiovoln [Method of Incoherent Scattering of Radio Waves]. Leningrad: Nauka. (in Russian).

Campbell-Brown, M.D., & Koschny, D. (2004). Model of the ablation of faint meteors. Astronomy & Astrophysics, 418, 751—758. http://doi.org: 10.1051/0004–6361:20041001–1

Campbell-Brown, M.D., & Jones, J. (2006). Annual variations of sporadic radar meteor rates. Monthly Notices of the Royal Astronomical Society, 367 (2), 709—716. http://doi.org: 10.1111/j.1365–2966.2005.09974.x

Campbell-Brown, M.D., & Close S. (2007). Meteoroid structure from radar head echoes. Monthly Notices of the Royal Astronomical Society, 382, 1309—1316. http://doi.org: 10.1111/j.1365–2966.2007.12471.x

Campbell-Brown, M.D. (2008). High resolution radiant distribution and orbits of sporadic radar meteoroids. Icarus, 196, 144—163. http://doi.org: 10.1016/j.icarus.2008.02.022

Campbell-Brown, M.D., & Wiegert, P. (2009). Seasonal variations in the North toroidal sporadic meteor source. Meteoritics and Planetary Science, 44, 1837—1848. URL: https://physics.uwo.ca/~pwiegert/papers/2009MAPS.pdf

Campbell-Brown, M.D., Borovicka, J., Brown, P.G., & Stokan, E. (2013). High-resolution modelling of meteoroid ablation. Astronomy & Astrophysics, 557, A41. http://doi.org: 10.1051/0004–6361/201322005

Campbell-Brown, M.D. (2017). Modelling a short-wake meteor as a single or fragmenting body. Planetary and Space Science, 143, 34—39. http://doi.org: 10.1016/j.pss.2017.02.012

Cannon, P.S. & Shukla, A.K. (1991). Optimum antenna spacing for diversity in meteor burst communications systems. In AGARD, Use or Reduction of Propagation and Noise Effects in Distributed Military Systems 13 p (SEE N91–30362 22–32).

Ceplecha, Z., (1987). Geometric, dynamic, orbital, and photometric data on meteoroids from photographic fireball networks. Bulletin of the Astronomical Institutes of Czechoslovakia, 38, 222—234.

Ceplecha, Z.J., Borovicka, J., Elford, W.G., ReVelle, D.O., & Hawkes, R.L. et al. (1998). Meteor phenomena and bodies. Space Science Reviews, 84, 327—471. http://doi.org: 10.1023/A:1005069928850

Ceplecha, Z., & ReVelle, D.O. (2005). Fragmentation model of meteoroid motion, mass loss, and radiation in the atmosphere. Meteoritics and Planetary Science, 40, 35—54. URL: https://adsabs.harvard.edu/pdf/2005M%26PS...40...35C

Cervera, M.A., & Reid, I.M. (2000). Comparison of atmospheric parameters derived from meteor observations with CIRA. Radio Science, 35 (3), 833—843. http://doi.org: 10.1029/1999RS002226

Chau, J.L., Woodman, R.F., & Galindo, F. (2007). Sporadic meteor sources as observed by the Jicamarca high-power large-aperture VHF radar. Icarus, 188, 162—174. http://doi.org: 10.1016/j.icarus.2006.11.006

Chebotarev, R.P., & Isamutdinov, Sh.O. (1970). Mnogoluchevoy indikator meteornogo radiolokatora [Multi-beam indicator of a meteor radar]. Bulletin of the institute of Astrophysics of the Republic of Tajikistan, (55), 34—39.

Chebotarev, R.P., Sidorin, V.N., & Polushkin, G.A. et al. (1970). Kompleks apparatury dlya radiolokatsionnykh issledovaniy meteorov v Dushanbe [Complex of equipment for meteor radar studies in Dushanbe]. Bulletin of the institute of Astrophysics of the Republic of Tajikistan, (55), 25—28. (in Russian).

Chernogor, L.F. (2018). Fizicheskie effekty Rumynskogo meteoroida [Physical effects of the Romanian meteoroid]. Kosmichna nauka i tekhnologiya, 24 (1), 49—70. (in Russian).

Chernyiy, B.F. (1962). Rasprostranenie radiovoln [Propagation of Radio Waves]. Moscow: Sov. Radio. (in Russian).

Chilson, P.B., Kirkwood, S., & Nilon, A. (1999). The Esrange MST radar: A brief introduction and procedure for range validation using balloons, Radio Science, 34, 427—436. URL: https://agupu.onlinelibrary.wiley.com/doi/pdf/10.1029/1998RS900023

Close, S., Oppenheim, M., Hunt, S., & Coster, A. (2004). A technique for calculating meteor plasma density and meteoroid mass from radar head echo scattering. Icarus, 168, 43—52. http://doi.org: 10.1016/j.icarus.2003.11.018

Close, S., Hamlin, T., Oppenheim, M., Cox, L., & Colestock P. (2008). Dependence of radar signal strength on frequency and aspect angle of nospecular meteor trails. Journal of Geophysical Research, 113, A06203, 113—128. http://doi.org:10.1029/2007JA012647

Cohen, D., Grant, W., & Steele, F. (1989). Meteor Burst System Communications Compatibility. National Telecommunications and Information Administration 89—241, March. 1989. URL: https://www.ntia.doc.gov/files/ntia/publications/89–241_ocr1_20130514113154_215619.pdf

Davis radar main antenna array. (n.d.). Australian Antarctic Division. Retrieved March 23, 2023. URL: http://www.antarctica.gov.au/about–antarctica/history/exploration–and–expeditions/modern–expeditions/this–week–in–antarctica/2003/davis2/vhf–radar–at–davis

Dimant, Y.S., & Oppenheim, M.M. (2017). Formation of plasma around a small meteoroid: Implications for radar head echo. Journal of Geophysical Research, 122 (4). http://doi.org:10.1002/2017JA023960

Draine, B.T. (1977). CRSR Report, № 669, Cornell University.

Draine, B.T., & Salpeter, E.E. (1979). On the physics of dust grains in hot gas. Astrophysical Journal, 231, 77—94. http://doi.org:10.1086/157165

Dyrud, L.P., Urbina, J., Fentzke, J.T., Hibbit, E., & Hinrichs, J. (2011). Global variation of meteor trail plasma turbulence. Annales Geophysicae, 29 (12), 2277—2286. http://doi.org:10.5194/angeo–29–2277–2011

Eshleman, V.R. (1957). The theoretical length distribution of ionized meteor trails, J. Atmospheric and Terrestrial Physics, 10 (2), 57—72.

Eshleman, V.R., & Mlodnoski, R.F. (1961). Harakteristiki napravlennosti meteornogo rasprostraneniya radiovoln [Directional characteristics of meteor propagation of radio waves]. In: Meteor communication on VHF. Moscow: Publ. House of Foreign Literature. (in Russian).

Evans, J.V. (1966). Radar Observation of Meteor Deceleration. Journal of Geophysical Research, 71, 171—188. http://doi.org: 10.1029/JZ071i001p00171

Fadeenko, Y.I. (1967). Razrusheniye meteornykh tel v atmosfere [Destruction of meteor bodies in the atmosphere]. Fizika goreniya i vzryva [Physics of combustion and explosion], 2, 276—280. (in Russian).

Fedynsky, V.V., Kascheev, B.L., & Nechitaylenko, V.A. (1972). Opredeleniye vektora preimushchestvennogo vetra po radionablyudeniyam meteorov [Determination of the predominant wind vector from radio observations of meteors]. Doklady Akademii nauk SSSR [Reports of the Academy of Sciences of the USSR], 203 (5), 1047—1049. (in Russian).

Fedynsky, V.V., Kascheev, B.L., Voloshchuk, Yu.I., & Dyakov, A.A. (1976). Radionablyudeniye meteorov s primeneniyem avtomatizirovannykh sistem [Radio observation of meteors using automated systems]. Vestnik Akademii nauk SSSR [Bulletin of the Academy of Sciences of the USSR], 10, 89—94. (in Russian).

Fernandez, J.A., & Jp, W.–H. On the time evolution of the cometary influx in the region of the terrestrial planets. Icarus, 54 (3), 377—387. http://doi.org:10.1016/0019–1035(83)90235–X

Fisher, W.J. (1934). Mass and Velocity of Meteorites and the Air Density Along Their Luminous Paths. Harvard College Observatory Circular, 385, 1—16.

Forsyth, P.A., Vogan, E.L., & Hines, C.O. (1957). The Principles of JANET — A Meteor-Burst Communications System. Proceedings of the IRE, 45 (12), 1642—1657. http://doi.org:10.1109/JRPROC.1957.278296

Fraser, D.D. (1994). Neural Networks and Early Fast Doppler for Prediction in Meteor-Burst Communications Systems. Submitted in University of KwaZulu-Natal, South Africa. December 1994. URL: https://ukzn–dspace.ukzn.ac.za/handle/10413/6886

Fraser, W.C., Dones, L., Volk, K., Womack, M., & Nesvorný, D. (2022). The Transition from the Kuiper Belt to the Jupiter-Family Comets, chapter in press for the book Comets III. Edited by K. Meech and M. Combi, University of Arizona Press. URL: https://arxiv.org/pdf/2210.16354.pdf

Friichtenicht, J.F., & Becker D.G. (1971). Measurements of the ionization probability of Cu and LaB6 simulated hydrometeors. Astrophysical Journal, 166, 717—724.

Friichtenicht, J.F., & Becker D.G. (1973). Determination of meteor parameters using laboratory simulation techniques, in Evolutionary and Physical Properties of Meteoroids. Edited by C.L. Hemingway, 53—81, NASA, Washington, D.C.

Friichtenicht, J.F., Slattery, J.C., & Hansen, D.O. (1967). Ionization from Fe atoms incident on various gas targets. Physical Review, 163 (1), 75—80. http://doi.org: 10.1103/PhysRev.163.75

Fukao, S., Hashiguchi, H., Yamamoto, M., Tsuda, T., Nakamura, T., & Yamamoto, M.K. et al. (2003). Equatorial Atmosphere Radar (EAR): system description and first results. Radio Science, 38 (3), 1053. http://doi.org:10.1029/2002RS002767

Galactic coordinate system. URL: https://en.wikipedia.org/wiki/Galactic_coordinate_system

Galindo, F.R., Urbina, J.V., Dyrud, J.V., & Fentzke, J. (2014). Modeling the role of atmosphere on the duration of non-specular meteor trails. IEEE Conference, Radio Science Meeting (USNC-URSI NRSM, Accession Number: 14693023). http://doi.org: 10.1109/USNC–URSI–NRSM.2014.6928098

Galligan, D.P., & Baggaley, W.J., (2005). The radiant distribution of AMOR radar meteors. Monthly notices of the Royal Astronomical Society, 359, 551—560. http://doi.org: 10.1111/j.1365–2966.2005.08918.x

Gharmonov, A.B., Filatov, A.G., & Savinkov, A.Y. (2000). Sposob poiska shirokopolosnogo signala i ustrojstvo dlja ego realizacii [Method for searching for a broadband signal and device for its implementation]. Patent No. 2159508 RU.

Glinka, N.L. (2010). Obshchaya khimiya: uchebnoye posobiye dlya vuzov [General chemistry: textbook for universities]. Moscow, Russia: KnoRus Press. (in Russian).

Gorbenko, I.D., Zamula, A.A., & Semenko, E.A. (2015). Ansambl' i korrelyatsionnye svoystva kriptograficheskikh signalov dlya primeneniya v sistemakh i setyakh svyazi [Ensemble and correlation properties of cryptographic signals for applications in telecommunications systems and networks]. Radioelektronika, 181, 110—117. (in Russian). URL: http://nbuv.gov.ua/UJRN/rvmnts_2015_181_15

Gorelov, D.Yu., & Voloshchuk, Yu.I. (2005). Issledovanie fizicheskogo faktora obnaruzhimosti [Study of the physical factor of detectability]. Radioelektronika: Vseukrainskiy mezhvedomstvennyy nauchno-tekhnicheskiy sbornik [Radioelectronics: All-Ukrainian Interdepartmental Scientific and Technical Collection], 143, 215—222. (in Russian).

Green, R.M. (1985). Spherical Astronomy. Cambridge University Press, Cambridge.

Greenhow, J.S., & Neufeld E.L. (1955). The diffusion of ionized meteor trails in the upper atmosphere. Journal of Atmospheric and Solar-Terrestrial Physics, 6, 133—140. http://doi.org: 10.1016/0021–9169(55)90020–9

Grigoryan, S.S. (1979). O dvizhenii i razrushenii meteoritov v atmosferah planet [On the motion and destruction of meteorites in the atmospheres of planets]. Kosmicheskie Issledovaniya [Cosmic Research], 17 (6), 875—893. (in Russian).

Hajduk, A., Hajdukova, M., Porubcan, V., Cevolani, G., & Grai, G. (1999). The ozone concentration in the meteor zone. In: Meteoroids 1998. Editors: W.J. Baggaley and V. Porubcan. Proceedings of the International Conference held at Tatranska Lomnica, Slovakia, August 17—21, 1998. Astronomical Institute of the Slovak Academy of Sciences, 91—97. URL: https://articles.adsabs.harvard.edu//full/1999md98.conf...91H/0000091.000.html

Handbook on national spectrum management [ITU-R edition 2015]. (2015). Geneva, Switzerland: ITU-R. URL: https://www.itu.int/dms_pub/itu–r/opb/hdb/R–HDB–21–2015–PDF–E.pdf

Handbook on radiometeorology (2015). Geneva, Switzerland: ITU-R. URL: https://www.itu.int/dms_pub/itu–r/opb/hdb/R–HDB–26–2013–OAS–PDF–E.pdf

Handbook on Radiometeorology, 2st ed. / ITU-R: Geneva, 2013.

Harris, F.D. (1978). Ispolzovanie okon pri garmonicheskom analize metodom diskretnogo preobrazovaniya Fure [The use of windows in harmonic analysis by the discrete Fourier transform method]. TIIER [Proceedings of the Institute of Electrical and Radioelectronics Engineers], 66 (1), 60—96. (in Russian).

Hasegawa, I.(1993). Historical records of meteor showers. Meteoroids and their parent bodies, Proceedings of the International Astronomical Symposium held at Smolenice, Slovakia, July 6—12, 1992, Bratislava: Astronomical Institute, Slovak Academy of Sciences, 1993. Edited by J. Stohl and I.P. Williams, 209—223.

Hawkes, R.L., & Jones J. (1975). A quantitative model for the ablation of dustball meteors. Monthly Notices of the Royal Astronomical Society, 173, 339—356. http://doi.org: 10.1093/mnras/173.2.339

Heacock, P.K. & Price, F.D. "How the USAF Talks on a Star!" Popular Communications (September 1984), 44—49.

Hellweg, G.A. (1987). Meteor-Burst Communications: Is This What The Navy Needs? Masters Thesis, Naval Post Graduate School, Monterey, CA, June 1987, 771—775. URL: https://core.ac.uk/download/pdf/36715588.pdf

Herlofson, N. (1948). The theory of Meteor ionization. Reports on Progress in Physics, 11, 444—445.

Hocking, W.K. (1987). Turbulence in the region 80—120 km. Advances in Space Research, 7 (10), 171—181. http://doi.org: 10.1016/0273–1177(87)90090–1

Hocking, W.K. (1997). System design, signal-processing procedures, and preliminary results for the Canadian (London, Ontario) VHF atmospheric radar. Radio Science, 32, 687—706. http://doi.org:10.1029/96RS03316

Hocking, W.K., Thayaparan T., & Jones, J. (1997). Meteor decay times and their use in determining a diagnostic mesospheric Temperature-pressure parameter: Methodology and one year of data. Geophysical Research Letters, 24, 2977—2980. http://doi.org:10.1029/97GL03048

Hocking, W.K., Jones, J., & Rendtel, J. (1998). Observations of the Geminids and Quadrantids using a stratosphere — troposphere radar. Monthly notices of the Royal Astronomical Society, 295 (4), 847—859. http://doi.org:10.1046/j.1365–8711.1998.01279.x

Hocking, W.K. (2000). Real-time meteor entrance speed determinations made with interferometric meteor radars. Radio Science, 35(5), 1205—1220. http://doi.org: 10.1029/1999RS002283

Hocking, W.K., Kelley, M., Rogers, R., Brown, W.O. J., Moorcroft, D., & St. Maurice, J.-P. (2001). Resolute Bay VHF radar: a multipurpose tool for studies of tropospheric motions, middle atmosphere dynamics, meteor physics, and ionospheric physics, Radio Science, 36, 1839—1857. http://doi.org: 10.1029/2000RS00100

Hocking, W. K., Fuller, B., & Vandepeer, B. (2001). Real-time determination of meteor-related parameters utilizing modern digital technology. Journal of Atmospheric and Solar-Terrestrial Physics 63 (2), 155—169. http://doi.org: 10.1016/S1364–6826(00)00138–3

Hocking, W.K. (2011). A Review of Mesosphere-Stratosphere-Troposphere (MST) Radar Developments and Studies, circa 1997—2008. Journal of Atmospheric and Solar-Terrestrial Physics, 73 (9), 848—882. http://doi.org:10.1016/j.jastp.2010.12.009

Hoff, J.A. (1988). The Utility of Meteor Burst Communications. IEEE Conference on Military Communications, [MILCOM 88, San Diego, CA, October 1988, vol. 2, 565—570]. http://doi.org: 10.1109/MILCOM.1988.13446

Holdsworth, D.A, Reid, I.M, & Cervera, M.A. (2004). The Buckland Park all-sky interferometric meteor radar-description and first results. Radio Science, 39 (5), 1—12. http://doi.org: 10.1029/2003RS003014

Holovan, E.V., & Kharchenko, V.N. (2020). Kontseptsiya postroeniya perspektivnoy meteornoy radiosvyazi [Concept of building a perspective meteor radio communication sys-

tem]. Radiofizika i Elektronika, 25 (2), 64—73. (in Russian). http://doi.org:10.15407/rej2020.02.064

Holovan, E.V., & Kharchenko, V.N. (2020). Tekhnologiya postroeniya meteornoy radiosvyazi s kodovym deleniem kanalov [Technology for building a meteor radio communication system with code division multiplexing]. Radiofizika i Elektronika, 25 (2), 74—81. (in Russian). http://doi.org:10.15407/rej2020.02.074

Hönl, H., Maue, A., & Westphal, K. (1964). Teoriya difraktsii [Theory of diffraction]. Ed. G.D. Malyuzhints; translation from German by N.G. Vakhitov, V.I. Ivanov, M.P. Sakharova. Moscow: Mir. (in Russian). URL: https://biblioclub.ru/index.php?page=book&id=487648

How Comets Move [Center for Scientific Creation]. URL: https://www.creationscience.com/onlinebook/Comets4.html

International Civil Aviation Organization. (2002). Rukovodstvo po Vsemirnoy geodezicheskoy sisteme-1984 (WGS-84) [Manual on the World Geodetic System-1984 (WGS-84)]. Doc 9674 AN/946 (2nd ed.). (in Russian).

Ishimaru, A. (1978). Wave propagation and scattering in random media. New York: Academic Press.

Ivanov, A.V., Yaroshevsky, A.A., & Ivanova M.A. (2019). Minerals of meteorite — a new catalog [Minerals of meteorite — a new catalog]. Geohimiya [Geochemistry], 64 (8), 869—932. (in Russian).

Jacchia, L.G. (1955). The Physical Theory of Meteors. VIII. Fragmentation as Cause of the Faint-meteor Anomaly. Astrophysical Journal, 121. http://doi.org:10.1086/146012

Jacchia, L.G. (1955). The Physical Theory of Meteors. VIII. Fragmentation as Cause of the Faintmeteor Anomaly. The Astrophysical Journal, 121, 521—527. http://doi.org:10.1086/146012

Janches, D., Hocking, W., Pifko, S., Hormaechea, J.L., Fritts, D.C., & Brunini, C. et al. (2014). Interferometric meteor head echo observations using the Southern Argentina Agile Meteor Radar. Journal of Geophysical Research: Space Physics, 119, 2269—2287. http://doi.org:10.1002/2013JA019241

Janches, D., Close, S., Hormaechea, J.L., Swarnalingam, N., Murphy, A., & O'Connor, D. et al. (2015). The Southern Argentina Agile Meteor Radar Orbital System (SAAMER-OS): An Initial Sporadic Meteoroid Orbital Survey in the Southern Sky. The Astrophysical Journal, 809 (1). http://doi.org: 10.1088/0004–637X/809/1/36

Janches, D., Bruzzone, J.S., Hormaechea, J.L., Weryk, R., Gural, P., & Matney, M. et al. (2019). A status update on Southern Hemisphere Meteoroid Measurements with SAAMER. First Int'l. Orbital Debris Conf. 2019 (LPI Contrib. No. 2109). URL: https://www.hou.usra.edu/meetings/orbitaldebris2019/orbital2019paper/pdf/6064.pdf

Janches, D., Bruzzone, J.S., Hormaechea, J.L., Weryk, R., Gural, P., & Matney, M. et al. (2019). A status update on Southern Hemisphere Meteoroid Measurements with SAAMER. First Int'l. Orbital Debris Conf. 2019 (LPI Contrib. No. 2109). URL: https://www.hou.usra.edu/meetings/orbitaldebris2019/orbital2019paper/pdf/6064.pdf

Jenniskens, P. (2006). Meteor Showers and their Parent Comets. Cambridge University Press, New York, USA.

Jernovics, J.P. (1990). Meteor Burst Communications: An Additional Means Of Long-Haul Communications. URL: https://www.globalsecurity.org/space/library/report/1990/JJP.htm

Jewitt, D. (2012). The Active Asteroids. Astron. J., 143, 66—70. http://doi.org:10.1088/0004–6256/143/3/66

Johnson, D.E. (1987). Ten years experience with SNOTEL meteor burst data acquisition system. Proc. Meteor Burst Commun. Sym., vol. SII, 5—20, Nov. 1987.

Jones, J., & Collins, J.G. (1974). The mass distribution of radio meteors and the full-wave scattering theory. Monthly Notices of the Royal Astronomical Society, 166, 529—542. URL: https://adsabs.harvard.edu/full/1974MNRAS.166..529J

Jones, J., McIntosh, B.A., & Šimek, M.(1990). Ozone and the Duration of Overdense Radio Meteors. Journal of Atmospheric and Solar-Terrestrial Physics, 52, 253—258. http://doi.org: 10.1016/0021–9169(90)90092–2

Jones, J., & Brown, P.G. (1993). Sporadic meteor radiant distribution: Orbital survey results. Monthly of the Royal Astronomical Society, 359, 1131—1136. http://doi.org:10.1093/mnras/265.3.524

Jones, J. (2004). Meteoroid Engineering Model — Final Report. SEE/CR-2004-400, June 2004. URL: https://www.nasa.gov/pdf/ 192930main_SEECR–2004–400_MOD_MEM.pdf

Jones, J., Brown, P., Ellis, K.J., Webster A.R., Campbell-Brown, M., & Krzemenski, Z. et al. (2005). The Canadian Meteor Orbit Radar: system overview and preliminary results. Planetary and Space Science, 53, 413—421. http://doi.org: 10.1016/J.PSS.2004.11.002

Jones, J., & Campbell-Brown, M., (2005). The initial train radius of sporadic meteors. Monthly Notices of the Royal Astronomical Society, 359 (3), 1131—1136. http://doi.org: 10.1111/j.1365–2966.2005.08972.x

Jones, W., & Jones J. (1990). Ionic diffusion in meteor trains. Journal of Atmospheric and Solar–Terrestrial Physics, 52 (3), 185—191. http://doi.org: 10.1016/0021–9169(90)90122–4

Jones, W. (1991). Theory of diffusion of meteor trains in the geomagnetic field. Planetary and Space Science, 39, 1283—1288. http://doi.org: 10.1016/0032–0633(91)90042–9

Jones, W. (1995). Theory of the initial radius of meteor trains. Monthly Notices of the Royal Astronomical Society, 275, 812—818. URL: https://adsabs.harvard.edu/full/1995MNRAS.275..812J

Jones, W. (1997). Theoretical and observational determinations of the ionization coefficient of meteors. Monthly Notices of the Royal Astronomical Society, 288 (4), 995—1003. http://doi.org: 10.1093/mnras/288.4.995

Kaiser, T.R. (1955). The Incident Flux of Total Meteoric Ionization. Journal of Atmospheric and Terrestrial Physics, 2, 55—64.

Kascheev, B.L., & Lebedinets, V.N. (1961). Radiolokatsionnye issledovaniya meteornykh yavlenii [Radar studies of meteor phenomena]. Moscow: Izdatelstvo AN SSSR [Publishing House of the Academy of Sciences of the USSR] (in Russian).

Kascheev, B.L., Lebedinets, V.N., & Lagutin, M.F. (1967). Meteornye yavleniya v atmosfere Zemli [Meteor phenomena in the Earth's atmosphere]. Moscow: Nauka. (in Russian).

Kascheev, B.L., Voloshchuk, Y.I., & Dudnik, B.S. et al. (1977). Meteornaya avtomatizirovannaya radiolokatsionnaya sistema [Meteor Automated Radar System]. Meteornye Issledovaniya [Meteor Research], 4, 11—61. (in Russian).

Kascheev, B.L., & Tkachuk, A.A. (1979). Rasprostranenie elementov orbit melkikh meteornykh tel [Distribution of elements of orbits of small meteor bodies]. Problemy Kosmicheskoi Fiziki [Problems of Space Physics], 14, 44—51. (in Russian).

Kascheev, B.L., Tkachuk, A.A., & Kremer, E.N. (1980). Rezultaty radiolokatsionnykh nablyudenii slabykh meteorov: Katalog orbit meteorov do +12. Materialy Mirovogo Tsentra dannykh "B" [Results of radar observations of weak meteors: Catalog of meteor orbits up to +12. Materials of the World Data Center "B"]. Moscow: Proizvodstvenno-izdatel'skii kombinat VINITI. (in Russian).

Kascheev, B.L., & Tkachuk, A.A. (1982). Rezultaty radiolokatsionnykh nablyudenii slabykh meteorov. Katalog orbit meteorov do +12m [Results of radar observations of weak meteors. Catalog of meteor orbits up to +12m]. Moscow: Materialy Mirovogo Tsentra dannykh "B" [Materials of the world data center "B"]. (in Russian).

Kascheev, B.L., Zhukov, E.T., Koval, Y.A., & Dudnik, B.S. (1989). Meteoraya sinkhronizatsiya shkal vremeni [Meteor Time Scale Synchronization]. (B.I. Makarenko, Ed.). Kiev: Naukova dumka. (in Russian).

Kascheev, B.L., Koval, Y.O., Gorbach, V.I., & Bondar, B.G. (1996). Meteory segodnya [Meteors today]. Kyiv: Tekhnika. (in Russian).

Kascheev, B.L., Leshchenko, L.N., & Semenov, A.I. (2000). Sezonnyie osobennosti mnogoletnih variatsiy temperaturyi sredney atmosferyi [Seasonal features of long-term variations of the

middle atmosphere temperature]. Report Russian Academy of Sciences, 374 (6), 816—819. (in Russian).

Kascheev, B.L., Proshkin, E.G., & Lagutin, M.F. (Eds.). (2002). Distantsionnyie metodyi issledovaniya protsessov v atmosfere Zemli [Remote sensing methods for studying processes in the Earth's atmosphere]. Kharkov: Kharkiv National University of Radio Electronics; Business Inform. (in Russian).

Kawamura, S., Tsutsumi, M., & Murayama, Y. (2007). Wind estimations with meteor observations by MF radars at Poker Flat, Alaska and Wakkanai. Japan, Journal of the National Institute of Information and Communications Technology, 54 (1—2), 67—75. URL: https://www.nict.go.jp/publication/shuppan/kihou–journal/journal–vol54no1.2/01–02C.pdf

Kazantsev, A.N. (Ed.). (1961). Meteornaya radiosvyaz na ultrakorotkikh volnak [Meteor Radio Communication on Ultra-Short Waves]. Moscow: Inostrannaya Literatura. (in Russian).

Kennedy, R. (1973). Kanaly svyazi s zamiraniyami i rasseivaniem [Channels of communication with fading and scattering], (I.A. Ovseevich, Trans.). Moscow: Sov. radio. (in Russian).

Kero, J. (2008). High resolution meteor exploration with tristatic radar methods IRF Scientific Report 293, 2008. URL: https://www.diva–portal.org/smash/get/diva2:141525/FULLTEXT01.pdf

Kero, J., Szasz, C., Nakamura, T., Meisel, D.D., Ueda, M., & Fujiwara, Y. et al. (2012). The 2009—2010 MU radar head echo observation programme for sporadic and shower meteors: radiant densities and diurnal rates. Monthly Notices of the Royal Astronomical Society, 425, 135—146. http: //doi.org: 10.1111/j.1365 2966.2012.21407.x

Kero, J., Szasz, C., Nakamura, T., Terasawa, T., Miyamoto, H., & Nishimura K. (2012). A meteor head echo analysis algorithm for the lower VHF band. Annales Geophysicae, 30, 639—659. http: //doi.org: 10.5194/angeo–30–639–2012

Kero, J., Kastinen, D., Vierinen, J., Grydeland, T., Heinselman, C., & Markkanen, J. et al. (2019). EISCAT 3D: the next generation international atmosphere and geospace research radar. Proceedings of the First NEO and Debris Detection Conference, Darmstadt, Germany, 22—24 January 2019. URL: https://conference.sdo.esoc.esa.int/proceedings/neosst1/paper/471

Khachaturov, V.R., Konovalchik, O.S., Kharchenko, V.M., Vdovichenko, Y.I., & Holovan', O.V. (2014). Sposib poshuku shirokosmugovogo signalu [Broadband signal search method]. Patent No. 91862 UA.

Khanukaeva, D.Yu. (2002). Aerotermoballistika yedinogo i drobyashchegosya meteoroida v neizotermicheskoy atmosfere [Aerothermoballistics of a single and fragmented meteoroid in a non-isothermal atmosphere]. (in Russian). URL: https://www.dissercat.com/content/aerotermoballistika–edinogo–i–drobyashchegosya–meteoroida–v–neizotermicheskoi–atmosfere

Kharchenko, H.V. (2008). Analiz vliyaniya parametrov kvantovatelya na kachestvo tsifrovoy obrabotki signalov s rasshirennym spektrom [Analysis of the influence of quantizer parameters on the quality of digital signal processing with an extended spectrum]. Systemy obrobky informatsiyi [Systems of Signal Processing], 2, 121—127. (in Russian).

Kharchenko, H.V., Tkalich, I.O., & Vdovychenko, Y.I. (2009). Two-criterial DS synchronization method efficiency research. Proceedings of 7th IEEE East-West Design and Test Symposium (EWDTS'09), 165—174. Kharkov—Moscow: KhNURE. http: //doi.org: 10.1109/EWDTS.2010.5742116

Kharchenko, H.V. (2010). Estimated formation probability of meteoric trails with specular reflection. Proceedings of 8-th IEEE East-West Design and Test Symposium (EWDTS'10), 289—291. Kharkov—St. Peterburg: KNURE.

Kharchenko, H.V. (2010). Mathematical model to estimate the probability of formation of the meteor trails with a specular reflection. Modern Problems of Radio Engineering, Telecommunications and Computer Science. Proceedings of the Xth International Conference TCSET'2010, 344. Lviv—Slavske. URL: https://ieeexplore.ieee.org/document/5445963

Kharchenko, H.V. (2010). Metod otsenki intervala rasseyaniya po zapazdyvaniyu pri otrazhenii signalov ot meteornykh sledov [Method for estimating the delay spread interval when reflecting signals from meteor trails]. Radiotekhnika, Kharkov: KhNURE, 160, 56—61. (in Russian).

Kharchenko, H.V. (2011). Metod rascheta oblastey naiboleye veroyatnogo poyavleniya meteornykh sledov, imeyushchikh tochku zerkal'nogo otrazheniya [Method for calculating the areas of the most probable occurrence of meteor trails having a point of specular reflection]. Radiotekhnika, Kharkov: KhNURE, 166, 186—192. (in Russian).

Kharchenko, H.V. (2011). Rasseyaniye radiosignala na meteornom slede [Scattering of a radio signal on a meteor trail]. Bulletin of Kharkiv National University. Radiofizyka ta elektronika [Radio Physics and Electronics], 966, 90—96. (in Russian). URL: http://irbis–nbuv.gov.ua/publ/REF–0000365292

Kharchenko, H.V. (2011). Rasseyaniye radiosignala na nedouplotnennom meteornom slede [Scattering of a radio signal on an underdense meteor trail]. Radiotekhnika, Kharkov: KhNURE, 167, 34—43.

Kharchenko, H.V. (2012). Model meteornogo radiokanala, osnovannaya na reshenii difraktsionnoy zadachi rasseyaniya signala na ionizirovannom slede [Model of the meteor radio channel based on the solution of the diffraction problem of signal scattering on an ionized trail], 164. (in Russian). URL: https://catalogue.nure.ua/document=146196

Kharchenko, H.V. (2012). Model meteornogo radiokanala, osnovannaya na reshenii difraktsionnoy zadachi rasseyaniya signala na ionizirovannom slede [Model of the meteor radio channel based on the solution of the diffraction problem of signal scattering on an ionized trail], 20. (in Russian). URL: https://openarchive.nure.ua/server/api/core/bitstreams/63f21612–8e8c–4729–9099–e9d81a7769d4/content

Kharchenko, H.V. (2012). Calculation of the areas most likely to appear suitable for communication meteor trails. International journal of electronic and telecommunications, 58 (2), 105—110. http://doi.org: 10.2478/v10177–012–0014–6

Kharchenko, V.N. (1988). Sintez optimalnogo priyemnika pri zamiraniyakh i rasseyanii signalov po zapazdyvaniyu [Synthesis of an optimal receiver in the presence of fading and dispersion of signals by delay]. Radiotekhnika, 6, 13—16. (in Russian).

Kharchenko, V.N., Lavrut, A.A., & Lavrut, T.V. (2006). Metod postroyeniya sistemy sinkhronizatsii slozhnykh sostavnykh signalov [Method of constructing a synchronization system for complex composite signals]. Radioelektronni ta kompiuterni systemy [Radioelectronics and Computer Systems], 5, 193—197. (in Russian). URL: http://nbuv.gov.ua/UJRN/recs_2006_5_34

Kolomiyets, S.V. (2012). Kharkiv automated meteor radio system "MARS": Its historical significance in radio astronomy. 2012 22nd International Crimean Conference "Microwave & Telecommunication Technology". Date of Conference: 10—14 September 2012. URL: https://ieeexplore.ieee.org/document/6335836

Korn, G., & Korn, T. (2003). Spravochnik po matematike dlya nauchnykh rabotnikov i inzhenerov [Handbook of mathematics for scientists and engineers]. Moscow: Nauka. (in Russian).

Korneev, V.A., Sidorov, V.V., & Epiktetov, L.A. (2007). Nanosekundnaya sinkhronizatsiya shkal vremeni po meteorinym radiootrazheniyam i ee primenenie k zashchite informatsii [Nanosecond synchronization of time scales based on meteoric radio reflections and its application to information security]. Uchenye Zapiski Kazanskogo Universiteta. Seriya Fiziko-Matematicheskie Nauki [Scientific notes of Kazan University. Series Physical and Mathematical Sciences], 149 (3), 83—96. (in Russian).

Koval, Y.A., Kostyrya, A.A., & Priymak, V.Y. (2012). Otsenivanie neopredelennosti izmereniy pri slicheniyah etalonov vremeni i chastotyi radiotehnicheskimi metodami [Estimation of measurement uncertainty during comparisons of time and frequency standards by radio

engineering methods]. Sistemy Obrabotki Informatsii [Information Processing Systems], 21(99), 30—33. (in Russian).

Kozin, I.D., Zelenkov, V.E., Vasilev, I.V., & Kipshakbaev, A.I. (2002). Method of meteor radio communication (options) and system for its implementation (options). Eurasian Patent Organization EA002406B1. (in Russian). URL: https://patents.google.com/patent/EA002406B1/ru

Kravtsov, Yu.A., Feyzulin, Z.I., & Vinogradov, A.G. (1983). [Passage of radio waves through the Earth's atmosphere]. Moscow: Radio i svyaz [Radio and communication]. (in Russian).

Kuiper Belt — Facts and Information [by Planets Education/Solar System]. URL: https://planetseducation.com/kuiper–belt–facts/

Kulikov, K.A. (1976). Kurs sfericheskoi astronomii [Course of spherical astronomy]. Moscow: Nauka. (in Russian).

Kuzmin, S.Z. (2000). Tsifrovaya radiolokatsiya. Vvedenie v teoriyu [Digital radiolocation. Introduction to theory]. Kiev: Izdatelstvo KViTS. (in Russian).

Kuznetsov, O. O., Kovalenko, A. M., Harchenko, H. V., & Nosik, O. M. (2007). Formuvannya velikikh ansamblei diskretnikh signaliv z polipshenimi korelyatsiynimi vlastivostyami [Formation of large ensembles of discrete signals with improved correlation properties]. Sistemi Ozbroennya I Viyskova Tekhnika, 1 (9), 94—98. (in Ukrainian). URL: http://nbuv.gov.ua/UJRN/soivt_2007_1_27

Landau, L.D., & Lifshitz, E.M. (1973). Teoriya polya [Field theory]. [6th corrected and supplemented edition]. Moscow: Nauka. (in Russian).

Larsen, J.D., Mawrey, R.S., & Weitzen J.A. (1992). The use of antenna beam steering to improve the performance of meteor burst communications systems. Military Communications Conference 1992. MILCOM '92 Conference Record. Communications Fusing Command Control and Intelligence. IEEE, 12—17, vol. 1.

Leavens, W.M. (1965). Scattering Resonances of a Cylindrical Plasma. RADIO SCIENCE Journal of Research of the National Bureau of Standards, 69D (10), 1321—1333. URL: https://nvlpubs.nist.gov/nistpubs/jres/69D/jresv69Dn10p1321_A1b.pdf

Levin, B.Y. (1956). Fizicheskaya teoriya meteorov i meteornoye veshchestvo v Solnechnoy sisteme [Physical theory of meteors and meteoric matter in the solar system]. Moscow: Gosudarstvennoye izdatelstvo fiziko-matematicheskoy literatury [State publishing house of physical and mathematical literature]. (in Russian).

Levin, B.Y. (1963). O fragmentatsii meteornykh tel [On the fragmentation of meteor bodies]. Astronomicheskiy zhurnal [Astronomical journal], 40 (2), 304—311. (in Russian).

Lindblad, B.A. (1967). Solar cycle variations in atmospheric density as deduced from meteor observations. Space Research, 7, 1029—1043.

Liou, K-N. (1972). Electromagnetic scattering by arbitrarily oriented ice cylinders. Applied Optics, 11 (3), 667—674. http: //doi.org: 10.1364/AO.11.000667

Losev, Yu.I., Berdnikov, A.G., Goykhman, E.Sh., & Sizov, B.D. (1988). Adaptivnaya kompensatsiya pomekh v kanalakh svyazi [Adaptive Interference Compensation in Communication Channels]. (Yu.I. Losev, Ed.). Moscow: Radio i svyaz. (in Russian).

Lowry, S.C., Fitzsimmons, A., Lamy, P., & Weissman, P. (2008) Kuiper-Belt Objects in the Planetary Region: The Jupiter Family Comets. In: Barrucci, M.A., Boehnhardt, H., Cruikshank, D.P., Morbidelli, A., & Dotson, Renee et al. The Solar System Beyond Neptune. Space Science Series. The University of Arizona Press, Tucson, USA, 397—410. URL: http://web.mit.edu/axs/Public/papers_to_print/Lowry_JFCs.pdf

Lykov, Y. V., Oleynikov, A. N., Kukush, V. D., & Shkarlet, A. I. (2010). Rezultaty issledovaniya parametrov meteornykh otrazheniy signalov televizionnogo veshchaniya raznesennoy radiolokatsionnoy sistemoi [Results of studying the parameters of meteor reflections of television broadcasting signals by a distributed radar system]. Systemy obrobky informatsiyi, 1 [Information Processing Systems, 1], 110—118. (in Russian). URL: http://nbuv.gov.ua/UJRN/soi_2010_1_29

Lyons, R. (2006). Tsifrovaya obrabotka signalov: Vtoroe izdanie [Digital signal processing: 2 ed. (Translated from English). Moscow: LLC "Binom Press". (in Russian).

Mak–Daniel, I. (1967). Protsessy stolknovenii v ionizirovannykh gazakh [Collision Processes in Ionized Gases]. (L.A. Artsimovich, Ed., & Trans.). Moscow: Mir. (in Russian).

Maksimov, F.A. (2013). Sverkhzvukovoe obtekhanie sistemy tel [Supersonic Flow around a System of Bodies]. Kompyuternyie issledovaniya i modelirovanie [Computer Research and Modeling], 5 (6), 969—980. (in Russian).

Marshall, R.A., Brown, P., & Close, S. (2017). Plasma distributions in meteor head echoes and implications for radar cross-section interpretation. Planetary and Space Science, 143, 203—208. http://doi.org:10.1016/j.pss.2016.12.011

Matsunanmi, A., Yamamura, Y., Itikawa, Y., Itoh, N., Kazumata, Y., & Miyagawa, S. et al. (1980). A semiempirical formula for the energy dependence of the sputtering yield. Radiation Effects and Defects in Solids, 57, 15—21. http://doi.org: 10.1080/01422448008218676

Mawrey, R.S., & Weitzen J.A. (1995). Measured performance of meteor burst systems using antenna beam steering. Communications IEEE Transactions, 43, 1467—1476. http://doi.org: 10.1109/26.380196

McCrea, I., Aikio, A., Alfonsi, L., Belova, E., Buchert, S., & Clilverd, M. et al. (2015). The science case for the EISCAT_3D radar. Progress in Earth and Planetary Sciences, 2, Article number: 21. http://doi.org: 10.1186/s40645–015–0051–8

McCrosky, R.E. (1955). Phisical and statistical studies of meteor fragmentation. Harvard Univ., 1955.

McCrosky, R.E. (1958). The Meteor Wake. Astronomical Journal, 63, 97—106.

McKinley, D.W.R. (1961). Meteor Science and Engineering. McGraw-Hill, New York.

McKinlay, D. (1964). Metody meteornoi radioastronomii [Methods of Meteor Radio Astronomy]. Moscow: Mir. (in Russian).

Medvedev, A.V. (2014). Razvitie metodov i apparatnykh sredstv radiofizicheskikh issledovanii verkhnei atmosfery Zemli na Irkutskom radarnekoherentnogo rasseyaniya [Development of Methods and Equipment for Radio Physics Research of the Upper Atmosphere of the Earth on the Irkutsk Incoherent Scatter Radar]. Siberian Branch of the Russian Academy of Sciences, Irkutsk. (in Russian). URL: http://ru.iszf.irk.ru/images/9/90/%D0%9C%D0%B5%D0%B4%D0%B2%D0%B5%D0%B4%D0%B5%D0%B2_%D0%B4%D0%B8%D1%81%D1%81%D0%B5%D1%80%D1%82%D0%B0%D1%86%D0%B8%D1%8F.pdf

Melville, S.W., Larsen, J.D., Letschert, R.Y., & Goddard, W.D. (1989). The classification of meteor trail reflections by a rule-based system. Transactions of the SAIEE, 80 (1), 104—116.

Melville, S.W., & Fraser, D.D. (1993). Meteor burst communication. Transactions of the SAIEE, 84 (3), 60—68.

Melville, S., Sutcliffe, G., & Fraser, D. (1996). Using Artificial Neural Networks for Meteor-Burst Communications Trail Prediction. Pacific Rim International Conferences on Artificial Intelligence 1996, 423—434. http://doi.org: 10.1007/3–540–61532–6_36

Menees, G.P., & Park, C. (1976). Nitric oxide formation by meteoroids in the upper atmosphere. Atmospheric Environment, 10, 535—545. http://doi.org: 10.1016/0004–6981(76)90180–3

Menzer, D.R. (1958). Difraktsiya i rasseyanie radiovoln [Diffraction and Scattering of Radio Waves]. Moscow: Sov. Radio. (in Russian).

Mie, G. (1908). Beiträge zur Optik trüber Medien, speziell kolloidaler Metallösungen. Leipzig, Annalen der Physik [Annals of Physics], 330, 377—445. (in German). http://doi.org: https://dx.doi.org/10.1002/andp.19083300302

Miroshnikov, V.I., Budko, P.A., & Zhukov G.A. (2019). Osnovnyye napravleniya razvitiya meteornoy svyazi [The main directions of development of meteor communication]. Naukoyemkiye tekhnologii v kosmicheskikh issledovaniyakh Zemli [Science-intensive technologies in space research of the Earth], 11 (4), 30—47. (in Russian). http://doi.org: 10.24411/2409–5419–2018–10277

Miroshnikov, V.I., Budko, P.A., & Zhukov, G.A. (2019). Sostavnoi trakt dovedeniya informatsii do robototekhnicheskikh kompleksov v severnykh moryakh [Composite Path for Information Delivery to Robotic Systems in the Northern Seas]. Tekhnika Sredstv Svyazi [Telecommunications Equipment Engineering], 3 (147), 2—26. (in Russian).

Mishenina, L.N., & Shelkovnikov, V.V. (2007). Spravochnye materialy po khimii [Reference Materials on Chemistry]. (2nd ed.). Tomsk: Izdatelstvo Tomskogo Universiteta. (in Russian).

Monzingo, R.A., & Miller, T.W. (1986). Adaptivnyye antennyye reshetki: Vvedeniye v teoriyu [Adaptive Antenna Arrays: Introduction to Theory]. (Translation edited by V.A. Lexachenko). Moscow: Radio i Svyaz. (in Russian).

Moorhead, A.V., Brown, P.G., Campbell-Brown, M.D., Heynen, D., & Cooke, W.J. (2017). Fully correcting the meteor speed distribution for radar observing biases. Planetary and Space Science, 143, 209—217. http://doi.org: 10.1016/j.pss.2017.02.002

Morris, R.J., Murphy, D.J., Reid, I.M., Holdsworth, D.A., & Vincent, R.A. (2004). First polar mesosphere summer echoes observed at Davis, Antarctica (68.6°S). Geophysical Research Letters, 31, L16111. http://doi.org: 10.1029/2004GL020352

Naishadham, K., & Piou, J.E. (2010). Analytical characterization and validation of creeping waves on dielectric coated and perfectly conducting cylinders. Radio Science, 45, RS5014. http://doi.org: 10.1029/2009RS004241

Nakamura, T., Tsuda, T., Tsutsumi, M., Kita, K., Uehara, T., & Kato, S. et al. (1991). Meteor wind observations with the MU radar. Radio Science, 26 (4), 857—869. http://doi.org: 10.1029/91RS01164

Nakamura, T., Tsuda, T., & Tsutsumi, M. (1997). Development of an external interferometer for meteor wind observation attached to the MU radar. Radio Science, 32 (3), 1203—1214. http://doi.org:10.1029/97RS00091

Narziev, M., & Chebotarev, R.P. (2017). O kataloge radjantov, skorostej, orbit i atmosfernyh traektorij 4500 radiometeorov, nablyudaemyh v Tadzhikistane. In O.V. Mozgovij (Ed.). Memorialna VII mizhnarodna konferentsiia z astronomii CAMMAC-2017, Vinnytsia, 26—28 veresnia 2017 r.: statti i tezy. Vinnytsia: FOP Pyshnyi O.A. (in Russian).

National Geospatial-Intelligence Agency (NGA). Standardization Document. (2014). [World Geodetic System 1984: Its Definition and Relationships with Local Geodetic Systems. NGA. STND. 0036_1.0.0_WGS84, Version 1.0.0, Department of Defense. Office of Geomatics]. URL: https://nsgreg.nga.mil/doc/view?i=4085

Neganov, V.A., & Osipov, O.V. (2000). Rasseyanie ploskih elektromagnitnyh voln na kiralyano–metallicheskom cilindre. Pis'ma v Zhurnal tekhnicheskoy fiziki, 26 (1), 77—83.

Nesvorný, D., Vokrouhlický, D., Pokorný, P., & Janches, D. (2011). Dynamics of dust particles released from Oort cloud comets and their contribution to radar meteors. The Astrophysical Journal, 743 (1), 37. http://doi.org: 10.1088/0004–637X/743/1/37

Nikolskij, V.V., & Nikolskaya, T.I. (1989). Elektrodinamika i rasprostranenie radiovoln [Electrodynamics and propagation of radio waves]. Moskva: Nauka.

Nussbaumer, G. (1981). Fast Fourier Transform and Convolution Algorithms. Springer—Verlag, Berlin, 1981.

Obrubov, Y.V. (1991). Kompleksy malyh tel Solnechnoj sistemy. [Complexes of small bodies of the solar system]. Astronomicheskiy Zhurnal [Astronomical journal], 68 (5), 1063—1073. (in Russian).

Olsson-Steel, D. (1988). Identification of meteoroid streams from Apollo asteroids in the Adelaide Radar Orbit surveys. Icarus 75, 64—96. http://doi.org: 10.1016/0019–1035(88)90127–3

Oort, J.H. (1950). The Structure of the Cloud of Comets surrounding the Solar System and a Hypothesis concerning its Origin. Bulletin of the Astronomical Institutes of the Netherlands, 11, 91—110. URL: https://articles.adsabs.harvard.edu/pdf/1950BAN....11...91O

Oort, J.H. (1951). Origin and Development of Comets. Observatory, 71, 129. URL: https://adsabs.harvard.edu/full/1951Obs....71..129O

Öpik, E. (1937). Researches on the physical theory of meteor phenomena. III. Basic of the physical theory of meteor phenomena. Publications of the Tartu Astrofizica Observatory, 29, 1—69. URL: https://adsabs.harvard.edu/full/1936PTarO..29E...1O

Öpik, E.J. (1958). Physics of Meteor Flight in the Atmosphere. Interscience Publishers, New York.

Ostergaard, J.C., Rasmuen, J.E., Sowa, M.J., Quinn, J.M., & Kossey, P.A. (1985). Characteristics of High-Latitude Meteor Scatter Propagation Parameters over the 45—104 MHz Band. In: AGARD Propagation Effects on Military Systems in the High Latitude Region 15 p (SEE N86-27531 18—32).

Pascale, M., Miano, G. & Forestiere, C. (2017). Spectral theory of electromagnetic scattering by a coated sphere. Journal of the Optical Society of America B, 34 (7), 1524—1535. http: //doi.org: 10.1364/JOSAB.34.001524

Pestryakov, V.B. (1969). Shumopodobnyye signaly v sistemakh peredachi informatsii [Noise-like signals in information transmission systems]. Moscow: Sov. radio. (in Russian).

Pokorný, P., Vokrouhlický, D., Nesvorný, D., Campbell-Brown, M., & Brown, P. (2014). Dynamical model for the toroidal sporadic meteors. The Astrophysical Journal, 789 (1), 25. http: //doi.org: 10.1088/0004–637X/789/1/25

Pokorný, P., Janches, D., Brown, P. & Hormaechea, J.L. (2017). An orbital meteoroid stream survey using the Southern Argentina Agile MEteor Radar (SAAMER) based on a wavelet approach. Icarus 290, 162—182. http: //doi.org: 10.1016/j.icarus.2017.02.025

Popkov, V.A., & Puzakov, S.A. (2010). Obshchaya khimiya: uchebnik [General chemistry: textbook]. Moscow: GEOTAR-Media. (in Russian).

Portnyagin, Y.I., Shprenger, K., Lysenko, I.A., Shminder, R., Orlyanskiy, A.D., & Grayziger, K.M. et al. (1978). Izmereniye vetra na vysotakh 90—100 km nazemnymi metodami [Wind measurement at heights of 90—100 km by ground-based methods]. Leningrad: Gidrometeoizdat. (in Russian).

Porubcan, V., Kornos, L., & Williams, I.P. (2004). Associations Between Asteroids and Meteoroid Streams. Earth, Moon and Planets, 95 (1—4), 697—712. http: //doi.org: 10.1007/s11038–005–2243–5

Porubcan, V., & Kornos, L. (2005). The Quadrantid meteor stream and 2003 EHl. Contributions of the Astronomical Observatory Skalnaté Pleso, 35 (1), 5—16. URL: https://www.ta3.sk/caosp/Eedition/FullTexts/vol35no1/pp5–16.pdf

Porubcan, V., Kornos, L., & Williams, I.P. (2006). The Taurid complex meteor showers and asteroids. Contributions of the Astronomical Observatory Skalnaté Pleso, 36 (2), 103—117. URL: https://www.ta3.sk/caosp/Eedition/FullTexts/vol36no2/pp103–117.pdf

Potekhin, A.I. (1948). Nekotoryye zadachi difraktsii elektromagnitnykh voln [Some problems of diffraction of electromagnetic waves]. Moscow: Sov. radio. (in Russian).

Potekhin, A.P., Setarov, A.G., Lebedev, V.P., Medvedev, A.V., & Kushnarev, D.S. (2016). Perspektivnyy radar NR-MST: potentsial i diagnosticheskiye vozmozhnosti [Prospective IS-MST radar: potential and diagnostic capabilities]. Solnechno-Zemnaya Fizika [Solar-Terrestrial Physics], 2 (3), 3—16. (in Russian).

Recommendation ITU-R F. 1113. Radio systems employing meteor-burst propagation (Question ITU-R 157/9)

Recommendations ITU-R P.372-8: Radio noise (Question ITU-R 214/3). URL: https://www.itu.int/dms_pubrec/itu–r/rec/p/R–REC–P.372–8–200304–S!!PDF–E.pdf

Recommendations ITU–R P.843–1: Communication by meteor burst propagation. (Question ITU-R 221/3, 08/28/1997). URL: https://www.itu.int/dms_pubrec/itu–r/rec/p/R–REC–P.843–1–199708–I!!PDF–E.pdf

Reid, I., Holdsworth, D., Morris, R., Murphy, D., & Vincent, R. (2006). Meteor observations using the Davis mesosphere-stratosphere-troposphere radar. J. Geophys. Res., 111, A05305. http: //doi.org: 10.1029/2005JA011443

Roberts, I.D., Hawkes, R.L., Weryk,R.J., Campbell-Brown, M.D., Brown, P.G., & Stokan, E. et al. (2013). Meteoroid structure and ablation implications from multiple maxima meteor light curves. Proceedings of the Meteoroids 2013. http://doi.org:10.48550/arXiv.1402.6002

Rogers, L.A., Hill, K.A., & Hawkes, R.L. (2005). Mass loss due to sputtering and thermal processes in meteoroid ablation. Planetary and Space Science, 53, 1341—1354. http://doi.org:10.1016/j.pss.2005.07.002

Rytove, S.M., Kravtsov, Y.A., & Tatarskiy, V.I. (1978). Vvedenie v statisticheskuyu radiofiziku. Chast 2. Sluchaynyie polya [Introduction to statistical radio physics. Part 2. Random fields]. Moscow: Nauka. (in Russian).

Safronov, V.S. (1972). Ejection of Bodies from the Solar System in the Course of the Accumulation of the Giant Planets and the Formation of the Cometary Cloud. The motion, evolution of orbits and origin of comets. Proceedings from IAU Symposium no. 45, held in Leningrad, U.S.S.R., August 4—11, 1970. (Eds Chebotarev G.A. et al.). D. Reidel, Dordrecht. 1972, 329—334. URL: https://adsabs.harvard.edu/full/1972IAUS...45..329S

Sato, K., Tsutsumi M., Sato, T., Nakamura, T., Saito, A., & Tomikawa, Y. et al. (2014). Program of the Antarctic Syowa MST/IS radar (PANSY). Journal of Atmospheric and Solar-Terrestrial Physics, 118, 2—15. http://doi.org:10.1016/j.jastp.2013.08.022

Schanker, J.Z. (1990). Meteor Burst Communications. Boston, London, Artech House Inc., 1990.

Schilling, D.L. (1993). Meteor Burst Communications: Theory and Practice. John Wiley & Sons, New York.

Schlyter, P. Computing planetary positions — a tutorial with worked examples. URL: http://stjarnhimlen.se/comp/tutorial.html

Schult, C. (2018). Studies of meteor head echo signatures at polar latitudes. URL: https://rosdok.uni-rostock.de/file/rosdok_disshab_0000001970/rosdok_derivate_0000057383/Dissertation_Schult_2018.pdf

Sekanina, Z. (1970). Statistical model of meteor streams I. Analysis of the model. Icarus, 13 (3), 459—474. http://doi.org:10.1016/0019–1035(70)90093–X

Sekanina, Z. (1970). Statistical model of meteor streams II. Major showers. Icarus, 13 (3), 475—493. http://doi.org:10.1016/0019–1035(70)90094–1

Sekanina, Z. (1973). Statistical Model of Meteor Streams. III. Stream Search Among 19303 Radio Meteors. Icarus, 18 (2), 253—284. http://doi.org:10.1016/0019–1035(73)90210–8

Sekanina, Z. (1976). Statistical model of meteor streams. IV. A study of radio streams from the synoptic year. Icarus, 27 (2), 253—284. http://doi.org:10.1016/0019–1035(76)90009–9

Senior, T.B.A. (1965). Obzor analiticheskikh metodov otsenki poperechnykh secheniy rasseyaniya [Review of analytical methods for scattering cross-sections evaluation]. TIIER [Proceedings of the Institute of Electrical and Electronics Engineers], 53 (8), 948—959. (in Russian).

Silber, E.A., Hocking, W.K., Niculescu, M.L., Gritsevich, M., & Silber, R.E. (2017). On shock waves and the role of hyperthermal chemistry in the early diffusion of overdense meteor trains. Monthly Notices of the Royal Astronomical Society, 469, 1869—1882. http://doi.org: 10.1093/mnras/stx923

Silber, E.A., Boslough, M., Hocking, W.K., Gritsevich, M., & Whitaker, R.W. (2018). Physics of Meteor Generated Shock Waves in the Earth's Atmosphere — A Review. Advances in Space Research, 62(3), 489—532. http://doi.org: 10.1016/j.asr.2018.05.010

Simonenko, A.N. (1973). K gipoteze drobleniya meteornykh tel putem otdeleniya melkikh chastits [On the hypothesis of fragmentation of meteor bodies by separation of small particles]. Meteoritics, 8 (4), 50—64. (in Russian).

SKiYMET Meteor Radar. [Website by Genesis Software Pty Ltd.]. URL: http://www.gsoft.com.au/productsandservices/skiymet

Sklyar, B. (2016). Tsifrovaya svyaz: teoreticheskie osnovy i prakticheskoe primenenie [Digital communication: theoretical foundations and practical applications]. (A.V. Nazarenko, Trans.). Moscow: Williams. (in Russian).

Slivinskiy, A.P., & Shulga, A.V. (2011). Odnopozitsionnyy punkt opredeleniya radianta meteornogo potoka po signalam TV peredatchika [Single-position point for determining the radiant of meteor stream by TV transmitter signals]. Nauka i tekhnologicheskiye razrabotki [Science and technological developments], 90 (2), 38—44. (in Russian).

Slyusar, V.I. (2004). SMART antenny poshli v seriyu [SMART antennas have gone into production]. Elektronika: nauka, tekhnologiya, biznes [Electronics: Science, Technology, Business], 2, 62—65. (in Russian).

Sokolova, M.G., & Sergienko, M.V. (2016). Asteroidyi, sblizhayuschiesya s zemley, kak vozmozhnyie roditelskie tela meteornyih potokov [Asteroids approaching the Earth as possible parent bodies of meteor streams]. Proceedings of Kazan University: Natural Sciences Series, 158 (4), 583—592.

Solovev, A.A. (2000). Peidzhingovaya svyaz [Paging communication]. Moscow: Eco-Trends. (in Russian).

Stasev, Y.V., Kuznetsov, A.A., Nosik, A.M., & Kachur, L.N. (2008). Formation of large ensembles of discrete signals using redundant codes. Zbirnyk naukovykh prats′ Kharkivs′koho universytetu Povitryanykh syl [Collection of scientific works of Kharkiv Air Force University], 2, 102—110. (in Ukrainian).

State Standard 4401—73. Standartnaya atmosfera. Parametryi [Standard atmosphere. Parameters]. Moscow: Izdatelstvo standartov [Standards Publishing House], 1977. (in Russian).

Steshenko, V.B. (2000). PLIS firmy Altera: proyektirovaniye ustroystv obrabotki signalov [Altera FPGA: designing signal processing devices]. Moscow: DODEKA. (in Russian).

Stokan, E., & Campbell-Brown, M.D. (2015). A particle-based model for ablation and wake formation in faint meteors. Monthly Notices of the Royal Astronomical Society, 447, 1580—1597. http: //doi.org: 10.1093/mnras/stu2552

Stokan, E., (2014). Fragmentation and Wake Formation in Faint Meteors: Implications for the Structure and Ablation of Small Meteoroids. Electronic Thesis and Dissertation Repository. 2581. URL: https://ir.lib.uwo.ca/etd/2581

Stulov, V.P. (1998). Analiticheskaya model posledovatelnogo drobleniya i ablyatsii meteornogo tela v atmosfere [Analytical model of sequential fragmentation and ablation of a meteor body in the atmosphere]. Astronomicheskiy vestnik [Astronomical Bulletin], 24 (12), 855—858. (in Russian).

Subasinghe, D., Campbell-Brown, M.D., & Stokan, E. (2016). Physical characteristics of faint meteors by light curve and high-resolution observations, and the implications for parent bodies. Monthly Notices of the Royal Astronomical Society, 457 (2), 1289—1298. http: //doi.org: 10.1093/mnras/stw019

Subasinghe, D. (2017). Physical Properties Of Faint Meteors Through High-Resolution Observations. Electronic Thesis and Dissertation Repository, 5077. URL: https://ir.lib.uwo.ca/etd/5077

Subasinghe, D., & Campbell-Brown, M. (2019). Properties of meteors with double peaked light curves. Monthly Notices of the Royal Astronomical Society, 457, 1121—1136. http: //doi.org: 10.1093/mnras/stz447

Sugar G., Oppenheim, M.M., Dimant, Y.S. & Close, S. (2019). Formation of Plasma Around a Small Meteoroid: Electrostatic Simulations. Journal of Geophysical Research: Space Physics, 124 (5), 3810—3826. http: //doi.org: 10.1029/2018JA026434

Sukara, R.E. (2013). Potential for Measurement of Mesospheric Ozone Density from Overdense Meteor Trains with a Monostatic Meteor Radar. Electronic Thesis and Dissertation Repository, Pap. 1789. Univ. of Western Ontario, Canada. URL: https://ir.lib.uwo.ca/etd/1789

Sverdlik, M.B. (1975). Optimalnyie diskretnyie signalyi [Optimal discrete signals]. Moscow: Sov. radio. (in Russian).

Tatarsky, V.I. (1967). Rasprostranenie voln v turbulentnoi atmosfere [Wave propagation in turbulent atmosphere]. Moscow: Nauka. (in Russian).

Taylor, A.D. (1991). A Meteor Orbit Radar. [ph.D. Dissertation, Department of Physics, University of Canterbury, New Zealand]. URL: http://dx.doi.org/10.26021/8130

Taylor, A.D. & McBride, N. (1997). A Radiant Resolved Meteoroid Model, Proceedings of the Second European Conference on Space Debris, 375—380, ESA-ESOC, Darmstadt, Germany. URL: https://www.nasa.gov/pdf/195790main_McNamara_04–MEM.pdf

Thomas, E., Horányi, M., Janches, D., Munsat, T., Simolka, J., & Sternovsky, Z. (2016). Measurements of the ionization coefficient of simulated iron micrometeoroids, Geophysical Research Letters, 43, 3645—3652. http: //doi.org:10.1002/2016GL068854

Tielens, A.G. G.M., McFee, C.F., Seab, C.G., & Hollenbach, D.J. (1994). The physics of grain-grain collisions and gas-grain sputtering in interstellar shocks. Astrophysical Journal, 431 (1), 321—340. http: //doi.org: 10.1086/ 174488

Tirskiy, G.A. (2000). Vzaimodeistvie kosmicheskikh tel s atmosferami Zemli i planet [Interaction of cosmic bodies with the atmospheres of the Earth and planets]. Sorosovskiy obscheobrazovatelnyiy zhurnal [Soros Educational Journal], 6 (5), 76—82. (in Russian).

Tkachuk, A.A. (1979). Sutochnye variatsii parametrov orbit nablyudaemykh radiometorov [Daily variations of the parameters of the orbits of observed radiometeors]. Problemy Kosmicheskoi Fiziki [Problems of Space Physics], 14, 52—61. (in Russian).

Tokhtasev, V.S. (1975). Obrazovanie i raspod meteornykh sledov [Formation and decay of meteor trails]. Dushanbe: DONISH. (in Russian).

Torrieri, D. (2022). Principles of Spread-spectrum communication systems. N.Y.: Springer.

Turin, D.L. (1980). Vvedenie v shirokopolosnye metody bor'by s mnogoluchevost'yu rasprostraneniya radiosignalov i ikh primenenie v gorodskikh sistemakh tsifrovoi svyazi [Introduction to broadband methods of combating multipath propagation of radio signals and their application in urban digital communication systems]. TIIER [Proceedings of the Institute of Electrical and Radioelectronics Engineers], 68 (3), 30—58. (in Russian).

Tuzov, G.I. (Ed.), Sivov V.A., & Prytkov V.I. (1985). Pomekhozashchishchennost radiosistem so slozhnymi signalami [Interference protection of radio systems with complex signals]. Moscow: Radio i svyaz. (in Russian).

Van de Hulst, G. (1961). Rasseyanie sveta malyimi chastitsami [Light Scattering by Small Particles]. (T.V. Vodopyanova, Trans.; V.V. Sobolev, Ed.). Moscow: Izdatelstvo inostrannoy literaturyi. (in Russian).

Van Tris, G. (1977). Teoriya obnaruzheniya, otsenok i modulyatsii: v 4-kh t. T. 3. Obrabotka signalov v radio- i gidrolokatsii i priem sluchaynykh gaussovykh signalov na fone pomekh [Theory of Detection, Estimation, and Modulation: in 4 vols. Vol. 3. Signal Processing in Radio and Hydro-Location and Reception of Random Gaussian Signals in the Presence of Noise]. (V.T. Goryainov, Trans. & Ed.). Moscow: Sov. radio. (in Russian).

Varakin, L.E. (1985). Sistemy svyazi s shumopodobnyimi signalami [Communication Systems with Noise-Like Signals]. Moscow: Radio i Svyaz. (in Russian).

Vendik, O.G., & Parnes, M.D. (2002). Antennyi s elektricheskim skanirovaniem (Vvedeniye v teoriyu) [Antennas with Electrical Scanning. Introduction to the Theory]. (L.D. Bakhrah, Ed.). Moscow: SAYNS PRESS. (in Russian). URL: https://techlibrary.ru/b/2j1f1o1e-1j1l_2w.2k.,_2x1a1r1o1f1s_2u.2l._2h1o1t1f1o1o2c_1s_2e1m1f1l1t1r1j1y1f1s1l1j1n_1s1l1a1o1j1r1p-1c1a1o1j1f1n._2001.pdf

Verniani, F. (1964). Luminousand Ionizing Efficiencies of Meteors. Astronomical Journal, 69, 561. http: //doi.org: 10.1086/109330

Volman, V.I., & Pimenov, Yu.V. (1971). Tekhnicheskaya elektrodinamika [Technical electrodynamics]. Moscow: Svyaz. (in Russian).

Voloshchuk, Y.I., & Gorelov, D.Yu. (2011). Meteornyye potoki i assotsiatsii, vyyavlennyye po rezultatam mnogoletnikh radiolokatsionnykh nablyudeniy meteorov v Kharkove [Meteoric streams and associations revealed from the results of long-term radar observations of meteors in Kharkiv]. Kharkiv: NTMT Press. (in Russian).

Voronin, S.V., Doroshenko, V.I., & Ksenofontov, Yu.G. (2019). Radiolinii meteornoy svyazi v telekommunikatsionnoy seti Severnogo morskogo puti [Radiolines of meteoric communication in the telecommunications network of the Northern Sea Route]. Trudy Uchebnykh Zavedeniy Svyazi [Proceedings of educational institutions of communication], 5 (3), 13—18. (in Russian). http://doi.org:10.31854/1813–324X–2019–5–3–13–18

Vvedensky, B.A. (Ed.). (1965). Dalnee troposfernoe rasprostranenie ultrakorotkih radiovoln [Distances tropospheric propagation of ultrashort radio waves]. Moscow: Sovetskoe radio. (in Russian).

Vyigodskiy, M.Y. (1976). Spravochnik po vyisshey matematike [Handbook of higher mathematics]. Moscow: Nauka. (in Russian).

Wait, J.R. (1955). Scattering of a plane wave from a circular dielectric cylinder at oblique incidence. Canadian Journal of Physics, 33, 189—195. http://doi.org: 10.1139/p55–024

Webster, A.R., & Hocking, W.K.(1998). An improved interferometer design for use with meteor radars. Radio Science, 33 (1), 55—65. http://doi.org: 10.1029/97RS03050

Webster, A.R., Brown, P.G., Jones J., Ellis, K.J., & Campbell-Brown, M. (2004). The Canadian Meteor Orbit Radar (CMOR). Atmospheric Chemistry and Physics, 4, 1181—1201. http://doi.org: 10.5194/acp–4–679–2004

Weitzen, J.A. Meteor Scatter Communication: A New Understanding, Chapter 1 of "Meteor Burst Communications Theory and Practice". Edited by D.L. Schilling, John Wiley. New York, 1993, 9—58.

Weitzen, J.A. (1993). Meteor Scatter Communication: A New Understanding. In: D.L. Schilling (Ed.), Meteor Burst Communications Theory and Practice, 9—58. Wiley-Interscience; 1st edition.

Weryk, R.J., & Brown, P. (2005). A search for interstellar meteoroids using the Canadian Meteor Orbit Radar (CMOR). Earth, Moon, and Planets, 95, 221—227. http://doi.org: 10.1007/s11038–005–9034–x

Weryk, R., & Brown, P.G. (2012). Simultaneous radar and video meteors-I: Metric comparisons. Planetary and Space Science, 62, 132—152. http://doi.org: 10.1016/j.pss.2011.12.023

Weryk, R.J., & Brown, P.G. (2013). Simultaneous radar and video meteors-II: Photometry and ionization. Planetary and Space Science, 81, 32—47. http://doi.org: 10.1016/j.p.2011.12.023

Weryk, R., Campbell-Brown, M.D., Wiegert, P., Brown, P.G., Krzeminski, Z., & Musci, R. (2013). The Canadian Automated Meteor Observatory (CAMO): System overview. Icarus, 225, 614—622. http://doi.org: 10.1016/j.icarus.2013.04.025

Whipple, F.L. (1938). Photographic meteor studies I. Proceedings of the American Philosophical Society, 79 (4), 499—548. URL: https://www.jstor.org/stable/984939

Whipple, F.L. (1943). Meteors and the Earth's atmosphere. Reviews of Modern Physics, 15 (3), 246—264. http://doi.org: 10.1103/RevModPhys.15.246

Whitman, K., Morbidelli, A., & Jedicke, R. (2006). The Size-Frequency Distribution of Dormant Jupiter Family Comets. Icarus, 183 (1), 101—114. http://doi.org: 10.1016/j.icarus.2006.02.016

Widrow, B., & Stearns, S. (1989). Adaptivnaya obrabotka signalov [Adaptive signal processing]. (V. Myasnikov, Trans.). Moscow: Radio i Svyaz. (in Russian).

Wiegert, P., Vaubaillon, J., & Campbell-Brown, M. (2009). A dynamical model of the sporadic meteoroid complex, Icarus, 201, 295—310. http://doi.org: 10.1016/j.icarus.2008.12.030

Wislez, J.-M. (1995). Forward scattering of radio waves off meteor trails. Proceedings of the International Meteor Conference, Brandenburg, Germany, 1995, 99—117. URL: https://adsabs.harvard.edu/full/1996pimo.conf...99W

Yakimchik, A.I. (2019). O preobrazovanii koordinat punktov iz sistemy CK-42 v sistem u WGS-84 [On the transformation of coordinates of points from the CK-42 system to the WGS-84 system]. Geofizicheskiy zhurnal [Geophysical journal], 41 (5), 165—189. (in Russian). http://doi.org: 10.24028/gzh.0203–3100.v41i5.2019.183641

Ye, Q-Z, & Han, S.X. (2017). Ozone measurements with meteors: a revisit. Monthly notices of the Royal Astronomical Society, 472 (1), 2—7. http://doi.org: 10.1093/mnras/stx1851

Younger, P.T., Astin, I., Sandford, D.J., & Mitchell, N.J. (2009). The sporadic radiant and distribution of meteors in the atmosphere as observed by VHF radar at Arctic, Antarctic and equatorial latitudes. Annales Geophysicae, 27 (7), 2831—2841. http://doi.org: 10.5194/angeo–27–2831–2009

Younger, J.P., Lee, C.S., Reid, I.M., Vincent, R.A., Kim, Y.H., & Murphy D.J. (2014). The effects of deionization processes on meteor radar diffusion coefficients below 90 km. Journal of Geophysical Research: Atmospheres, 119 (16), 10,027—10,043. http://doi.org:10.1002/2014JD021787

Zharov, V.E. (2006). Sfericheskaya astronomiya [Spherical astronomy]. Fryazino: Vek 2. (in Russian).

Zhdan, I.A., Stulov, V.P., Stulov, P.V., & Turchak, L.I. (2007). Koeffitsientyi soprotivleniya tel meteornyih form [Drag coefficients of meteor-shaped bodies]. Astronomicheskiy Vestnik [Astronomical Bulletin], 51 (6), 544—547. (in Russian).

Zherebtsov, G.A., Potekhin, A.P., Kurkin, V.I., Matvienko, G.G., Medvedev, A.V., & Mikhalev A.V. (2011). Radio and optical instruments of the National Helio-Geophysical Complex of the Russian Academy of Sciences. In Proceedings of the XXIII All-Russian Scientific Conference on Radio Wave Propagation, 47—54. Yoshkar-Ola: MarGTU. (in Russian).

Zotov, V.Y. (2003). Proektirovanie tsifrovykh ustroystv na osnove PLIS firmy XILINX v SAPR WebPACK ISE [Designing digital devices based on XILINX FPGAs in CAD WebPACK ISE]. Moscow: Goryachaya Liniya Telekom. (in Russian).

Zouros, G.P., Roumeliotis, J.A., & Stathis, G-T. (2011). Electromagnetic scattering by an infinite cylinder of material or metamaterial coating eccentrically a dielectric cylinder. Journal of the Optical Society of America A: Optics and Image Science, and Vision, 28 (6), 1076—1085. http://doi.org: 10.1364/JOSAA.28.001076

У монографії представлені дослідження, засновані на системному аналізі опублікованих праць у галузі метеорної фізики, а також оригінальні дослідження авторів книги. Запропоновано прогностичні моделі та алгоритми оцінки характеристик радіосигналів при бістатичному розсіюванні на іонізованому метеорному сліді у процесі його формування та розвитку, а також концепція та технологія побудови перспективної системи метеорного радіозв'язку.

Книга може бути корисною різним категоріям читачів: науковцям та конструкторам, які займаються метеорним радіозв'язком; геофізикам, що досліджують іоносферу у метеорній зоні; астрономам, які шукають нові взаємозв'язки між метеороїдами та їхніми батьківськими тілами; аспірантам, викладачам вищих навчальних закладів та студентам відповідних спеціальностей.

Наукове видання

НАЦІОНАЛЬНА АКАДЕМІЯ НАУК УКРАЇНИ
ІНСТИТУТ РАДІОФІЗИКИ ТА ЕЛЕКТРОНІКИ
ім. О.Я. УСИКОВА НАН УКРАЇНИ

ГОЛОВАНЬ Олена Вікторівна
ХАРЧЕНКО Віктор Миколайович

ПЕРЕДАЧА ІНФОРМАЦІЇ ПО МЕТЕОРНИХ РАДІОКАНАЛАХ

Англійською мовою

Редактор *Тетяна Ярмола*

Художнє оформлення *Євгена Ільницького*
Технічне редагування *Тетяни Шендерович*
Виготовлення ілюстрацій *Тетяни Лук'яненко*
Комп'ютерна верстка *Ніни Кучеренко*

Підписано до друку 29.10.2024. Формат 70×100/16. Гарн. Minion Pro.
Ум. друк. арк. 20,47. Обл.-вид. арк. 22,64. Тираж 100 прим. Зам. № 7448

Видавець і виготовлювач
Видавничий дім «Академперіодика» НАН України
вул. Терещенківська, 4, Київ, 01024, Україна

Свідоцтво про внесення до Державного реєстру суб'єктів
видавничої справи серії ДК № 544 від 27.07.2001